Realistic Strain Capacity Models for Pipeline Construction and Maintenance

Contract No. DTPH56-10-T-000016
Final Report

Prepared for

US Department of Transportation
Pipeline and Hazardous Materials Safety Administration
Office of Pipeline Safety

Prepared by

Ming Liu, Yong-Yi Wang, Fan Zhang, and Kunal Kotian

Center for Reliable Energy Systems
5960 Venture Dr., Suite B

Dublin, OH 43017

614-808-4872

December 9, 2013

Notice

This project was funded by the Department of Transportation, Pipeline and Hazardous Materials Safety Administration under the Pipeline Safety Research and Development Program. The views and conclusions contained in this document are those of the authors and should not be interpreted as representing the official policies, either expressed or implied, of the Pipeline and Hazardous Materials Safety Administration, or the U.S. Government.

This work is the contribution of an agency of the U.S. government, and is not subject to copyright.

Acknowledgement

This report was prepared for the U.S. Department of Transportation Pipeline and Hazardous Materials Safety Administration (US DOT PHMSA). Many individuals have provided valuable contributions throughout this multi-year effort. The project team is particularly grateful for the guidance and encouragement of Mr. Steve Nanney and Mr. James Merritt of DOT PHMSA for their support and guidance. Mr. Nanney served as the technical manager on behalf of US DOT PHMSA.

An industry advisory committee was formed to assist the development of the work scope, execution of the work plan, and the review of the work outputs. Members of the advisory committee are

- Dr. Mamdouh Salama of ConocoPhillips,
- Dr. Millan Sen of Enbridge,
- Drs. Daming Duan and Cindy Guan of TransCanada Pipelines,
- Mr. Alex Afaganis of Alliance Pipeline,
- Dr. Laurie Collins of Evraz NA, and
- Mr. Rick Gailing and Mr. Paul Lee of Southern California Gas.

Their insightful and constructive inputs to the project are gratefully acknowledged.

Realistic Strain Capacity Models for Pipeline Construction and Maintenance

Executive Summary

Traditional pipeline designs primarily focus on pressure containment through limiting the hoop stress to a certain percentage of the specified minimum yield stress (SMYS). Pipeline failures due to longitudinal strains are relatively rare events. Strain-based design (SBD) refers to pipeline design methodologies which have a specific goal of maintaining pipeline services and integrity under high longitudinal plastic strains (typically defined as strains greater than 0.5 %). Such large strains may come from frost heave and thaw settlements in arctic regions, seismic activities, landslides, mine subsidence, slope movement, or other events that alter the support conditions of pipelines. For offshore pipelines, large longitudinal strains may be induced by upheaval or lateral buckling or pipeline movements due to underwater landslides. The principles and procedures of SBD may also be applied to the maintenance of existing pipelines in areas of ground movement. Such process is sometimes termed strain-based design and assessment (SBDA).

Contrary to some misconception, stress- and strain-based designs are not mutually exclusive. The traditional pipeline design lacks precise methodologies required to design against high longitudinal strains. Strain-based design provides systematic and quantitative procedures to count for the effect of high longitudinal strains. Therefore, strain-based design should be viewed as a complementary tool to the traditional stress-based design.

The strain-based design encompasses both strain demand (i.e., applied strain) and strain capacity (i.e., strain limit). At least two limit states are associated with the SBD: tensile rupture and compressive buckling. A major focus of this project is the development of refined compressive strain models. The tensile strain models developed in a previous project (DOT agreement number DTPH56-06-T000014) are applied concurrently with the newly developed compressive strain models in the ranking and evaluation of both limit states.

The sophistication of compressive strain models is somewhat lagging prior to this project in comparison to that of tensile strain models. The existing compressive strain models in current standards typically include a limited number of parameters such as D/t ratio and internal or external pressure. It is known that many other factors affect the compressive strain capacity, including but not limited to, pipe geometry imperfection, shape of stress-strain curves, pipe material's strain hardening behavior, girth weld, and net-section stress.

The major deliverables of this project are:

- Refined compressive strain models,
- A ranking system for strain-based design using the newly developed compressive strain models and recently developed tensile strain models,
- Guidelines on critical elements of strain-based design, and
- Identification of additional gaps that further research may address.

The refined compressive strain models developed in this project recognize the following parameters:

- Pipe *D*/*t* ratio;
- Internal pressure;
- Pipe Y/T ratio;
- Geometry imperfection, specifically the height (from peak to valley) of pipe surface undulation;
- Pipe uniform strain;
- Pipe Lüder's strain; and
- Net-section stress (only tension currently).

Compared with other existing compressive strain models, the refined compressive strain models provide the following key improvements:

- The refined models are developed using a set of modeling procedures that provide realistic representation of field conditions;
- The refined models recognize an increased number of key controlling parameters compared with the existing models;
- The applicable range of each controlling parameter is extended or similar to the largest range of the existing models;
- The effects of the pipe *D*/*t* ratio and internal pressure are more precisely captured than the existing models;
- The compressive strain capacity (CSC) can be greatly affected by geometry imperfections. The magnitude of geometry imperfections is usually not available. Recommendations on the median, lower, and upper bound levels of geometry imperfections are provided. The upper bound geometry imperfections can lead to reasonably conservative CSC. The median and upper/lower geometry imperfections can lead to more realistic range of CSC with balanced conservatism.
- The effect of the girth weld, especially the effect of the high-low misalignment, is more properly accounted for than the existing models.

Together with the previously developed tensile strain models, the refined compressive strain models can be used for both the design of new pipelines and the evaluation of existing pipelines.

For new pipeline construction projects, the compressive and tensile strain models can be used for

- Setting linepipe specifications,
- Setting requirements for girth weld qualification,
- Helping the selection of field inspection procedures, and
- Determining flaw acceptance criteria.

For the integrity management of existing pipelines, these models may be used for

- Assessing the risk of tensile rupture and compressive buckling,
- Facilitating the decision on mitigation options, and
- Determining the intervention threshold in allowable strain demand.

The ranking system may be applied to serve a number of critical functions.

- At the design stage, the ranking system can be used to optimize the design conditions to balance the safety and cost of the pipeline by maintaining balanced safety margins for the tensile and compressive limit states.
- For pipeline maintenance, the output of the ranking system can be used to identify the relative risks in tensile and compressive failures, direct the mitigation plans, and optimize maintenance activities.

Guidelines on some key issues of strain-based design are provided. The needs to refine linepipe specifications and girth weld procedure qualification, including adoption of rigorous testing procedures, are highlighted. The potential negative consequence of not having these refinements is described.

The current status of strain-based design is summarized in the last section. Gaps and future research directions in regulatory requirements, strain demand, strain capacity, testing procedures, and codes and standards are highlighted. Finally, the needs of fully documenting testing data and testing procedures are noted in order to achieve the best possible strain-based design and assessment.

Realistic Strain Capacity Models for Pipeline Construction and Maintenance

Technical Summary on Compressive Strain Models

S.1. Introduction

The output of this project covers key elements related to strain-based design and assessment (SBDA). However, the key development in this project is the refined compressive strain models. To facilitate the understanding of this key development, this technical summary is provided to cover the key features of the development process and the results.

The development of the refined compressive strain models involves comprehensive review of existing compressive strain capacity (CSC) models, development of modeling processes that represent field conditions, systematic sensitivity studies on parameters affecting the compressive strain capacity (CSC), and detailed model evaluation.

S.2. Review of Existing Models

The following existing CSC models were reviewed in details:

- CSA Z662;
- DNV OS F101;
- API RP 1111;
- University of Alberta (UOA);
- JFE; and
- C-FER.

The comprehensive review demonstrates that the existing CSC models have:

- large differences in input parameters and their applicable ranges;
- large differences in computed CSC, especially for pressurized conditions;
- large differences in recommended safety factors; and
- inconsistent trends on model conservatism.

The model predictions depend on the processes adopted in the model development. The observed differences in the computed CSC from the different CSC models are partially due to the differences in the experimental and/or numerical modeling processes used to develop those CSC models, including but not limited to:

- the bases of the model development, e.g., experimental vs. numerical;
- the representation of material properties;
- the representation of field conditions;
- the definition/measurement of the compressive strain and strain capacity;
- the construction of the finite element models.

S.3. Modeling Processes

Proper modeling processes should give close representation of actual material behaviors and field conditions. Through systematic investigations on various (experimental and/or numerical)

modeling factors, improved modeling processes were established. The recommended modeling processes are summarized in the following.

S.3.1. Representation of Material Properties

S.3.1.1. Background

The linepipe materials often show material anisotropy, i.e., different stress-strain behaviors in their longitudinal and circumferential directions and different stress-strain behaviors under tension and compression. For example, the circumferential properties of UOE pipes often have higher strength but lower strain hardening capacity than their longitudinal properties. The pipes made from other manufacturing processes may show different characteristics of material anisotropy. Although the CSC mainly depends on the pipe's longitudinal properties, the material anisotropy is also believed to affect the CSC. For example, for the UOE pipes, the increase of the strength in the hoop direction tends to increase the CSC, however, the decrease of the strain hardening capacity in the hoop direction tends to decrease the CSC.

In the existing CSC models, the material's full stress-strain behaviors are often represented by selected key material parameters, e.g., yield strength, yield to tensile ratio (Y/T), and strain hardening exponent, etc. However, the key material parameters cannot uniquely define a full stress-strain curve. As a result, even for the same key material parameters, the full stress-strain behaviors used in different CSC models and the resulting CSC could be different.

S.3.1.2. Findings and Recommendations

The effect of the material anisotropy on the CSC was investigated through finite element analyses (FEA) in this project. For the UOE pipes with anisotropic stress-strain properties, it was found that compared with the different tensile and compressive properties, the anisotropic longitudinal and circumferential properties often play a secondary role on the CSC. The CSC is mainly determined by the pipe's longitudinal compressive properties. Therefore, the longitudinal compressive stress-strain curves should be used for the assessment of the CSC when available.

In this project, a set of mathematical equations for constructing the full stress-strain curves of the linepipes are recommended (see Section 3.2.3) and used in the development of the refined CSC models. The key material parameters representing the longitudinal tensile stress-strain properties are used in those equations. The equations are consistent with those used to construct the PRCI-CRES tensile strain models. The constructed stress-strain curves statistically show a good match with the experimentally measured stress-strain curves.

If the longitudinal compressive stress-strain curve is available, in order to properly use the CSC models, the compressive stress-strain curve must be converted to its equivalent tensile stress-strain curve. The key material parameters (i.e., model input parameters) should be obtained from the equivalent tensile stress-strain curve (see Section 3.2.1). It should be noted that the equivalent tensile stress-strain curve converted from the compressive stress-strain curve could be different from the tensile stress-strain curve measured from uni-axial tensile tests.

S.3.2. Representation of Field Conditions

S.3.2.1. Representation of Loads and Constraints

S.3.2.1.1. Background

High longitudinal strains in a pipeline segment are often induced by ground movement hazards, which usually apply distributed loads to a pipeline through pipe-soil interactions. The pipeline segment which is exposed to the ground movement is connected to the rest of the pipeline. The longitudinal strain is generated by the longitudinal force and bending moment generated by the distributed load and the constraint from the rest of the pipeline. The pipeline also experiences longitudinal stresses/strains from operating loads such as internal pressure and temperature change.

The variation of the loading and constraint conditions in fields can result in different combinations of bending moment and longitudinal forces to the pipeline and affect the CSC. For example, the CSC under uniform longitudinal compressive force is about half of the CSC under pure bending (see Section 2.3.5). Under bending-dominant conditions, the increase of the longitudinal tensile force tends to increase the CSC, while the increase of the compressive force tends to decrease the CSC.

The existing CSC models were developed under different loading and constraint conditions which produced different combinations of the bending moment and longitudinal force. As a result, the CSC computed from different models may not be equivalent. However, the existing CSC models do not distinguish the differences in the loading and constraint conditions and the computed CSC is treated equally.

Furthermore, different from the typical field conditions, in most numerical models and experimental tests including those used to develop the existing CSC models, the bending moment and longitudinal force were applied at the two ends of a pipe specimen without longitudinal displacement constraints and distributed loads.

S.3.2.1.2. Findings and Recommendations

In this project, various loading and constraint conditions and their effects on the CSC were investigated with FEA. It is found that the CSC under distributed soil loads tends to be smaller than the CSC under the loads applied at the pipe ends. On the other hand, the longitudinal displacement constraint tends to generate a tensile force in the longitudinal direction under bending due to elongation of the pipe segment, which tends to increase the CSC compared with the CSC under pure bending.

Based on the above discussions, for bending-dominant field conditions, the bending moment (applied at pipe ends) without the longitudinal constraint and net-section force is recommended for future numerical modeling and experimental tests if the exact magnitude of the longitudinal force in fields is not available. For compression-dominant conditions, the loading with uni-axial compressive force is recommended. The details on the loading conditions can be found in Sections 3.3.2 and 3.3.3.

S.3.2.2. Representation of Loading Sequences

S.3.2.2.1. Background

Under ground movement hazards, the buried pipeline can experience complicated loading sequences. The ground movement can take place in one occasion or multiple occasions and at

different pressure levels. The change of the internal pressure can take place before, during, and/or after the ground movement.

However, in typical numerical models and experimental tests, simplified loading sequences are often used. For example, the pipe specimen is firstly pressurized to a pre-determined pressure level. The bending moment and/or longitudinal force are then applied until a wrinkle is formed while the pressure is held constant.

Under plastic deformation, the stress and strain generated in the pipe depend on not only the magnitude of the load but also the loading sequence. Therefore, the CSC and the maximum moment may vary with the loading sequence.

S.3.2.2.2. Findings and Recommendations

The FEA conducted under this project demonstrated that both the CSC and the maximum moment can be affected by the loading sequence. The simplified loading sequence used by the existing numerical models and tests can produce conservative CSC compared with the CSC from other loading sequences analyzed. However, the simplified loading sequence may over-estimate the maximum/limit bending moment. The detailed discussion can be found in Section 3.3.4.

S.3.2.3. Length of Specimen for Experiments

The length of the specimen for experimental testing is often limited by the testing equipment. The length of the pipeline segment experiencing large longitudinal strain is typically longer than the testing specimen.

The pipe specimen for experimental testing has end plates to contain internal pressure and to transfer loads. The end plates reinforce the end section of the specimen and affect the strain, i.e., the end effect. Therefore, the testing specimen needs to be long enough to prevent the end effect from affecting the wrinkle formation and the CSC.

Detailed FEA conducted in this project on the testing specimens demonstrated that the CSC and the maximum (or limit) bending moment both depend on the length of the specimen. The CSC and the maximum bending moment increase with the increase of the specimen length. The length effect diminishes when the specimen length is longer than 6*D* (i.e., six times of pipe OD). The recommended minimum specimen length is 4*D*. The recommended specimen length is for those tests where the bending moment and longitudinal force are applied at the two ends of the pipe specimen where the end plates are attached. The length does not include the length of the pipe end sections with reinforcement. The detailed discussion can be found in Section 3.3.5.

S.3.3. Calculation and Measurement of Compressive Strain Capacity

S.3.3.1. Background

The bending moment and compressive strain are not uniform along the length of a pipe in most field conditions and in typical loading and constraint conditions adopted by most numerical models and experimental tests (Section 3.3.3.1). Therefore, wrinkles tend to be formed at the locations having the highest bending moment and compressive strain. The maximum (or limit) bending moment and CSC should be calculated/measured at the wrinkle location.

On the other hand, small wrinkles are often generated before the CSC is reached which can induce strain localization. To minimize the effect of the strain localization on the measured CSC

values, the average strain within a certain gauge length in the wrinkle area is usually used for determining the CSC. However, the selection of the gauge length varies in the current practice. The typical gauge length can be 1*D* (i.e., one pipe OD), 2*D*, and up to the full specimen length. The reported CSC values increase as the gauge length decreases. Therefore, selecting a proper gauge length is important for ensuring the consistent measure of the CSC. The gauge length used to define the CSC in most existing CSC models is not known.

S.3.3.2. Findings and Recommendations

The determination of the proper gauge length should consider the definition of strain demand. Since the CSC is eventually compared with the strain demand, the strain definition for the strain capacity and the demand needs to be consistent. The strain demand can be obtained from finite element simulations. In the finite element simulations of the strain demand, beam elements are often used. The beam elements cannot capture the wrinkle formation and wrinkle induced strain localization.

In this project, the strain demand and strain capacity were obtained for the same loading condition using finite element simulations. The results showed that to obtain consistent strain demand and capacity, the gauge length should be 2*D*. Additional details can be found in Section 3.4. It should be noted that the strain demand can also be obtained from direct measurement of the curvature of the pipeline. Under that circumstance, it is recommended to use 2*D* as the gauge length for calculating the strain demand too.

S.3.4. Finite Element Models

Shell and three-dimensional solid elements are often used in the finite element simulations of pipe buckling and wrinkle formation. The three-dimensional solid elements should be preferred, especially for the pipes containing girth welds and for post buckling analyses where significant displacement and strain localization are expected.

Proper mesh convergence tests are needed to demonstrate the mesh refinement is adequate. In general, finer mesh is needed for the pressurized conditions than that for the non-pressurized conditions. Therefore adequate mesh refinement needs to be demonstrated for high pressure conditions. Details on the mesh refinement are discussed in Section 3.5.

S.4. Systematic Sensitivity Studies

Systematic sensitivity studies were carried out on the influencing parameters for the CSC via FEA. The key findings are summarized in the following:

S.4.1. Pipe D/t Ratio and Internal Pressure

The pipe *D*/*t* ratio and internal pressure are the two most recognized influencing parameters to the CSC in the existing CSC models. Sensitivity studies in this project demonstrate a coupled effect between the *D*/*t* ratio and internal pressure, i.e., the increase of the CSC due to increasing pressure is more significant for small *D*/*t* pipes than large *D*/*t* pipes. However, most models do not recognize the coupling between the two parameters and also overestimate the increase of the CSC due to the internal pressure. The CSA models, although recognize the coupling between the internal pressure and pipe *D*/*t* ratio, produce an opposite trend to what is observed in the sensitivity studies. Additional details on this issue can be found in Sections 3.6.1, 4.4.1, 4.4.2,

and B.2.

S.4.2. Pipe Properties: Yield Strength, Strain Hardening, Lüder's and Uniform Strains

The pipe yield strength is used to evaluate the pressure effect on the CSC in most existing models, i.e., to calculate the pressure factor - the ratio between the pressure induced hoop stress and yield (or flow) strength. It should be noted that the yield strength for calculating the pressure factor is the hoop property and could be different from the longitudinal strength due to material anisotropy.

In addition to being used for calculating the pressure factor, the yield strength is used in some models to show the dependence of the CSC on pipe properties. In some other models, the strain hardening capacity, such as the pipe Y/T ratio and strain hardening exponent (n), is used instead of the yield strength. It should be noted that the pipe yield strength and strain hardening capacity are often related. In general, the pipe with lower yield strength often has higher strain hardening capacity. The sensitivity studies through FEA in the project showed that without the variation of the strain hardening capacity, the change of the yield strength alone has secondary effect on the CSC. On the other hand, the increase of the Y/T ratio can decrease the CSC greatly. The details on the effects of the yield strength and strain hardening capacity on the CSC can be found in Sections 3.6.3 and B.4.

The CSC can be affected by the shape of the linepipe's stress-strain curves. The pipes with discontinuous stress-strain curves containing Lüder's strains (or Lüder's extension) are often believed to have less CSC than the pipes with round and smooth stress-strain curves (assuming other conditions are the same). The sensitivity studies showed that if the CSC of the pipe with the Lüder's strain is higher than the Lüder's strain, the CSC of the pipe with the Lüder's strain is usually higher than the CSC of the pipe with round and smooth stress-strain curves (assuming same yield strength and Y/T ratio) and vise versa. The details on the effect of the Lüder's strain on the CSC can be found in Sections 3.6.5 and B.6.

The pipe uniform strain is not used by the existing CSC models. Small uniform strains are observed in the stress-strain curves of some pipes (especially modern linepipe materials). Similar to the yield strength, the uniform strain and the strain hardening capacity are also often correlated, i.e., the pipes with higher uniform strain often have higher strain hardening capacity. The sensitivity studies in this project showed that the change of the pipe uniform strain alone (i.e., the pipe yield strength and Y/T ratio are kept unchanged) has a secondary effect on the CSC unless the uniform strain becomes extremely low. Methods to taking account of the uniform strain are established and the details can be found in Sections 3.6.4 and B.5.

S.4.3. Pipe Geometry Imperfection

The pipe geometry imperfections can greatly affect the CSC. The imperfections studied in this project are those generated during pipe manufacturing which are typically in the form of an ovality (i.e., out-of-roundness of cross section), eccentricity, and non-uniform diameter or wall thickness. Mechanical damages and corrosion defects are not considered. The outside surface of the pipe is not perfectly round and smooth due to the combination of the imperfections. The variation of the outside surface from the perfect shape can be found in both pipe circumferential and longitudinal directions. The variation in the pipe circumference alone, such as the ovality

uniform along the length of the pipe is found to have a limited effect on the CSC. A wave-like surface variation along the length of the pipe (referred to as surface undulation) has been found in UOE pipes and can greatly reduce the pipe CSC. Both the height and the wavelength of the surface undulations are found critical to the CSC. Only the surface undulations with critical wavelengths are found to reduce the CSC greatly and the critical wavelength is the wavelength of the wrinkles formed at the maximum moment.

However, there is very limited data on measured surface undulations. The lack of the data on the surface undulations makes the application of some CSC models which require the geometry imperfection as input difficult. In this project, recommended median, upper, and lower bound surface undulations were developed for the application of those CSC models. It is believed that the surface undulations can be used as the generic representation of the geometry imperfections in different types of pipes due to their large detrimental effect on the CSC compared with other types of geometry imperfections. However, it should be noted that the recommendations are based on limited experimental data for UOE pipes. It is not clear if the other types of pipes, e.g., ERW, spiral, etc., have similar types of surface undulations. Additional details on the pipe geometry imperfections can be found in Sections 3.6.2, 4.4.4, and B.3.

S.4.4. Net-Section Force

Most existing CSC models are targeted for bending-dominant loading conditions and claim to be applicable to combined bending and longitudinal force. Although the longitudinal net-section force is found to affect the CSC, most existing CSC models do not adopt it as an input parameter. In addition, the existing CSC models adopted different loading conditions in their development processes. For example, some models used pure bending without net-section force. Some models allowed the net-section force generated by the pressure on the end plates (i.e., the longitudinal stress is in tension and is half of the hoop stress). Some models used data generated from mixed loading conditions. As a result, the difference in the applied net-section force in the models is partially responsible for the large difference in their computed CSC.

An assessment method for treating the net-section tensile force was developed in this project. Future work is still needed to properly consider the effect of the net-section compressive force on the CSC. Details on the net-section force effects can be found in Sections 3.6.7 and B.9.

S.4.5. Girth Weld

For pipes with girth welds, the CSC can be affected by both the girth welds and the geometry imperfections of the plain pipes. Mixed results have been reported in the published experimental data on the effects of girth welds on CSC. Some test data showed that the girth welds, especially those with high-low misalignment can greatly reduce the CSC. The other tests however, showed that girth welds with or without misalignment do not reduce the CSC.

The work in this project found that within reasonable ranges, the weld profile (e.g., cap size etc), welding residual stress, and strength mismatch have marginal effects on the CSC, compared with the plain pipes with reasonable geometry imperfections, e.g., a surface undulation of 4%t (t is wall thickness).

The high-low misalignment also shows relatively limited effect on the CSC especially under pressurized conditions. For the weld high-low misalignment (h_m) up to 50%t, the effect of the

misalignment on the CSC is equivalent to a 4%*t* and 15%*t* geometry imperfection in a plain pipe under high and zero pressure conditions, respectively. The 4%*t* ~ 15%*t* geometry imperfection is within the range of reasonable geometry imperfections found in plain pipes. The mixed testing results on the effect of the girth welds on the CSC could be explained by the different geometry imperfections in the tested pipes.

It should be noted that excessive high-low misalignment could induce significant stress/strain concentration on the tensile side of the pipe under bending. The maximum bending moment can be reached due to necking on the tensile side. The event corresponds to the tensile limit state and the tensile strain models should be able to capture this limit state. As a result, the compressive strain at the maximum moment should not be used as the critical strain for buckling failure.

On the other hand, the radial shrinkage due to the welding of the girth welds tends to create a geometry imperfection in the form of the surface undulation near the girth weld and reduce the CSC. The geometry imperfection induced by the girth weld shrinkage can be assessed with the surface undulations of plain pipes.

Based on the above observations, the CSC of pipes with girth welds can be assessed with the CSC models for plain pipes using equivalent geometry imperfections. Details on the girth weld studies can be found in Sections 3.6.6 and B.8.

S.5. Experimental Database and Model Evaluation

An experimental database was compiled using testing data published in public domain and was used to evaluate the refined compressive strain capacity models. The database consists of 48 full-scale bending tests and experimentally measured CSC was provided for 40 out of the 48 tests. Fifteen (15) of the 48 tests contain a girth weld. The database covers the following range,

- OD (D): 6.6 - 48 (inch)
- WT (t): 0.13 - 0.93 (inch)
- D/t: 22 - 104
- Grade: X52 - X100
- YS (σ_y): 55 - 98 (ksi)
- Y/T: 0.77 - 0.91
- Lüder's strain (ε_e): < 1.6%
- Pressure factor (f_p): 0 - 0.82
- Net-section stress factor (f_n): -0.42 - 0.62
- CSC: 0.23 - 6.2 (%)

The predicted CSC for the seven tests with measured geometry imperfections matches the measured CSC very well. For all test data, the recommended median imperfection values provide fairly reasonable predictions of the measured CSC. Using the upper bound geometry imperfections, reasonably conservative predictions can be obtained.

Table of Contents

Notice i
Acknowledgement ii
Executive Summary iii

Nomenclature 1
Abbreviations 1
Symbols 1
Organizations 2
1 Introduction 4
1.1 Background on Strain-Based Design 4
1.1.1 Stress- vs. Strain-Based Design 4
1.1.2 General Concept of Strain-Based Design 4
1.2 Scope and Objective of This Project 4
1.2.1 Scope of This Project 4
1.2.2 Project Objectives 5
1.2.3 Relationship of Current Work and Public Safety 5
1.3 Structure of the Report 5
2 Status of Existing Compressive Strain Models 7
2.1 Role of Compressive Strain Models 7
2.2 Overview of Models for Compressive Strain Limit 8
2.3 Review of Compressive Strain Models 8
2.3.1 CSA Z662 Models 8
2.3.2 DNV OS F101 Models 9
2.3.3 API RP 1111 Models 10
2.3.4 University of Alberta (UOA) Models 10
2.3.5 JFE Models 12
2.3.6 C-FER Models 13
2.4 Comparison of Selected Models 13
2.5 Limitations of Existing Models 16
3 Processes for the Development of Compressive Strain Models 17
3.1 Overview 17
3.2 Representation of Material Properties 17
3.2.1 Introduction of Stress-Strain Curves 17
3.2.2 Pipe Property Anisotropy 19
3.2.3 Mathematical Representation of Stress-Strain Curves 20
3.2.4 Pipe Properties and Geometries Used in the Analyses 21
3.3 Representation of Field Conditions 23
3.3.1 Introduction of Field and Testing/Numerical Modeling Conditions 23
3.3.2 Modeling of Field Loading and Constraints 26
3.3.3 Effect of Modeling Conditions on CSC 27

3.3.4 Modeling of Loading Sequences 31
3.3.5 Lengths of Specimens 34
3.4 Definition and Calculation of Compressive Strain Capacity 36
3.5 Finite Element Models 38
3.5.1 Shell vs. Three-Dimensional (3-D) Solid Models 38
3.5.2 Sample 3-D Solid Models 39
3.5.3 Mesh Refinement of 3-D Solid Models 39
3.6 Parameters Affecting Compressive Strain Limit 40
3.6.1 Pipe *D*/*t* Ratio and Internal Pressure 41
3.6.2 Geometry Imperfection 41
3.6.3 Pipe Yield Strength and Y/T Ratio 42
3.6.4 Pipe Uniform Strain 42
3.6.5 Pipe Lüder's Strain 42
3.6.6 Girth Weld 43
3.6.7 Net-Section Force 43
3.7 Summary of the Analysis Process 44
3.7.1 Representation of Material Properties 44
3.7.2 Representation of Field Conditions 45
3.7.3 Calculation and Measurement of Compressive Strain Capacity 46
3.7.4 Finite Element Models 47
4 Refined Compressive Strain Models 48
4.1 Structure of the Refined Compressive Strain Models 48
4.2 Refined Compressive Strain Models 48
4.3 Applicable Range 49
4.4 Trend Analyses and Comparison of with Existing Models 49
4.4.1 Pipe *D*/*t* Ratio 49
4.4.2 Internal Pressure 49
4.4.3 Pipe Y/T Ratio 50
4.4.4 Pipe Geometry Imperfection 50
4.5 Model Evaluation 52
4.5.1 Experimental Database 52
4.5.2 Evaluation with Test Data Having All Input Parameters 53
4.6 Recommended Geometry Imperfections 56
4.7 Summary Remarks of the Refined Compressive Strain Models 57
5 Tensile Strain Models 62
5.1 Role of Tensile Strain Models 62
5.2 Physical Process of Tensile Rupture 63
5.3 Key Elements of Tensile Strain Design 64
5.4 Tensile Strain Models 64
5.4.1 PRCI-CRES Models 65
5.4.2 Other Tensile Strain Models 71
5.5 Summary Remarks about Tensile Strain Models 71

6 A Ranking System for Strain-Based Design 73
6.1 Basis of the Ranking System 73
6.2 Structure and Function of the Ranking System 73
6.3 Sample Application of the Ranking System 74
6.4 Summary Remarks of the Ranking System 78
7 Guidelines on Some Key Elements in Strain-Based Design 79
7.1 Introduction 79
7.2 Role of Strain-Based Design 79
7.3 General Philosophy of Strain-Based Design 79
7.4 Linepipe Specifications 81
7.4.1 Importance of Linepipe Specifications 81
7.4.2 Shortcomings of Linepipe Specifications in Current Standards 81
7.4.3 Recommendations on Linepipe Specifications 82
7.4.4 Key Issues in Linepipe Specifications and Rationales for Recommendations 84
7.5 Girth Weld Specifications / Qualification 91
7.5.1 Girth Welding Procedure Qualification 91
8 Gaps for Further Studies 99
8.1 Introduction 99
8.2 Tensile Strain Models for Girth Welds of Equal Wall Thickness 99
8.2.1 Flaw Interactions 99
8.2.2 Applicable Strain Ranges 99
8.3 Compressive Strain Models for Girth Welds of Equal Wall Thickness and Plain Pipes 100
8.3.1 Effect of Net-Section Axial Compressive Force 100
8.3.2 Effect of Compression Induced Hoop Strain 100
8.4 Tensile and Compressive Strain Models for Transition Welds 100
8.5 Burst Pressure and Tensile/Compressive Strain Models for Corroded Pipes 103
8.5.1 Burst Pressure 103
8.5.2 Tensile and Compressive Strains 104
8.6 Compressive Strain Models for Dented Pipes 106
9 Concluding Remarks 109
9.1 Tensile Strain Models 109
9.2 Compressive Strain Models 110
9.3 Gaps in Strain-Based Design and Future Directions 111
9.3.1 Regulatory Requirements 112
9.3.2 Strain Demand 113
9.3.3 Strain Capacity under Realistic Conditions 113
9.3.4 Testing Procedures and Material Qualification 115
9.3.5 Codes and Standards 115
9.4 Summary 116
10 References 117
Appendix A Construction of Pipe and Weld Stress-Strain Curves A-1
A.1 Background A-1

A.2 Ramberg-Osgood vs. CSA Stress-Strain Curve Equations A-2
A.3 Representation of Pipe Stress-Strain Curves A-3
A.4 Representation of the Weld Metal Stress-Strain Curves A-6
A.5 Evaluation of the Constructed Stress-Strain Curves A-9
A.6 References for Appendix A A-10
Appendix B Influencing Parameters for CSC B-1
B.1 Overview of Influencing Parameters B-1
B.2 Pipe *D*/*t* Ratios and Internal Pressure B-1
B.3 Geometry Imperfections B-5
B.3.1 Shape of Geometry Imperfections B-5
B.3.2 Modeling of Geometry Imperfections B-6
B.3.3 Effect of the Type of Geometry Imperfections on CSC B-7
B.3.4 Critical Wavelength of Geometry Imperfections B-9
B.3.5 Effect of the Height of Geometry Imperfections on CSC B-13
B.4 Pipe Yield Strength and Strain Hardening Capacity B-13
B.5 Pipe Uniform Strains B-16
B.6 Pipe Lüder's Strains B-17
B.7 Pipe Property Anisotropy B-24
B.8 Girth Welds B-27
B.8.1 Overview of Girth Weld Effect B-27
B.8.2 Effect of Weld Profile and Strength Mismatching B-27
B.8.3 Weld Residual Stresses B-29
B.8.4 Weld High-Low Misalignment B-32
B.8.5 Summary of the Girth Weld Effect on the CSC B-33
B.9 Net-Section Longitudinal Force B-33
B.10 Summary of Sensitivity Studies B-37
B.10.1 Pipe D/t Ratio and Internal Pressure B-37
B.10.2 Pipe Properties: Strength, Strain Hardening, Lüder's and Uniform Strains B-37
B.10.3 Pipe Geometry Imperfection B-38
B.10.4 Net-Section Force B-39
B.10.5 Girth Weld B-39
B.11 References of Appendix B B-40
Appendix C Experimental Database C-1
C.1 Experimental Data C-1
C.2 References of Appendix C C-3

Nomenclature

Abbreviations

3-D	Three dimensional,
CSC	Compressive strain capacity,
CTOD	Crack tip opening displacement,
$CTOD_A$	Apparent CTOD toughness,
$CTOD_F$	CTOD driving force,
FEA	Finite element analysis,
OD	Outside diameter,
OM	Weld strength mismatch ratio, ratio between weld and pipe UTS,
OV	Cross section ovality, $(D_{max}-D_{min})/(D_{max}+D_{min})$,
SBD	Strain based design,
SMYS	Specified minimum yield strength,
SSC	Stress-strain curves,
TSC	Tensile strain capacity,
uEL	Uniform strain (uniform elongation),
UOE	'U', 'O', and expansion,
UTS	Ultimate tensile strength,
WT	Wall thickness,
YS	Yield strength,
Y/T	Yield to tensile strength ratio,

Symbols

a	Flaw height,
c	Flaw half length,
D	Pipe outside diameter (OD),
D_{max}	Maximum pipe outside diameter,
D_{min}	Minimum pipe outside diameter,
E	Young's modulus,
f_p	Pressure factor: $(p_i - p_e)\, D / (2\, t\, \sigma_y)$,
h_g	Height of pipe geometry imperfection (surface undulation),
h_m	Height of girth weld high-low misalignment,
L	Length of pipe specimen in full-scale bending test,
L_b	Wavelength of surface undulation in pipe axial (longitudinal) direction,
L_w	Wavelength of wrinkle in pipe axial (longitudinal) direction,

l_g	Gauge length for CSC measurement,
n	Strain hardening exponent,
p_i	Internal pressure,
p_e	External pressure,
t	Pipe wall thickness,
σ	Stress,
σ_a	Applied axial (longitudinal) stress,
σ_u	Pipe ultimate tensile strength (UTS),
σ_u^w	Weld metal ultimate tensile strength,
σ_y	Pipe yield strength (YS),
σ_y^w	Weld metal yield strength,
ε	Strain,
ε_c	Average compressive strain,
ε_c^{crit}	Compressive strain capacity (CSC) under bending-dominant loading,
ε_{ac}^{crit}	Compressive strain capacity (CSC) under pure axial compression,
ε_e	Strain where Lüder's extension (or Lüder's strain) ends,
ε_t	Average tensile strain within a given gauge length,
ε_u	Pipe uniform strain or uniform elongation (uEL),
α	Angle of geometry imperfection in pipe circumferential direction,
δ	Cross section ovality (OV), $\delta = (D_{max}-D_{min})/(D_{max}+D_{min})$,
δ_A	Apparent CTOD toughness ($CTOD_A$),
ν	Poison's ratio,
η	Normalized flaw depth: a/t,
β	Normalized flaw length: $2c/t$,
ψ	Normalized girth weld high-low misalignment: h_m/t,
ρ	Normalized geometry imperfection: h_g/t,
ξ	Pipe yield to tensile strength ratio (Y/T): σ_y/σ_u,
ϕ	Weld strength mismatch ratio measured by UTS (OM): σ_u^w/σ_u,

Organizations

API	American Petroleum Institute,
ASME	American Society of Mechanical Engineers,
CRES	Center for Reliable Energy Systems,
CSA	Canadian Standards Association,
DNV	Det Norske Veritas,

DOT	Department of Transportation,
UOA	University of Alberta,
PHMSA	Pipeline and Hazardous Materials Safety Administration,
PRCI	Pipeline Research Council International.

1 Introduction

1.1 Background on Strain-Based Design

1.1.1 Stress- vs. Strain-Based Design

Traditional pipeline designs primarily focus on pressure containment through limiting the hoop stress to a certain percentage of the specified minimum yield stress (SMYS). For instance, the concept of class location effectively limits the maximum applied hoop stress as a percentage of SMYS. Potential failures due to longitudinal strains are relatively rare events. Consequently design against longitudinal stress is typically not a primary concern.

Strain-based design (SBD) refers to pipeline design methodologies which have a specific goal of maintaining pipeline services and integrity under large longitudinal plastic strains (typically defined as strains greater than 0.5 %). Such large strains may come from frost heave and thaw settlements in arctic regions, seismic activities, landslides, mine subsidence, or other events. For offshore pipelines, large longitudinal strains may be induced by upheaval or lateral buckling or pipeline movements due to underwater landslides. In North America, the need for the SBD is primarily driven by northern pipeline projects (e.g., in Alaska). Pipelines in the northern regions may traverse areas of discontinuous permafrost. In other parts of the world, the SBD is playing an increasingly important role in the design and maintenance of pipelines going through areas of seismic activities and mine subsidence. The principles and procedures of the SBD may also be applied to the maintenance of existing pipelines in areas of ground movement which is one of the leading causes of girth weld failure.

Contrary to some misconception, the stress- and strain-based designs are not mutually exclusive. The traditional pipeline design lacks the precise methodologies required to design against high longitudinal strains. The strain-based design provides systematic and quantitative procedures to count for the effects of high longitudinal strains. Therefore, the SBD should be viewed as a complementary tool to the traditional stress-based design.

1.1.2 General Concept of Strain-Based Design

The strain-based design encompasses at least two limit states: tensile rupture and compressive buckling. The tensile rupture is an ultimate limit state which is related to the breach of the pressure boundary. The compressive buckling could be either a service limit state or an ultimate limit state. To design for these limit states, it is necessary to quantify the magnitude of strain demands (applied strains) and strain capacity (strain limits).

The strain demand is the strain imposed on the pipeline by its operational and environmental conditions. The strain capacity is the limit of the tolerable strain level beyond which a failure condition is reached. A single design condition would require that the strain capacity be greater than the strain demand by an appropriate margin.

1.2 Scope and Objective of This Project

1.2.1 Scope of This Project

This project is intended to continue the development of refined strain capacity models. Considerable efforts have been devoted to the development of tensile strain design models

worldwide in the recent years [1,2,3]. A comprehensive set of tensile strain models has been developed through the joint funding of US DOT PHMSA and the pipeline industry [4,5]. The tensile strain design models have become much more sophisticated and realistic in comparison to those available only a few years ago. For instance, the effects of linepipe and weld properties, internal pressure, and girth weld misalignment are fully accounted for in the PRCI-CRES tensile strain models [4].

However, in comparison to the tensile strain models, the sophistication of the compressive strain models is somewhat lagging. Models in the current standards typically include a very limited number of parameters, such as the *D*/*t* ratio and the internal or external pressure, but it is known that many other factors have an effect on the compressive strain capacity as well, such as pipe geometric imperfection, pipe strain hardening behaviors, girth welds, and net-section stress, etc.

The major focus of this project is:

(1) developing more refined compressive strain models,

(2) implementing a ranking system for strain-based design using the newly developed compressive strain models and recently developed tensile strain models,

(3) drafting guidelines on some critical elements of strain-based design,

(4) highlighting gaps in the current approaches and further research needs.

1.2.2 Project Objectives

The objectives of this project are to:

(1) develop more refined compressive strain models than those in the current standards,

(2) implement a ranking system for strain-based design, and

(3) provide updated guidelines on key elements of strain-based design.

1.2.3 Relationship of Current Work and Public Safety

The current work has public safety implications both immediate and over the long term. Although the compressive buckling is usually not considered an ultimate limit state because the bucking typically does not lead to an immediate loss of pressure containment. Over a longer term, the buckled pipes can have reduced fatigue lives and diminished abilities to sustain further deformation, should such an event occur. The tensile rupture leads to an immediate loss of pressure containment, therefore, can have serious environmental and safety implications.

1.3 Structure of the Report

In Section 2 of this report, the existing compressive strain models are reviewed and compared. The features of these models are highlighted. The review leads to the recognition of the areas that need further refinement. Section 3 covers the development process of refined compressive strain models through systematic analysis of the influence of various parameters. In Section 4, the refined compressive strain models and their applicable range are provided. The models are compared with other existing models and evaluated against available experimental test data. Section 5 provides a review of tensile strain models with focus on the PRCI-CRES models. The use of the newly developed compressive strain models and the PRCI-CRES tensile

strain models in a ranking system for strain-based design is shown in Section 6 through a few example problems. In Section 7, guidelines on key elements of strain-based design are provided with a focus on practice to achieve adequate strain capacity. Certain gaps and practical issues related to compressive strain capacity are described in Section 8. In Section 9, the overall status and use of strain-based design is summarized.

2 Status of Existing Compressive Strain Models

2.1 Role of Compressive Strain Models

Pipelines may fail by buckling when subjected to compressive strains in the longitudinal direction. The compressive strains can be generated by bending and/or net-section compression. The buckling is accompanied by the formation of wrinkles (Figure 2-1). Depending on the level of the internal pressure when the wrinkle forms, the wrinkle can be either in a form of an inward kink into the pipe surface (under low or no internal pressure) or an outward bulge (under high internal pressure).

The formation of a wrinkle does not typically lead to an immediate failure (or breach of the pressure boundary) of the pipeline. Therefore, the buckling is usually considered a service limit state not an ultimate limit state. A wrinkle can however reduce the load carrying capacity of the pipeline, interfere with the in-line inspection tools, induce stress and strain concentrations, and reduce fatigue life. The buckling can be an ultimate limit state and lead to an immediate failure if the pipeline is under load-controlled conditions such as free span.

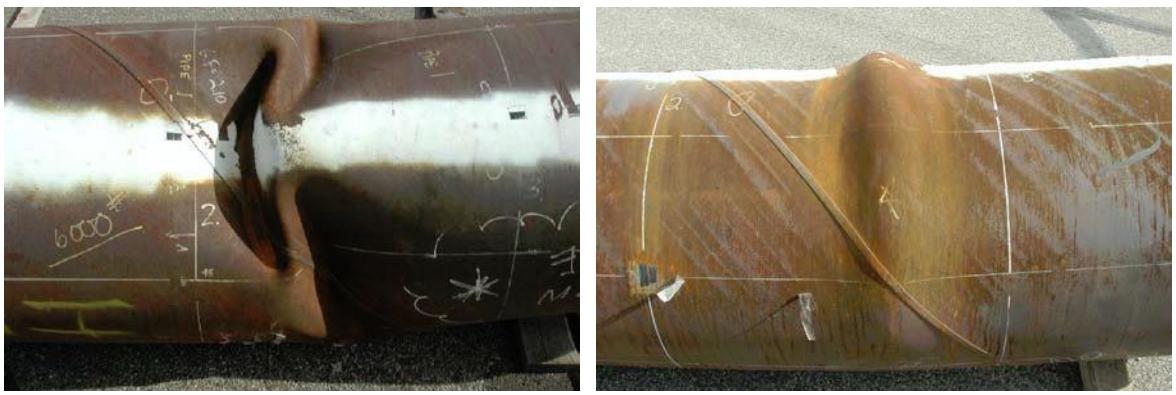

(a) wrinkle formed at no internal pressure (b) wrinkle formed at high internal pressure

Figure 2-1 Wrinkles in pipe [6]

Compressive strain models were developed to capture the compressive strain at the initiation of the buckling. The compressive strain models may be used in the design phase of a pipeline or in the integrity management of an existing pipeline. In the design phase, the compressive strain models may be used for

- Setting linepipe specifications,
- Setting requirements for girth weld qualification,
- Helping the selection of field inspection procedures, and

For the integrity management of existing pipelines, the compressive strain models may be used for

- Assessing the risk of compressive buckling,
- Facilitating the decision on mitigation options, and
- Determining the intervention threshold in allowable strain demand.

The compressive strain models can be powerful tools in the entire life cycle of pipelines.

2.2 Overview of Models for Compressive Strain Limit

There are many limit state equations for the compressive strain capacity (CSC) in codes and standards such as DNV OS F101 [7], CSA Z662 [8], and API RP 1111 [9]. In recent years, however, many efforts have been undertaken to develop improved CSC models, such as those by University of Alberta (UOA) [10], JFE [11, 12, 13], C-FER [14, 15], Atkins Boreas [16], and many others [17, 18].

All the CSC equations address local buckling (i.e., wrinkle formations) under bending and/or longitudinal (i.e., axial) compression. The local buckling is an event of instability triggered by the localization of compressive stresses/strains and the reduction of load carrying capacity. In most models, the CSC is defined as the compressive strains corresponding to the maximum loads (i.e., bending moments or axial compressive forces). In the UOA models, the CSC is defined as the compressive strains at the initiation of strain localizations [19].

Those equations are better suited for displacement-controlled loading conditions. However, if proper correlations between stresses and strains can be established, those equations can also be applied to load-controlled conditions.

It is well known that the CSC is greatly affected by the pipe *D*/*t* ratio (the ratio between pipe outside diameter and wall thickness) and the pressure. All the above CSC equations recognize those two parameters.

It has been found that other parameters such as pipe's strain hardening properties, shapes of stress-strain curves, girth welds, and geometry imperfections can also affect the CSC. However, the significance and working mechanism of those parameters have not been fully understood and therefore, the acceptance of those parameters by different models varied greatly.

Due to the different targeting applications of those models, the applicable range of those models also varies greatly. For example, the DNV and API models are mainly for offshore applications and therefore are targeted for pipes of small *D*/*t* ratios. The detailed review of each model is included in the following section.

2.3 Review of Compressive Strain Models

2.3.1 CSA Z662 Models

The CSA Z662 equations (in Clause C.6.3.3 of Annex C) were originated from the work by Gresnigt in 1980s [20]. These equations were developed by fitting a curve to the lower bound of the measured strains in an experimental database. The equations in the recent versions of the CSA codes, i.e., 2007 and 2011 [8], were modified to correct possible non-conservative predictions under high internal pressure. The CSA equations can be used for the conditions with combined bending and axial (longitudinal) compression under internal overpressure (i.e., internal pressure ≥ external pressure).

The CSA Z662 equations are shown in the following. The unit of the CSC ($\varepsilon_c^{\text{crit}}$) is in/in.

$$\varepsilon_c^{\text{crit}} = \left\{0.5\frac{t}{D} - 0.0025 + 3000\left[\frac{f_p\sigma_y}{E}\right]^2\right\} \quad \text{if } f_p < 0.4 \tag{2-1}$$

$$\varepsilon_c^{\text{crit}} = \left\{0.5\frac{t}{D} - 0.0025 + 3000\left[\frac{0.4\sigma_y}{E}\right]^2\right\} \quad \text{if } f_p \geq 0.4 \tag{2-2}$$

The pressure factor (f_p) can be calculated from the following equation.

$$f_p = \frac{(p_i - p_e)D}{2t\sigma_y}.$$

In the above equations, t represents the pipe's wall thickness, D represents the OD, σ_y represents the pipe's yield strength, E represents the Young's modulus of the pipe, p_i represents the internal pressure, and p_e represents the external pressure.

The CSA equations explicitly recognize two parameters, i.e., the pipe's D/t ratio and pressure. However, since the equations were obtained by fitting experimental data, the pipe's strain hardening properties (such as Y/T ratios) and geometry imperfections were implicitly taken into account. It is likely that the upper bound pipe Y/T ratios and/or geometry imperfections (of the pipes in the experimental database) were used by the models since the lower bound of the experimentally measured strains were used. It is not clear if the experimental database used to derive the CSA equations had specimens with girth welds.

The applicable range of the input parameters is not explicitly specified for the CSA equations. Based on the original work led to the CSA equations [20], the applicable D/t ratio should be between 20 and 120. A small safety factor of 1.25 was recommended by the CSA codes.

2.3.2 DNV OS F101 Models

In DNV OS F101 [7], two sets of CSC equations are provided for load- and displacement-controlled loading conditions, respectively. For the displacement-controlled loading conditions, two separate equations, i.e., internal overpressure (i.e., $p_i \geq p_e$) and external overpressure (i.e., $p_i \leq p_e$), are provided. The focus of this review is on the equations for the displacement-controlled conditions with internal overpressure. The displacement-controlled equations (with internal overpressure) were based on finite element results. A slight change to the flow stress for calculating the pressure effect was made in the recent 2007 version of the DNV codes which makes the calculated CSC slightly less conservative for pipes with Y/T ratios greater than 0.87.

The DNV equation for plain pipes is given in Eq. (2-3) and the DNV equation for pipes with girth welds is given in Eq. (2-4) where the unit of the CSC ($\varepsilon_c^{\text{crit}}$) is in/in,

$$\varepsilon_c^{\text{crit}} = 0.78\left(\frac{t}{D} - 0.01\right)\left[1 + 5.75\frac{(p_i - p_e)}{p_b}\right]\xi^{-1.5}, \tag{2-3}$$

$$\varepsilon_c^{\text{crit}} = 0.78\left(\frac{t}{D} - 0.01\right)\left[1 + 5.75\frac{(p_i - p_e)}{p_b}\right]\xi^{-1.5}\alpha_{gw}, \tag{2-4}$$

where,

$$p_b = \frac{2t}{D-t}\frac{2}{\sqrt{3}}\min\left(\sigma_y, \frac{\sigma_u}{1.15}\right),$$

$$\xi = \frac{\sigma_y}{\sigma_u},$$

$$\alpha_{gw} = \begin{cases} 1 & if\ \frac{D}{t} \leq 20 \\ 1 - 0.01\left(\frac{D}{t} - 20\right) & if\ \frac{D}{t} > 20 \end{cases}.$$

In the above equations, σ_u represents the pipe's ultimate tensile strength (UTS).

In addition to the pipe's D/t ratio and pressure, the DNV equations include the pipe's Y/T ratio to account for the effect of the material's strain hardening capacity on the CSC. The DNV equations also recommend a CSC correction factor (α_{gw}) for pipes with girth welds. The girth weld correction factor was developed using the experimental data published by University of Alberta in 1994 [19].

The DNV equations are limited to the pipes with $D/t \leq 45$, which are typical for offshore pipelines. No limits on the applicable pipe grades or Y/T ratios are specified in the codes. The recommended safety factors are between 2.0 and 3.3.

2.3.3 API RP 1111 Models

The API RP 1111 equation [9] was developed for offshore applications and is applicable to external overpressure only (i.e., $p_i \leq p_e$). The API equation is given in Eq. (2-5) as shown below. The unit of the CSC ($\varepsilon_c^{\text{crit}}$) is in/in.

$$\varepsilon_c^{\text{crit}} = \left[\frac{1}{1+20\delta} - \frac{(p_e - p_i)}{p_c}\right]\frac{t}{2D}, \tag{2-5}$$

where,

$$\delta = \frac{(D_{max} - D_{min})}{(D_{max} + D_{min})},$$

$$p_c = \frac{p_y p_e{}'}{\sqrt{p_y{}^2 + p_e{}'^2}},$$

$$p_y = 2\sigma_y \frac{t}{D}, \text{ and}$$

$$p_e{}' = 2E\left(\frac{t}{D}\right)^3 \frac{1}{(1-\nu^2)}.$$

In the above equations, δ is the so-called ovality (i.e., the out of roundness) of the pipe cross section and ν is Poisson's ratio of the pipe materials. The $D_{\max}$ and $D_{\min}$ are the maximum and minimum OD of a given cross section.

The API RP 1111 equation includes the effect of the D/t ratio, pressure, and ovality of the pipe's cross section. The equation is limit to $D/t \leq 50$ and $p_i \leq p_e$. The recommended safety factor is 2.

2.3.4 University of Alberta (UOA) Models

The UOA models (2006) [10], developed by researchers at University of Alberta, were based on extensive FEA. The FEA were done under bending and internal pressure (i.e., $p_e = 0$).

The UOA models consist of four (4) sets of equations: (1) plain pipes with round stress-strain curves (Eq. 2-6), (2) plain pipes with yield plateau (i.e., Lüder's extension) in stress-strain curves (Eq. 2-7), (3) pipes of round stress-strain curves with girth welds (Eq. 2-8), and (4) pipes of yield plateau in stress-strain curves with girth welds (Eq. 2-9). The unit of the CSC in Eqs. (2-6) to (2-9) is %.

$$\varepsilon_c^{\text{crit}}(\%) = \left(\frac{2.9398}{D/t}\right)^{1.5921}\left(1 - 0.8679 f_p\right)^{-1}\left(\frac{E}{\sigma_y}\right)^{0.8542}\left[1.2719 - \left(\frac{h_g}{t}\right)^{0.1501}\right], \tag{2-6}$$

$$\varepsilon_c^{\text{crit}}(\%) = 40.4\left(\frac{t}{D}\right)^2\left(1-0.906f_p\right)^{-1}\left(\frac{E}{\sigma_y}\right)^{0.8}\left[1.12-\left(\frac{h_g}{t}\right)^{0.15}\right], \tag{2-7}$$

$$\varepsilon_c^{\text{crit}}(\%) = \left(\frac{8.995}{D/t}\right)^{1.724}\left(1-0.892f_p\right)^{-1}\left(\frac{E}{\sigma_y}\right)^{0.701}\left[1.087-\left(\frac{h_m}{t}\right)^{0.086}\right], \tag{2-8}$$

$$\varepsilon_c^{\text{crit}}(\%) = 106\left(\frac{t}{D}\right)^2\left(1-0.5f_p\right)^{-1}\left(\frac{E}{\sigma_y}\right)^{0.7}\left[1.10-\left(\frac{h_m}{t}\right)^{0.09}\right]. \tag{2-9}$$

In addition to the *D*/*t* ratio and pressure factor, the UOA models include pipe's yield strength and geometry imperfections as model parameters. For the pipes with girth welds, the geometry imperfections refer to the high-low misalignment (i.e., h_m) of the girth welds. For plain pipes, the geometry imperfections refer to a local outward bulge (i.e., h_g) on the pipe's outside surface [21] as shown in Figure 2-2. The bulge has a total width of *D*/2 (i.e., $L_b = D/2$) along the length of the pipe and covers 90° (i.e., $\alpha = 90°$) in the pipe's circumference.

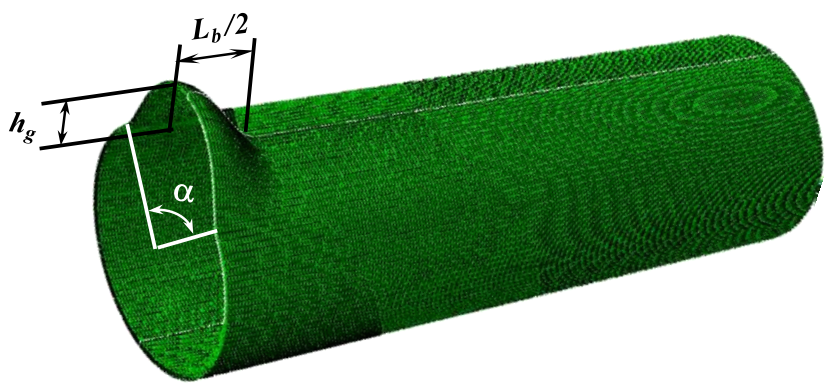

Figure 2-2 Representation of the geometry imperfections in plain pipes by UOA models

In most other models, the pipe's yield strength is used only to calculate the pressure effect, e.g., pressure factor. In the UOA models, in addition to calculating the pressure factor, the yield strength is used as an input parameter to capture the effect of material's properties on the CSC. Two different shapes of the pipe stress-strain curves (i.e., continuous/round vs. discontinuous yielding) are considered. For the stress-strain curves with discontinuous yielding, a Lüder's extension up to 0.5% strain is assumed [22].

The applicable range of the UOA equations depends on the FEA database used in the model development. The FEA database covers pipe grades from X52 to X80 (with yield strength from 359 MPa to 550 MPa). It should be noted that different Y/T ratios were used for different pipe grades. The Y/T ratios used in the FEA database ranges between 0.78 (for X52) and 0.87 (for X80) [22]. The pipe *D*/*t* ratio covers from 50 to 90. The height of the geometry imperfection (h_g) is between 2% and 30% of wall thickness. The girth weld high-low misalignment (h_m) is up to 1/8 in (3.0 mm). The maximum hoop stress induced by the internal pressure is 80% SMYS.

In the FEA for developing the UOA models, the plates (i.e., end caps) attached to the ends of the pipe to hold internal pressure during experimental tests were modeled. Therefore, with internal pressure, a net-section tensile force can be generated in the longitudinal direction (i.e., end cap effect). The net-section tensile force is known to be able to increase the CSC.

2.3.5 JFE Models

The JFE models [11] included two separate sets of CSC equations for pure axial compression (Eqs. 2-10 and 2-11) and pure bending (Eq. 2-12), respectively.

The equations for axial compression were originated from their work in 2002 [12] which were based on the analytical solution developed by Gerard in 1956 [23] for non-pressurized conditions. In their recent (2008) work [11], the equations in [12] were modified by calibrating those equations with FEA results to incorporate the effect of internal pressure and to improve the accuracy of the prediction by considering pipe geometry imperfections.

The CSC equations for axial compression [11] at zero-pressure are given below. The unit of the CSC for axial compression ($\varepsilon_{ac}^{\text{crit}}$) is in/in:

$$\varepsilon_{ac}^{\text{crit}}{}_{(f_p=0)} = (\varepsilon_{pc} + \frac{A\varepsilon_{pc}^{n}}{E} - 0.0005), \tag{2-10}$$

where,

$$\varepsilon_{pc} = \frac{4}{3}\sqrt{n}\left(\frac{t}{D}\right) - \frac{\sigma_y}{2E}(1+n),$$

and A and n are the constants in the fitted power function of the tensile stress-strain curves as shown in the following,

$$\sigma = A\varepsilon_p^n,$$

where ε_p is the plastic strain.

The CSC equations for axial compression at pressurized conditions are given as,

$$\varepsilon_{ac}^{\text{crit}} = m_1\varepsilon_c^{AC}{}_{(f_p=0)} - m_2 \tag{2-11}$$

The CSC equations for pure bending [11] are given as,

$$\varepsilon_c^{\text{crit}} = m_3\varepsilon_{ac}^{\text{crit}}, \tag{2-12}$$

The constants m_1, m_2, and m_3 in Eqs. (2-11) and (2-12) are given for three pressure factors of 0.50, 0.60, and 0.72 as shown in the following,

$$f_p = 0.50: m_1 = 1.4;\ m_2 = 0.2; m_3 = 2.02,$$
$$f_p = 0.60: m_1 = 1.6;\ m_2 = 0.3; m_3 = 2.07,$$
$$f_p = 0.72: m_1 = 2.0;\ m_2 = 0.5; m_3 = 2.10.$$

The factors (m_3) to convert the CSC of axial compression to pure bending were developed by FEA of pipes under pure bending and axial compression. From Eq. (2-12), it is seen that the CSC for pure bending is about twice of the CSC for pure axial compression.

The JFE equations recognize the pipe *D*/*t* ratios, pressure factor, yield strength, and strain hardening exponent. Although the pipe geometry imperfection is not explicitly included in the JFE equations, typical geometry imperfections observed in UOE pipes made by JFE [24, 25, 13] were built into the FEA models for calibrating the analytical solution of Gerard and developing the converting functions for incorporating the pressure effect and bending. The typical geometry

imperfection reported in [24, 25, 26, 13] is about 4% - 8% of the pipe's wall thickness. The FEA in the model development covered pipe *D*/*t* ratios from 46.9 to 66.3 and Y/T ratios from 0.79 to 0.90. The internal pressure was not applied to the pipe ends and no net-section longitudinal force due to the internal pressure was included.

2.3.6 C-FER Models

The C-FER models (2009) include two separate equations [15] as shown below. The unit of the CSC ($\varepsilon_c^{\text{crit}}$) is in/in:

$$\varepsilon_c^{\text{crit}} = \left[0.75\left(\frac{t}{D}\right) - 0.0075\right](1.2 - 0.005n)\left(1 - 0.85\frac{h_m}{t}\right) + 3000\left(\frac{p_i D}{2Et}\right)^2, \qquad (2\text{-}13)$$

$$\varepsilon_c^{\text{crit}} = \left[0.75\left(\frac{t}{D}\right) - 0.0075\right](1.2 - 0.005n)\left(1 - 0.85\frac{h_m}{t}\right)\left(\frac{p_y}{p_y - C\,p_i}\right), \qquad (2\text{-}14)$$

where

$$p_y = \sigma_y \frac{2t}{D},$$

and *C* in Eq. (14) equals to 0.868 and 0.892 for plain pipes with round stress-strain curves and girth-welded pipes with round stress-strain curves, respectively. The *n* is the strain hardening exponent of the tensile stress-strain curves which follow the equation,

$$\varepsilon = \frac{\sigma}{E} + \left(0.005 - \frac{\sigma_y}{E}\right)\left(\frac{\sigma}{\sigma_y}\right)^n.$$

The C-FER equations include pipe *D*/*t* ratio, girth weld high-low misalignment (h_m), strain hardening exponent (*n*), and internal pressure. The part of the Eqs. (2-13) and (2-14) which calculates the CSC for non-pressurized conditions is modified from the equation developed in [14]. The equation in [14] was developed from a series of FEA which covered *D*/*t* from 15 and 35, σ_y from 480 to 660 MPa, *n* from 17 to 50, and h_m from 0 to 1/8 in (0 to 3 mm). The yield strength (σ_y) was found to have no effect on the CSC and therefore was not included in the equation. An ovality of 0.6% was used in all the FEA models.

The two equations adopted different approaches to account for the pressure effect. Equation (2-13) uses the pressure term in the CSA models and Eq. (2-14) uses the pressure terms in the UOA models.

2.4 Comparison of Selected Models

The CSC calculated with some selected models is compared in Figure 2-3 to Figure 2-5 for different pressure factors (i.e., f_p = 0.0, 0.40, and 0.72). A safety factor of 1.0 was used for all the models. The UOA models for plain pipes with round stress-strain curves and the DNV models for plain pipes were used in the comparison.

For non- pressurized conditions, the CSA models only consider the pipe *D*/*t* ratio. Compared with the CSA models, the DNV and API models consider the pipe Y/T ratio and the pipe ovality (OV), respectively. In Figure 2-3 (a), three Y/T ratios (i.e., 0.77, 0.87, and 0.94) were used in the DNV calculations to show the range of the CSC for typical Y/T ratios. Similarly, three OV values (i.e., 0%, 1%, and 2%) were used in the API calculations to show the range of the CSC for

typical OV values. As shown in Figure 2-3 (a), the API and CSA models predict very similar results, while the DNV models give higher CSC than the CSA and API models.

The UOA models recognize the pipe yield strength (σ_y) and geometry imperfection (h_g). The CSC for typical yield strength values (52 - 85 ksi) and imperfection sizes (4%t - 12%t) is shown in Figure 2-3 (b) where Y/T = 0.87 and OV = 1% are used for the DNV and API models, respectively. As shown in Figure 2-3 (b), the UOA models for high yield strength (85 ksi) pipes give similar CSC with that by the DNV and CSA models for $D/t \leq 45$ and $D/t > 45$, respectively. While the UOA models for low yield strength (52 ksi) pipes give higher CSC than those by the DNV and CSA models.

From Figure 2-4 and Figure 2-5, it is seen that at medium to high internal pressure levels, the DNV models give significantly higher CSC than the CSA models. The CSC by the UOA models is, in general, between that by the CSA and DNV models. The API models are not applicable for the conditions with internal overpressure and are not shown in Figure 2-4 and Figure 2-5. Under pressurized conditions, the CSC given by the CSA models depends on the pipe yield strength. The CSA calculation indicates that increasing the yield strength increases the CSC as shown in Figure 2-4 (a) and Figure 2-5 (a). The trend is opposite to what is given by the UOA models as shown in Figure 2-4 (b) and Figure 2-5 (b).

In Figure 2-3 to Figure 2-5, the safety factors recommended by the codes and standards are not used. In Figure 2-6, the CSC calculated with selected codes with their recommended safety factors is compared. Without internal pressure, as shown in Figure 2-6 (a), after applying the recommended safety factors, the CSC by the API models and the CSC by the DNV models with the upper bound safety factor are very similar and are the most conservative. The CSC by the CSA models and the CSC by the DNV models with the lower bound safety factor are very similar and are less conservative. With internal pressure, as shown in Figure 2-6 (b), the CSC by the CSA models is much lower than the CSC by the DNV models.

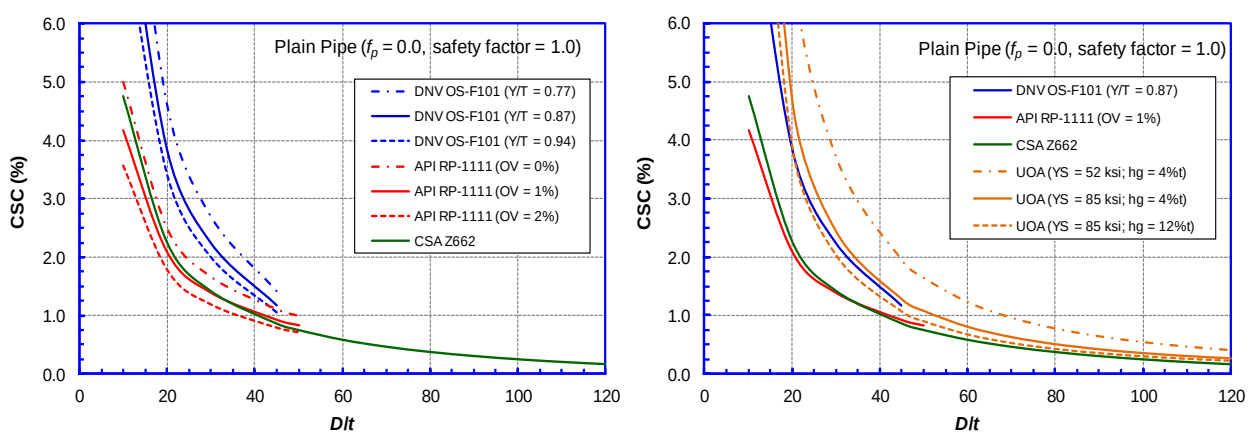

(a) Selected codes (b) Selected codes and UOA equations

Figure 2-3 Comparison of CSC calculated by selected models - no safety factors (f_p = 0.0)

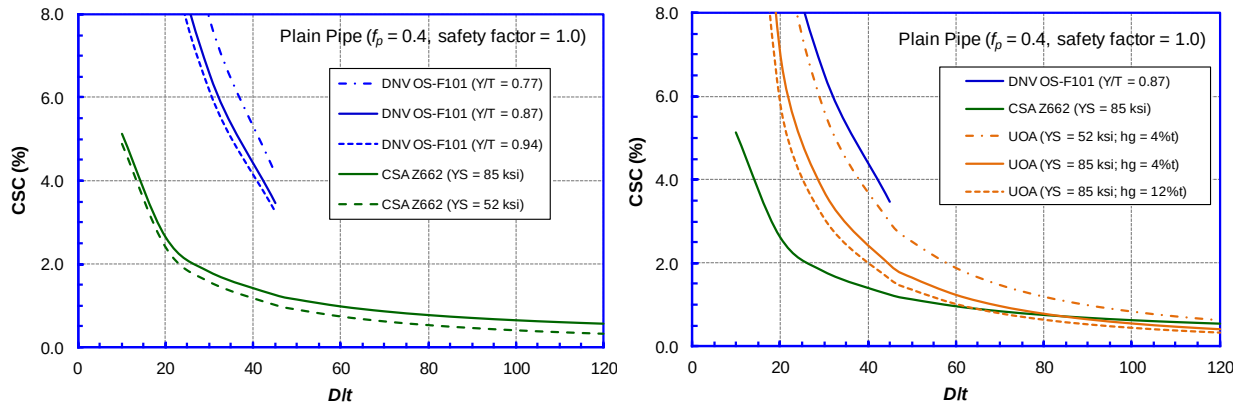

(a) Selected codes (b) Selected codes and UOA equations

Figure 2-4 Comparison of CSC calculated by selected models - no safety factors (f_p = 0.4)

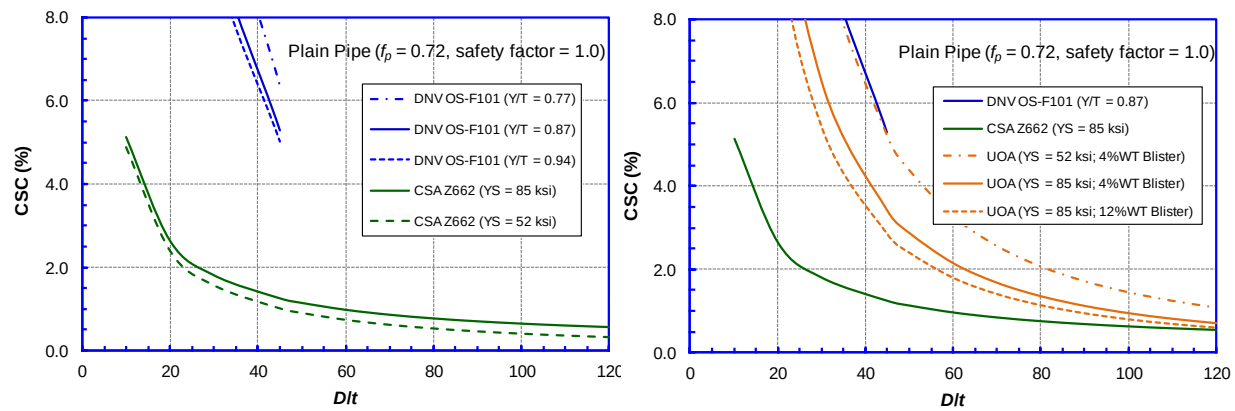

(a) Selected codes (b) Selected codes and UOA equations

Figure 2-5 Comparison of CSC calculated by selected models - no safety factors (f_p = 0.72)

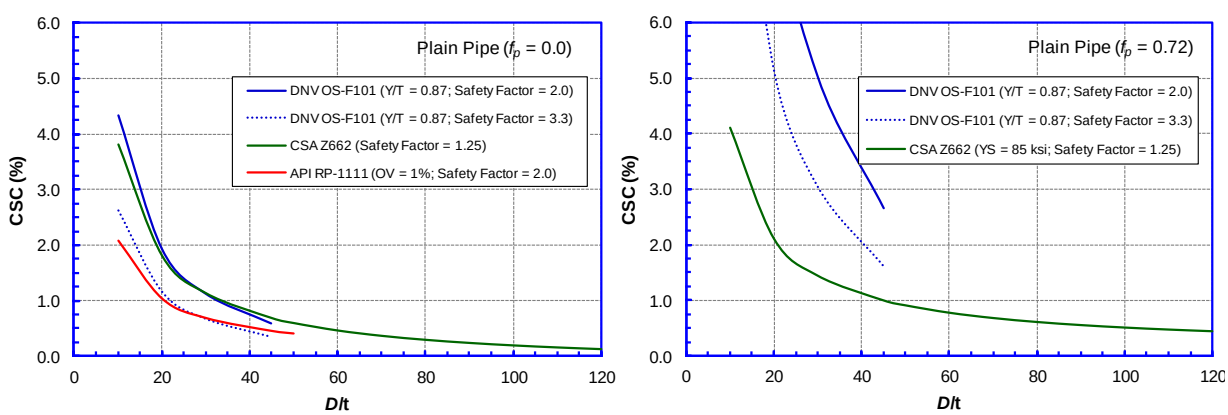

(a) without pressure (f_p = 0.0) (b) with high pressure (f_p = 0.72)

Figure 2-6 Comparison of CSC calculated by selected models - with safety factors

2.5 Limitations of Existing Models

The comprehensive review demonstrates that the existing CSC models have:

- large differences in input parameters and their applicable ranges;
- large differences in computed CSC, especially for pressurized conditions;
- large differences in recommended safety factors; and
- inconsistent trends on the conservatism of CSC.

For example, the CSC can be affected by many parameters to various degrees. However, the recognition of the influencing parameters by the existing models is quite different. The pipe *D*/*t* ratio and pressure are the only two parameters which are used by all models. The CSA models only explicitly recognize the *D*/*t* ratio and pressure. The UOA models explicitly consider four (4) input parameters: the *D*/*t* ratio, pressure, pipe's yield strength, and geometry imperfection (or weld high-low misalignment).

Features and characteristics of the CSC models are affected by their development processes. The observed differences in the CSC computed using different CSC models are partially due to the different processes used in developing those CSC models, including but not limited to:

- the bases of the model development, e.g., experimental data vs. numerical analysis;
- the representation of material properties;
- the representation of field conditions;
- the definition/measurement of the compressive strain and strain capacity;
- the construction of finite element models.

For example, the CSA models were developed by fitting the lower bound CSC measured in a set of experimental tests. The development of the DNV and UOA models involved extensive FEA. The loading conditions used to develop different models were often different too. In some models, pure bending without net-section force was used. In other models, net-section force in the longitudinal direction existed while bending was applied.

The definition of the compressive strain in different models is not always consistent. Since the strain along the pipe is not uniform, the average compressive strain over a specified gauge length in the pipe's longitudinal direction is often used. However, the selection of the gauge length (therefore, the reported/computed compressive strain) varied in different experiments and FEA.

In addition to the definition of the compressive strain, the definition of the compressive strain capacity (CSC) also varies. The CSC in the UOA models is defined as the compressive strain at the initiation of strain localization, while the CSC in the other models is generally defined as the compressive strain at the maximum load/moment.

Due to the differences in their modeling processes, those compressive models do not always represent the same conditions which partially contributes to the differences in the calculated CSC.

3 Processes for the Development of Compressive Strain Models

3.1 Overview

As discussed in Section 2.5, the differences of the existing CSC models are partially caused by the different modeling processes used in their development. In this section, systematic studies were conducted to evaluate the relative importance of various factors in fields. Consistent processes which can give close representations of field conditions were established. The following factors were studied:

- representation of material properties;
  - basics of stress-strain curves: tensile and compressive stress-strain curves;
  - anisotropic properties: longitudinal vs. circumferential, tensile vs. compressive stress-strain curves;
  - mathematical representation of pipe stress-strain curves;
- representation of field conditions;
  - loading and constraints: bending, axial force/constraint, and soil load;
  - loading sequences;
  - length of pipes being modeled or tested;
- definition/measurement of the compressive strain and strain capacity;
  - gauge length by which the compressive strain capacity is computed;
- construction of the finite element models.
  - shell vs. solid elements;
  - requirement on model refinement;
- influencing parameters;
  - D/t ratio and internal pressure;
  - geometry imperfection;
  - pipe yield strength and Y/T ratio;
  - pipe uniform strain;
  - pipe Lüder's strain;
  - girth weld (i.e., weld profile, strength mismatch, residual stress, and high-low misalignment); and
  - net-section force.

The key components for the development of the CSC models are summarized in Figure 3-1.

3.2 Representation of Material Properties

3.2.1 Introduction of Stress-Strain Curves

Two types of stress-strain curves (SSC) are often used in engineering stress analyses, i.e., true and engineering SSC. From uni-axial tensile/compressive tests, the engineering stress vs. strain curves are often generated. The engineering stress is the ratio between the load and the

original (i.e., before deformation) cross-section area of the specimen. The engineering strain is the ratio between the elongation and the original length of the specimen. The common material parameters such as the yield strength, tensile strength, uniform strain, Y/T ratio, are measured from the engineering SSC.

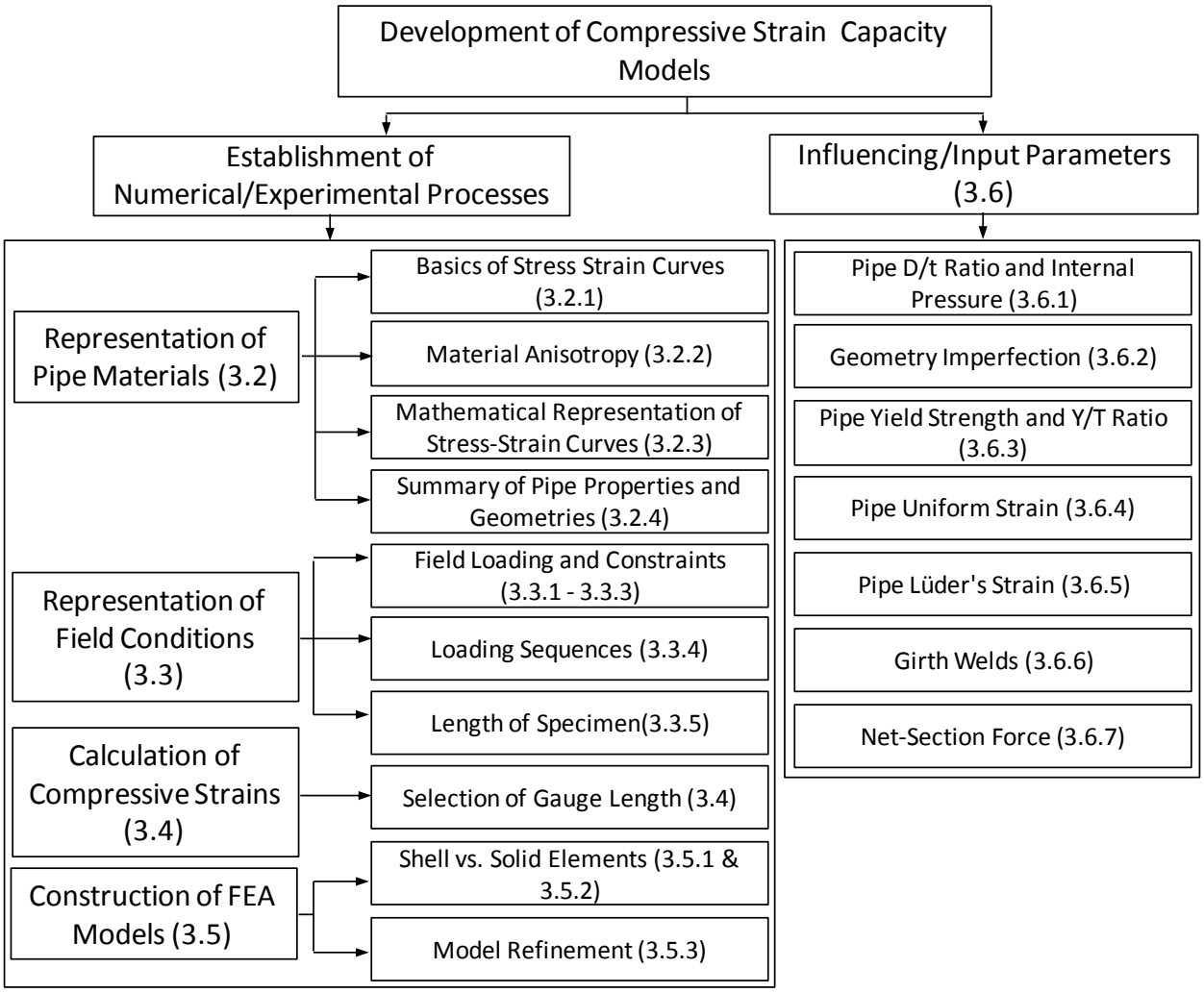

Figure 3-1 Key components for the development of the CSC models

During a tensile test, as the specimen is elongated, its cross section area tends to reduce due to the Poisson's effect. As a result, the engineering stress can underestimate the actual stress in the specimen. The true stress is defined as the ratio between the load and the actual cross-section area of the specimen at the moment the load is applied. On the other hand, the engineering strain tends to overestimate the actual strain. Therefore, the true strain is developed to take account of the increase of the length of the specimen. The true stress - true strain relationship can represent the true behavior of the materials. The true and engineering stress/strain can be correlated using the following equations:

$$\varepsilon_{true} = \ln\left(1.0 + \varepsilon_{eng}\right) \tag{3-1}$$

$$\sigma_{true} = \sigma_{eng}\left(1.0 + \varepsilon_{eng}\right) \tag{3-2}$$

where σ_{eng} and ε_{eng} are engineering stress and strain, respectively; and σ_{true} and ε_{true} are true stress and true strain, respectively. Under tension, the stress and strain are both positive. Under compression, the stress and strain are both negative.

In a compressive test, as the specimen is compressed, its cross section area tends to expand due to the Poisson's effect. Therefore, opposite to the tensile tests, the engineering stress (the absolute value) in the compressive tests is higher than the true stress and the engineering strain (the absolute value) is smaller than the true strain.

As a result, the tensile and compressive engineering stress - strain curves appear differently even if the material behaves the same under tension and compression (i.e., the same true stress - strain relationship) as shown in Figure 3-2. The compressive and tensile engineering stress - strain curves in Figure 3-2 are derived from the same true stress - strain curve. It should be noted that under compression, the stress and strain should be negative and in the figure, the absolute values of the stress and strain are plotted. The compressive stress - strain curve shows seemingly much higher strain hardening capacity than the tensile stress - strain curve. But, the difference between the tensile and compressive engineering stress - strain curves in Figure 3-2 is due to the mathematical representation of the stress and strain and is not due to different material behaviors.

3.2.2 Pipe Property Anisotropy

On the other hand, the actual (or physical) behaviors of a linepipe steel (i.e., the true stress - true strain curves) can be different under tension and compression. In addition, the linepipe steels often show different properties (strength and strain hardening capacity) in the longitudinal and circumferential (hoop) directions, i.e., material anisotropy. For example, for UOE pipes, the hoop properties often show higher tensile strengths and Y/T ratios (i.e., smaller strain hardening capacities) than the longitudinal properties. The pipes made from other manufacturing processes may show different characteristics of material anisotropy.

The findings on the effect of the material's anisotropy on the CSC are mixed. For UOE pipes, the low strain hardening capacity in the hoop direction alone was found detrimental to the CSC [27, 28, 29] and the elevated tensile strength in the hoop direction alone was found beneficial to the CSC [30]. Finite element analyses using the actual anisotropic properties measured in a UOE pipe (with both anisotropic tensile strengths and strain hardening capacities) showed that the CSC was reduced by the material's anisotropy [31]. Therefore, the anisotropic strain hardening capacities tend to play a more dominant role on the CSC than the anisotropic strengths.

The effect of the material anisotropy (i.e., tensile vs. compressive properties and longitudinal vs. hoop properties) on the CSC was investigated with FEA (see details in Section B.7). The results indicate that the CSC is mainly determined by the longitudinal compressive stress-strain curve (SSC) of the material. The difference between the tensile SSC of the longitudinal and hoop directions plays a secondary role. Therefore, the compressive SSC of the longitudinal direction is recommended for buckling analyses and the isotropic material's models could be adequate.

However, the direct use of the compressive engineering SSC in CSC models often has some challenges. Firstly, the compressive SSC is often hard to obtain because of the complications of the uni-axial compression tests, especially to large strains. Secondly, due to the compression

and the expansion of the cross-section area, the necking seen in the tensile tests may not take place. As a result, the key material parameters widely used in the tensile SSC such as the tensile strength, Y/T ratio, and uniform strain could be difficult to obtain. Therefore, in the following analyses, the engineering SSC are presented in the tensile format.

It should be noted that the use of the tensile format does not mean only the engineering SSC from the tensile tests should be used. In fact, the engineering SSC from the compressive tests are still preferred for the study of the CSC. However, to obtain the material parameters such as the yield and tensile strength and Y/T ratio, the compressive engineering SSC need to be converted to equivalent tensile engineering SSC through the engineering-true stress and strain relationships (i.e., Eqs. 3-1 and 3-2).

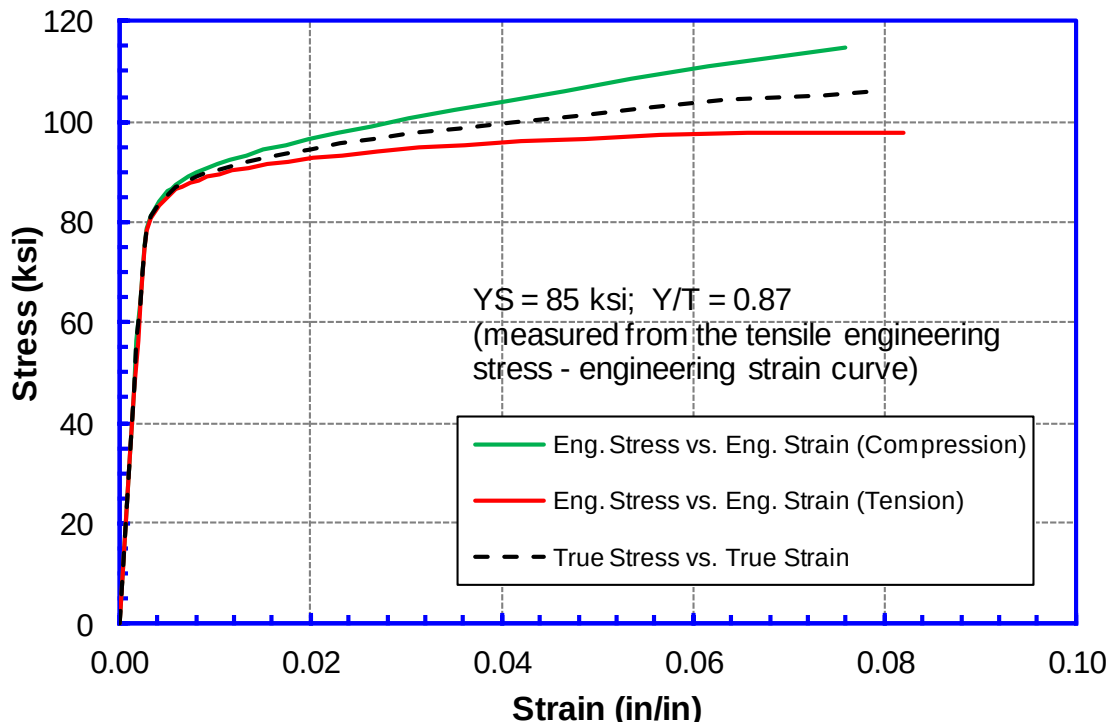

Figure 3-2 Comparison of true and engineering stress-strain curves

3.2.3 Mathematical Representation of Stress-Strain Curves

The CSC is known to depend on the actual shape of the pipe stress-strain curves. However, it is more practical to use the key material parameters (e.g., the yield strength, tensile strength and uniform strain etc.) as the input to the CSC models than to use the full stress-strain curves.

Nevertheless, the full stress-strain curves were actually used in the FEA for developing the compressive strain models. Those stress-strain curves could be obtained from experimental tests or created by some mathematical equations. Because of the difference in constructing the full stress-strain curves, the same material parameters (e.g., the yield strength, Y/T ratio, or strain hardening exponent) used by those different models may actually represent different stress-strain curves. The difference in the stress-strain curves may induce differences in the calculated CSC and contribute partially to the large difference of the CSC given by the different CSC models. Therefore, reliable procedures for constructing full stress-strain curves are needed.

The mathematical equations developed under a DOT and PRCI co-sponsored project [4,5,32, 33,34] were used to construct the full (tensile) stress-strain curve using two material parameters, i.e., the YS and Y/T ratios. The mathematical equations were based on the CSA Z662 equation and can (1) uniquely determine a full (tensile) engineering stress - engineering strain curve using the YS and Y/T ratio, and (2) statistically give a reasonable representation of the tensile stress-strain curves of actual pipe materials. The details of the mathematical equations can be found in Appendix A.

3.2.4 Pipe Properties and Geometries Used in the Analyses

3.2.4.1 Pipe properties

A large range of material properties (i.e., strength and strain hardening capacity) were used in this project to investigate the relationship between the pipe properties and the CSC. The key tensile properties of the longitudinal direction (i.e., yield strength, tensile strength, uniform strain, and Y/T ratio) are given in Table 3-1. The yield strength (YS) ranges from 69 to 115 ksi; the Y/T ratio ranges from 0.76 to 0.96; and the uniform strain (uEL) ranges from 0.04 to 0.13 in/in. The given YS corresponds to 4 ksi plus the mean of the minimum and maximum YS specified in API 5L for pipe grades X52 to X100. The given tensile strength (UTS) is varied to give the specified Y/T ratios.

The full stress-strain curves constructed for the material parameters in Table 3-1 are shown in Figure 3-3. All stress-strain curves are of round-house shape with continuous yielding behavior without obvious yield point. The key material parameters (in Table 3-1) and stress-strain curves (in Figure 3-3) represent the material's tensile properties (or the equivalent tensile properties converted from the compressive properties) of the longitudinal direction.

As discussed in Section 3.2.2, although the engineering stress - strain curves are constructed in their tensile format with the equations in Appendix A, the engineering stress - strain curves from the uni-axial compression tests are still preferred for assessing the CSC. The compressive engineering stress - strain curve needs to be converted to its equivalent tensile engineering stress - strain curve. The key material parameters (e.g., YS, UTS, uEL, and Y/T) should be obtained from the equivalent tensile engineering stress - strain curves.

In addition to the stress-strain curves given in Figure 3-3, the longitudinal tensile stress-strain stress curve of an actual X100 pipe was also used in some of the FEA. The stress-strain curve of the X100 pipe is shown in Figure 3-4.

The effect of the shape of the full stress-strain curve, i.e., the stress-strain curves with very low uniform strains or various Lüder's extensions, on the CSC was also investigated (Sections 3.6.4 and 3.6.5). In addition, full stress-strain curves of girth welds (Section 3.6.6) were also constructed to study the effect of weld strength mismatch on the CSC. The stress-strain curves adopted in those studies are given in those related sections.

3.2.4.2 Pipe Geometries

A range of pipe geometries, i.e., outside diameter (D), wall thickness (t), and pipe length (L), were used in this project to investigate the relationship between the pipe size and the CSC (as shown in Table 3-2). It is well known that the CSC is affected by the pipe D/t ratio and not the

absolute pipe outside diameter (OD) and wall thickness. The *D*/*t* ratio used in this study ranges from 20 to 104. The OD ranges from 10 to 48 inch (254.0 to 609.6 mm) and the wall thickness ranges from 0.25 to 0.50 in (6.35 to 12.7 mm). The full length of the pipe specimen is 6 times of OD. In Section 3.4, the effect of the length of the pipe specimen on the CSC was studied and the full length of the pipe was varied from 2 to 20.

Table 3-1 Key material parameters (longitudinal tension) used in analyses

Material Properties					
YS		UTS		uEL	Y/T
(ksi)	(MPa)	(ksi)	(MPa)	(in/in)	
69	473	90	624	0.127	0.76
75	517	92	633	0.103	0.82
85	587	98	679	0.082	0.87
95	658	105	725	0.065	0.91
115	793	120	827	0.041	0.96

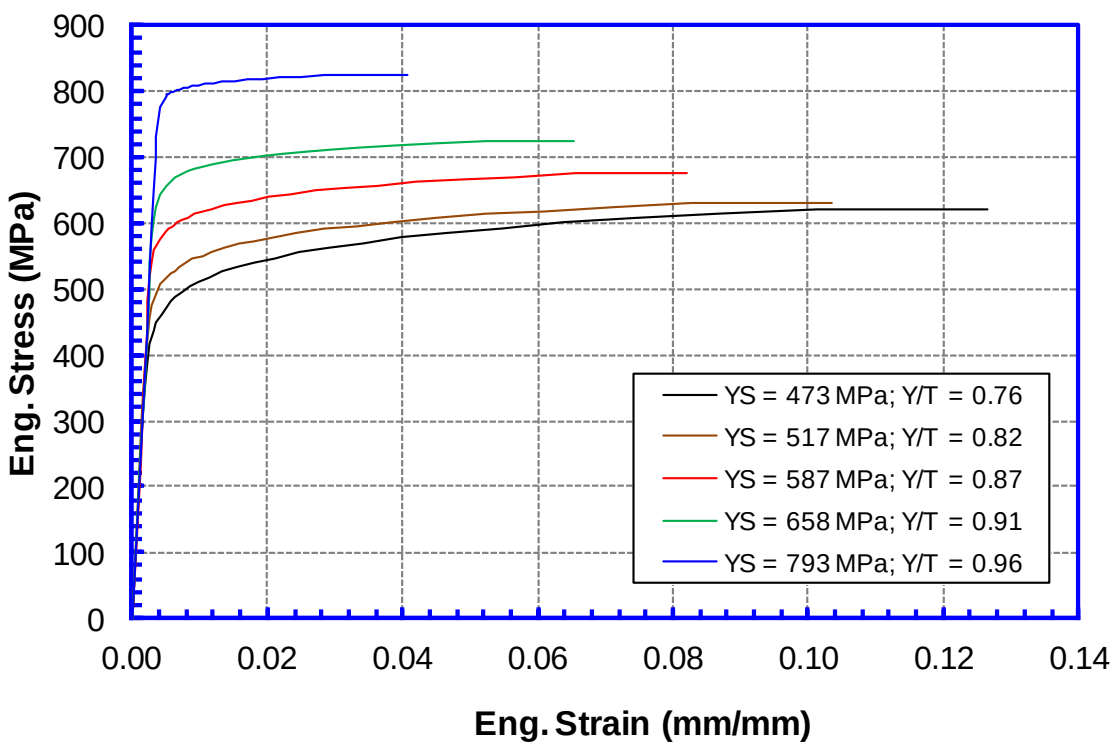

Figure 3-3 Stress-strain curves (longitudinal tension) used in analyses

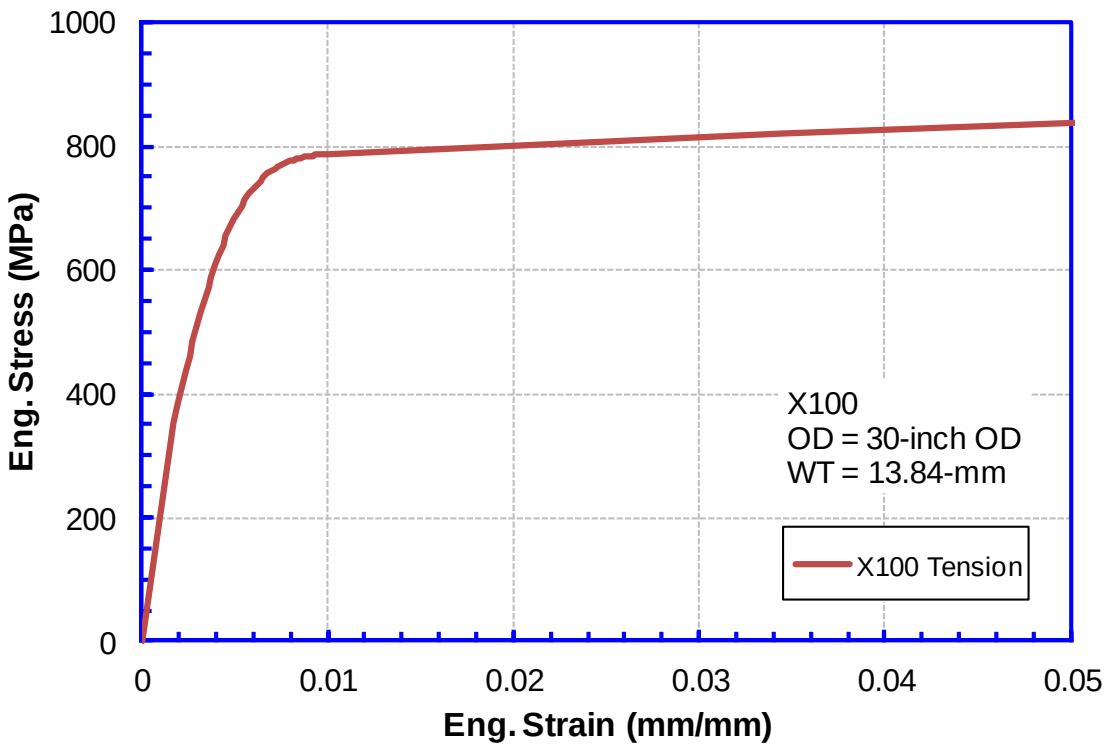

Figure 3-4 Stress-strain curves (longitudinal tension) of an X100 pipe

Table 3-2 Key pipe geometry parameters

Pipe Geometry							
OD (D)		Wall Thickness (t)		Total Length (L)		L/D	D/t
(inch)	(mm)	(inch)	(mm)	(inch)	(mm)		
10	254.0	0.500	12.70	60	1524.0	6	20
11	279.4	0.250	6.35	66	1676.4	6	44
16	406.4	0.250	6.35	96	2438.4	6	64
30	762.0	0.375	9.53	180	4572.0	6	80
48	1219.2	0.461	11.70	288	7315.2	6	104
24	609.6	0.500	12.70	144	3657.6	6	48

3.3 Representation of Field Conditions

3.3.1 Introduction of Field and Testing/Numerical Modeling Conditions

In typical field conditions, pipelines are buried under ground. Ground movements, such as frost heave, thaw settlement, and mining subsidence (e.g., Figure 3-5), can induce longitudinal strains to the pipeline. The longitudinal strains are typically generated by the bending moment and longitudinal/axial force applied through pipe-soil interactions in the form of distributed loads. The pipeline segment exposed to the ground movement is connected to the rest of the pipeline

which can provide additional constraint to the pipeline segment. The pipeline may also experience longitudinal strains/stresses from the operating pressure and temperature change.

The representative loading conditions of a buried pipeline segment experiencing ground movement hazards are shown in Figure 3-6. The distributed load along the length of the pipe represents the load from pipe-soil interactions. The force and moment at the ends of the pipe segment represent the constraint (or reaction force and moment) provided by the connected pipelines.

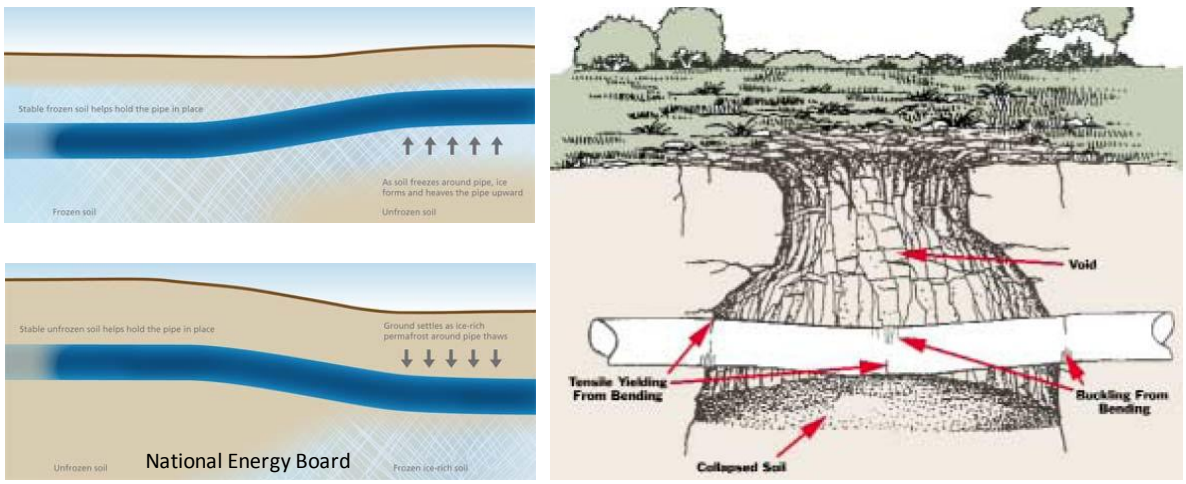

(a) frost heave and thaw settlement (b) mining subsidence

Figure 3-5 Example ground movement and pipeline deformation

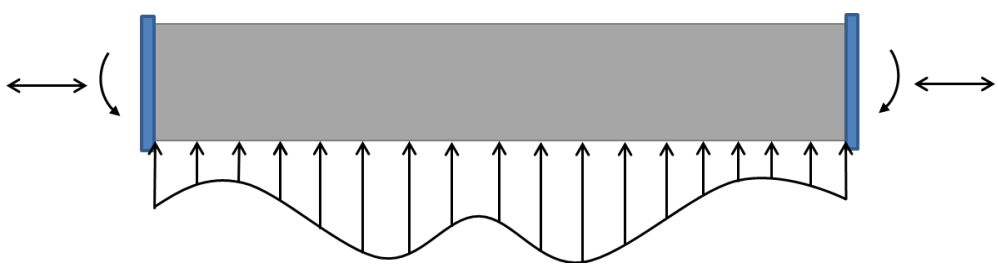

Figure 3-6 Representative loading conditions of buried pipeline segment experiencing ground movement hazards

To obtain compressive strain capacity (CSC), experimental testing is often used. There are many variations in testing setups. A schematic drawing of a typical experimental setup is shown in Figure 3-7. Depending on the relative magnitude of the externally applied forces *P* and *F*, the pipe specimen may be exposed to pure bending moment, combined bending moment and tension, and combined bending moment and compression. It should be noted that if the test is done with internal pressure, an additional tensile force is applied to the pipe specimen in the longitudinal direction due to the internal pressure applied to the end plates (i.e., the end cap effect). The end caps are referred to the steel plates welded onto the ends of the pipe specimen to hold internal pressure and transfer load and moment. For example, if the internal pressure is applied and $P = F$, the pipe specimen is exposed to combined bending moment and longitudinal tension instead of pure bending moment. It is well accepted that the longitudinal tensile force can increase the

CSC, while the longitudinal compressive force can reduce the CSC. Therefore, to properly use the experimentally measured CSC in pipeline design, it is critical to understand the loading conditions associated with the measured CSC.

Compared with the representative loading conditions for a buried pipeline segment (as shown in Figure 3-6), the distributed loads from the pipe-soil interactions are not included in the typical testing setup (Figure 3-7). To the authors' knowledge, experiments for studying the effect of the pipe-soil interactions on the behavior of a pipe under compressive strains are being planned in some future tests.

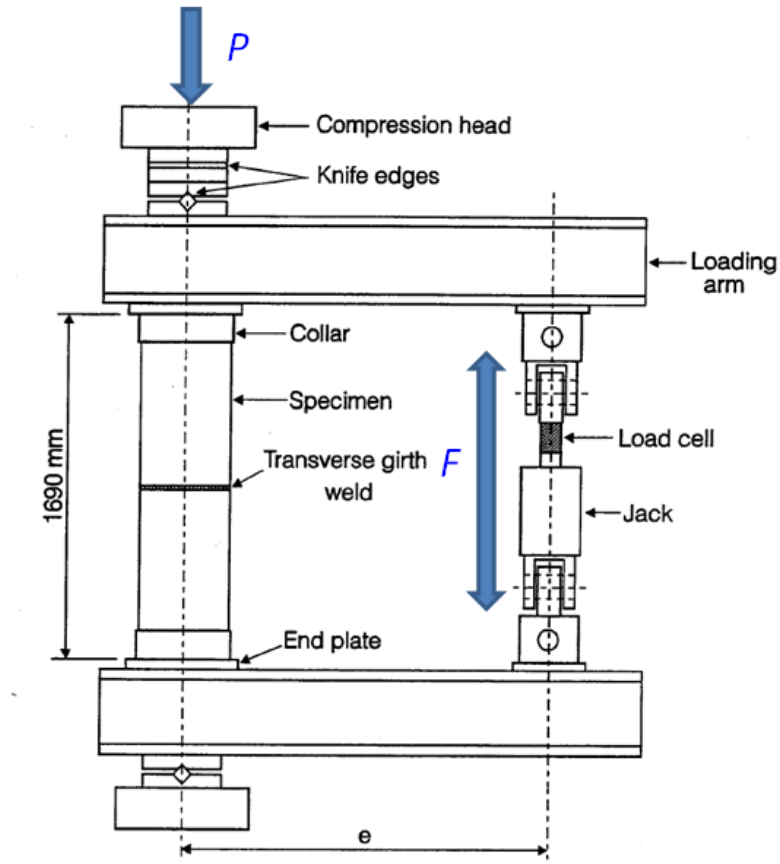

Figure 3-7 Representative testing setup of CSC measurement [19]

Finite element analyses (FEA) are also widely used for calculating the CSC. Similar to the experimental tests, the distributed loads due to pipe-soil interactions are typically not modeled in the FEA. Bending moment and external (longitudinal) force are applied at the ends of the pipe segment.

The longitudinal tensile force induced by the internal pressure (i.e., the end cap force) is handled differently in different FEA. The end cap force was applied in some FEA such as those for the development of the DNV and UOA models. The end cap force was not modeled in some other FEA such as those for the development of the JFE models. If the end cap force is modeled, with internal pressure (especially high pressure), the calculated CSC is higher than the CSC from the FEA without the end cap force.

3.3.2 Modeling of Field Loading and Constraints

3.3.2.1 Bending, Axial Force/Constraint, and Soil Load

As discussed in Section 3.1, the buried pipeline segments exposed to ground movements can experience very complicated loadings, i.e., the distributed load due to pipe-soil interactions, the end moment/load due to the constraint from the rest of the pipeline, and the longitudinal load due to operating pressure and thermal loadings.

Five representative loading conditions were investigated as shown in Figure 3-8, i.e., ER-NLF_P, ER-NLF_0, ER-LD_0, SP-LD_0, and SP-NLF_P. The meaning of the symbols is summarized in the following:

- ER (End Rotation): the bending is applied by enforcing rotation angles at the ends of the pipe.
- SP (Soil Pressure): the bending is applied by applying distributed pressure along the length of the pipe to simulate the pipe-soil interaction.
- NLF (Net Longitudinal Force):
  - NLF_0: the net longitudinal force is zero.
  - NLF_P: the net longitudinal force is generated by the internal pressure to the end cap.
- LD (Longitudinal Displacement):
  - LD_0 - the longitudinal displacements at the two ends of the pipeline segment is fixed to zero which represent the longitudinal constraints to the pipeline segment during bending.

The ER series are used to simulate the typical experimental conditions and the SP series are used to simulate the pipe-soil interactions for buried pipelines.

ER-NLF_P, ER-NLF_0, and ER-LD_0 represent typical conditions in experimental testing where the bending is induced by rotation at the ends of the pipe. Under ER-NLF_P, a net-section tensile force is generated to the pipe by the internal pressure (i.e., the end cap effect) and the resulting longitudinal stress is half of the hoop stress generated by the internal pressure. It is known that this net-section tensile force can increase the CSC. To minimize the effect of the net-section tensile force, in some experimental tests, an external compressive force is applied to the ends of the pipe specimen to counterbalance the pressure induced tensile force. As the result, the net-section longitudinal force is zero as shown in ER-NLF_0. ER-LD_0 represents the constraints from the pipeline. The longitudinal displacements at the ends of the pipe specimen are kept to be zero which represents a very strong constraint.

SP-LD_0 and SP-NLF_P represent the distributed soil loads from the pipe-soil interactions. Uniform pressure representing the soil loads is applied to one side of the pipe to generate the bending deformation. In SP-LD_0, the longitudinal displacements at both ends of the pipe are kept to be zero which represents a strong constraint from the pipeline. In SP-NLF_P, the end of the pipe is free to move in the longitudinal direction and a net-section tensile force is generated to the pipe by the internal pressure.

3.3.2.2 End Conditions

In most FEA conducted in this project, the ends of the pipe specimens were modeled as rigid planes to simulate the effect of the thick plates welded to the ends of the pipe specimen (to hold internal pressure and transfer load) in the experiments. Simulations with deformable pipe ends were also conducted for comparisons where the cross section of the pipe end can deform. Under typical field conditions, the ends of the pipeline segment experiencing ground movement are often deformable.

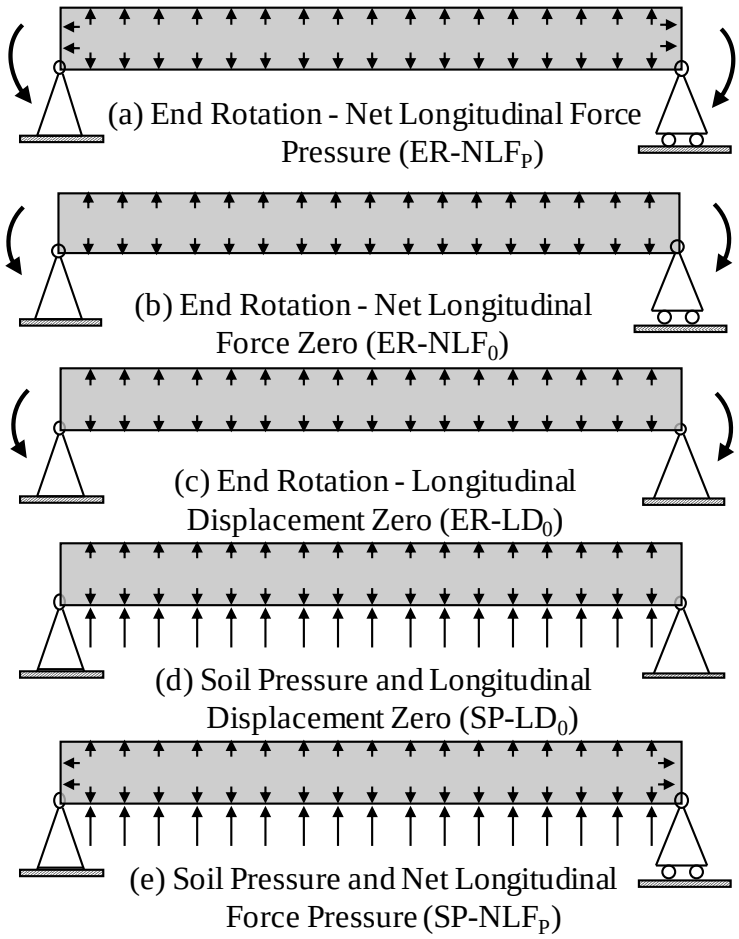

Figure 3-8 Representative loading conditions

3.3.3 Effect of Modeling Conditions on CSC

3.3.3.1 Moment and Strain Distributions

The distribution of the calculated bending moment along the length of the pipe is shown in Figure 3-9. The bending moment is normalized by the moment at the symmetry plane (i.e., the center along the length of the pipe). The plot was obtained at the time when the moment at the symmetry plane reaches the maximum. The results show that the moment is not uniform along the length of the pipe for all cases except for ER-NLF$_P$. The moment is close to uniform along the length of the pipe for ER-NLF$_P$. For ER-NLF$_0$, SP-LD$_0$, and SP-NLF$_P$, the moment decreases from the center of the pipe to the end of the pipe.

For ER-LD_0, the bending moment increases from the center of the pipe to the end of the pipe. The maximum moment is at the pipe ends. Therefore, when the moment at the symmetry plane reaches the maximum moment, the moment at the end may not reach the maximum value.

Due to the non-uniform bending moment along the length of the pipe, the compressive strain may also vary along the length of the pipe (as shown in Figure 3-10). In Figure 3-10, the strains were calculated at the compressive side of the pipe on both OD and ID surfaces at the maximum bending moment. At the maximum moment, a small wrinkle was formed at the symmetry plane. The half length of the wrinkle is slightly more than one (1) OD and the strain inside the wrinkle shows a wave-like variation. For ER-NLF_p, the strains outside the wrinkle are uniform along the length of the pipe because of its uniform bending moment. For ER-NLF_0, the strains outside the wrinkle decrease gradually towards the pipe end which is consistent with the moment distribution.

3.3.3.2 Extent of End Effects

The effect of the rigid and deformable ends on the strain distribution is also shown in Figure 3-10. For the deformable end, the strains near the pipe end are uniform. However, for the rigid end condition, a wrinkle also forms near the end indicated by the wave-like strain variations near the pipe end. The length of the wrinkle near the pipe end is about one (1) OD.

3.3.3.3 Tensile vs. Compressive Strains

Different longitudinal loads and constraints also lead to different components of bending and membrane strains. The relationship between the tensile and compressive strains calculated at the symmetry plane is shown in Figure 3-11. All strains were calculated as the average strains of a 2*D* gauge length. The tensile strain was calculated at the tensile side (top) of the pipe and the compressive strain was calculated at the compressive side (bottom) of the pipe.

The magnitudes of the compressive and tensile strains are almost the same for NLF_P and LD_0. The results are consistent with the experimental results reported in [35] where the test condition is close to NLF_p. For LD_0, as the bending deformation increases, the pipe is elongated due to the displacement constraints at the ends of the pipe. As a result, a net-section tensile force can be developed.

For NLF_0, the magnitude of the compressive strain is much higher than that of the tensile strain. The difference can be more than a factor of three. The similar difference between the tensile and compressive strains has been reported in experiments in [19].

For the condition ER-LD_0, the wrinkle tends to form near the two ends of the pipe where the highest bending moment is reached. This condition ER-LD_0 was not used in the further studies of the CSC since a 2*D* gauge length cannot be properly defined for calculating the CSC.

3.3.3.4 Loading Conditions vs. CSC

The effect of the different loading conditions on the calculated CSC is shown in Figure 3-12. The CSC of ER-NLF$_p$ and ER-NLF$_0$ clearly demonstrates that the net longitudinal tensile force generated by the internal pressure can increase the CSC. The CSC from SP-LD$_0$ and SP-NLF$_p$ is almost identical due to the similar bending and membrane strain components generated by the LD$_0$ and NLF$_p$ conditions. It is found that the distributed load from the pipe-soil interaction reduces the CSC. The higher the soil load, the higher the reduction on the CSC. The increase of the CSC due to the net longitudinal force generated by the internal pressure or longitudinal displacement constraints can be offset if the soil load is sufficiently high.

Although under certain circumstances, a net-section tensile force may exist in the pipeline, the distributed soil load may reduce the beneficial effect of the net-section force on the CSC. The ER-NLF$_0$ can provide reasonably conservative CSC. Therefore, the ER-NLF$_0$ is selected for model development. But, it should be noted that the ER-NLF$_0$ may not give conservative CSC if the net-section longitudinal force is in compression.

Because of the non-uniform distributions of the moment and strain caused by the loading condition, to properly determine the maximum moment and CSC, the bending moment and CSC should be always calculated at the location where the wrinkle forms.

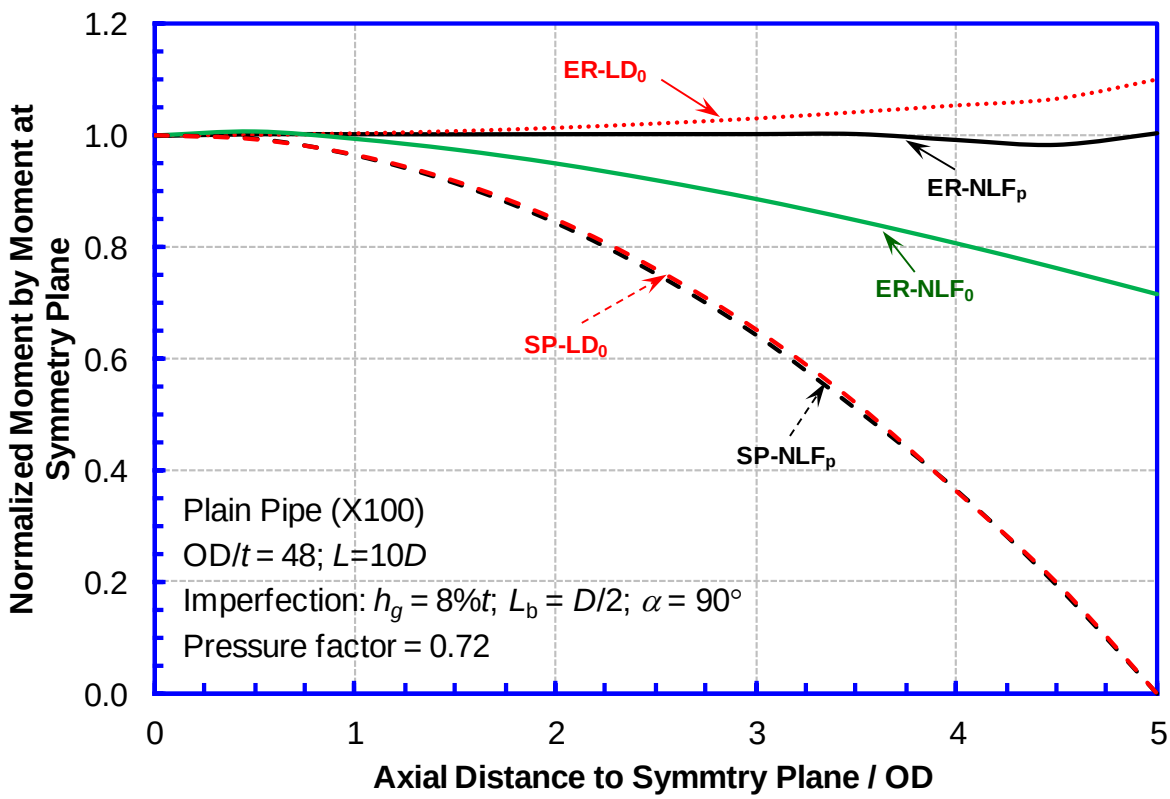

Figure 3-9 Bending moment along the length of pipe - effect of loading conditions

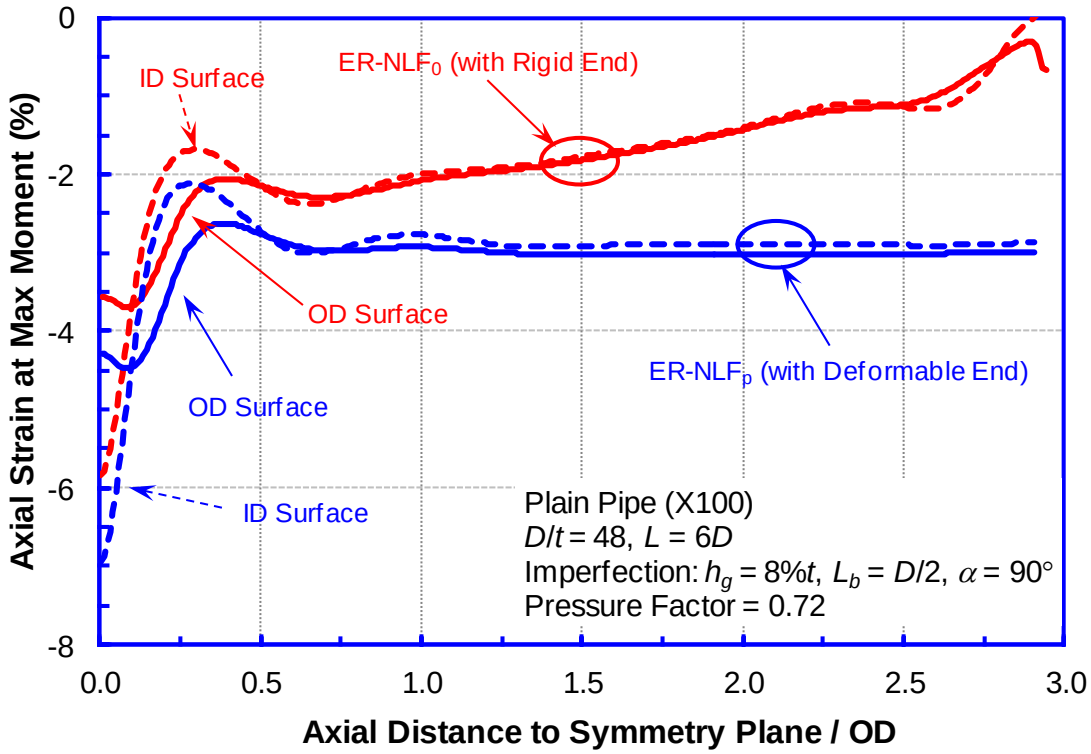

Figure 3-10 Effect of loading conditions on strain distributions at maximum moment

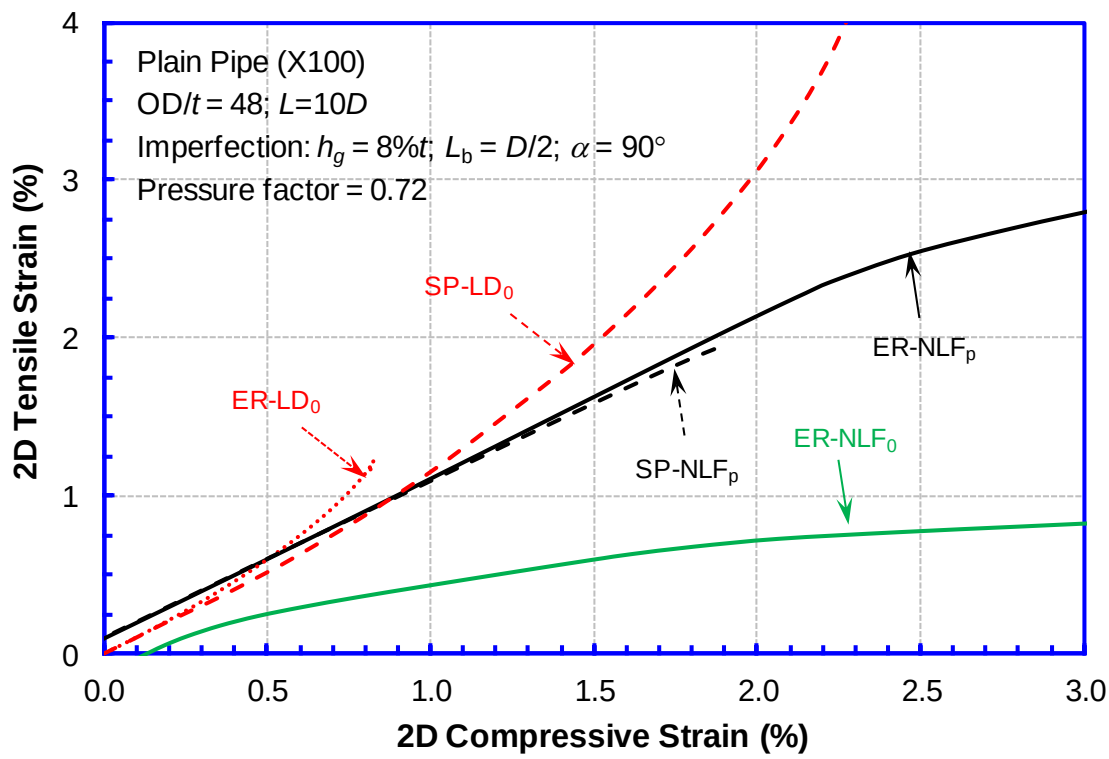

Figure 3-11 Tensile vs. compressive strains - effect of longitudinal loads and constraints

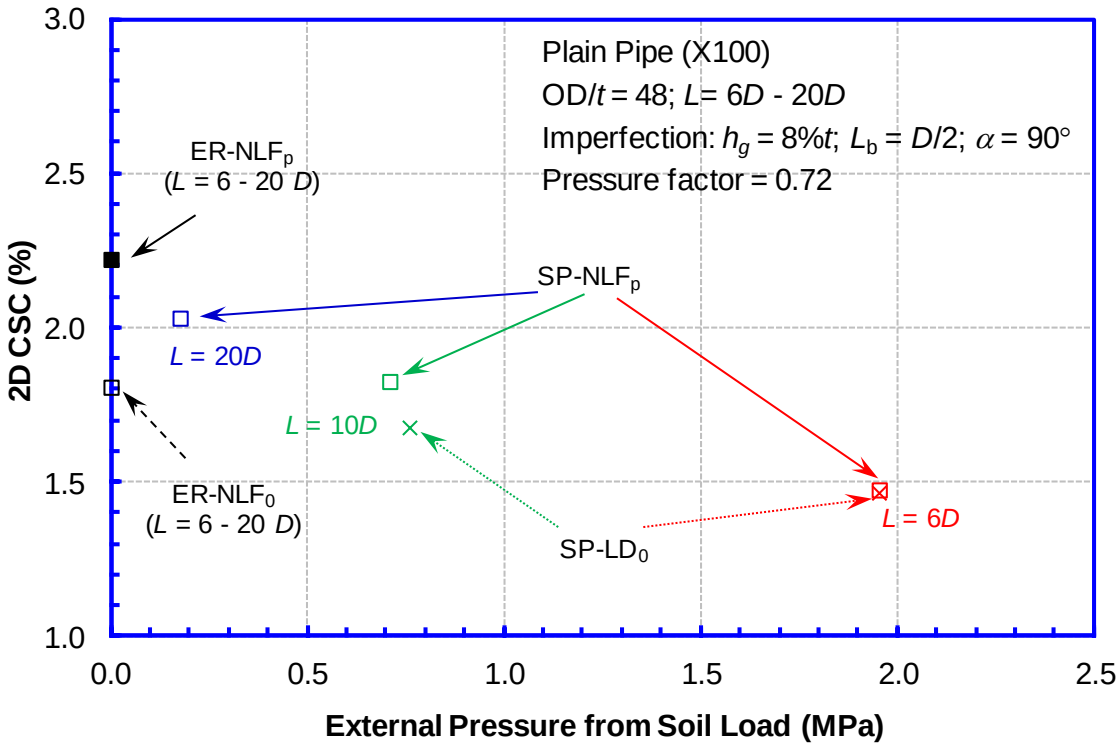

Figure 3-12 CSC vs. loading conditions

3.3.4 Modeling of Loading Sequences

The sequence of the loading experienced by a pipeline under ground movement is also very complicated. The ground movement (i.e., bending and longitudinal loading) may take place in operations or system shut downs (i.e., different pressure levels). The operating pressure may change or the system may need a shut down for maintenance before or after the ground movement. In experiments and numerical models, two loading sequences are widely used: (1) bending without internal pressure (for the ground movement during system shut downs) and (2) bending with pre-applied constant internal pressure (for the ground movement in operations).

Whether or not the two loading sequences used in the experiments and numerical models can represent the various loading sequences experienced by a pipeline in the field needs to be studied. For example, if a pipeline experienced and survived a ground movement event during operations (with internal pressure), will the pipeline survive a system shut down after the ground movement without load mitigations.

The following four loading sequences were studied, where the loading condition, ER-NLF$_P$, was used in all the analyses:

(1) Apply bending without internal pressure until wrinkle forms;

(2) Apply internal pressure (72% YS) → hold internal pressure constant and apply bending until wrinkle forms;

(3) Apply bending without pressure to a strain close to the CSC → hold the applied strain constant and apply internal pressure (72% YS) → continue bending with internal pressure until wrinkle forms;

(4) Apply internal pressure (72% YS) → hold the internal pressure constant and apply bending to different strains → hold the applied strain constant and reduce the internal pressure to zero → continue bending without pressure until wrinkle forms.

The moment - compressive strain relationships for loading sequences (1), (2), and (3) are shown in Figure 3-13. As shown in results for loading sequences (1) and (2), the existence of the internal pressure increases the CSC, but reduces the maximum bending moment. The result of loading sequence (3) shows that increasing the pressure with holding the bending strain reduces the bending moment. The moment eventually decreases to the value similar to that in loading sequence (2). When additional bending deformation is applied after the pressure is applied, the moment-compressive strain relationship follows that of loading sequence (2).

The results of loading sequence (4) are shown in Figure 3-14. For loading sequence (4a), the internal pressure was applied first and the pipe was then bent with the internal pressure to a compressive strain which is very close to the CSC of the pipe with no internal pressure. The internal pressure was then reduced to zero with holding the compressive strain and after which the additional bending was applied. The result shows that when the internal pressure decreases to zero, the bending moment slightly decreases. When the additional bending is applied, the bending moment quickly increases to the maximum which is similar to that of the pipe without internal pressure. The CSC is slightly increased compared with that of loading sequence (1), i.e., bending without internal pressure.

For loading sequence (4b), the pipe was bent with the internal pressure to a compressive strain which is very close to its CSC. The internal pressure was then reduced to zero while holding the compressive strain, after which additional bending was applied. The result shows that when the internal pressure decreases to zero, the bending moment greatly decreases. As the additional bending is induced (without the internal pressure), the bending moment rapidly increases and reaches its maximum which is similar to the maximum moment of the pipe with internal pressure (i.e., much lower than the maximum moment the pipe can withhold without the internal pressure). The CSC is slightly higher than the strain at which the depressurization starts and is much higher than the CSC of the pipe in loading sequence (1), i.e., bending without internal pressure.

The results show that the two loading sequences often used in the existing experiments and numerical models, i.e., (1) and (2), can produce conservative CSC for the bending without and with internal pressure, respectively. However, loading sequence (1) may overestimate the maximum bending moment without internal pressure for certain loading sequences such as loading sequence (4b).

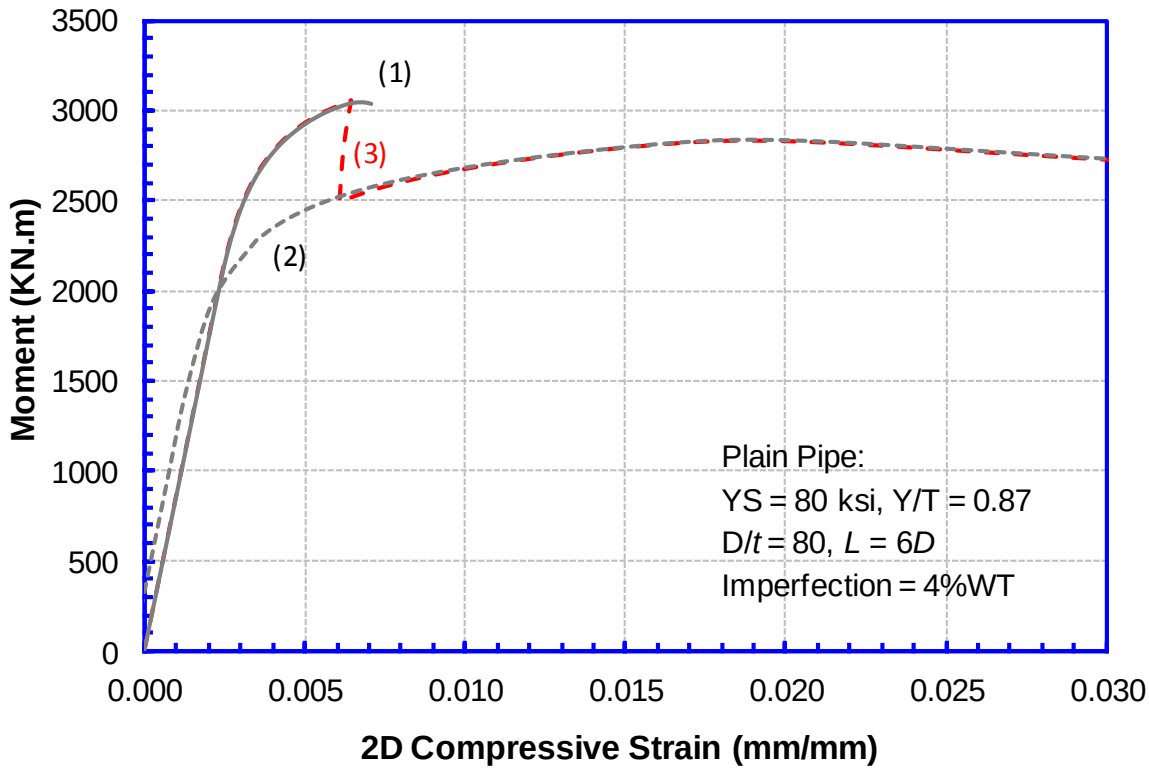

Figure 3-13 Effect of loading sequences on CSC (effect of pressure increase) - ER-NLF$_p$

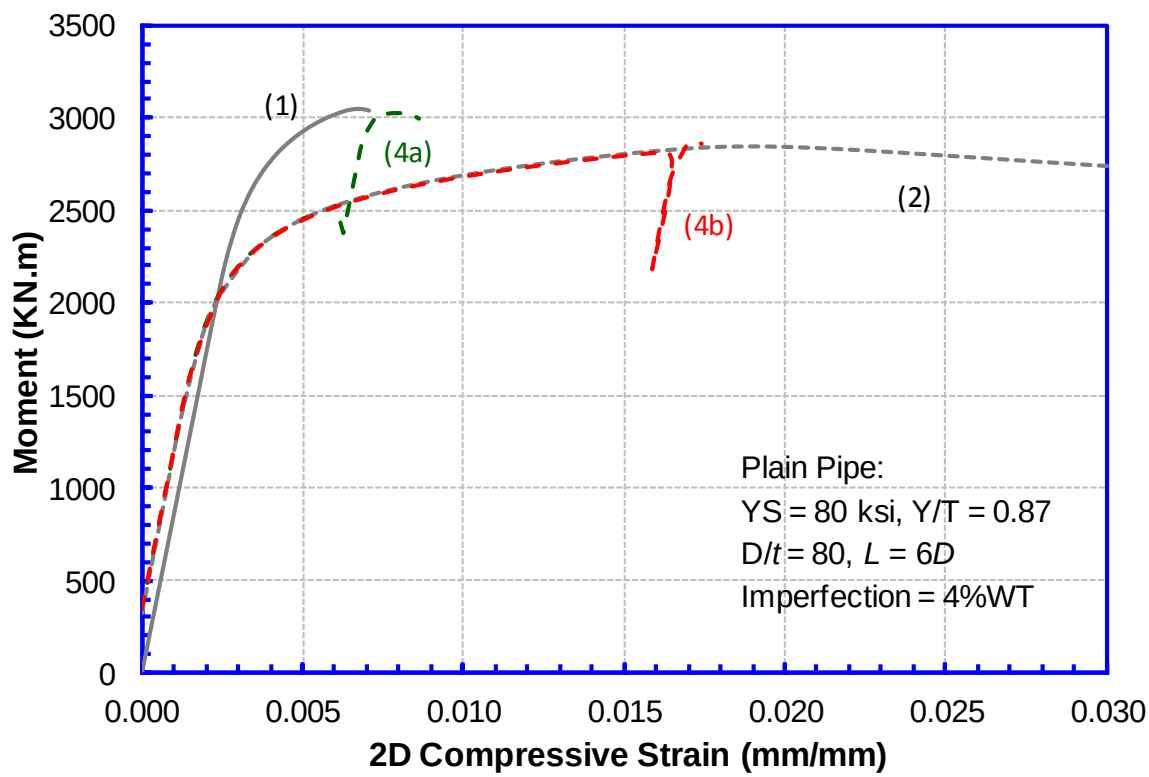

Figure 3-14 Effect of loading sequences on CSC (effect of pressure decrease) - ER-NLF$_p$

3.3.5 Lengths of Specimens

The relationship of the bending moment vs. compressive strains is shown in Figure 3-15 for various specimen lengths (L). The bending moment was calculated at the symmetry plane where the wrinkle forms and the compressive strain was calculated as the average strain within the $2D$ gauge length centered at the wrinkle location. The loading condition ER-NLF$_P$ was used in the simulation to produce constant bending moment along the pipe length.

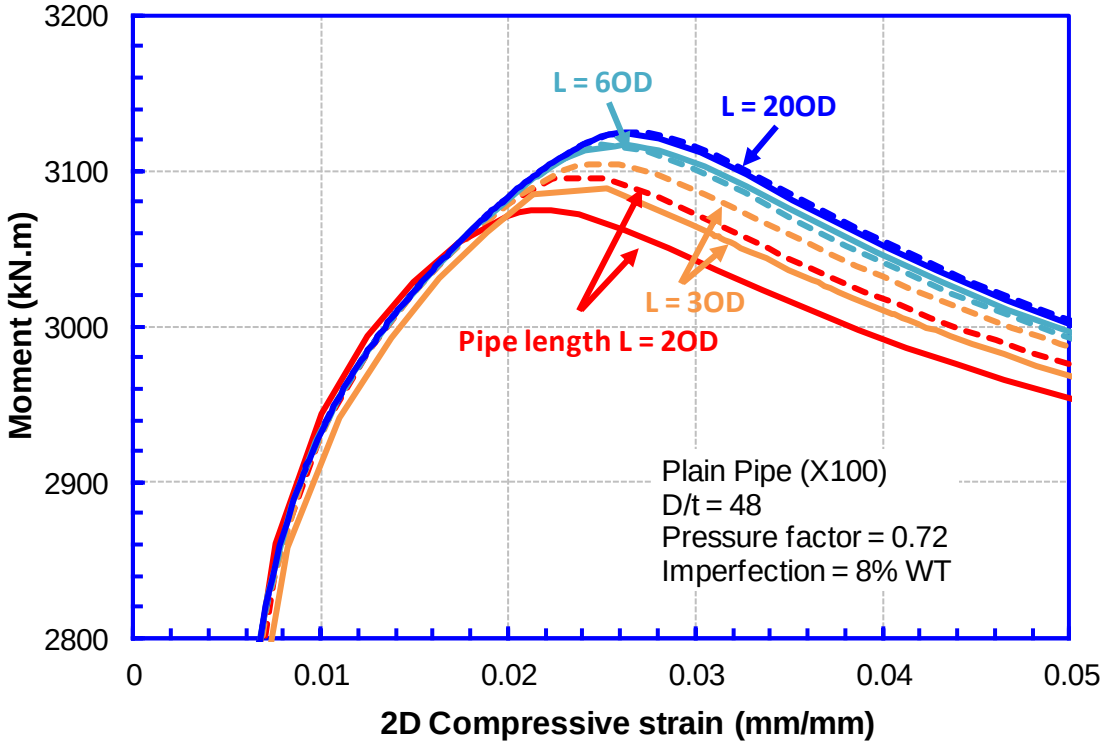

Figure 3-15 Moment (at wrinkle location) vs. compressive strain - effect of end conditions and model lengths - ER-NLF$_p$ (dashed line: deformable end; solid line: rigid end)

The results show that increasing the length of the specimen increases the maximum moment and CSC. If the length of the specimen is greater than six (6) OD (i.e., $L \geq 6D$), the calculated maximum moment and CSC become almost independent of the length. The CSC with the rigid end condition is slightly smaller than the CSC from the deformed end condition if $L < 6D$. The difference in the CSC calculated from those two end conditions is trivial when $L \geq 6D$. Similar observations can be found for the loading condition ER-NLF$_0$ (Figure 3-16) where no net-section force exists in the longitudinal direction.

The longitudinal strains at the maximum moment for the rigid end condition are shown in Figure 3-17. The wave-like strain variations near the symmetry plane and pipe end can be seen due to the wrinkle formed at those locations. The half length of the wrinkle near the symmetry plane is about one and half cycles similar to the full length of the wrinkle at the pipe end. To avoid strain interactions of the wrinkles at the pipe end and the symmetry plane, the total length of the full specimen should be greater than six (6) times of the wavelength of the wrinkles.

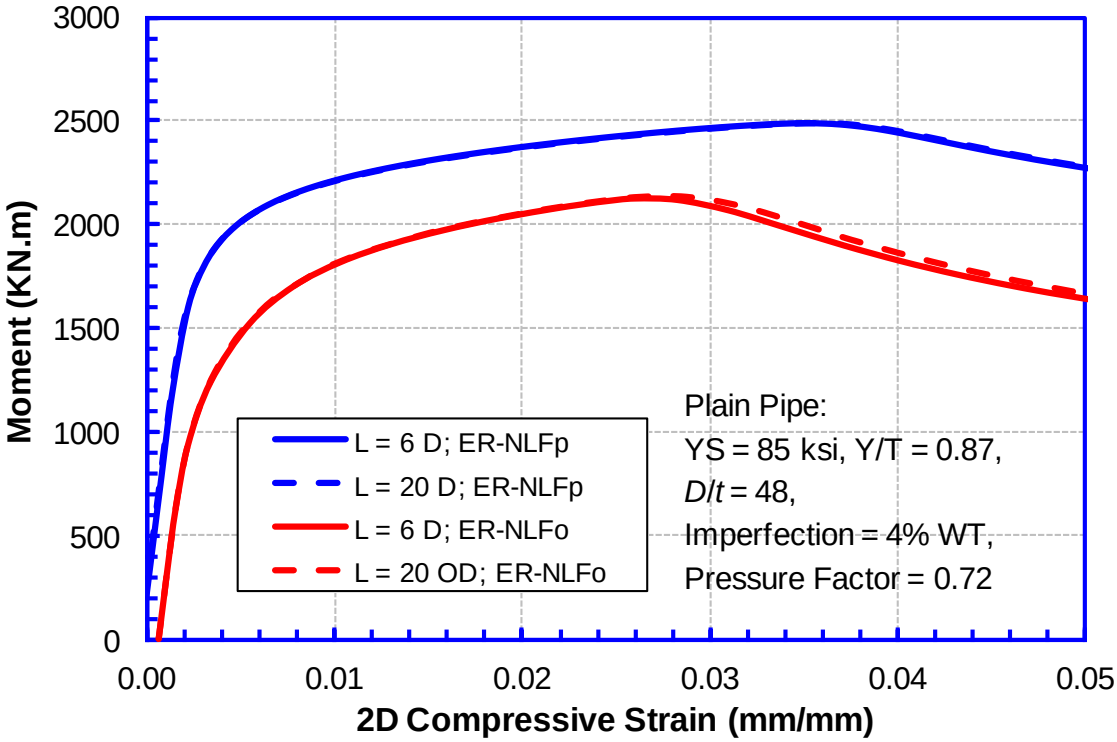

Figure 3-16 Moment (at wrinkle location) vs. compressive strain - effect of end conditions and model lengths - ER-NLF$_0$ vs. ER-NLF$_p$

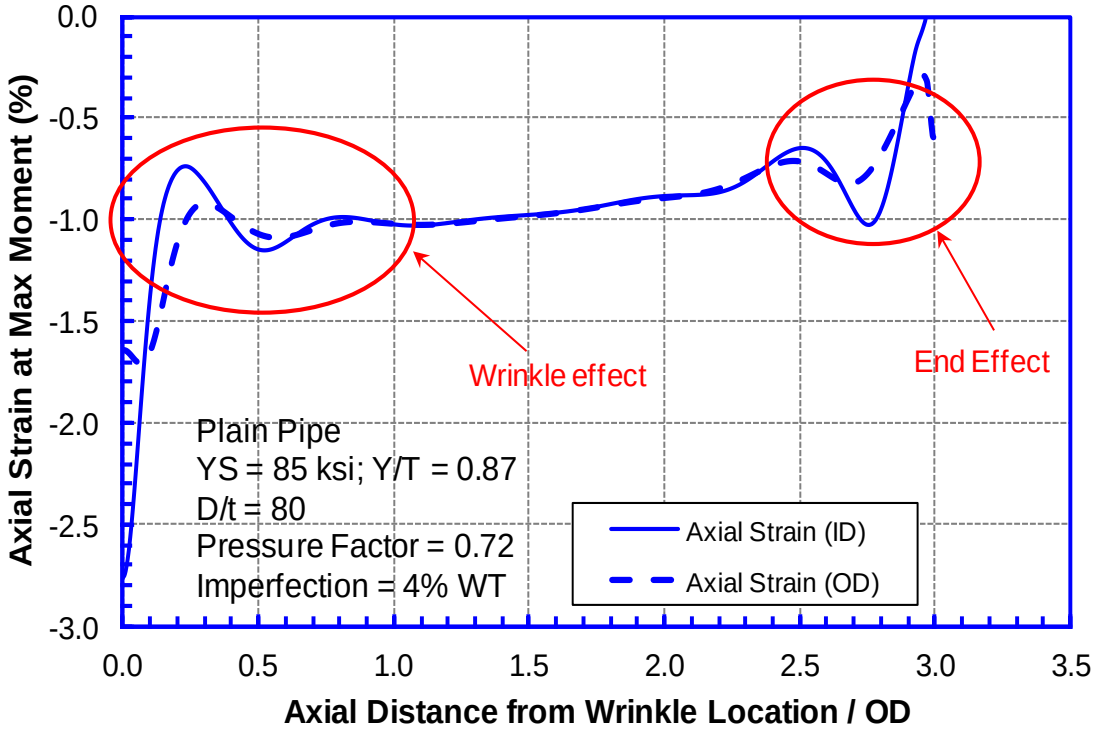

Figure 3-17 Effect of end conditions on the strain distribution along pipe length (ER-NLF$_0$)

The wavelength of the wrinkles, which is in general about 0.2*D* - 0.6*D*, depends on the pipe *D*/*t* ratio and internal pressure (see Section 3.6.2). To avoid any end effect, the length of the pipe specimen should be at least 4*D* (i.e., six times of the wrinkle wavelength), which is similar to what is shown in Figure 3-15. However, it should be noted that if the minimum length cannot be satisfied in an experiment, due to the end effect, the CSC tends to be under estimated and the measured CSC is conservative. In the following analyses, the total length of the pipe specimens is kept at 6*D* (i.e., $L = 6D$).

3.4 Definition and Calculation of Compressive Strain Capacity

When the applied bending moment approaches the maximum moment the pipe can withstand, a wrinkle with a small amplitude is often formed. Although the wrinkle is usually small and may not be visible, it can induce a large degree of strain localizations. For example, Figure 3-17 shows a typical distribution of the longitudinal (i.e., axial) strains along the length of a pipe at the maximum moment. The strains on the compressive side of the pipe at both ID and OD surfaces are shown. The formation of the wrinkle creates local bending deformation as indicated by the difference between the strains on the ID and OD surfaces. The peak strain at the wrinkle location can be nearly three times as much as the strain away from the wrinkle. Because of the wrinkle formation and strain localization, the strains along the length of the pipe are not uniform. The average compressive strain within a given gauge length is often used to measure the strain.

As discussed in Section 2, different definitions of the compressive strain capacity (CSC) have been used in the existing compressive strain models. The UOA models defined the CSC as the average compressive strain at the initiation of strain localization. The average compressive strain at the maximum moment was defined as the CSC in the other compressive strain models. Under this project, the CSC is defined as the average compressive strain at the maximum moment.

Since the average compressive strain varies with the gauge length, the CSC is affected by the selection of the gauge length. For example, Figure 3-18 shows that the CSC decreases with the increase of the gauge length for calculating the average compressive strain. Although the gauge length of one or two OD has been often used in the calculation of the average compressive strain and CSC, no commonly accepted gauge length exists.

The pipe integrity is often assessed by comparing the strain capacity with the strain demand. As a result, the calculation of the strain capacity should be consistent with the calculation of the strain demand. One of the major differences between the current practice in the calculations of the strain demand and capacity is the selection of finite element models. The strain demand is usually calculated with the beam-type elements which do not have the mechanisms for modeling the wrinkle formation and strain localization. The strain capacity is usually calculated with shell or solid elements where the wrinkle formation and strain localization can be produced. Due to the strain localization, the strain capacity can be overestimated compared with the strain demand if proper gauge length is not used.

To better understand the effect of the wrinkle formation on the local strains, two pipe models were conducted with 3-D solid finite elements. One pipe model was constructed with geometry imperfections and the other pipe model was constructed without geometry imperfections. The geometry imperfection promotes the wrinkle formation and reduces the maximum moment and

CSC. As a result, when the applied moment approaches to the maximum moment corresponding to the pipe with geometry imperfections, the wrinkle and strain localization can be observed in the pipe with geometry imperfections. While, the pipe without geometry imperfections is still under uniform deformation without strain localizations (as shown in Figure 3-19).

Therefore, the pipe model with geometry imperfections represents the models used for strain capacity studies. The pipe model without imperfections represents the model for strain demand studies. Figure 3-19 shows that the CSC determined with the 2*D* gauge length from the pipe with geometry imperfections matches the strain demand. It is recommended that the gauge length for the calculation of the CSC should be two (2) times the OD.

The average compressive strain (ε_c) can be calculated using the following equation with experimental and FEA data (see Figure 3-20):

$$\varepsilon_c = \varepsilon_t - D\frac{(\theta_2-\theta_1)}{l_g}, \tag{3-3}$$

where, the ε_t is the average tensile strain within a 2*D* gauge length measured from the tensile side of the pipe, the θ_1 and θ_2 are the angles of rotation of the ends of the gauge section, and l_g is the gauge length which is 2*D* (i.e., two times of the pipe OD). The CSC ($\varepsilon_c^{\text{crit}}$) is the average compressive strain at the maximum moment.

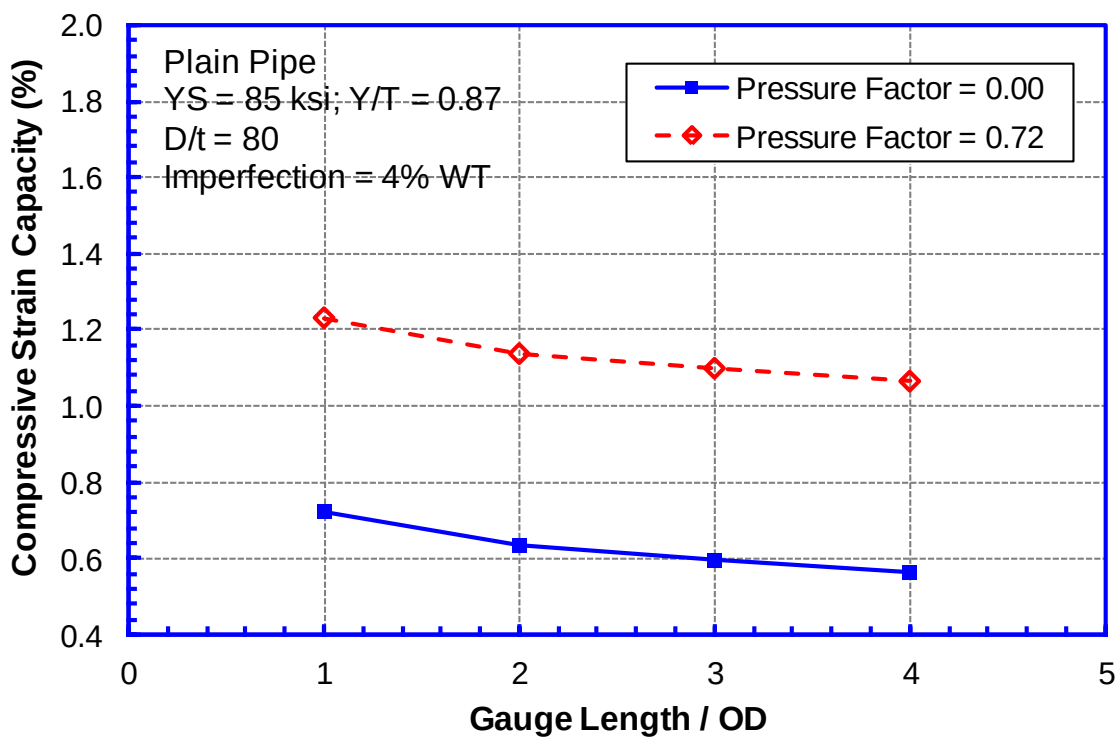

Figure 3-18 Effect of gauge length on measured CSC

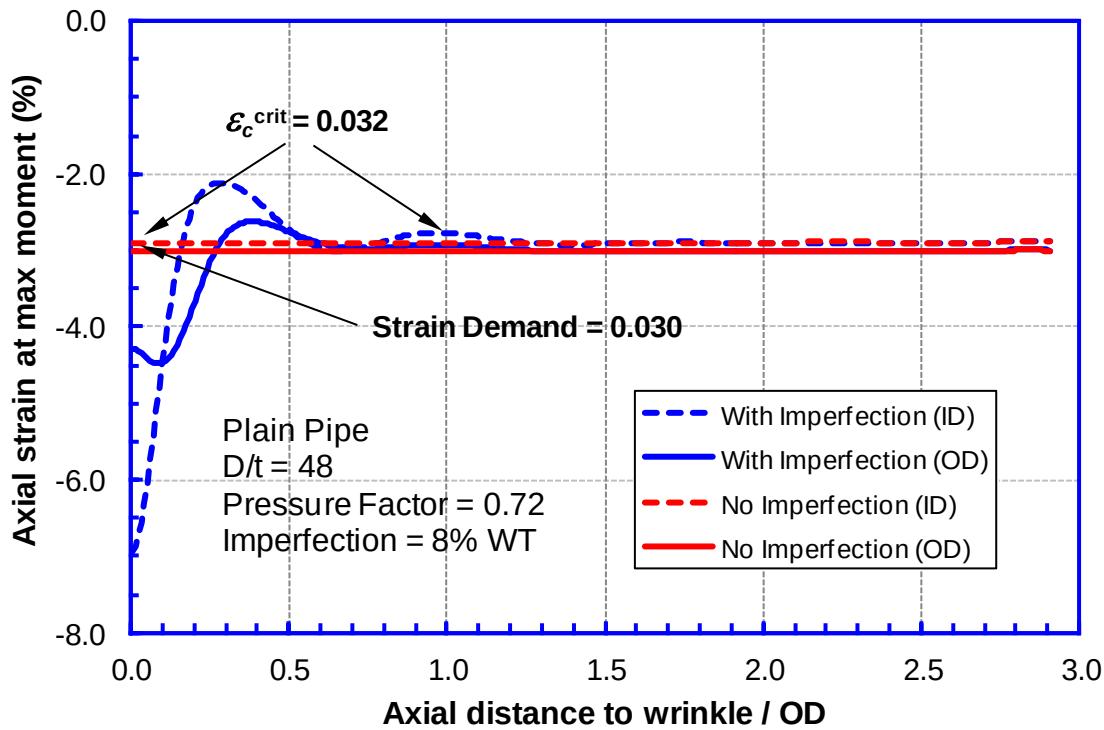

Figure 3-19 Effect of wrinkle formation on local strains

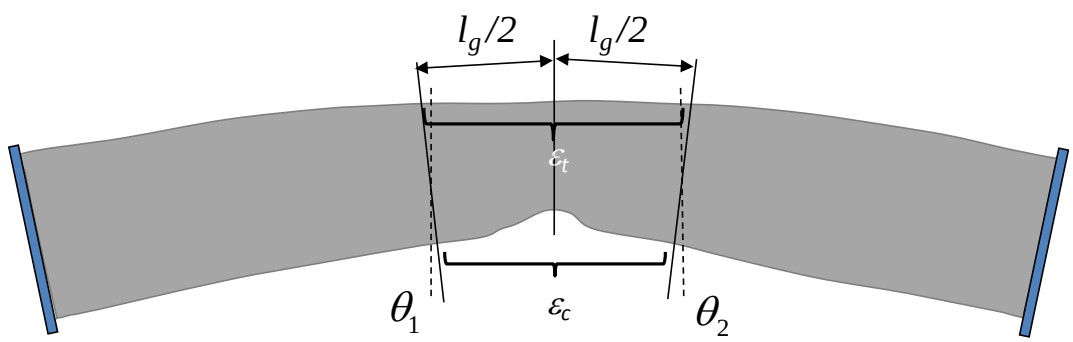

Figure 3-20 Calculation of compressive strain capacity

3.5 Finite Element Models

3.5.1 Shell vs. Three-Dimensional (3-D) Solid Models

Shell models have been frequently used in existing finite element analyses (FEA) of the CSC. In [36, 37], Souza and Murray recommended the 'best' type of shell models for analyzing the CSC. Although the shell models were widely accepted in calculating the CSC, the limitations of the shell models has also been recognized, e.g.,

(1) The shell models do not have adequate resolutions for precisely representing the non-homogeneous weld and heat affected zone (HAZ) properties and complex weld geometries such as bevel, cap, width, and high-low misalignment.

(2) Using the shell models, converged solutions especially for the post-buckling behavior cannot be established as the mesh refinement is increased monotonically.

In the typical FEA with shell elements, the mesh refinement and configuration are generally determined by calibrating/tuning the mesh to match the FEA results with experimental results [36, 37]. The calibrated mesh is then used for further parametric studies of the CSC.

Compared with the shell models, the 3-D solid models, although are more expensive in terms of computational costs, do not have the above limitations. The 3-D solid models have been more and more used in recent FEA.

3.5.2 Sample 3-D Solid Models

Three dimensional solid finite element models were used for bending simulations. A sample finite element model used in the analysis is shown in Figure 3-21. Due to the symmetric boundary conditions, a quarter of a full pipe specimen (half length and half circumference) was modeled. Symmetry conditions were applied to the proper planes. Rotation with and without internal pressure was applied to the end of the pipe until reaching the maximum moment.

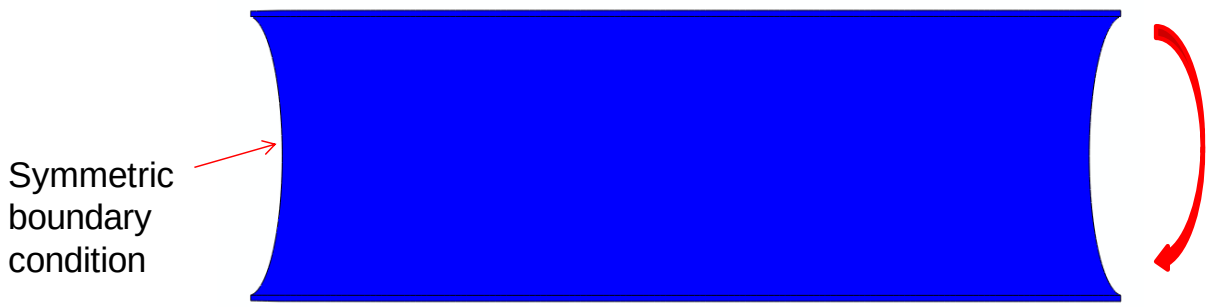

Figure 3-21 A sample FEA model

Different types of geometry imperfections were used in the finite element model (see Section 3.6.2). If not mentioned otherwise, the outward bulge type of geometry imperfections utilized by the UOA models (see Figure 2-2) were used in the following simulations.

3.5.3 Mesh Refinement of 3-D Solid Models

Comprehensive mesh convergence studies were carried out under this project. The mesh size for converged solutions is found proportional to the wall thickness or pipe OD. It is also found that the required mesh refinement for obtaining converged solutions at pressurized conditions is higher than that at zero pressure conditions. The sample results of the convergence studies are given in Figure 3-22.

In Figure 3-22, the letter H represents the hoop direction, the WT represents the thickness direction and the L represents the length direction. The number after the letters indicates the number of elements in that direction. For example, H60 means that 60 elements were used in the hoop direction, WT6 means that 6 elements were used in the thickness direction and L76 means that 76 elements were used in the length direction.

The minimum mesh refinement required to obtain converged solutions is summarized in the following:

(1) The maximum element size in the wall thickness direction is $\leq t/4$,

(2) The maximum element size in the hoop direction is $\leq \pi D/80$,

(3) The maximum element size in the longitudinal direction is ≤ $D/204$,

To obtain accurate results, the following mesh size was used in this project:

(1) The maximum element size in the wall thickness direction is $t/6$,

(2) The maximum element size in the hoop direction is $\pi D/120$,

(3) The maximum element size in the Longitudinal direction is $D/300$.

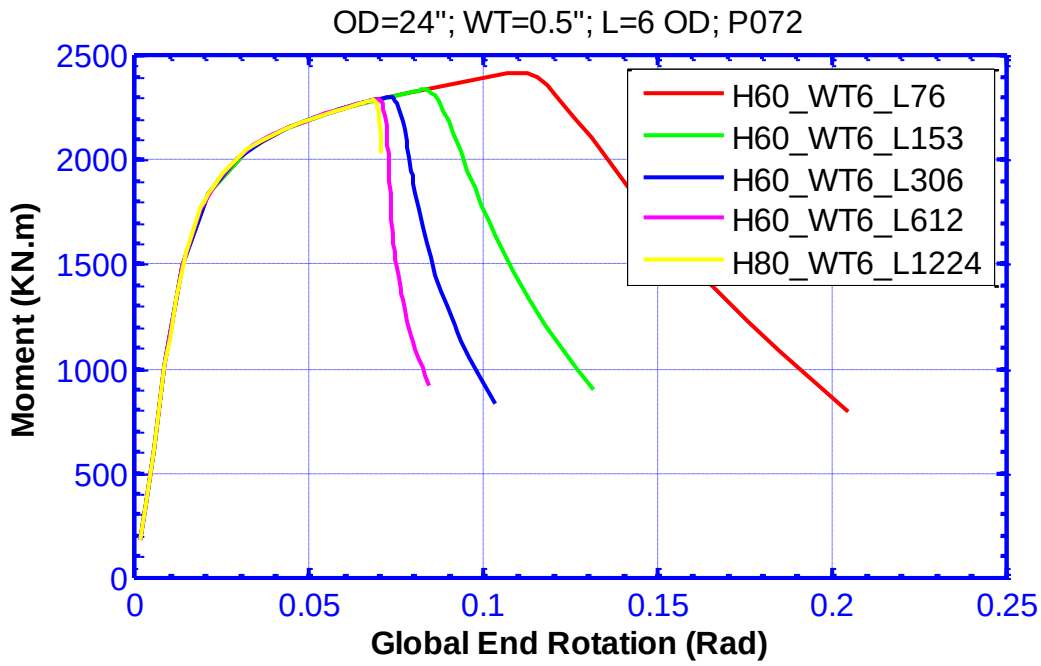

Figure 3-22 Sample results of mesh convergence studies (e.g., H60: 60 elements in hoop direction; WT6: 6 elements in thickness; L76: 76 elements in length direction)

3.6 Parameters Affecting Compressive Strain Limit

All the existing CSC models recognize the pipe's D/t ratios and pressure factors. The CSC was found to be also affected by other parameters such as the geometry imperfections, material properties, and girth welds.

However, the adoption of those parameters by different models varies greatly. For example, in the API equations, the pipe ovality (i.e., the out of roundness of pipe cross section) was used to evaluate the effect of the pipe geometry imperfection on the CSC. However, the UOA equations recognize the undulation of pipe outside surface as the geometry imperfection.

As for the material properties, the DNV, C-FER, and JFE equations all recognize the strain hardening capacity of the pipe materials, i.e., the Y/T ratio for the DNV equations and the strain hardening exponent (n) for both the C-FER and JFE equations. While, the UOA equations adopt the yield strength of the pipe materials.

The parameters that can affect the pipe's compressive strain capacity are briefly discussed in this section. The detailed discussions can be found in Appendix B.

3.6.1 Pipe *D*/*t* Ratio and Internal Pressure

All the existing CSC models recognize the pipe *D*/*t* ratio and pressure factor (f_p). The CSC decreases when the pipe *D*/*t* ratio increases and the increase of the internal pressure can increase the CSC. In most models, the effect of the *D*/*t* ratio and pressure factor is modeled with separate functions that are multiplied together. As a result, the ratio of the CSC at two pressure levels (f_p) is independent of the pipe *D*/*t* ratio, which is however, not always the case.

3.6.2 Geometry Imperfection

The geometry imperfections discussed herein are those generated during pipe manufacturing. The imperfections due to mechanical damages (such as dents and gauges) and corrosion defects are not included.

The out of roundness of the pipe's cross section, i.e., ovality, can reduce the pipe's CSC. The effect of the ovality on the pipe's CSC is recognized by API RP-1111. However, the reduction of the CSC due to the ovality is small for the ovality up to 1% as shown in Figure 2-3. Therefore, the typical ovality from pipe manufacturing has very limited effect on the CSC.

The seamless pipes inherently possess eccentricity (unequal ID & OD centers) which causes inconsistent wall thickness around the pipe's circumference. The thickness variation along the circumference has been proven to have a significant effect on the collapse resistance of the pipe. Similar to that, in recent studies, the geometry imperfection in the form of wave-like variation of the pipe's outside surface along the length of the pipe (referred to as surface undulations), was found to be critical for the pipe's CSC under bending. The surface undulation can be attributed to the variation of the pipe's outside diameter and/or wall thickness.

The surface undulations were adopted by the UOA and JFE models. In the UOA models, the height of the surface undulation is an input parameter. In the JFE models, the undulation is not explicitly used as a model input, but the size and shape of the surface undulations measured in representative JFE UOE pipes were built into the FEA used for the development of the JFE CSC models.

The surface undulations consist of waves of multiple wavelengths often with one dominant wavelength. The dominant wavelength varies from pipe to pipe and may be related to the pipe manufacturing process. However, it should be noted that the existing data on the pipe's surface undulations (e.g., shape and size), at the time of the report, are all from UOE pipes. It is not clear if the pipes of other manufacturing processes, e.g., ERW, spiral, etc., carry similar types of surface undulations.

Based on the research work performed under this project, the wavelength of the undulations is found to be critical to the pipe's CSC, in additional to the height of the surface undulations. Only the surface undulations of certain (i.e., critical) wavelengths are found to be detrimental to the pipe's CSC. The surface undulations with wavelengths much smaller or larger than the critical wavelengths have marginal effects on the CSC despite of the height of the undulations (within the realistic range) which is similar to what was reported in [38]. The critical wavelength of the surface undulation is similar to the wavelength of the wrinkles formed at the maximum moment (i.e., wrinkle's wavelength). The wrinkle's wavelength dependents on the pipe's dimensions and loading conditions (such as internal pressure and bending vs. longitudinal

compression). The wrinkle wavelength varies from 0.2D to 0.6D when $20 \leq D/t \leq 100$ and $0.0 \leq f_p \leq 0.8$.

3.6.3 Pipe Yield Strength and Y/T Ratio

The pipe's Y/T ratio (the ratio between the yield and tensile strength) measures the material's strain hardening capacity. The pipe's Y/T ratio and its yield strength are often related, e.g., the low grade (or strength) pipes often have lower Y/T ratios (i.e., higher strain hardening capacities) than the high grade pipes. In other words, pipes of different yield strengths often have different Y/T ratios. As a result, the difference of the CSC of the pipes with different strengths could be caused by the difference in their strain hardening capacities.

The acceptance of the pipe's yield strength and strain hardening capacity by the existing CSC models varies. The DNV, JFE, and C-FER models accept the strain hardening capacity (e.g., DNV - Y/T ratio; JFE and C-FER - strain hardening exponent, n). The CSA and UOA models use the pipe's yield strength.

Through the numerical simulations conducted in this research, the yield strength alone (i.e., the Y/T ratio is kept constant for various yield strengths) was found to have trivial effects on the CSC which is similar to the early findings by [14,15]. On the other hand, decreasing the pipe's Y/T ratio (i.e., increasing the strain hardening capacity) can lead to the increase of the CSC.

3.6.4 Pipe Uniform Strain

It is known that the pipe's CSC is affected by the shape of the full stress-strain curves. In addition to the yield strength and Y/T ratio, the uniform strain is another key parameter often used for characterizing the full stress-strain curves.

Under this research project, the effect of the pipe's uniform strain on the CSC was studied with numerical simulations. In the simulations, the uniform strain was reduced gradually from a base value while the pipe's yield strength and Y/T ratio were kept unchanged. The reduction of the uniform strain shows no effect on the pipe's CSC as long as the reduced uniform strain is still greater than the CSC obtained from the base uniform strain (i.e., the base CSC). However, if the uniform strain is smaller than the base CSC, the CSC will be reduced to the uniform strain.

3.6.5 Pipe Lüder's Strain

In addition to the uniform strain, the Lüder's strain (i.e., the plateau in the stress-strain curve after the yield point) can alter the shape of the stress-strain curves and therefore the CSC. The existence of the Lüder's strain can sometimes increase the CSC and sometimes reduce the CSC [16, 39]. The UOA models adopt separate equations for the pipes with and without Lüder's strains. It should be noted that the Lüder's strain ends at 0.5% strain in the UOA models.

Under this research project, the effect of the Lüder's strain on the CSC was investigated with numerical simulations. In the simulations, the magnitude of the Lüder's strains (i.e., the strain where the Lüder's plateau ends) was varied while the pipe's yield strength, Y/T ratio, and uniform strain were kept unchanged. The CSC of the pipes without the Lüder's strains (i.e., round-house stress-strain curves) was also obtained and used as the base CSC.

The results showed that if the base CSC is greater than the magnitude of the Lüder's strain, the existence of the Lüder's strain increases the CSC. However, if the base CSC is smaller than the magnitude of the Lüder's strain, the existence of the Lüder's strain reduces the CSC.

3.6.6 Girth Weld

The studies on the effect of girth welds on the CSC also showed mixed results. In the DNV codes [7], the existence of a girth weld was treated as detrimental. A 40% strain reduction was recommended in the DNV codes for D/t = 50 based on a set of bending tests for 12" X52 ERW pipes conducted at Univ. of Alberta (UOA) in 1994 [19]. However, the tests on a set of 20" X56 DSAW pipes of D/t = 60 in the same UOA work [19] didn't show detrimental effects of the girth welds.

The effects of the welding residual stress [36,37] and weld high-low misalignment [36, 37, 40, 41] on the CSC were studied with finite element simulations. The weld high-low misalignment was identified as the key parameter that reduces the CSC. Based on FEA, separate models were developed for pipes with girth welds in the UOA models, where the magnitude of the high-low misalignment was used as an input parameter.

The effects of the girth weld profile (such as cap size and root width), welding residual stress, weld and HAZ strength mismatch, and weld high-low misalignment on the CSC were studied in this project with numerical simulations. The results indicated that within reasonable ranges, the weld profile, welding residual stress, and strength mismatch have minimal effects on the CSC, compared with the plain pipes with reasonable geometry imperfections, e.g., a surface undulation of 0.04t. The high-low misalignment also shows relatively limited effect on the CSC especially under pressurized conditions. If no internal pressure is applied, a high-low misalignment up to 0.5t is equivalent to a 0.15t surface undulation. Under high internal pressure, the high-low misalignment doesn't show an obvious effect on the CSC.

The shrinkage of the girth weld tends to create a surface undulation near the girth weld. The surface undulation induced by the girth weld shrinkage can be treated in the same way as those in plain pipes.

3.6.7 Net-Section Force

The net-section force is known to affect the pipe's CSC under bending, e.g., the net-section tensile force can increase the CSC, while the net-section compressive force can reduce the CSC. The work by JFE [11] indicated that under pure longitudinal compressive force, the pipe's CSC is half of that under bending. However, due to the scatters of the CSC measured in bending tests, the change of the CSC due to the net-section force is often buried by the testing scatters.

Most existing models were developed under bending dominant conditions, although the models are recommended for combined bending and longitudinal forces.

There have been some studies on the effect of the net-section force on the CSC. However, no reliable correlations between the net-section force and the CSC have been established. In this project, the effect of the net-section tensile force on the CSC was studied and a correlation equation was established between the tensile force and the CSC.

3.7 Summary of the Analysis Process

Proper modeling processes should give close representation of actual material behaviors and field conditions. Through systematic investigations on various (experimental and/or numerical) modeling factors, improved modeling processes were established in the current project. The recommended modeling processes are summarized in the following.

3.7.1 Representation of Material Properties

3.7.1.1 Background

The linepipe materials often show material anisotropy, i.e., different stress-strain behaviors in their longitudinal and circumferential directions and different stress-strain behaviors under tension and compression. For example, the circumferential properties of UOE pipes often have higher strength but lower strain hardening capacity than their longitudinal properties. The pipes made from other manufacturing processes may show different characteristics of material anisotropy. Although the CSC mainly depends on the pipe's longitudinal properties, the material anisotropy is also believed to affect the CSC. For example, for the UOE pipes, the increase of the strength in the hoop direction tends to increase the CSC, however, the decrease of the strain hardening capacity in the hoop direction tends to decrease the CSC.

In the existing CSC models, the material's full stress-strain behaviors are often represented by selected key material parameters, e.g., yield strength, yield to tensile ratio (Y/T), and strain hardening exponent, etc. However, the key material parameters cannot uniquely define a full stress-strain curve. As a result, even for the same key material parameters, the full stress-strain behaviors used in different CSC models and the resulting CSC could be different.

3.7.1.2 Findings and Recommendations

The effect of the material anisotropy on the CSC was investigated through finite element analyses (FEA) in this project. For the UOE pipes with anisotropic stress-strain properties, it was found that compared with the different tensile and compressive properties, the anisotropic longitudinal and circumferential properties often play a secondary role on the CSC. The CSC is mainly determined by the pipe's longitudinal compressive properties. Therefore, the longitudinal compressive stress-strain curves should be used for the assessment of the CSC when available.

In this project, a set of mathematical equations for constructing the full stress-strain curves of the linepipes are recommended (see Section 3.2.3) and used in the development of the refined CSC models. The key material parameters representing the longitudinal tensile stress-strain properties are used in those equations. The equations are consistent with those used to construct the PRCI-CRES tensile strain models. The constructed stress-strain curves statistically show a good match with the experimentally measured stress-strain curves.

If the longitudinal compressive stress-strain curve is available, in order to properly use the CSC models, the compressive stress-strain curve must be converted to its equivalent tensile stress-strain curve. The key material parameters (i.e., model input parameters) should be obtained from the equivalent tensile stress-strain curve (see Section 3.2.1). It should be noted that the equivalent tensile stress-strain curve converted from the compressive stress-strain curve could be different from the tensile stress-strain curve measured from uni-axial tensile tests.

3.7.2 Representation of Field Conditions

3.7.2.1 Representation of Loads and Constraints

3.7.2.1.1 *Background*

High longitudinal strains in a pipeline segment are often induced by ground movement hazards, which usually apply distributed loads to a pipeline through pipe-soil interactions. The pipeline segment which is exposed to the ground movement is connected to the rest of the pipeline. The longitudinal strain is generated by the longitudinal force and bending moment generated by the distributed load and the constraint from the rest of the pipeline. The pipeline also experiences longitudinal stresses/strains from operating loads such as internal pressure and temperature change.

The variation of the loading and constraint conditions in fields can result in different combinations of bending moment and longitudinal forces to the pipeline and affect the CSC. For example, the CSC under uniform longitudinal compressive force is about half of the CSC under pure bending (see Section 2.3.5). Under bending-dominant conditions, the increase of the longitudinal tensile force tends to increase the CSC, while the increase of the compressive force tends to decrease the CSC.

The existing CSC models were developed under different loading and constraint conditions which produced different combinations of the bending moment and longitudinal force. As a result, the CSC computed from different models may not be equivalent. However, the existing CSC models do not distinguish the differences in the loading and constraint conditions and the computed CSC is treated equally.

Furthermore, different from the typical field conditions, in most numerical models and experimental tests including those used to develop the existing CSC models, the bending moment and longitudinal force were applied at the two ends of a pipe specimen without longitudinal displacement constraints and distributed loads.

3.7.2.1.2 *Findings and Recommendations*

In this project, various loading and constraint conditions and their effects on the CSC were investigated with FEA. It is found that the CSC under distributed soil loads tends to be smaller than the CSC under the loads applied at the pipe ends. On the other hand, the longitudinal displacement constraint tends to generate a tensile force in the longitudinal direction under bending due to elongation of the pipe segment, which tends to increase the CSC compared with the CSC under pure bending.

Based on the above discussions, for bending-dominant field conditions, the bending moment (applied at pipe ends) without the longitudinal constraint and net-section force is recommended for future numerical modeling and experimental tests if the exact magnitude of the longitudinal force in fields is not available. For compression-dominant conditions, the loading with uni-axial compressive force is recommended. The details on the loading conditions can be found in Sections 3.3.2 and 3.3.3.

3.7.2.2 Representation of Loading Sequences

3.7.2.2.1 *Background*

Under ground movement hazards, the buried pipeline can experience complicated loading sequences. The ground movement can take place in one occasion or multiple occasions and at different pressure levels. The change of the internal pressure can take place before, during, and/or after the ground movement.

However, in typical numerical models and experimental tests, simplified loading sequences are often used. For example, the pipe specimen is firstly pressurized to a pre-determined pressure level. The bending moment and/or longitudinal force are then applied until a wrinkle is formed while the pressure is held constant.

Under plastic deformation, the stress and strain generated in the pipe depend on not only the magnitude of the load but also the loading sequence. Therefore, the CSC and the maximum moment may vary with the loading sequence.

3.7.2.2.2 *Findings and Recommendations*

The FEA conducted under this project demonstrated that both the CSC and the maximum moment can be affected by the loading sequence. The simplified loading sequence used by the existing numerical models and tests can produce conservative CSC compared with the CSC from other loading sequences analyzed. However, the simplified loading sequence may over-estimate the maximum/limit bending moment. The detailed discussion can be found in Section 3.3.4.

3.7.2.3 Length of Specimen for Experiments

The length of the specimen for experimental testing is often limited by the testing equipment. The length of the pipeline segment experiencing large longitudinal strain is typically longer than the testing specimen.

The pipe specimen for experimental testing has end plates to contain internal pressure and to transfer loads. The end plates reinforce the end section of the specimen and affect the strain, i.e., the end effect. Therefore, the testing specimen needs to be long enough to prevent the end effect from affecting the wrinkle formation and the CSC.

Detailed FEA conducted in this project on the testing specimens demonstrated that the CSC and the maximum (or limit) bending moment both depend on the length of the specimen. The CSC and the maximum bending moment increase with the increase of the specimen length. The length effect diminishes when the specimen length is longer than 6*D* (i.e., six times of pipe OD). The recommended minimum specimen length is 4*D*. The recommended specimen length is for those tests where the bending moment and longitudinal force are applied at the two ends of the pipe specimen where the end plates are attached. The length does not include the length of the pipe end sections with reinforcement. The detailed discussion can be found in Section 3.3.5.

3.7.3 Calculation and Measurement of Compressive Strain Capacity

3.7.3.1 Background

The bending moment and compressive strain are not uniform along the length of a pipe in most field conditions and in typical loading and constraint conditions adopted by most numerical

models and experimental tests (Section 3.3.3.1). Therefore, wrinkles tend to be formed at the locations having the highest bending moment and compressive strain. The maximum (or limit) bending moment and CSC should be calculated/measured at the wrinkle location.

On the other hand, small wrinkles are often generated before the CSC is reached which can induce strain localization. To minimize the effect of the strain localization on the measured CSC values, the average strain within a certain gauge length in the wrinkle area is usually used for determining the CSC. However, the selection of the gauge length varies in the current practice. The typical gauge length can be 1*D* (i.e., one pipe OD), 2*D*, and up to the full specimen length. The reported CSC values increase as the gauge length decreases. Therefore, selecting a proper gauge length is important for ensuring the consistent measure of the CSC. The gauge length used to define the CSC in most existing CSC models is not known.

3.7.3.2 Findings and Recommendations

The determination of the proper gauge length should consider the definition of strain demand. Since the CSC is eventually compared with the strain demand, the strain definition for the strain capacity and the demand needs to be consistent. The strain demand can be obtained from finite element simulations. In the finite element simulations of the strain demand, beam elements are often used. The beam elements cannot capture the wrinkle formation and wrinkle induced strain localization.

In this project, the strain demand and strain capacity were obtained for the same loading condition using finite element simulations. The results showed that to obtain consistent strain demand and capacity, the gauge length should be 2*D*. Additional details can be found in Section 3.4. It should be noted that the strain demand can also be obtained from direct measurement of the curvature of the pipeline. Under that circumstance, it is recommended to use 2*D* as the gauge length for calculating the strain demand too.

3.7.4 Finite Element Models

Shell and three-dimensional solid elements are often used in the finite element simulations of pipe buckling and wrinkle formation. The three-dimensional solid elements should be preferred, especially for the pipes containing girth welds and for post buckling analyses where significant displacement and strain localization are expected.

Proper mesh convergence tests are needed to demonstrate the mesh refinement is adequate. In general, finer mesh is needed for the pressurized conditions than that for the non-pressurized conditions. Therefore adequate mesh refinement needs to be demonstrated for high pressure conditions. Details on the mesh refinement are discussed in Section 3.5.

4 Refined Compressive Strain Models

4.1 Structure of the Refined Compressive Strain Models

Systematic sensitivity studies were carried out for the parameters discussed in Section 3.4 via finite element analyses. The following key parameters for the compressive strain models were selected based on the sensitivity studies:

(1) Pipe's *D*/*t* ratio;

(2) Internal pressure;

(3) Pipe's Y/T ratio;

(4) Height (from peak to valley) of the surface undulation (geometry imperfection);

(5) Pipe's uniform strain;

(6) Pipe's Lüder's strain; and

(7) Net-section force (tension).

Most existing compressive strain models adopted a multiplying form, where a single-variable function was developed for each selected parameter and the single-variable functions were then multiplied together. The multiplying function form has been proven to be effective.

The similar function form was used in the new compressive strain models. Single-variable equations were established for characterizing the effect of the Y/T ratio, surface undulation, and net-section force and multiplied together. However, the simple multiplying form was found not able to capture the complicated relationship between the internal pressure and pipe *D*/*t* ratio. A refined function for the internal pressure and pipe *D*/*t* ratio was established.

4.2 Refined Compressive Strain Models

The refined compressive models (i.e., CRES models) are given in the following,

$$\varepsilon_c^{\text{crit}}(\%) = \min\left(\varepsilon_u, F_{LD} * \varepsilon_r\right), \tag{4-1}$$

$$F_{LD} = \begin{cases} 1 - 0.50 * (1 - 0.75\varepsilon_r^{-0.23})\left[1 + \tanh\left(8.0\frac{\varepsilon_e}{\varepsilon_r} - 8.2\right)\right] & \text{SSC with Lüder's strain} \\ 1 & \text{Round SSC} \end{cases}, \tag{4-2}$$

$$\varepsilon_r(\%) = F_{DP} * F_{YT} * F_{GI} * F_{NF}, \tag{4-3}$$

$$F_{DP} = \begin{cases} 980 * \left[0.5\left(\frac{D}{t}\right)^{-1.6} + 1.9 * 10^{-4}\right], & \text{if } f_p < f_{pc} \\ 980 * (1.06 f_p + 0.5)\left(\frac{D}{t}\right)^{-1.6}, & \text{if } f_p \geq f_{pc} \end{cases}, \tag{4-4}$$

$$f_{pc} = 1.8 * 10^{-4} * \left(\frac{D}{t}\right)^{1.6}, \tag{4-5}$$

$$F_{YT} = 2.7 - 2.0\xi, \tag{4-6}$$

$$F_{GI} = 1.84 - 1.6\left(\frac{h_g}{t}\right)^{0.2}, \tag{4-7}$$

$$F_{NF} = \begin{cases} 1.2{f_n}^2 + 1, & \text{if } f_n \geq 0 \\ 1, & \text{if } f_n < 0 \end{cases}. \tag{4-8}$$

In the above equations, ε_u is pipe's uniform strain, ε_e is the strain where the Lüder's extension ends, f_p is the pressure factor (i.e., the ratio between the pressure induced hoop stress and pipe's yield strength), h_g is the height (from peak to valley) of the geometry imperfection, f_n is the net-section stress factor (i.e., the ratio between the longitudinal stress induced by the net-section force and pipe's yield strength), D is pipe's OD, t is pipe's wall thickness, and ξ is pipe's Y/T ratio.

4.3 Applicable Range

The applicable range of the refined compressive strain models is determined by the range of the parameters used in the finite element analyses. The applicable range of the compressive strain models is given in the following:

(1) $20 \le D/t \le 104$;

(2) $0 \le f_p \le 0.80$;

(3) $0.70 \le \xi \le 0.96$;

(4) $0.01t \le h_g \le 0.30t$;

(5) ε_e (%) ≤ 2.0; and

(6) $0 \le f_n \le 0.40$.

4.4 Trend Analyses and Comparison of with Existing Models

4.4.1 Pipe *D/t* Ratio

Figure 4-1 shows the trend of the predicted CSC with respect to pipe's *D/t* ratios by different models. The CSC was normalized by the CSC of *D/t* = 44. A set of FEA results were also included for comparisons. The conditions used in the FEA are given in the plot. For the DNV and UOA models, the trend in Figure 4-1 is independent of the other parameters due to the function forms adopted in those models. For the CSA and CRES models, the trend depends on the pressure. The pressure factor was set to zero for the CSA and CRES models in Figure 4-1.

Although the methods to derive the different models are different and the functions used by different models also seem to be very different, Figure 4-1 shows the predicted trends by the different models are very similar.

4.4.2 Internal Pressure

The trend of the predicted CSC with respect to the pressure factor (f_p) by different models is shown in Figure 4-2. The CSC was normalized by the CSC of zero pressure. FEA results (for *D/t* = 30, 64, and 104) were also included for comparisons. The FEA results indicate that the CSC- f_p relationship depends on pipe's *D/t* ratio. The internal pressure shows more beneficial effect on the CSC for small *D/t* pipes than the CSC for large *D/t* pipes.

However, for the DNV and UOA models, the trend shown in Figure 4-2 is independent of the other parameters due to the function forms adopted in those models. Therefore, the dependence of the CSC- f_p relationship on pipe's *D/t* ratios is not be captured. In addition, the DNV models siginificantly overestimate the beneficical effect of the internal pressure. The UOA models also overpredicte the pressure effect. The overestimation of the pressure effect by the DNV and UOA models can be partially attributed to the loading conditions used in the model developement. In the DNV and UOA models, the loading conditions equivalent to ER-NLF$_p$ were used. However,

the conditon ER-NLF$_0$ was used in the FEA shown in the plot. At ER-NLF$_p$, the net-section force genereated by the internal pressure can further increase the CSC.

The CSC- f_p relationship predicted by the CSA and CRES models is shown in Figure 4-2 for *D/t* = 30 and 104. The CSA models incorretly predict the dependence on pipe's *D/t* ratios. As a resutlt. the CSA models may be overly conservative for small *D/t* pipes but not conservative for large *D/t* pipe for pressurized condtions. The CRES models capture the dependences on the *D/t* ratio reasonably well.

4.4.3 Pipe Y/T Ratio

Figure 4-3 shows the trend of the predicted CSC with respect to the pipe's Y/T ratio by the CRES and DNV models, since only these two models take the Y/T ratio into account. Sample FEA results were also included for comparisons. The CSC was normalized by the CSC of Y/t = 0.87. The trend in Figure 4-3 is independent of the other parameters due to the function forms adopted in those models. It is seen from Figure 4-3 that both models closely capture the decrease of the CSC with an increase in the Y/T ratio.

4.4.4 Pipe Geometry Imperfection

The trend of the predicted CSC with respect to the geometry imperfection (h_g) is shown in Figure 4-4. The CSC is calculated by the CRES and UOA models, since only these two models explicitly take the geometry imperfection into account. A set of FEA results were also included for comparisons. The CSC was normalized by the CSC of h_g = 4%*t*. The trend in Figure 4-4 is independent of the other parameters due to the function forms adopted in those models. It is seen from Figure 4-4 that both models closely capture the decrease of the CSC with an increase in the geometry imperfections.

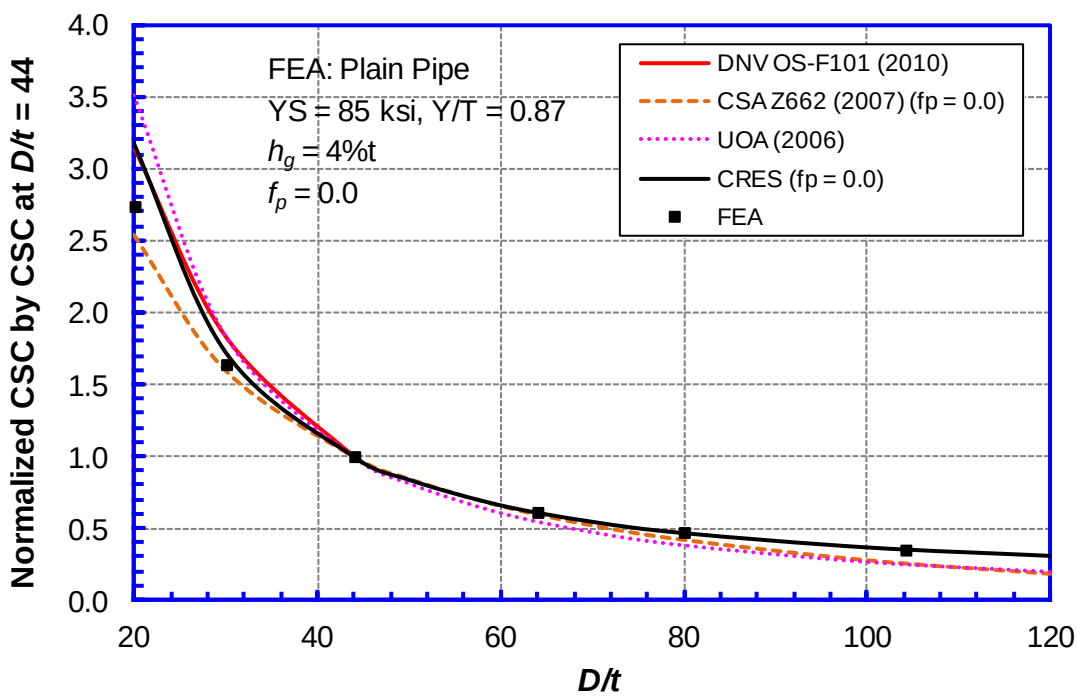

Figure 4-1 Comparison of normalized CSC from various models vs. *D/t* and FE results

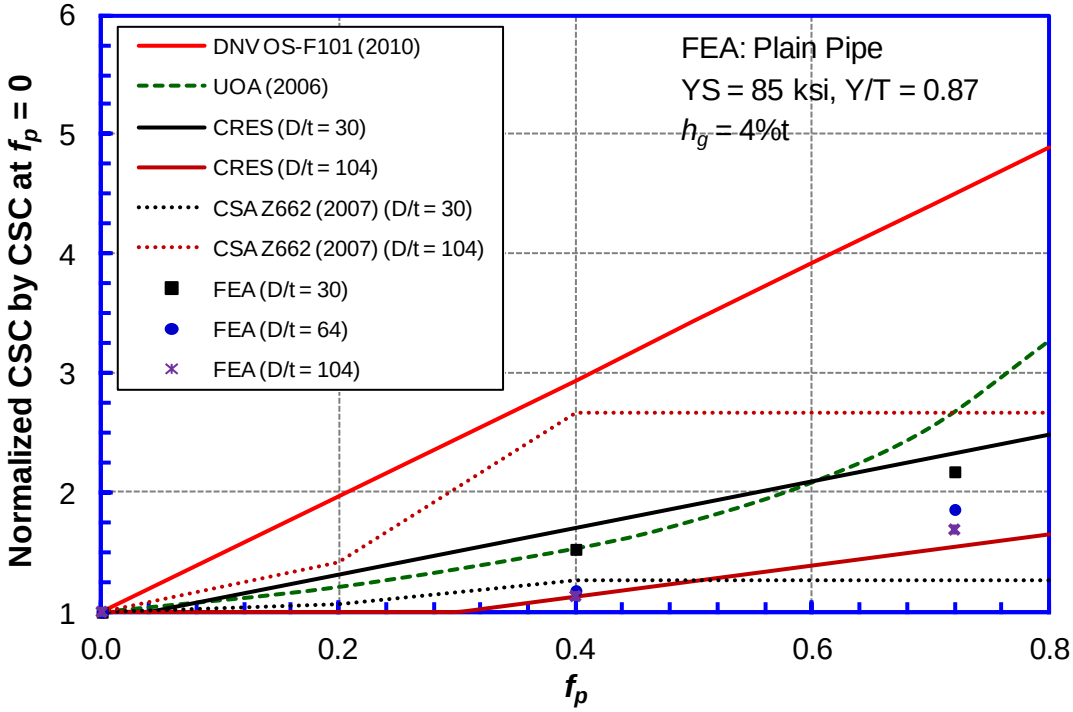

Figure 4-2 Comparison of normalized CSC from various models vs. pressure factor (f_p) and FE results

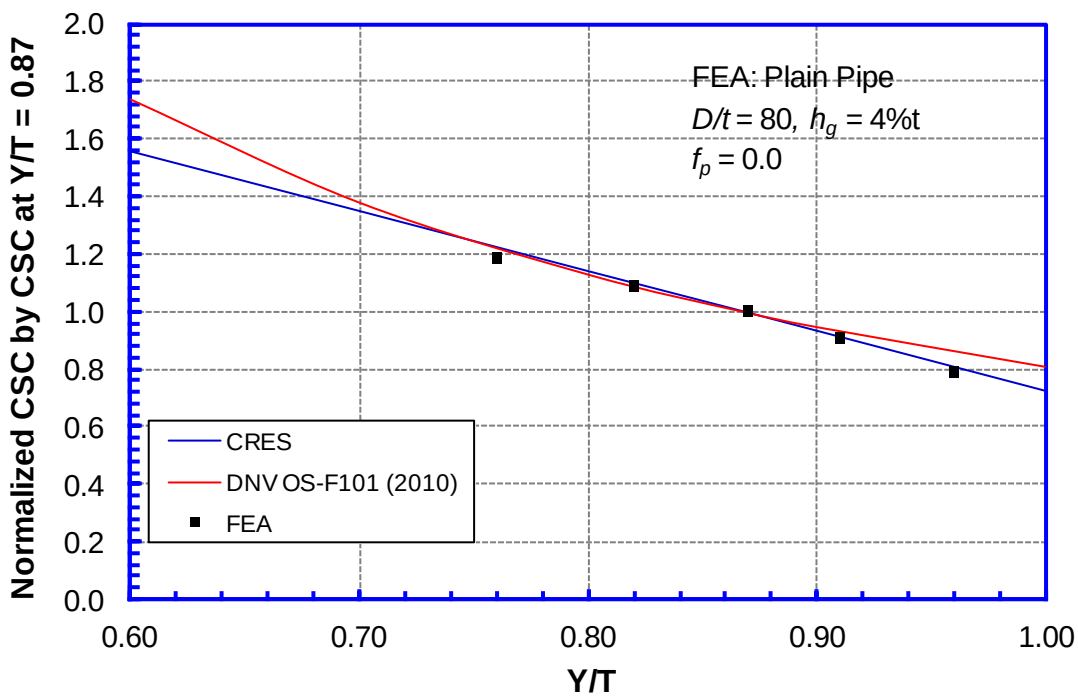

Figure 4-3 Comparison of CSC from CRES and DNV models vs. Y/T and FE results

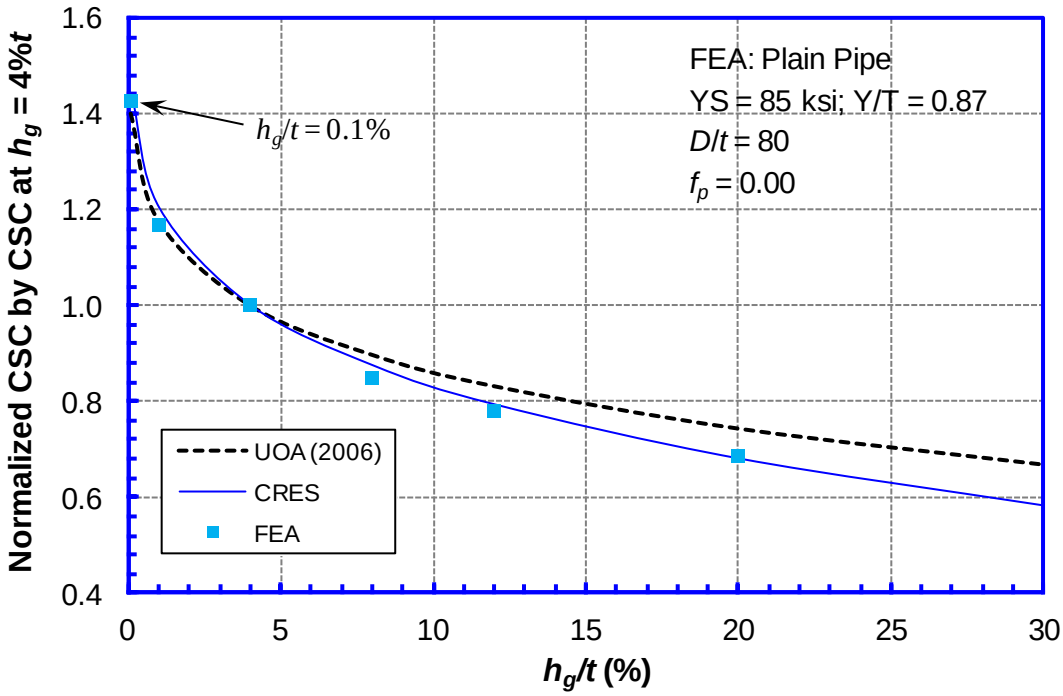

Figure 4-4 Comparison of normalized CSC from CRES and UOA models vs. geometry imperfection (h_g) and FE results

4.5 Model Evaluation

An experimental database was compiled using testing data published in public domain and was used to evaluate the refined compressive strain models. Details of the database can be found in the following section.

4.5.1 Experimental Database

The database consists of 48 full-scale bending tests and the experimentally measured CSC was provided for 40 out of the 48 tests. The database covers the following range,

- OD (D): 6.6 - 48 (inch)
- WT (t): 0.13 - 0.93 (inch)
- D/t: 22 - 104
- Grade: X52 - X100
- YS (σ_y): 55 - 98 (ksi)
- Y/T: 0.77 - 0.91
- Lüder's strain (ε_e): < 1.6%
- Pressure factor (f_p): 0 - 0.82
- Net-section stress factor (f_n): -0.42 - 0.62
- CSC: 0.23 - 6.2 (%)

The pipe grades covered in the test database range from X52 to X100. The number of tests for each pipe grade is almost evenly distributed for the grades up to X80 and there is only one test for X100 (Figure 4-5). The database covers *D/t* ratios ranging from 22 to 104 where about 52% of the tests fall in the *D/t* range between 50 and 80, as shown in Figure 4-6. The database covers pressure factors from 0 to 0.82, with 29% of the tests having zero pressure and 31% of the tests having high internal pressure ($f_p > 0.6$) (Figure 4-7). The Y/T ratios in the database range from 0.77 to 0.91, where 44% of the tests have pipes with Y/T > 0.85, as shown in Figure 4-8. The details of each individual test in the database are given in Appendix C.

4.5.2 Evaluation with Test Data Having All Input Parameters

The geometry imperfections are found to be critical to the CSC and recognized by the CRES compressive strain models. As shown in Figure 4-4, the CSC can differ by more than a factor of two (2) depending on the size of the geometry imperfections. The geometry imperfections may not be easily available, however, especially for the pipelines in service.

Except for seven (7) tests, the geometry imperfection was not given for the rest of the tests in the database. All required input parameters by the CRES models are available for the seven tests. The comparison of predicted and measured CSC values for the seven tests is shown in Figure 4-9. It is seen that the predicted CSC matches the measured ones very well.

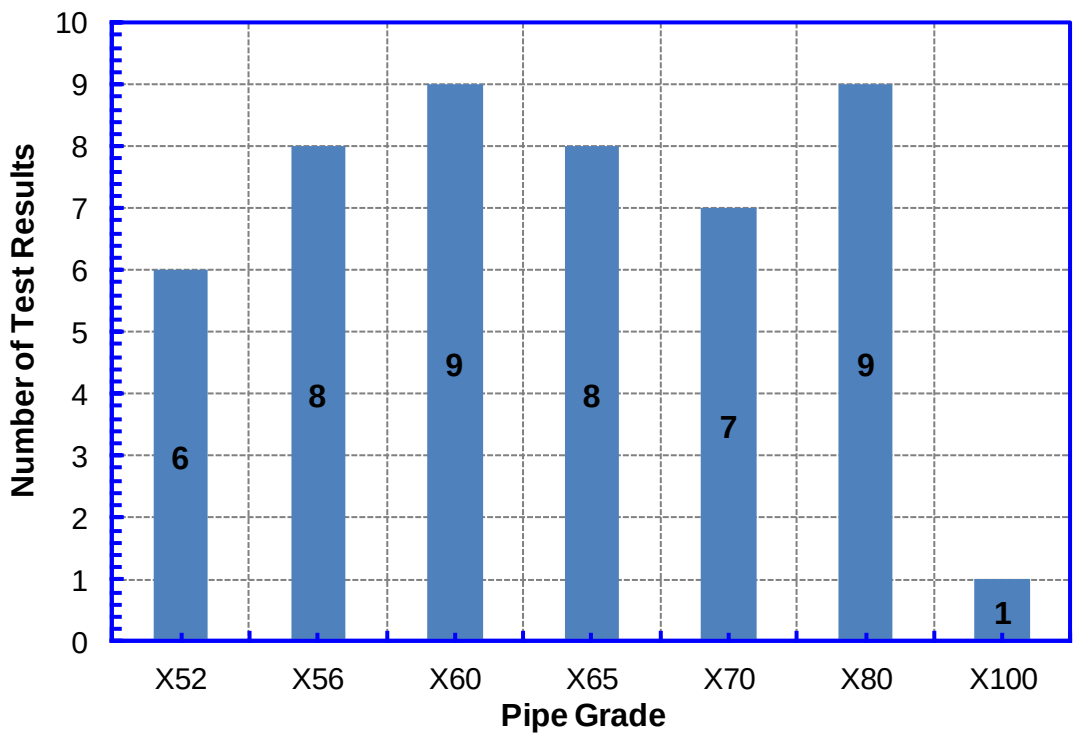

Figure 4-5 Distribution of test database over pipe grade

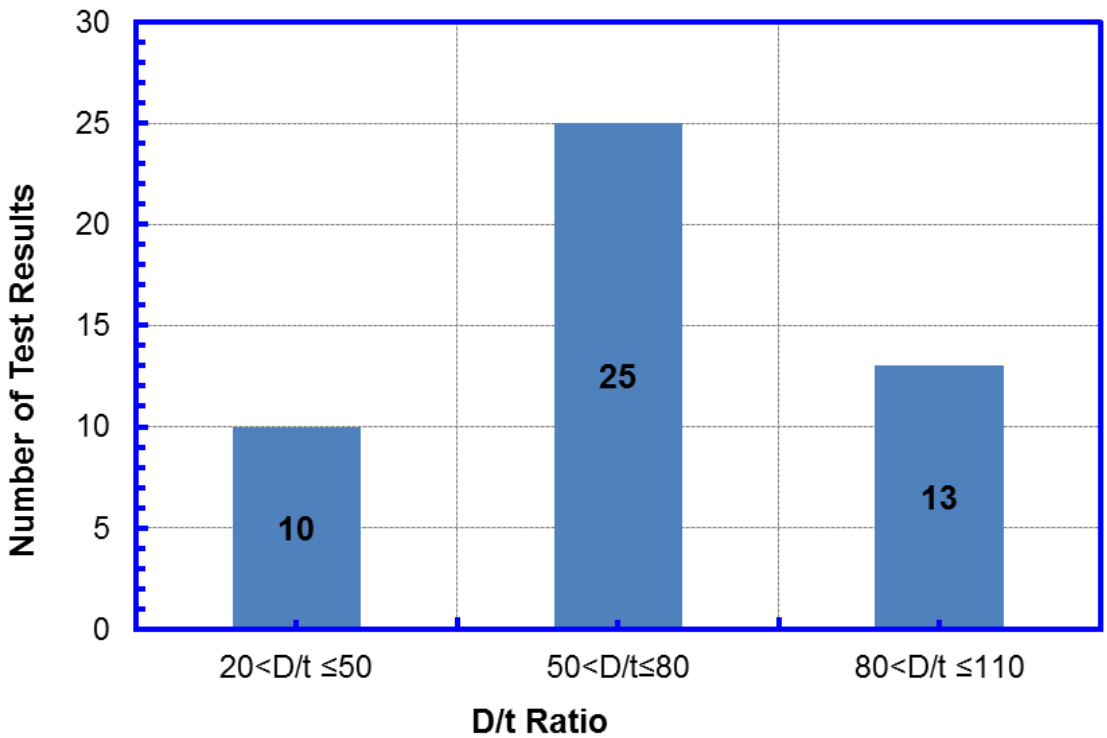

Figure 4-6 Distribution of test database over D/t ratio

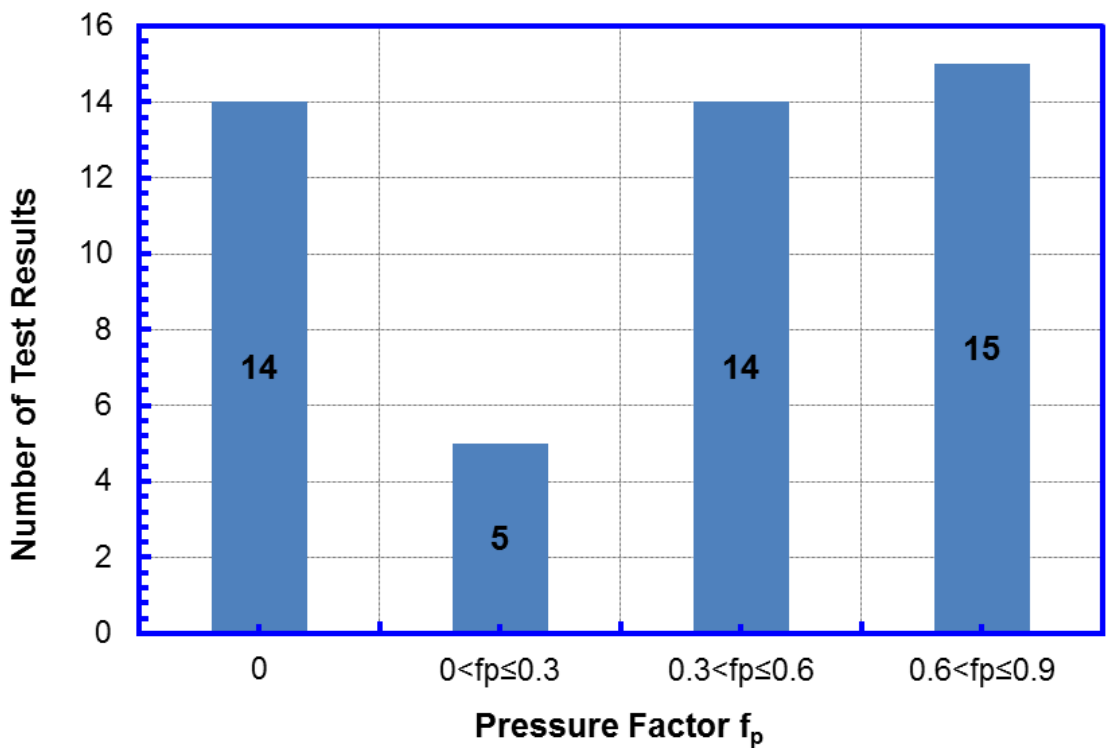

Figure 4-7 Distribution of test database over pressure factor

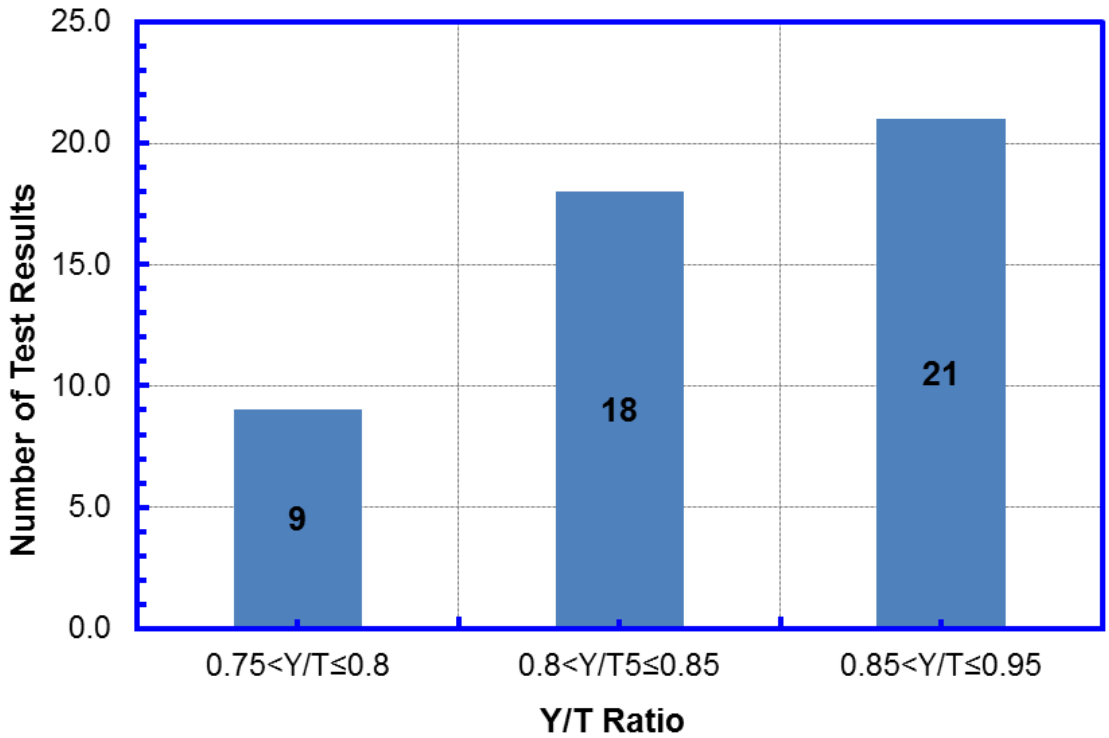

Figure 4-8 Distribution of test database over Y/T ratio

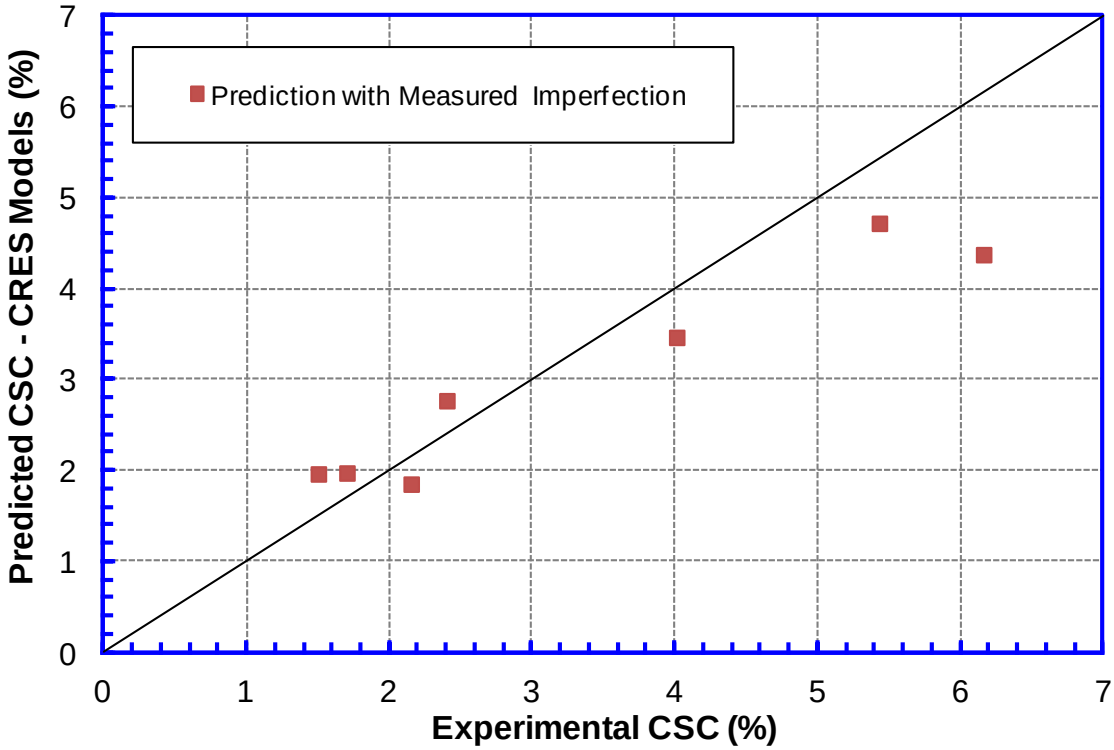

Figure 4-9 Comparison of predicted and measured CSC - with measured imperfections

4.6 Recommended Geometry Imperfections

To properly apply the newly developed compressive strain models (i.e., UOA and CRES), it is critical to have a reasonable estimation of the geometry imperfections if the actual data are not available. There exist very limited data on the geometry imperfections in the public domain. Figure 4-10 shows the geometry imperfections measured from the seven pipe specimens in Figure 4-9. All the imperfections are in the form of surface undulations. The data indicate that the height (from peak to valley) of the imperfections varies between 0.06%*D* and 0.14%*D* and 2%*t* and 8%*t*. It should be noted that all the seven pipe specimens are UOE pipes and it is not clear whether or not other types of pipes will have similar geometry imperfections. Considering the data are very limited and are from UOE pipes made in recent years, the range of the geometry imperfections in Figure 4-10 may not represent the actual range of the geometry imperfections. The size of the geometry imperfections is recommended as the following,

$$\text{Median } h_g = \max\,(0.13\%D, 8\%t),$$

$$\text{Lower Bound } h_g = \max\,(0.05\%D, 1\%t),$$

$$\text{Upper Bound } h_g = \max\,(0.2\%D, 15\%t).$$

The median imperfection height (h_g) is recommended to be the greater of 0.14%*D* and 8%*t*, i.e., the upper bound values observed in Figure 4-10. The lower bound height is the greater of 0.06%*D* and 2%*t*, i.e., the lower bound values observed in Figure 4-10. The upper bound height is determined by simply setting the median value in the middle of the upper and lower bound values. A very large girth weld high-low misalignment (up to 50% of wall thickness) is also considered in developing the upper bound imperfection.

The comparison between the experimentally measured CSC and the CSC predicted using the recommended median or measured (if available) geometry imperfections is shown in Figure 4-11 for the full database. It is seen that the predicted CSC using the recommended median geometry imperfections captures the trend of the overall experimental data very well.

The comparison between the experimentally measured CSC and the CSC predicted using the recommended lower bound and upper bound geometry imperfections is shown in Figure 4-12, and Figure 4-13, respectively.

The ratio between the experimentally measured CSC and the model predicted CSC was also calculated. If the ratio is greater than one, the prediction is conservative. The statistics of the calculated ratios of the full database are summarized in the following,

- Median imperfection: average = 0.99, standard deviation = 0.30
- Lower bound imperfection: average = 0.82, standard deviation = 0.26
- Upper bound imperfection: average = 1.18, standard deviation = 0.38

The average ratio calculated with the median imperfection is 0.99 with a standard deviation (SD) of 0.30. The recommended median imperfection provides fairly reasonable predictions of the testing results.

The average ratios calculated with the lower bound and upper bound imperfections are 0.82

(SD = 0.26) and 1.18 (SD = 0.38), respectively. Therefore, in general, reasonably conservative predictions can be obtained with the upper bound imperfections.

It is known that the predictions of the CSA models are often overly conservative. The CSC predicted by the CSA models is compared with the experimental data in Figure 4-14. It is seen that the CSA models provided conservative predictions for almost all the tests. The predictions seem to be overly conservative for most tests.

The predicted CSC by the CSA and CRES models (using the recommended upper bound geometry imperfections) is compared in Figure 4-15. From the comparisons shown in Figure 4-13 and Figure 4-15, it is seen that the CRES models with the upper bound imperfections can provide reasonably conservative predictions. The overly conservative predictions of the CSA models especially for those tests showing large CSC can be avoided.

4.7 Summary Remarks of the Refined Compressive Strain Models

The refined compressive strain models recognize the following parameters:

- Pipe *D*/*t* ratio;
- Internal pressure;
- Pipe Y/T ratio;
- Height (from peak to valley) of the surface undulation (geometry imperfections);
- Pipe uniform strain;
- Pipe Lüder's strain; and
- Net-section force (tension).

Compared with the other existing compressive strain models, the refined compressive strain models provide the following key improvements:

- The refined models are developed using a set of modeling procedures that provide realistic representation of field conditions;
- The refined models recognize an increased number of key controlling parameters compared with the existing models;
- The applicable range of each controlling parameter is extended or similar to the largest of the existing models;
- The effects of the pipe *D*/*t* ratio and internal pressure are more precisely captured than the existing models;
- Compressive strain capacity (CSC) can be greatly affected by geometry imperfections which are usually not available. Recommendations on median, lower, and upper bound geometry imperfections are provided. The upper bound geometry imperfections can produce reasonably conservative CSC for pipeline design. The median and upper/lower geometry imperfections can produce the realistic range of CSC for reliability based assessment.
- The effect of the girth weld, especially the effect of the high-low misalignment, is more properly accounted for than the existing models.

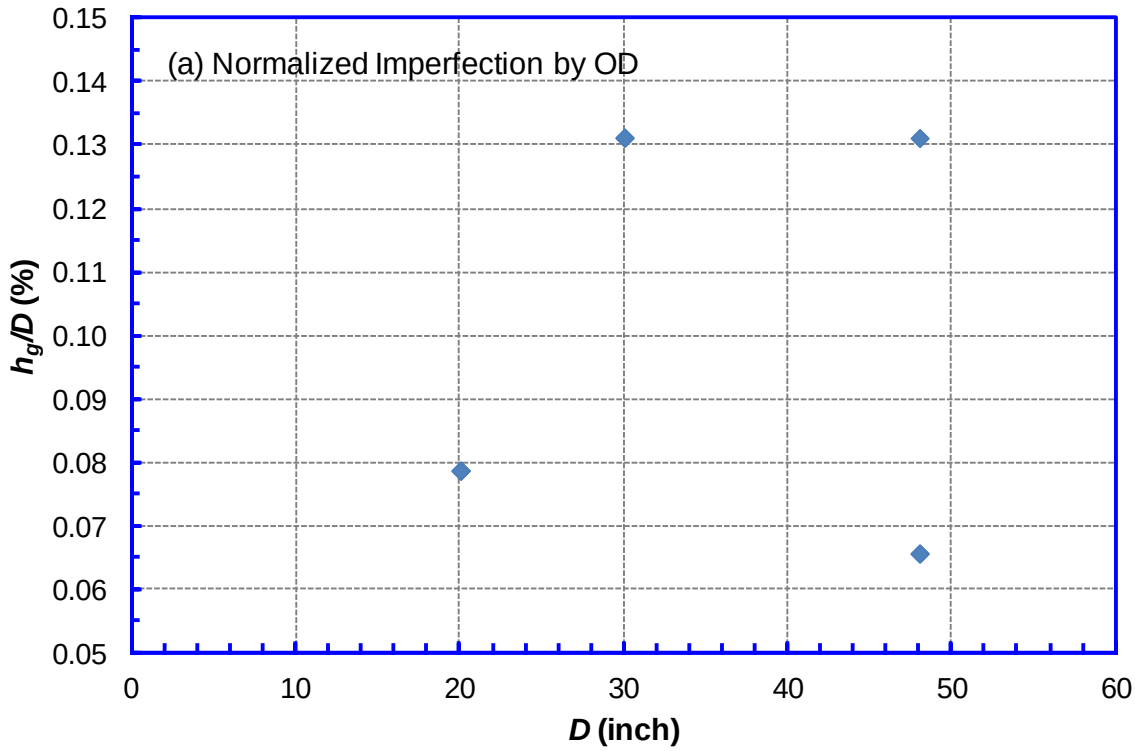

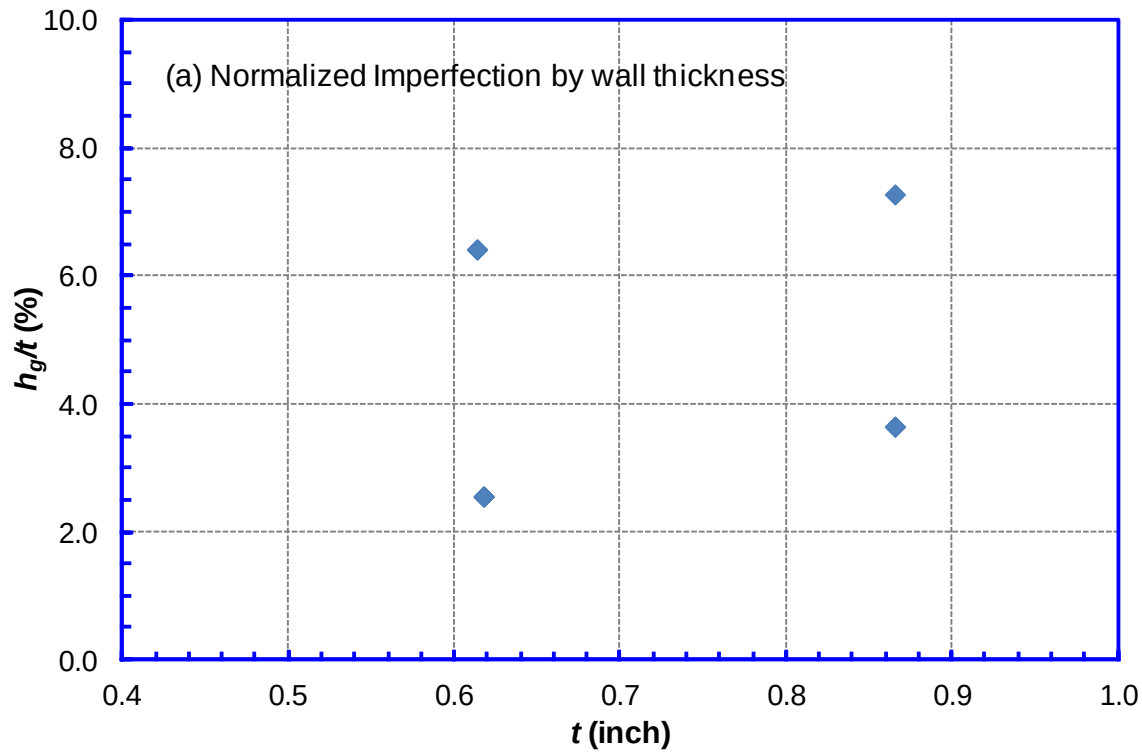

Figure 4-10 Measured geometry imperfections

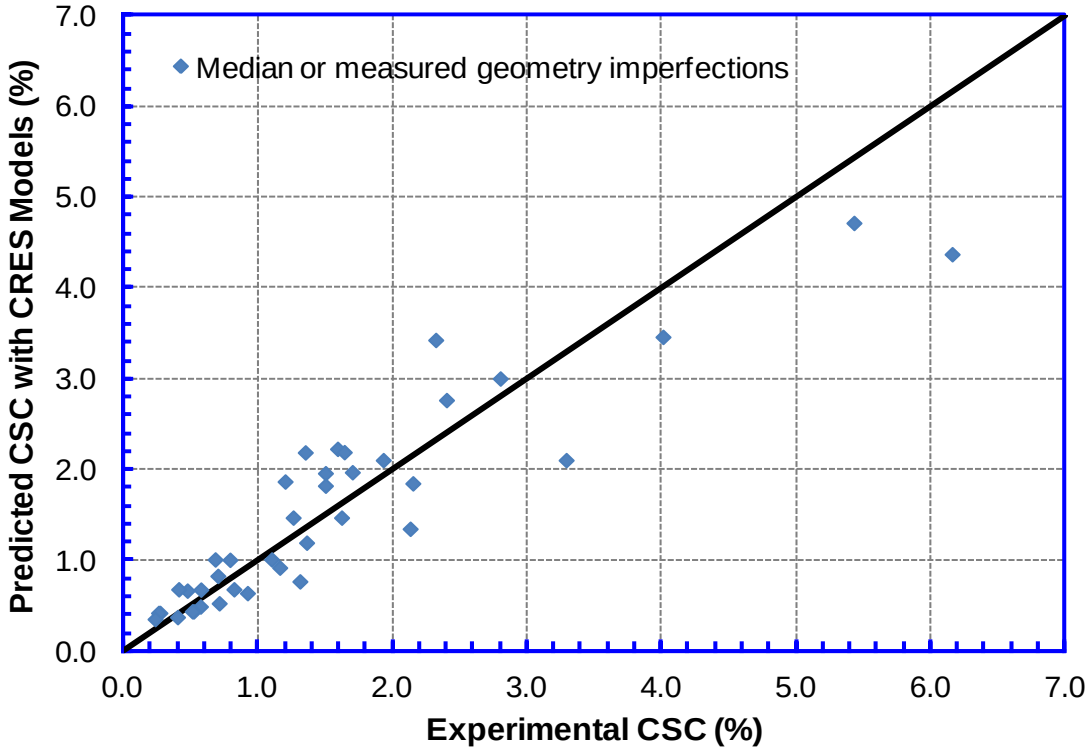

Figure 4-11 Comparison of experimentally measured CSC and predicted CSC from CRES models using median or measured imperfections (40 test data)

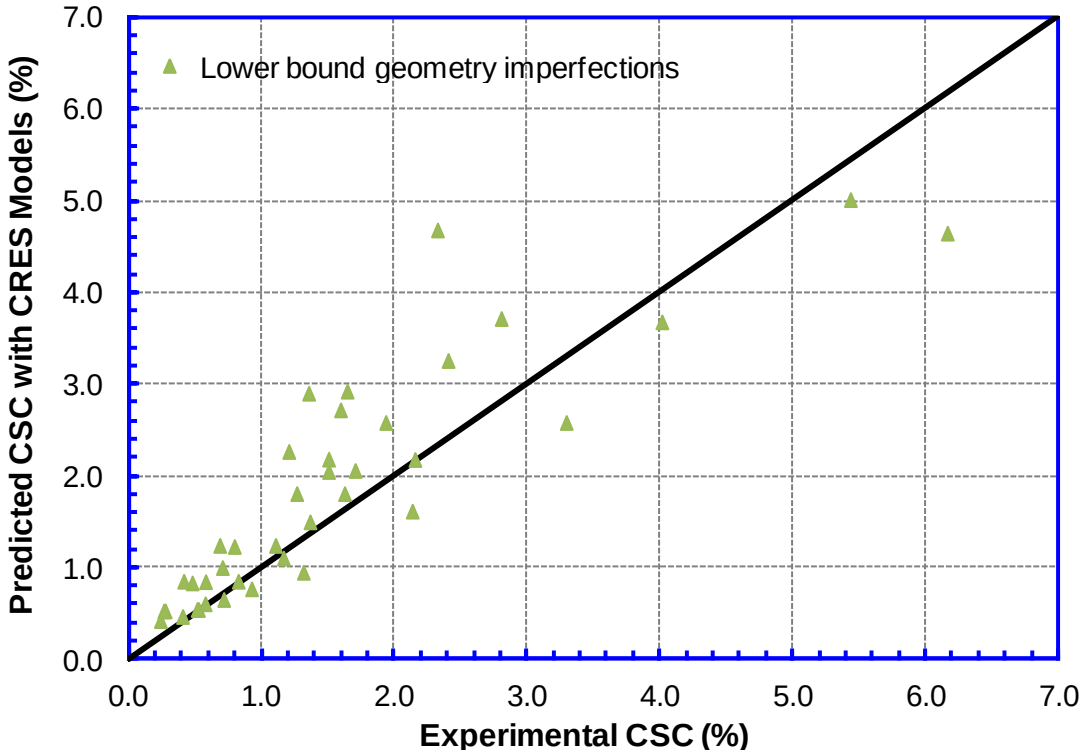

Figure 4-12 Comparison of experimentally measured CSC and predicted CSC from CRES models using lower bound imperfections (40 test data)

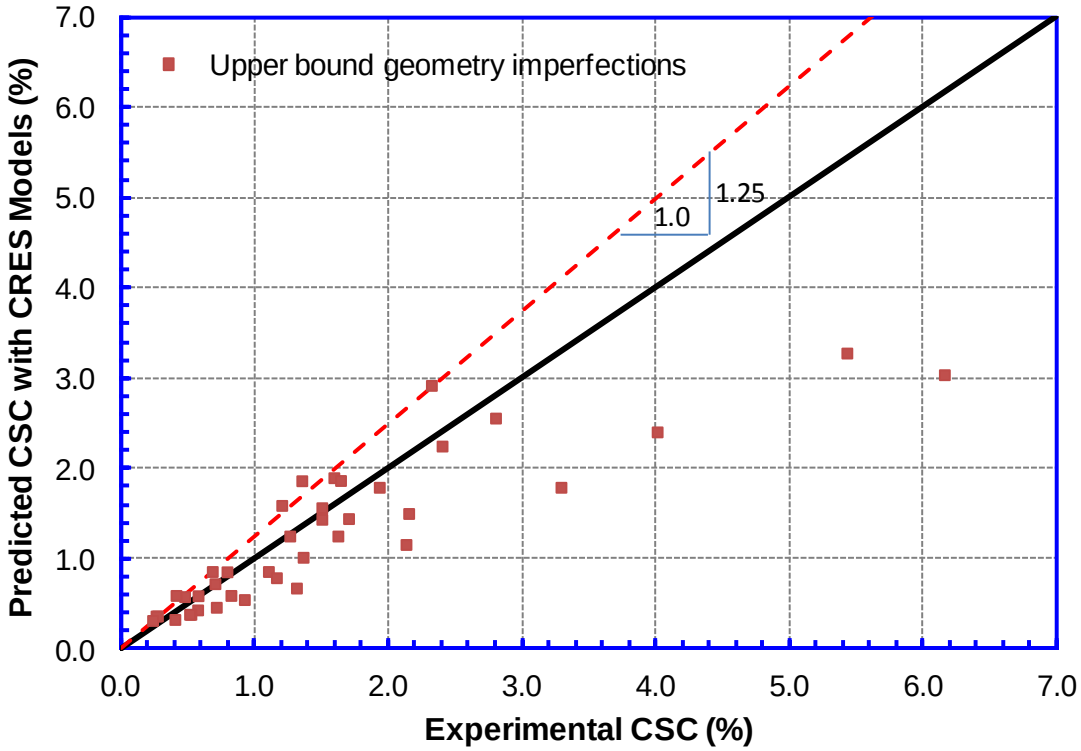

Figure 4-13 Comparison of experimentally measured CSC and predicted CSC from CRES models using upper bound imperfections (40 test data)

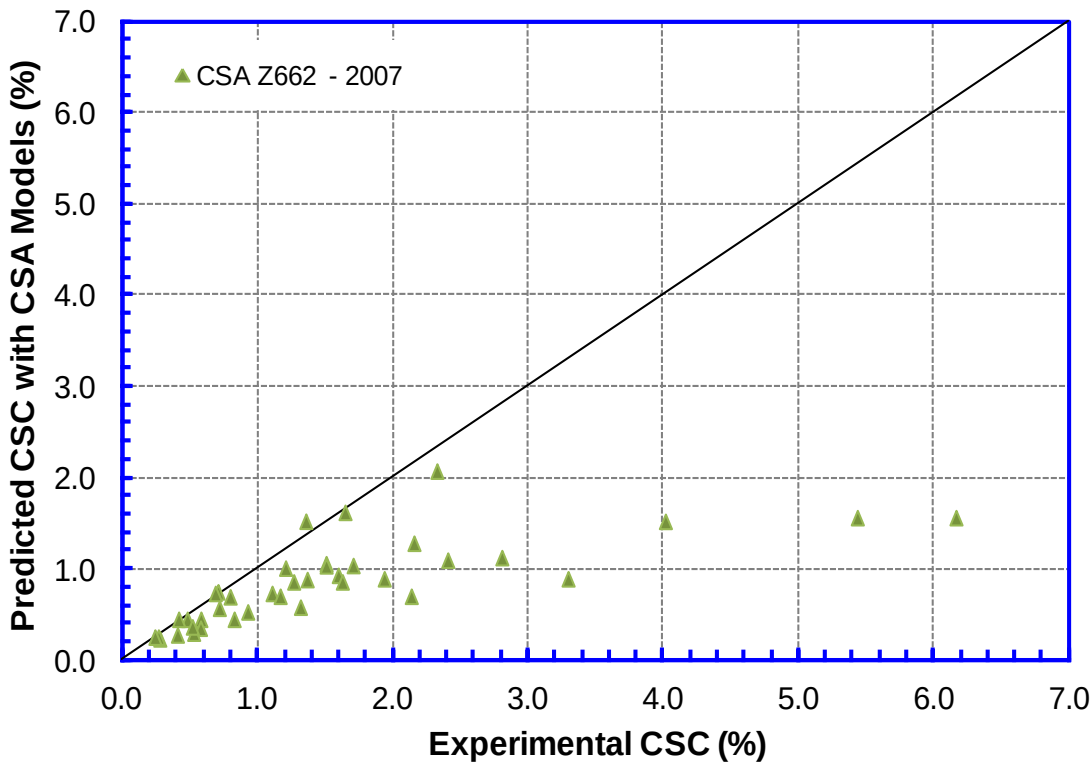

Figure 4-14 Comparison of experimentally measured CSC and predicted CSC from CSA models (40 test data)

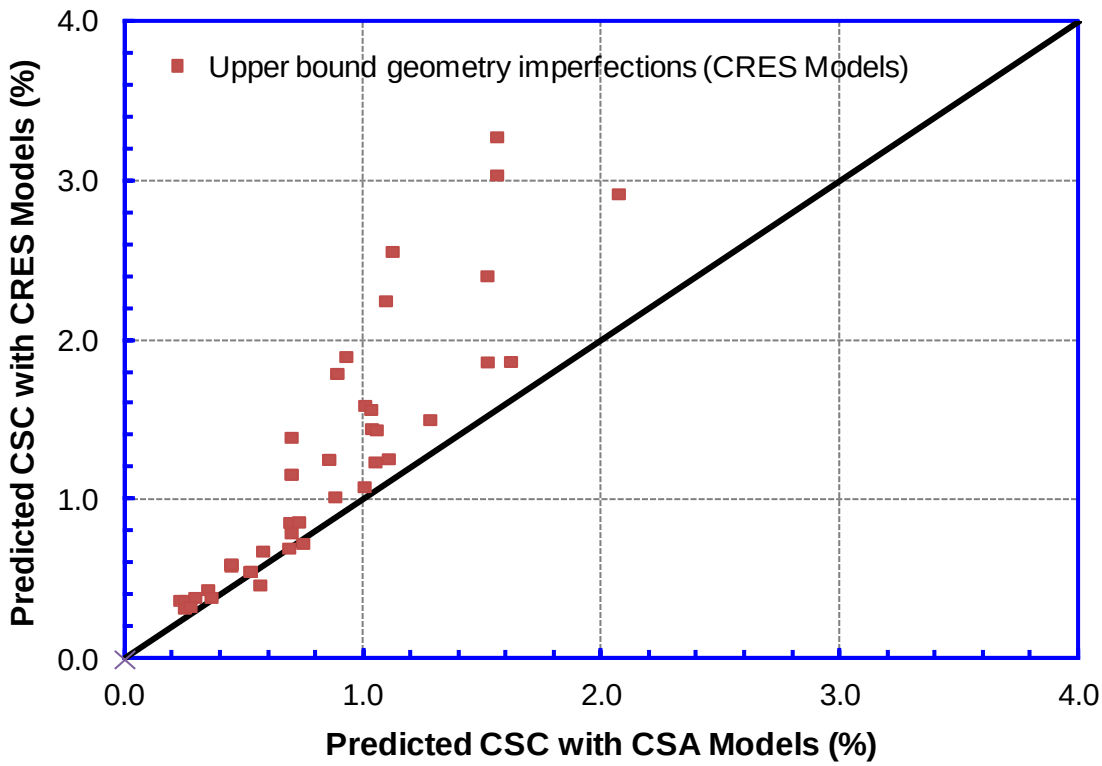

Figure 4-15 Comparison of predicted CSC with CRES models (using upper bound imperfections) and CSA models (40 test data)

5 Tensile Strain Models

5.1 Role of Tensile Strain Models

As described in Section 1.0, pipelines may fail by tensile rupture when they are subjected to tensile longitudinal strain. Girth welds are typically the weak link due to the existence of weld imperfections and less favorable material properties in the weld region than in pipe base materials. A few examples of girth weld rupture are shown in Figure 5-1. In some cases, gas may ignite at the ruptured girth welds, causing injuries and/or property damage as exemplified by the image in Figure 5-2.

Tensile strain models may be used in the design phase of a pipeline or in the integrity management of an existing pipeline. In the design phase, tensile strain models may be used for

- Setting linepipe specifications,
- Setting requirements for girth weld qualification,
- Helping the selection of field inspection procedures, and
- Determining flaw acceptance criteria.

For the integrity management of existing pipelines, tensile strain models may be used for

- Assessing the risk of tensile rupture,
- Facilitating the decision on mitigation options, and
- Determining the intervention threshold in allowable strain demand.

Figure 5-1 Sample of cases of girth weld rupture due to tensile longitudinal loading, and typically, existence of weld imperfections [42]

Figure 5-2 Girth weld rupture and resulting fire from a TV news report

Tensile strain models, when used appropriately, can be a powerful tool in the entire life cycle of pipelines.

5.2 Physical Process of Tensile Rupture

The physical process of a tensile strain failure starting from a planar girth weld flaw may be described as follows. Under increasing stress or strain, the flaw first blunts from the initial sharp flaw. The blunted flaw initiates ductile tearing upon further loading. The small ductile tear then grows in size, and eventually forms a growing flaw with a sharp tip. The initial blunted profile remains behind the sharp flaw. The evolution of the flaw profiles is shown in Figure 5-3.

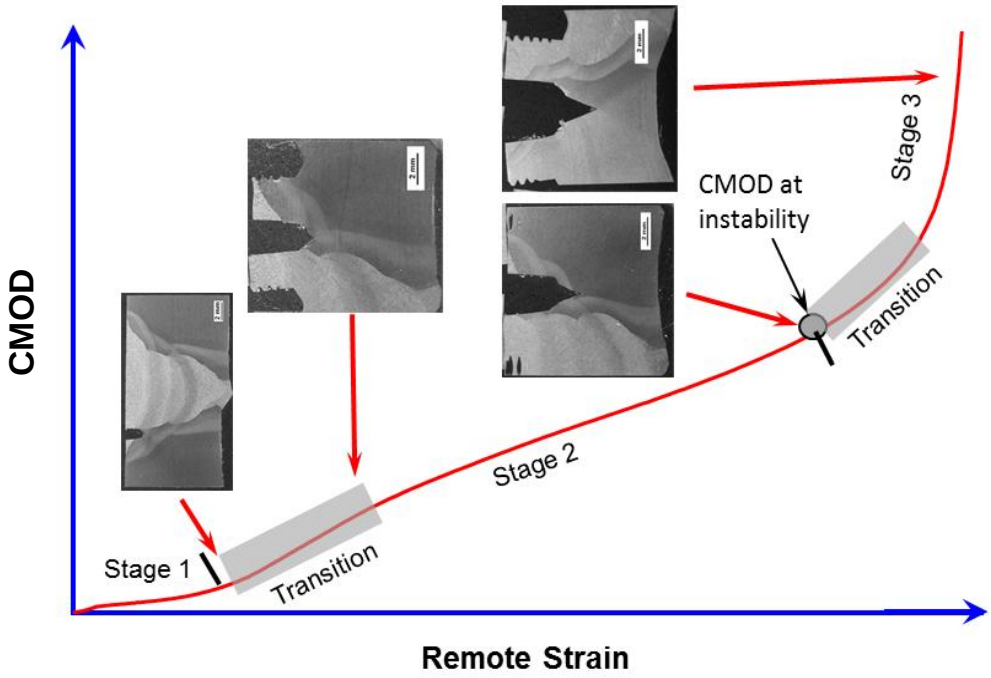

Figure 5-3 Evolution of a girth weld flaw under increasing longitudinal tensile strain

The importance of flaw growth is shown by the sequence of the growth relative to the tensile strain. The strain vs. flaw growth history of full-scale tests conducted by JFE is shown in Figure 5-4 [43]. It is evident that the strain at 0.02 in (0.5 mm) flaw growth is very close to the strain of leakage, whereas the amount of flaw growth at the point of leakage is much greater than 0.02 in (0.5 mm). However most of the growth occurs near the final leakage point accompanied by a small increase of remote strain. *This and other similar tests have shown that once a flaw growth rate starts to accelerate, the remaining additional strain capacity is limited. Much of the strain capacity comes from the straining process prior to the flaw growth. Therefore setting initiation as the limit state for strain capacity is physically sound and accurate in representing material's strain capacity*.

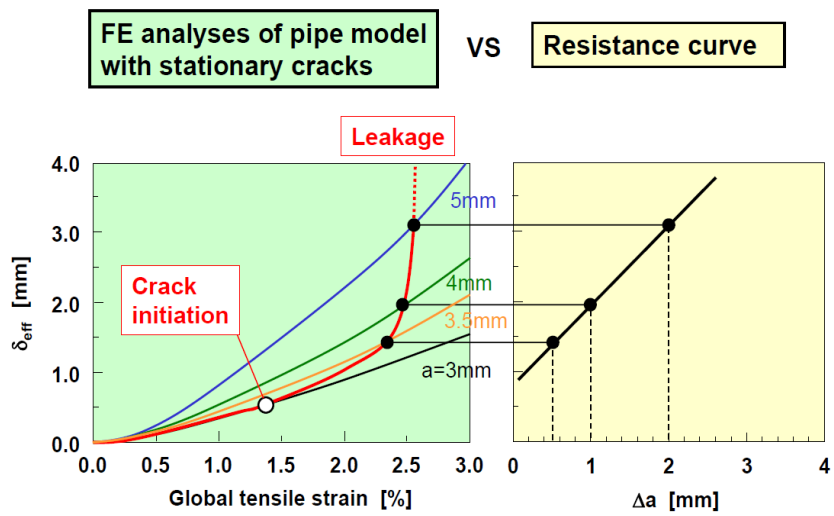

Figure 5-4: Flaw growth vs. strain history from full-scale pipe tests

5.3 Key Elements of Tensile Strain Design

Tensile strain design consists of three interdependent key elements:

- Linepipe specifications / qualification,
- Girth weld specifications / qualification, and
- Tensile strain models.

The first two elements, linepipe specifications/qualification and girth weld specifications/qualification, are covered in Section 7. Tensile strain models are covered in this section.

5.4 Tensile Strain Models

The tensile strain capacity of a pipeline is controlled by the tensile strain capacity of its girth welds. The girth welds here refer to the entire weld region, including the weld metal, fusion boundary, and the heat-affected zone (HAZ). Girth welds tend to be the weakest link due to the possible existence of weld defects and often deteriorative metallurgical and/or mechanical property changes from welding thermal cycles. Consequently, tensile strain capacity (TSC) is intrinsically related to the girth welding procedure qualification and flaw acceptance criteria. The welding procedure qualification involves the control of essential variables to ensure the

equivalence of procedure qualification welds and field production welds, and the definition and execution of mechanical tests of welds. The flaw acceptance criteria are implemented for field production welds to ensure a certain level of performance is achieved with respect to overall TSC.

Some of the earliest work specifically targeted to develop assessment procedures for strain-based design was supported by PRCI. The tensile limit state was formulated around the concept of crack driving force (demand) and apparent toughness (capacity) [44,45,46,47,48]. This approach was subsequently adopted in Annex C of CSA Z662 2007 Edition [49].

Considerable efforts have been devoted to the development of tensile strain design models worldwide in the recent years [1,2,3]. A number of tensile strain models are at various stages of development and maturity. They include the relatively new models from the University of Gent [50] and TWI [51], and more established models from PRCI [44,45,46,47,52], SINTEF [2,53,54], ExxonMobil [3,55,56,57,58], and JFE [59,60,61]. The PRCI models have undergone a major update (which are named the second generation models, i.e., PRCI-CRES models) and are fully documented in two comprehensive reports to PHMSA [4,5] and in conference publications [32,33,34,62,63]. The PRCI-CRES models have been shown to provide consistent trends with experimental test data for pipe grades including X56, X65, X80, and X100. The models have been used in the design and construction of X70 and X80 large-diameter pipelines in areas of mine subsidence [64,65].

5.4.1 PRCI-CRES Models

5.4.1.1 Development process

The development of the PRCI-CRES models involved a multi-discipline approach that fully utilized the distinctive capabilities of experimental techniques and modern computational mechanics. The overall development process is schematically illustrated in Figure 5-5. Some of the key steps are as follows:

- Develop pipe specifications based on the best understand at the time. The main criteria were the range of Y/T ratios and sufficient ductility of the material.
- Select welding procedures with the primary goal of having appropriate weld metals that provided desired levels of weld strength mismatch.
- Conduct initial numerical analysis to determine (a) spacing of the girth welds in full-scale test specimens, (b) spacing of multiple flaws in a single girth weld, (c) appropriate size of flaws to be installed in the girth welds, and (d) the instrumentation plans for full-scale and curved-wide plate tests.
- Conduct large-scale tests.
- Perform post-test physical examination of the large-scale test specimens.
- Develop second generation models that include a list of key parameters to account for the factors affecting the tensile strain capacity.
- Evaluate the second generation models against experimental test data.
- Formulate guidance for tensile strain design.

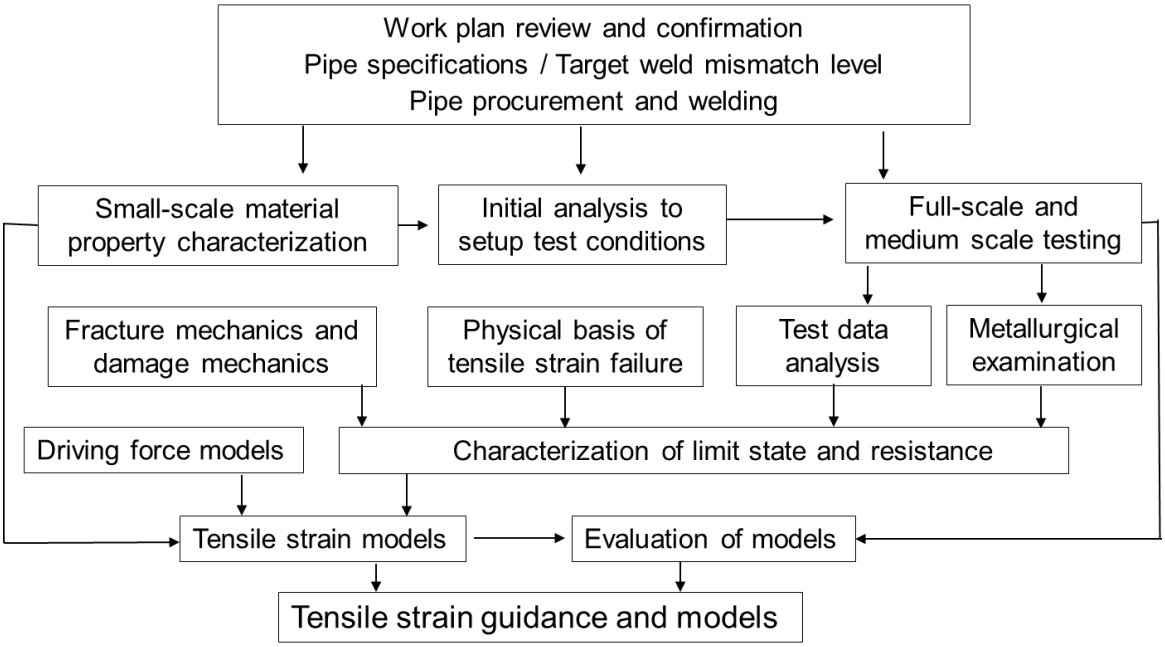

Figure 5-5 Schematic illustration of the development process of the PRCI-CRES tensile strain models

5.4.1.2 Failure Modes and Limit States

5.4.1.2.1 *Limit State Based on Initiation Control*

The initiation-based tensile limit state is defined as $CTOD_F = CTOD_A$, where $CTOD_F$ is the crack-driving force and $CTOD_A$ (or δ_A) is the apparent toughness. The apparent toughness is the toughness corresponding to the onset of stable tearing. Both $CTOD_F$ and $CTOD_A$ are represented by the crack tip opening displacement, i.e., CTOD.

5.4.1.2.2 *Limit State Based on Ductile Instability*

The limit state is defined as the tangent point of the crack driving force curve and the fracture toughness curve. Both curves are represented in the form of toughness versus flaw size.

5.4.1.3 Structure of PRCI-CRES Models

The PRCI-CRES models are organized in four levels as shown in Figure 5-6.

Level 1 – Initial Screening and Feasibility Studies

The Level 1 model is intended for quick estimations of the likely tensile strain capacity. The TSC is tabulated for selected pipe dimensions, material properties, and flaw size. The apparent toughness is estimated from upper shelf Charpy impact energy.

Level 2 – Nominal Assessment with Standard Toughness Data

The Level 2 models are given in a library of parametric equations. The apparent toughness can be estimated from either upper shelf Charpy impact energy or the upper shelf standard CTOD toughness.

Level 3 – Advanced Assessment with Low-Constraint Toughness

The Level 3 models have two options. Level 3a uses an initiation control limit state. Level

3b uses a ductile instability limit state. In Level 3a, the TSC is obtained by the use of the same library of parametric equations as in Level 2. The apparent toughness may be obtained by a number of low constraint test options, including shallow-notched SE(B), SE(T), or CWP. In Level 3b, the crack driving force is expressed as a function of remote strain and flaw depth using the parametric equations of Level 2. At the same time, material's resistance is expressed as a function of flaw depth, i.e., customary resistance curve. These two relationships are solved at the point of (1) the same flaw growth and (2) cracking driving force being the same as material's resistance. The strain corresponding to this point is the strain of ductile instability.

Level 4 Models – Advanced Analysis with Direct FEA Calculation

The Level4 models are structured with two limit state options. In contrast to Level 3 models, where the driving force relations are expressed in parametric equations, the driving force relations are directly obtained from FEA in this level. The toughness options are the same as in Level 3. This level allows for special cases when the specific weld geometry and material property conditions do not allow the use of the first three options. The Level 4 models should only be exercised by seasoned experts.

Level	Limit State	Target Application	Format of Models	Toughness Option
I	Initiation	Initial screening, feasibility study	Tabular	Upper shelf Charpy energy
2	Initiation	Nominal analysis	Equations	Upper shelf Charpy energy, CTOD or J from SENB
3a	Initiation	Advanced analysis	Equations	Single value CTOD or J from shallow-notched SENB, SENT, or CWP
				CTOD or J resistance curves from shallow-notched SENB, SENT, or CWP
3b	Ductile instability	Advanced analysis	Equations	CTOD or J resistance curves from shallow-notched SENB, SENT, or CWP
4a	Initiation	Case specific-analysis	Expert finite element analysis	Single value CTOD or J from shallow-notched SENB, SENT, or CWP
				CTOD or J resistance curves from shallow-notched SENB, SENT, or CWP
4b	Ductile instability	Advanced analysis	Expert finite element analysis	CTOD or J resistance curves from shallow-notched SENB, SENT, or CWP

Figure 5-6 Overall structure of the PRCI-CRES tensile strain models

5.4.1.4 Input Parameters of TSC Equations

Although the case-specific finite element analysis is an option in Level 4 of the PRCI-CRES models, the most valuable part of the models is the library of parametric equations which give the tensile strain capacity as a function of input parameters. The other advantage of the PRCI-CRES models is that multiple forms of toughness data may be used, including

- Charpy impact,
- Standards three-point bend CTOD,
- Shallow-notched three-point bend CTOD,

- SENT (single edge notched tension), and
- CWP (curved wide plate).

The images of some toughness test options are given in Figure 5-7. The input parameters for the computation of tensile strain capacity are given in Table 5-1.

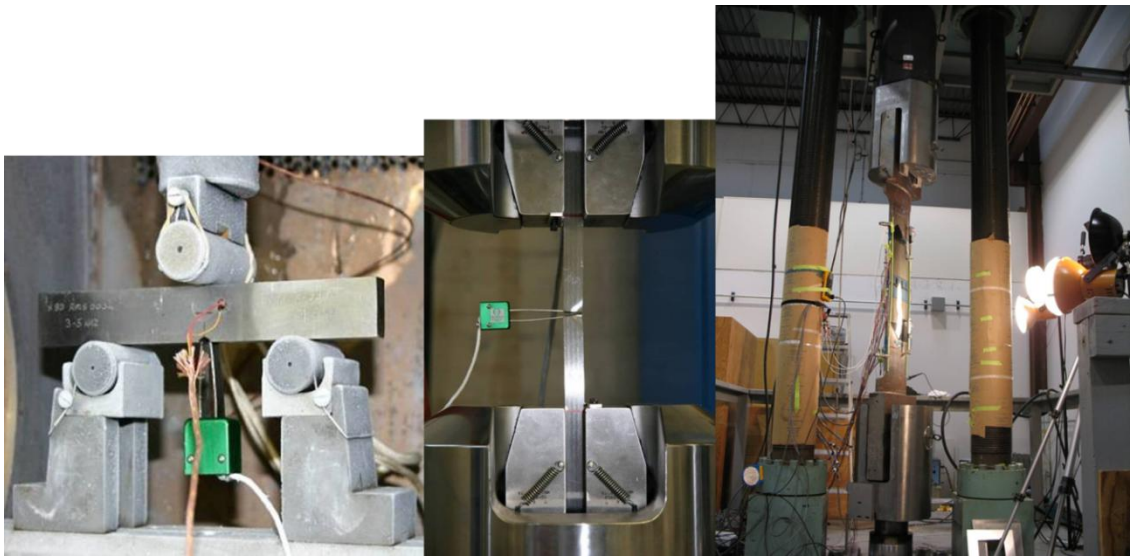

Figure 5-7 Images of various toughness test options that may be exercised to apply the PRCI-CRES tensile strain models. Left: standard three-point bend CTOD; Middle: SENT; and Right: CWP

Table 5-1: List of input parameters to the CRES TSC equations

Parameters	Unit	Description
OD	mm	Pipe outside diameter
t	mm	Pipe wall thickness
a	mm	Initial flaw height
$2c$	mm	Initial flaw length
h	mm	Misalignment at girth weld
σ_y	MPa	Yield strength of base metal at 0.5% total elongation strain
σ_u	MPa	Ultimate tensile strength of base metal
σ_u^W	MPa	Ultimate tensile strength of girth weld
δ_A	mm	Apparent toughness $CTOD_A$
p_i	MPa	Internal pressure
$\eta = a/t$		Normalized flaw depth
$\beta = 2c/t$		Normalized flaw length
$\psi = h/t$		Normalized misalignment at girth weld
$\xi = \sigma_y / \sigma_u$		Ratio of yield strength to tensile strength of base metal
$\phi = \sigma_u^W / \sigma_u$		Weld strength mismatch ratio
f_p		Internal pressure factor (the ratio of hoop stress to yield strength of base metal)

5.4.1.5 Sample Applications

The PRCI-CRES tensile strain models are very versatile. They may be used to estimate the tensile strain capacity (TSC) for a given set of conditions as shown in Figure 5-8. One of the major applications is the development of flaw acceptance criteria for field girth welding as shown in Figure 5-9. The models may also be used to play "what-if" scenarios to meet the same target level of TSC as shown in Figure 5-10. For instance, a balance approach between weld toughness and strength mismatch may be developed against practical limits of welding processes and realistically-achievable material properties.

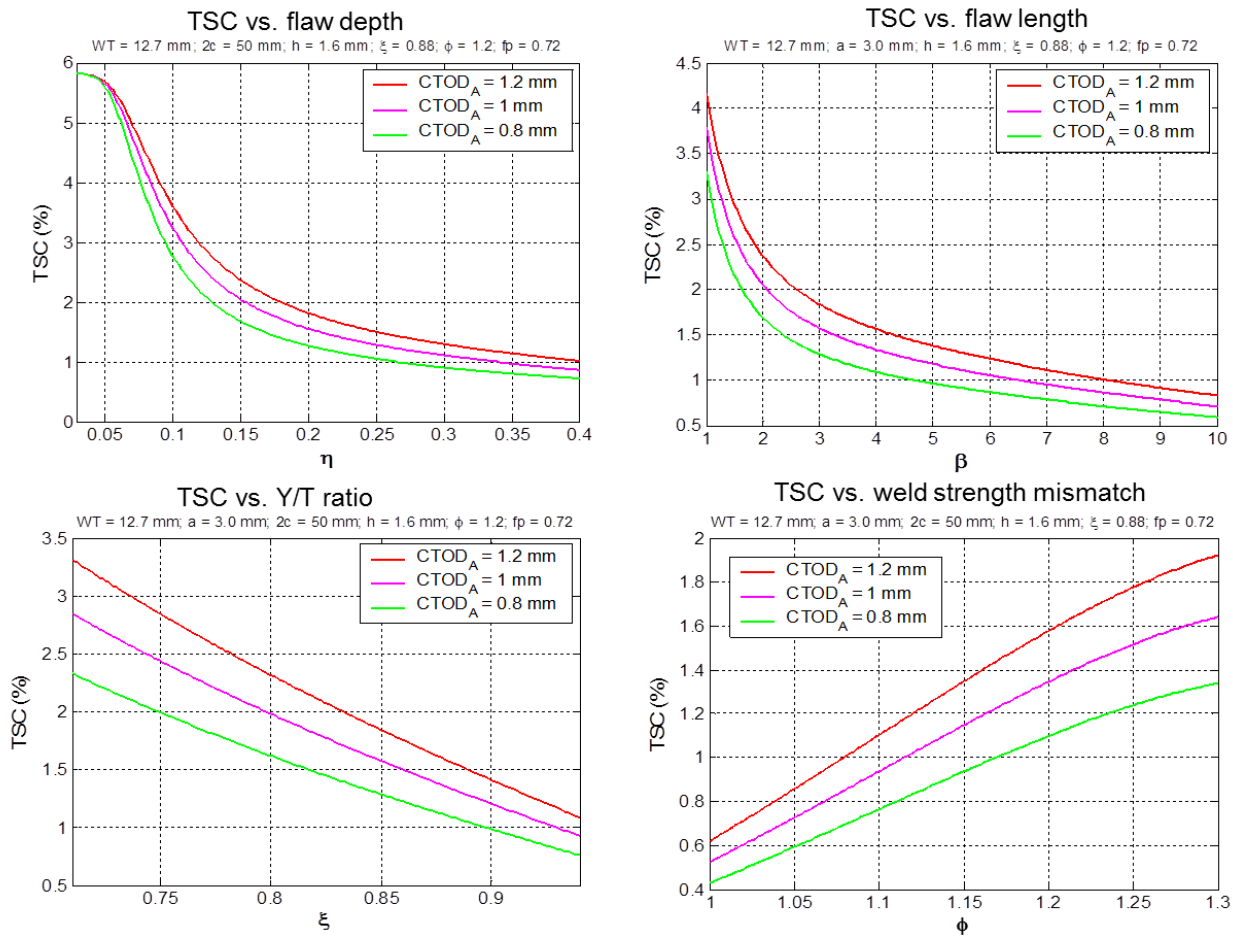

Figure 5-8 Sample applications of the PRCI-CRES tensile strain models in the form of tensile strain capacity (TSC) vs. various physical parameters

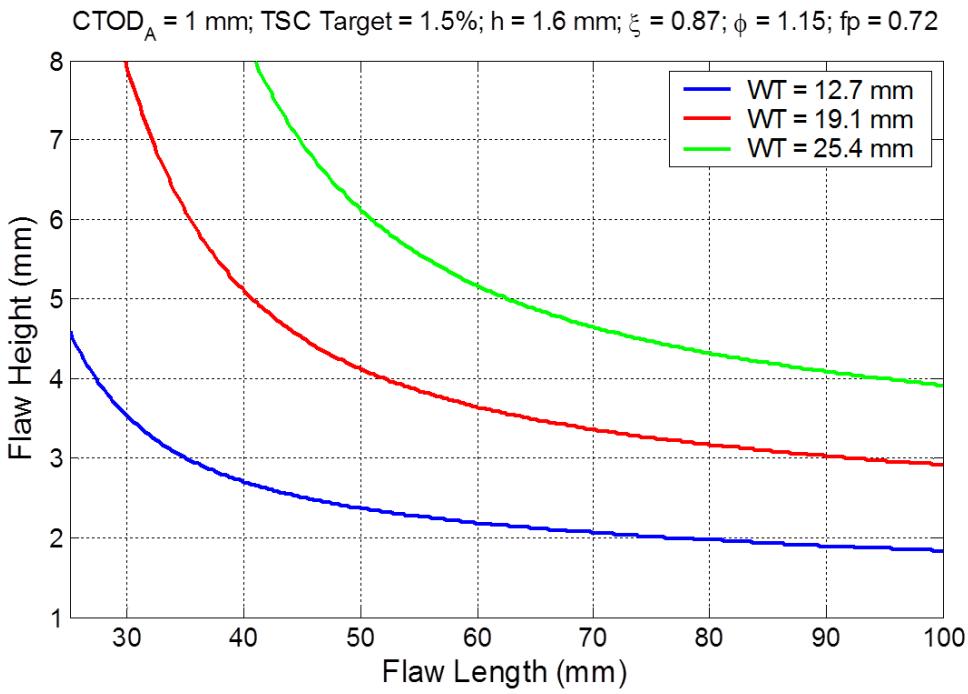

Figure 5-9 Sample applications of the PRCI-CRES tensile strain models in the form of flaw acceptance criteria with a target tensile strain capacity (TSC) of 1.5%

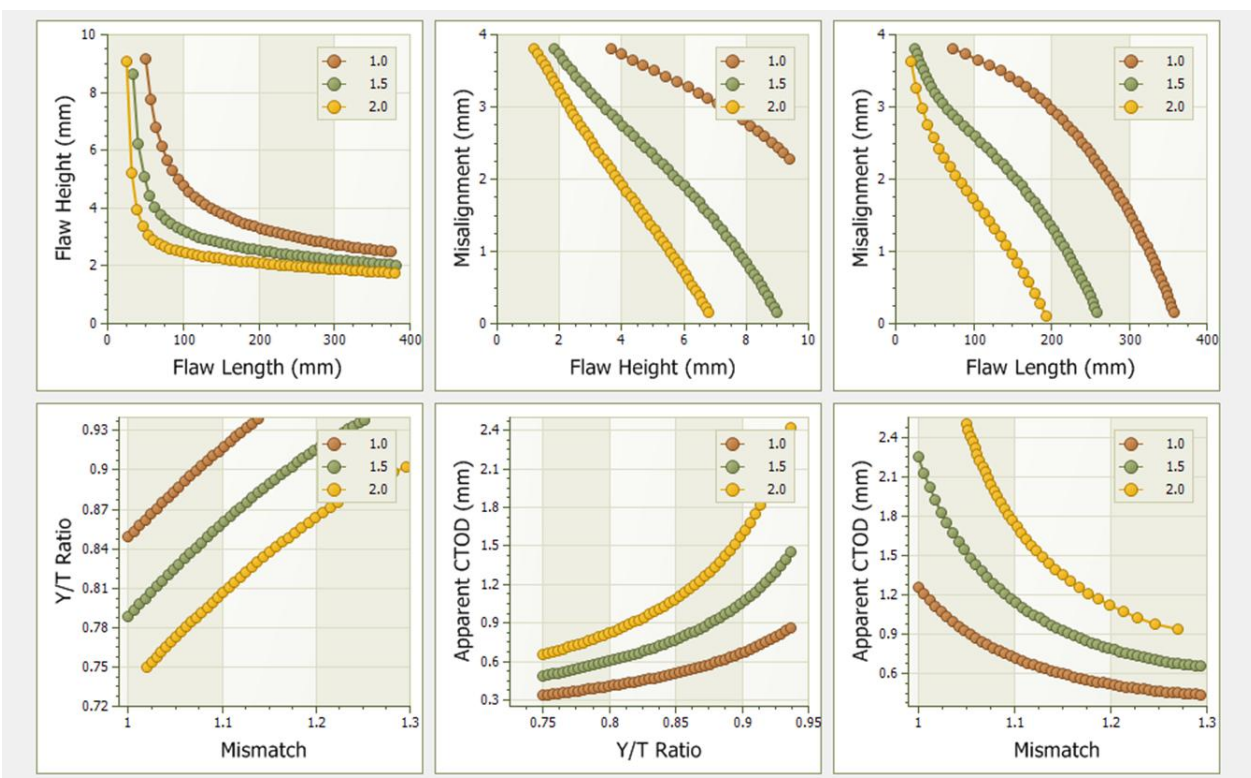

Figure 5-10 Sample applications of the PRCI-CRES tensile strain models at various levels of target tensile strain capacity (TSC)

5.4.2 Other Tensile Strain Models

5.4.2.1 Ductile Instability Approach

The ductile instability approach establishes a limit state at which point the driving force is in equilibrium with material's resistance. The effects of flaw growth on the driving force and resistance are explicitly accounted for. The crack driving force, in terms of CTOD or *J*-integral, is derived from finite element analysis for various structural geometries (including flaw size) and material properties. The resistance curve (*R*-curve) is directly measured from test specimens. The failure point or the unstable ductile tearing point is determined by the traditional tangency criteria (discussed in 5.4.1.2.2). Models from SINTEF [2,53,54] and ExxonMobil [3,55,56,57] utilize the ductile instability approach.

5.4.2.2 Osaka University and JFE Approach

The Osaka/JFE approach relies on the failure loci relating the stress triaxiality and equivalent plastic strain at a crack tip. The so-called two-parameter approach has been applied to a wide variety of fracture mechanics applications [66,67]. Igi and Suzuki applied this methodology for the prediction of tensile strain limit of X80 pipes [59]. The SENT and CWP specimens were tested to establish the failure loci. Igi and Suzuki demonstrated the effects of internal pressure and Y/T on tensile strain limits using this method. The reduction of tensile strain limits were shown to be a factor of 1.8 for low Y/T material (Y/T=0.76) and over 5.0 for high Y/T material (Y/T=0.95).

5.5 Summary Remarks about Tensile Strain Models

The essential features of the PRCI-CRES tensile strain models are as follows:

(1) Two limits states are recognized: (1) initiation control and (2) ductile instability.

(2) Two weld bevel geometries are recognized: (a) narrow-groove, typical of mechanized GMAW welds and (b) standard groove, typical of FCAW and SMAW welds.

(3) There are no inherent limits on pipe grade. The pipe tensile properties are represented by its longitudinal Y/T ratio, which serves as a representation of pipe's strain hardening capacity.

(4) The weld should not have gross strength undermatching.

(5) The target optimum strain range of the models is from 1.0% to one half of the pipe's uniform elongation. The stress-strain curves beyond one half of the pipe's uniform elongation can be very flat, particularly those of some modern microalloyed steels. As a result, remote strains of very different values produce essentially the same stress states at the girth welds. Therefore determining the precise remote strain values when the stress-strain curves become very flat is very difficult.

(6) The models are applicable to one single flaw in a girth weld. If multiple flaws were to exist in a single girth weld, the flaws need to be sufficiently far apart, so that the existence of other flaws does not affect the behavior of the flaw being evaluated.

(7) No flaw interaction rules are established and applied in the models.

(8) No embedded safety factor is applied or implied.

(9) The models should not be used for flaw acceptance after repair welding without further evaluation.

(10) The potential impact of material anisotropy on the tensile strain capacity is not considered in the models.

The fundamental basis of the tensile strain models does not assume or rely on material property data of any particular grade. The parametric representations of the tensile properties of the pipes and welds were developed using a material database which covered grades from X65 to X100. The tensile strain design models are, in principle, applicable to all GMAW and FCAW/SMAW processes, provided that appropriate mechanical property data are within the applicable range of the models.

The major advantage of the PRCI-CRES models are the flexibility in toughness option and the inclusion of both initiation and ductile instability limit states. In contrast, models that only recognize ductile instability, such as the ExxonMobil models, rely solely on the availability of resistance curves. When applying the tensile strain models to existing pipelines, resistance curves are generally not available. Furthermore, obtaining resistance curves of girth welds of thin-walled pipes (e.g., wall thickness ≤ 3/8 inch), which many onshore transmission pipelines fall under, can be difficult. The relative advantage of initiation vs. ductile instability limit states is discussed in Section 9.

6 A Ranking System for Strain-Based Design

6.1 Basis of the Ranking System

In Section 4, the new refined compressive strain models (termed CRES compressive strain models) developed in this project were fully described. In Section 5 the key features of the PRCI-CRES tensile strain models were reviewed. The development of these tensile and compressive strain models involved in-depth numerical analysis using fundamental mechanics principles. The models are further evaluated against experimental test data.

The input parameters of the tensile and compressive strain models, which essentially represent the features those models are capable of considering, are shown in Table 6-1. It is evident from the list that, with the development of the new compressive strain models, key geometric, material, and operational parameter can be evaluated on a consistent basis with the similar level of refinement. These models are used in a ranking system by which the criticality of the tensile and compressive limit states is ranked for a given set of geometric, material, and operational conditions. Similarly the same ranking system may be used to achieve balanced safety margin against both possible tensile and compressive failures.

Table 6-1 Input parameters of the PRCI-CRES tensile strain models and the CRES compressive strain models

Parameters		PRCI/CRES TSC Models	CRES CSC Models
Geometry	Outside Diameter	Considered	Input Para.
	Wall Thickness	Input Para.	Input Para.
Material Properties	Pipe Yield Strength	Input Para.	Input Para.
	Pipe Tensile Strength	Input Para.	Input Para.
	Weld Tensile Strength	Input Para.	Considered
	Girth Weld Toughness	Input Para.	Not Relevant
Flaws / Imperfections	Girth Weld Flaw Depth	Input Para.	Not Relevant
	Girth Weld Flaw Length	Input Para.	Not Relevant
	Weld High-Low Misalignment	Input Para.	Considered
	Pipe Geometric Imperfections	Not Relevant	Input Para.
Pressure	Pressure	Input Para.	Input Para.
Other Features	Weld Type	Input Para.	Not Relevant

The parameters marked "considered" mean that the effect of the parameters is found to be secondary through detailed sensitivity studies. These parameters are excluded in further model development. Consequently they are not part of the parameters in the final tensile and compressive strain models.

6.2 Structure and Function of the Ranking System

A ranking system for evaluating the tensile (TSC) and compressive strain capacity (CSC) of a pipeline is established based on the tensile and compressive strain models. The structure of the ranking system is shown in Figure 6-1. The inputs to the ranking system are the pipe and weld properties and the strain demands. The core of the ranking system is the tensile and compressive

strain models given in Sections 5 and 4, respectively. The output of the ranking system includes:

(1) the critical limit state (tensile rupture vs. compressive buckling) of the pipeline for the given strain demands;

(2) the optimized pipeline design with balanced safety margin for both TSC and CSC.

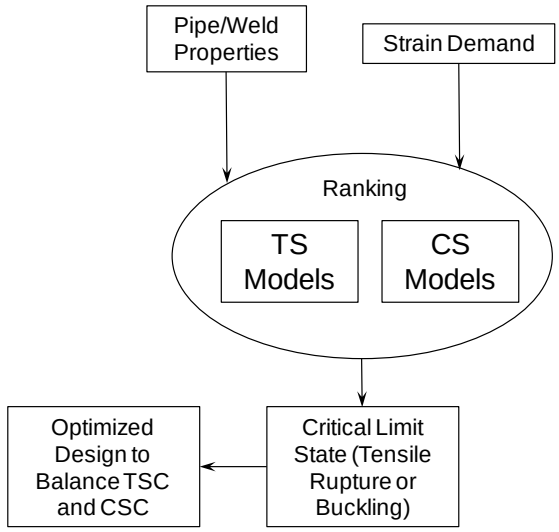

Figure 6-1 Structure of the ranking system

6.3 Sample Application of the Ranking System

A sample application of the ranking systems is introduced in this section. The preliminary design parameters of the pipeline are given in the following:

- Strain demands: tensile and compressive strains 0.75%
- Pipeline parameters
  - Materials: X80, YS = 85 ksi, Y/T = 0.90;
  - Pipe OD and wall thickness: D = 48 inch; t = 0.75 in (19.1 mm);
- Weld parameters
  - Minimum strength mismatch ratio (OM): ϕ = 1.25;
  - Allowable high-low misalignment: h_m = 1/16 in (1.6 mm);
  - Minimum apparent toughness: δ_A = 0.047 in (1.2 mm);
- Girth weld flaws and pipe geometry imperfections
  - Flaw depth: a = 0.12 in (3.0 mm);
  - Flaw length: $2c$ = 2.0 in (50.0 mm); and
  - Pipe geometry imperfection: h_g = 15%t;
- Pressure factor: f_p = 0.72

The tensile rupture and compressive buckling typically cause different consequences to the pipeline. The tensile rupture is considered to be an ultimate limit state, i.e., an immediate threat to the pressure integrity. The compressive buckling is usually considered to be a serviceability

limit state which does not show immediate threat to the pressure integrity.

The evaluation of the tensile and compressive experimental results indicates that the tensile and compressive strain capacity has different levels of uncertainties. The tensile tests often show larger testing scatters than the compressive tests.

As a result, different safety factors for the tensile and compressive strain models should be used. The safety factors and corresponding target strain capacity (i.e., multiplying the safety factors to the strain demands) are given in the following:

- Safety factors: tension - 2.0; compression - 1.2[1];
- Target strain capacity: TSC = 1.5%, CSC = 0.9%.

The TSC and CSC calculated using the tensile and compressive strain models with those preliminary design parameters are shown in Figure 6-2 for various pressure factors. The TSC decreases with the increase of the pressure factor, while the CSC increases with the increase of the pressure factor. The minimum TSC is about 2.5% for pressure factors greater than 0.6. The minimum CSC is about 0.6% for no pressure condition. Therefore, using the preliminary design parameters, the target TSC (1.5%) is satisfied, but the target CSC (0.9%) is not.

The target CSC can be satisfied by increasing the wall thickness to 1.0 inch (25.4 mm) as shown in Figure 6-3. But in the same time, the minimum TSC will be increased to 3.3% which is much higher than the target TSC. Although the design requirement is satisfied, the high TSC, therefore the potential high cost associated with it, may not be necessary.

The target allowable high-low misalignment of 1/16 in (1.6 mm) may be very difficult to achieve in the field, especially for large diameter pipes and the associated cost could be very high. Due to the increase of the wall thickness (to meet the design requirement on the CSC), the allowable high-low misalignment can be increased to 0.16 in (4.0 mm) as shown in Figure 6-4. Therefore, a better design in the sense of balancing the integrity and cost can be achieved by introducing the modifications to the preliminary design parameters in the following:

- Pipe wall thickness: t = 1.0 in (25.4 mm) (changed from 0.75 in, i.e., 19.1 mm);
- Allowable maximum high-low misalignment: h_m = 0.16 in (4.0 mm)[2] (changed from 1/16 in, i.e., 1.6 mm).

The design parameters can be further optimized to satisfy the project requirements as shown in the iso-strain curve of Figure 6-5. The target TSC and CSC are always satisfied as the design parameters (i.e., the weld strength mismatch and high-low misalignment) are adjusted along the iso-curve. For example, the target TSC and CSC can be satisfied if the minimum weld mismatch ratio is 1.25 and the maximum high-low misalignment is 0.16 in (4.0 mm). If the high-low misalignment can be controlled within 0.10 in (2.5 mm), the required minimum weld mismatch ratio can be reduced to 1.10. Depending on the preference for controlling the high-low misalignment and weld strength mismatch, the design parameters can be optimized.

---

[1] The safety factors used here are examples only and are not code requirements or recommendations.

[2] The high-low misalignment in field welds of large diameter onshore pipelines can be 1/8 inch and higher.

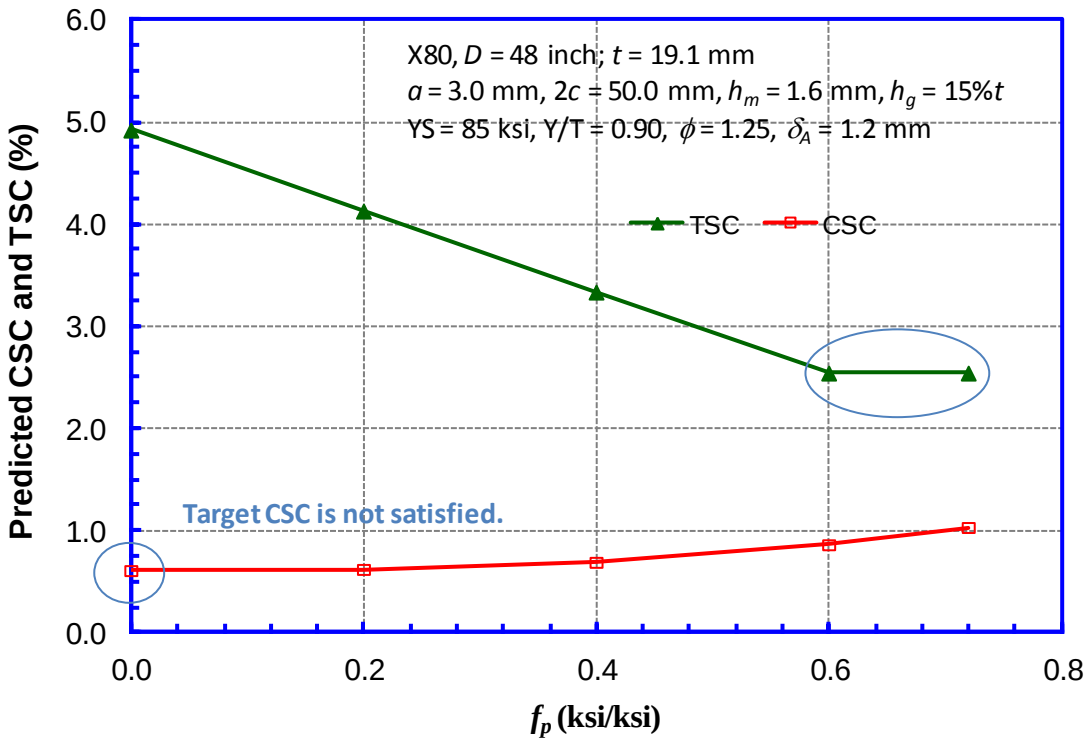

Figure 6-2 Predicted CSC and TSC for different pressure factors (f_p) using preliminary design parameters

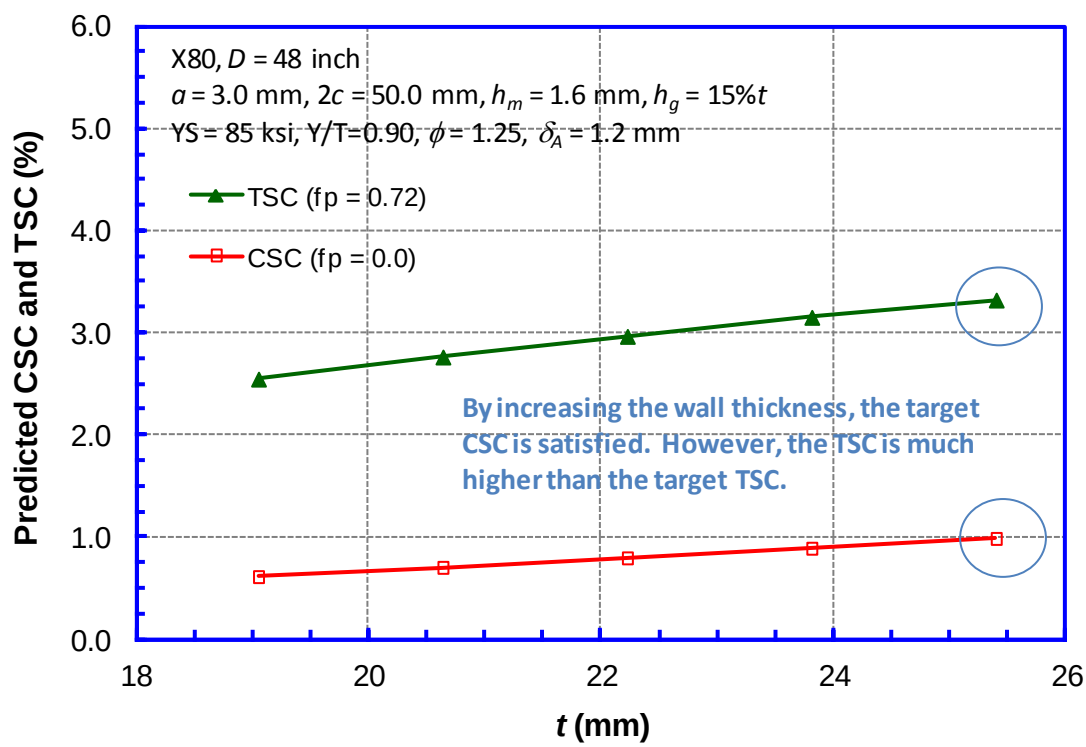

Figure 6-3 Effect of pipe wall thickness (t) on the predicted CSC and TSC

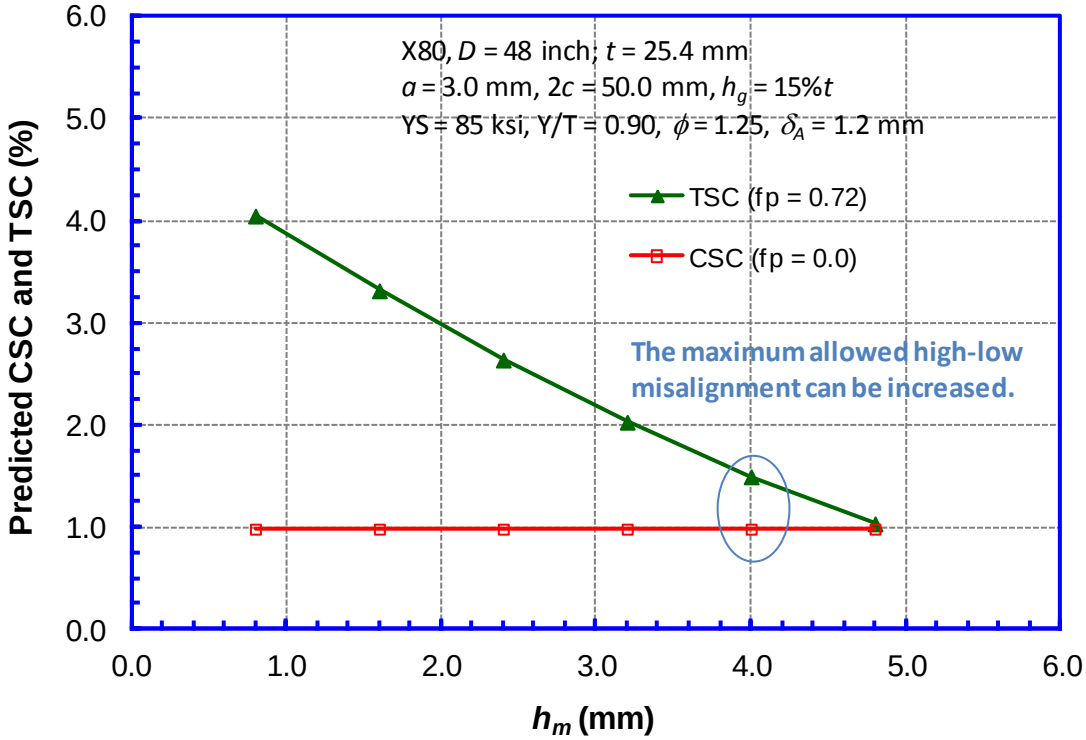

Figure 6-4 Predicted TSC and CSC for different high-low misalignment (h_m) using modified design parameters

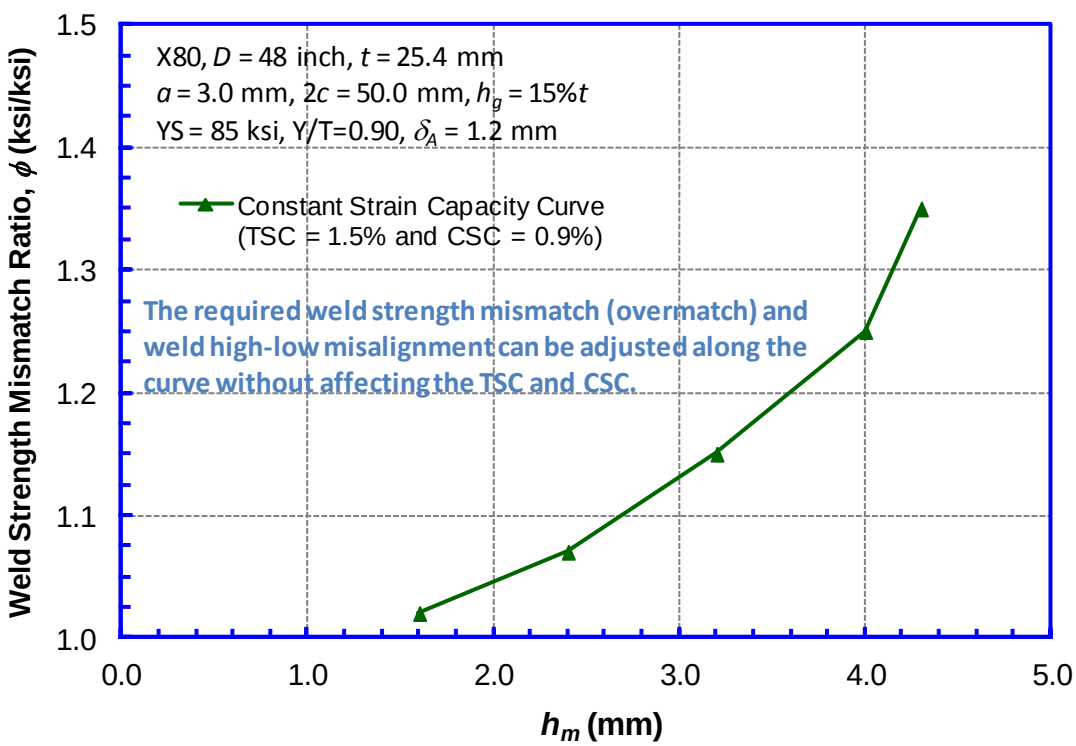

Figure 6-5 Constant strain capacity curve: relationship between weld strength mismatch ratio (ϕ) and weld high-low misalignment (h_m)

6.4 Summary Remarks of the Ranking System

The core of the ranking system is the tensile and compressive strain models. The inputs to the ranking system are the design/working conditions of the pipeline such as the pipe and weld properties and the strain demands.

The ranking system is used to evaluate, rank, and optimize the tensile (TSC) and compressive strain capacity (CSC) of a pipeline. The direct output of the ranking system is the tensile (TSC) and compressive (CSC) strain capacity of the pipeline and the ranking of the relative risk for reaching the tensile or compressive limit states.

For pipeline maintenance, the output of the ranking system can be used to identify the highest risk between the tensile and compressive failures, direct the mitigation planning, and optimize the maintenance efficiency (both cost and safety).

At the design stage, the ranking system can be used to optimize the design conditions to balance the safety and cost of the pipeline by maintaining balanced safety margins for the TSC and CSC.

7 Guidelines on Some Key Elements in Strain-Based Design

7.1 Introduction

This section covers general guidelines of some key elements in strain-based design. The guidelines are not meant to be all-inclusive. Instead, particular attention is given to areas in which current standards or traditional industry practice is inadequate either in scope and/or in specificity. Guidelines are first given, followed by rationales which are meant to further elucidate the key issues. The focus of the guidelines is on strain capacity, although strain demand is also addressed to a lesser extent.

7.2 Role of Strain-Based Design

All pipeline designs start with the evaluation of the desired throughput and the associated hydraulics. The pressure and temperature profile of the line hydraulics form the basis for the operational requirements. The initial wall thickness is then computed from the requirements of pressure containment, and, in gas pipelines, class location specified by relevant standards and regulatory requirements.

The initial design conditions may be further evaluated under construction and operational conditions at locations with special features. For instance, stress conditions at tie-in points may be evaluated when the tie-in points are associated with steep slopes, crossings, and large bend angles. Adjustment to wall thickness and/or pipe grade may be made to meet the design stress requirements, such as those in ASME B31.4 [68] and B31.8 [69].

The entire pipeline route may be evaluated for possible high longitudinal strains, such as locations of fault crossings, mine subsidence, frost heave and thaw settlement, discontinuous permafrost, or unstable slopes. Although ASME B31.4 and B31.8 permit high longitudinal strains up to 2% when the quality of the girth welds are verified and the integrity of the pipeline is maintained, the standards do not specify ways the integrity assurance may be achieved. In practice, most onshore pipelines are designed to combined stress and individual stress criteria. By the combined stress criterion, the Mises or Tresca equivalent stress is limited to 90% of SMYS. Individual longitudinal stress is also limited to 90% SMYS. The combined stress limit of 90% SMYS corresponds to compressive strain limit of approximately 0.13% in X70 pipelines for Class 1 design. Similarly individual stress limit of 90% SMYS would limit the tensile longitudinal strain to 0.21% for X70 pipelines. However, the pipeline industry generally uses 0.5% as the demarcation point between traditional stress-based design and strain-based design. It is generally agreed that current standards do not adequately address conditions with longitudinal strains greater than 0.5%. At the same time, conditions with longitudinal strains in the range of approximately 0.2% to 0.5% are in fact a grey area.

For the purpose of consistency with the pipeline industry practice, 0.5% longitudinal strain is used as starting point for strain-based designs.

7.3 General Philosophy of Strain-Based Design

A few practical steps to achieve sound strain-based design are as follows:

(1) *Reduce strain demand.* This may be accomplished through the judicious selection of pipeline routes which impose low strain demand, using specially designed trenches and backfill, and other strain reduction methods.

(2) *Select appropriate line pipes*. A few features which are beneficial to the strain capacity are (1) high strain hardening capacity and (2) an upper bound of strength distribution that is as low as possible for manufacturing and yet still meets the minimum specifications. Rigorous specifications and verifications throughout the line pipe manufacturing processes are necessary to ensure the expected properties are achieved.

(3) *Minimize the likelihood of gross strain concentration at welds*. When there is gross strain concentration at a weld, i.e., the weld experiencing higher strains than the pipe body, the overall strain capacity is typically below yield strain (0.5%) because most of the applied displacement is imposed on the weld. The leading causes of gross strain concentration at the welds are high levels of high-low misalignment and low weld strength overmatching. It is necessary to ensure sufficient weld overmatching for expected high-low misalignment to prevent gross strain concentration.

(4) *Ensure upper-shelf toughness behavior.* To have a sufficient level of tensile strain capacity at the expected service temperatures, it is necessary to ensure that the material behavior is ductile.

(5) *Balance the selection of pipe grade and pipe wall thickness.* Pipes of thicker walls are beneficial to both tensile and compressive strain capacity. For the same pressure containing capacity, a thicker wall would allow the use of lower grade of pipes. Lower grade pipes can more easily be made to have higher strain hardening capacity. However, the increased strain hardening capacity cannot be automatically assumed for lower grade pipes. Rigorous specifications and verifications are still needed.

(6) *Control flaw size and distribution.* Weld flaws, particularly planar flaws, are detrimental to tensile strain capacity. The flaw size and distribution need to be controlled with appropriate welding and NDT procedures. It should be emphasized that overly aggressive flaw size limits may lead to unnecessary repairs. Since repair welds typically have more inferior properties than mechanized welds, there needs to be a proper balance between flaw size limits and repair rates.

(7) *Follow a rigorous program on material qualification, including consistent and robust experimental test procedures for material property characterization.* Strain-based design is significantly more sensitive to material properties and their variations than traditional stress-based design. It is necessary to ensure that all test data are generated using a consistent set of test procedures among all labs, including specimen extraction and preparation, instrumentation, data reduction, and reporting.

(8) *Ensure consistency and exercise rigorous quality control in field construction.* It should be recognized that good specifications in paper do not guarantee good outcome unless those specifications are implemented in practice. Similarly weld properties achieved in qualification welds can only be obtained in field production welds when welding procedures are implemented by equally qualified welders and welding equipment. In

critical locations, it may be necessary to sample the production welds through destructive testing to confirm weld quality.

Specific recommendations to achieve the general philosophy described above are provided below.

7.4 Linepipe Specifications

7.4.1 Importance of Linepipe Specifications

Linepipe tensile properties are a basic governing parameter to all aspects of a pipeline's service life. The *tensile properties* refer to a comprehensive set of property measures. The most commonly referenced strength parameter, the specified minimum yield strength or SMYS, is only one of the measures. Examples of other measures include ultimate tensile strength, total elongation, yield to tensile (or Y/T) ratio, uniform elongation, and transverse (hoop) vs. longitudinal properties.

7.4.2 Shortcomings of Linepipe Specifications in Current Standards

Although the linepipe specifications in current standards have served the industry well, some aspects of the specifications can be strengthened for strain-based design.

(1) The current definition of yield strength can become problematic for high-strength pipes, particularly for "high-strain" linepipes manufactured specifically for strain-based design. The nonlinear elastic response in some of those materials can lead to under-presentation of yield strength, high variability of measured yield strength, and overly optimistic representation of material's strain hardening capacity. A possible revision of the yield strength definition has been proposed by Wang, et al. [70].

(2) The range of upper bound strength and the specified minimum strength is very generous. Having a narrower range, i.e., specifying lower values of upper bound strength than those in API 5L and other equivalent standards, is advisable for achieving adequate weld strength mismatch while maintaining adequate toughness and ductility.

(3) The maximum allowed Y/T ratio in API 5L could be too high for strain-based design. Even for pipelines of traditional stress-based design, some strain hardening capacity is necessary. The maximum allowed Y/T ratios of 0.97 and 0.99 for X100 and X120 are too high for realistic pipeline applications.

(4) Tensile property variation within a joint of pipe or pipes made of the same heat of steels is worthy of further investigation. Given the progressively lower strain hardening capacity of linepipes with microalloyed steels, and in particular high strength steels, the tensile property variation can have greater consequences than older linepipes (Q&T steels) which had greater strain hardening capacity.

(5) Modern linepipe steels are known to have anisotropy. For example, the strain hardening capacity of UOE pipes in the hoop direction is often lower than that in the longitudinal direction. The low strain hardening in the hoop direction is shown to have detrimental

effects on the strain capacity under pressurized conditions. The idea that the strain capacity of a pipe is determined by its longitudinal property is not entirely correct[3].

(6) Specimen shapes and dimensions can affect the reported stress-strain behavior for the same material. It is therefore necessary to specify the geometry and dimensions of test specimens when tensile specifications are given. For heavy wall and/or large diameter pipes, the position of the specimen in the thickness direction can affect the test results and should be specified.

(7) The shape of stress-strain curves can be altered by strain-ageing.

7.4.3 Recommendations on Linepipe Specifications

7.4.3.1 Recommendations and Steps to Address Inadequate Practice

(1) Full stress-strain curves (i.e., up to UTS or uniform strain) shall be required for all tensile tests.

(2) Tensile tests shall be conducted on aged (e.g., due to FBE coating) materials.

(3) The upper bound of tensile properties relative to those in API 5L and other equivalent standards shall be lowered in consultation with feasibility of production.

(4) A modified yield strength definition may be considered if the stress-strain curves exhibit a large degree of nonlinear elasticity [70].

(5) A meaningful representation of material's strain hardening capacity should be defined. API 5L upper limit on Y/T ratio is too high for strain-based design.

(6) Specifications on tensile properties shall include values, test specimen forms and dimensions, and test conditions.

(7) The quality of the test data should be checked and verified. Some of the possible checks are described in Section 7.4.3.4.

The recommended format of tensile property specifications is summarized in Table 7-1.

7.4.3.2 Recommendations for Tensile Test of Hoop Properties

(1) Round-bar specimens without flattening should be tested for hoop properties.

(2) Within the reduced gauge section of the specimen where the test data are taken, the length-to-diameter ratio should be no less than four.

(3) The mounting points of the extensometer should be sufficiently far away from the shoulder (the transition zone from the reduced gauge section to the end tab) to assure uniform deformation within the gauge section.

(4) The test results of round-bar specimens can be affected by the through-thickness property variations. The diameter of the reduced gauge section should be as large as possible while meeting the requirement of length to diameter ratio.

[3] Most analyses of strain capacity assume isotropic material properties, i.e., assuming the material properties in the hoop direction are identical to those in the longitudinal direction. Therefore the effects of the difference in the longitudinal and hoop properties are not captured.

7.4.3.3 Recommendations for Tensile Test of Longitudinal Properties

(1) Full thickness strap or round-bar specimens should be tested for longitudinal properties. It should be noted that the total elongation from round bar specimens is lower than that from full-thickness straps.

(2) The specimen should be of "dogbone" shape with a reduced gauge section in the middle of the specimen.

(3) No parallel-sided strip specimens, similar to those in the main body of API 1104 20th Edition, should be used.

(4) Within the reduced gauge section where the test data are taken, the length over the diameter/thickness ratio should be no less than four.

(5) The mounting points of the extensometer should be sufficiently far away from the shoulder to assure uniform deformation within the gage section.

(6) The diameter of the reduced gage section should be as large as possible for the round-bar specimens.

Table 7-1 Summary of Linepipe tensile property specifications

Property Parameters	Orientation	Features	Current Requirement	Stress-based design in addition to the generic issues	Strain-based design in addition to the generic issues	Generic Issues to Be Considered
Yield Strength and UTS	Hoop	Test Form	Flattened strap	Round bar and/or ring expansion	Round bar and/or ring expansion	Definition of yield strength, test specimen form and dimensions, test temperature, effects of strain ageing, effects of cyclic plastic strain
		Minimum	Yes	Yes	Yes	
		Maximum	No for PSL 1, Yes for PSL 2	Yes	Yes, lower than the current code limits	
	Longitudinal	Test Form	Not required	Optional, Full-thickness strap or round bar	Full-thickness strap or round bar	
		Minimum	Not required	Optional	Yes	
		Maximum	Not required	Optional	Yes	
Y/T Ratio	Hoop	Maximum	No for PSL 1, Yes for PSL 2	Yes	Yes	
	Longitudinal	Test Form	Not required	Optional	Yes	
Total Elongation	Hoop	Minimum	Yes	Yes	Yes	
	Longitudinal	Minimum	Not required	Optional	Yes	
Uniform Strain or Elongation	Hoop	Minimum	Not required	Optional	Optional	
	Longitudinal	Minimum	Not required	Optional	Yes	
Shape of Stress-Strain Curve	Hoop		Not required	Optional	Optional	
	Longitudinal		Not required	Optional	Yes	

7.4.3.4 Test Procedures and Data Check to Ensure Quality

7.4.3.4.1 *Data Check for Elastic Slope*

The initial part of a stress-strain curve should be checked against theoretical elastic (Young's) modulus. The initial slope of the stress-strain curve at the stress level up to one third of the UTS should be computed and compared with the elastic modulus. If the initial slope differs by more than 10 % from the theoretical value[4], possible sources of the discrepancy should be examined. After the possible sources of systematic errors are eliminated, the test data may be updated by applying a compliance correction.

Elastic slope can be an invaluable "marker" of data quality. While small deviation from the theoretical value is understandable and tolerable, in some egregious cases reported slopes have been much lower than the theoretical value or even, in some cases, much greater than the theoretical value. Some of the possible contributing factors to the incorrect elastic slope are (1) straightness of the test specimens, (2) dimension of the test specimens, particularly the reduced gage width (diameter) to length ratio, (3) location of the clip gage relative to the transition of the reduced section, and (4) post-test data processing. While the elastic slope is generally not viewed as a material parameter in strain-based design, the elastic slope directly affects the reported yield strength. This influence is particularly acute for stress-strain curves of high-strength steel exhibiting non-linear behavior prior to the yield point, see Figure 7-1. An incorrect elastic slope can directly lead to incorrect yield strength, hence incorrect *Y*/*T* ratio and incorrect conclusion on the pass/fail of the strength requirement. It also affects the qualification of the weld strength mismatch if the mismatch is defined at the yield strength.

A joint industry project (JIP) is under way to investigate the yield strength variations and to develop best practice to minimize the variability [71].

7.4.3.4.2 *Data Check for Uniform Elongation*

When the stress-strain curves are flat around the point of UTS, a curve fit around the point should be conducted to "smooth" out the local data oscillations. The point of UTS should be determined by obtaining the maximum stress level of the fitted curve. The corresponding uniform elongation can be obtained accordingly from the same procedure.

7.4.4 Key Issues in Linepipe Specifications and Rationales for Recommendations

7.4.4.1 Yield Strength

The yield strength is a fundamental parameter that affects all phases of a pipeline's life, including design, construction, and maintenance. The yield strength is typically reported as the strength at 0.5 % total strain or the strength at the 0.2 % offset strain [72,73]. In response to the requirements for strain-based design, a number of pipe manufacturers have developed manufacturing processes aimed at improving the stress-strain response of the linepipes, including having so-called round-house stress-strain curves (without obvious yield point and Lüder's extension), high strain hardening, and resistance to strain ageing during pipe coating [74,75,76]. A representative stress-strain curve is shown in Figure 7-1 [74]. When the yield strength is

[4] The theoretical value of the Young's Modulus of steels is 206,700 MPa (30,000 ksi).

measured at either 0.5 % total strain or 0.2 % offset strain, the reported yield strength, as given in Figure 7-1 and Table 7-2, can be much lower than the "physical" yield strength, which may be understood as the "knee" of the stress-strain curve. The low value of yield strength directly leads to a low Y/T ratio. The strength values reported by in Table 7-2 for a high-strength steel are not representative of the material's true yield strength. The under-representation of the yield strength is attributable to the nonlinearity in the "elastic" part[5] of the stress-strain curve prior to reaching the 0.5 % total strain. For this type of high-strength material with nonlinear "elastic" behavior, using the 0.2 % offset strain for the measurement of yield strength produces similar under-representation of the material's yield strength.

Having proper representation of the yield strength of the linepipe is critical for a wide variety of pipeline design and maintenance considerations. One of the fundamental problems in having a yield strength measured on the elastic part of the stress-strain curve is that the reported values can have large variations from one test to another, even when the overall stress-strain responses are almost identical. The large variations of the reported yield strength introduce uncertainties about the strength of linepipes. Such uncertainties can be a major headache for virtually every stakeholder, including pipe mills, pipeline owner companies, pipeline designers, and pipeline construction contractors.

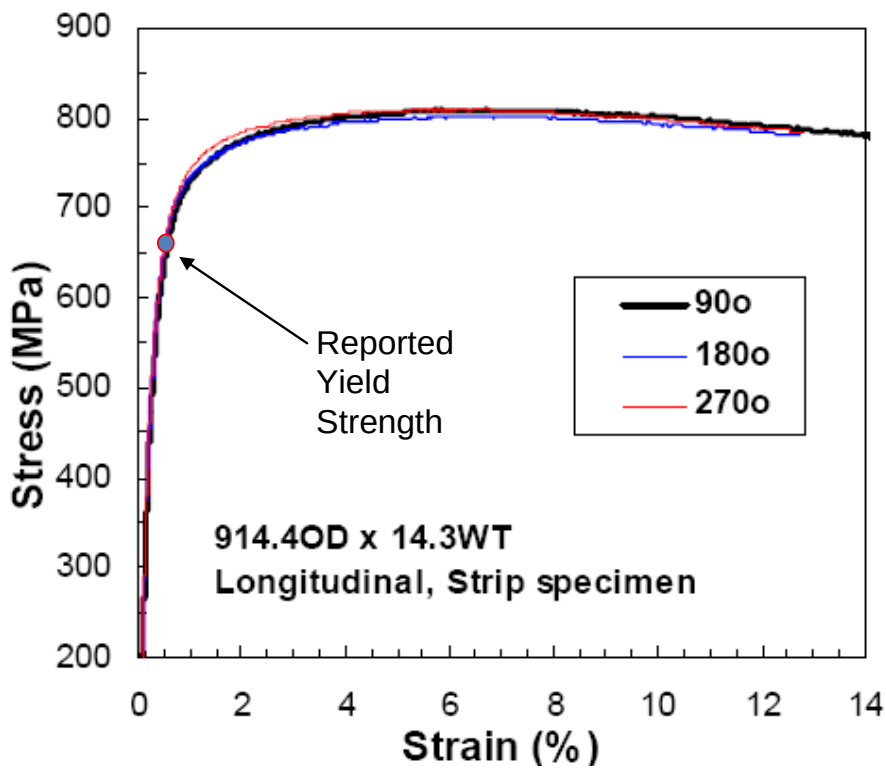

Figure 7-1 Stress-strain curves of a "high-strain" pipe and the associated yield strength measured according to current codes [72]

[5] The source of nonlinearity prior to the "knee" of the stress-strain curve is not well understood. It's not known if the nonlinearity is fully reversible when the stress level is reduced to zero. Micro-scale plasticity may explain the nonlinearity if the nonlinearity is not fully reversible.

Table 7-2 Reported strength values using current codes [72]

Pipe No.	Direction	Base metal tensile properties *1					Trans weld
		YS (MPa)	TS (MPa)	Y/T (%)	uEl (%)	σ_r *2 $\sigma_{1.5}/\sigma_{0.5}$	TS (MPa)
A	Trans.	713	824	87	-	-	819
	Longi.	668	835	80	7.3	1.17	-
B	Trans.	713	836	85	-	-	825
	Longi.	659	811	81	6.9	1.18	-

*1 Trans: round bar specimen, Longi.: Rectangular strip specimen

*2 Stress ratio, defined by the ratio of stress at ε=1.5% to that at ε=0.5% (σ1.5/σ0.5)

Strain hardening has been recognized as one of the critical parameters in strain-based design [77]. The strain hardening capacity of linepipe materials is often expressed in terms of the Y/T ratio. The under-representation of the yield strength leads to overly optimistic representation of the strain hardening capacity characterized by the Y/T ratio.

One of the most critical considerations in strain-based design is the weld strength mismatch level. It is now generally accepted that weld strength overmatching is preferred for strain-based design. One of the most common definitions of weld strength mismatch is based on the yield strengths of base metal and weld metal. If the yield strength of the pipe material is under-represented but not that of the weld metal, the weld mismatch level can in turn misrepresent the true strength difference between the pipe material and the weld metal. The under-representation of the yield strength can give an impression that the weld metal overmatches the pipe material by a very large margin if the strength mismatch is measured by the yield strength. The full stress-strain curves would suggest that the overall degree of overmatching is much lower.

Consumable manufacturers rely on the mismatch requirements for their product development and delivery. When the yield strength of the pipe material is artificially under represented, pipe mills may choose to increase the overall strength level to meet the yield strength requirement. The increased strength level of the pipe would lead to an increased strength requirement of the weld metal. At very high strength level, the weld metal ductility and toughness may have to be sacrificed to meet the strength requirement.

7.4.4.2 Upper Bound of Linepipe Strength

In API 5L and ISO 3182 [72,73], the permissible upper-bound strength is significantly higher than the specified minimum strength for PSL 2 pipes [72,73]. There are no upper bound limits for PSL 1 pipes. For instance, for pipe grades X70 and lower, the upper-bound ultimate tensile strength (UTS) is 110 ksi (758 MPa) for PSL 2 pipes. For grades X80 to X100, the upper-bound yield strength is about 22-ksi (150-MPa) higher than the SMYS. For grade X120, the upper-bound yield strength is about 32-ksi (220-MPa) higher than the SMYS. For grades X80 and X90, the upper-bound UTS is about 29-ksi (200-MPa) and 32-ksi (220-MPa) higher than the specified minimum UTS, respectively. For X100 and X120, the upper-bound UTS is 33-ksi (230-MPa) higher than the specified minimum UTS.

One of the major concerns about the upper limits of yield strength and UTS is its potential impact on the level of the weld metal strength mismatch. Weld strength overmatching relative to the pipe body strength is generally considered preferable in design and construction to prevent strain localization in the weld region. The wide range of tensile properties permitted for a given grade of linepipes makes it difficult to select proper consumables and welding processes to achieve a certain level of desired mismatch. For instance, the specified minimum yield strength of X80 pipes is 80 ksi (555 MPa) and the upper-bound limit of the yield strength is 102 ksi (705 MPa). Assume that the yield strength of the weld is at 91 ksi (630 MPa), i.e., the average of the SMYS and upper-bound yield strength. The 91-ksi (630-MPa) yield strength produces 13.5% overmatching if the pipe yield strength is at the SMYS or 10.6 % under matching if the pipe yield strength is at the upper-bound value of 102 ksi (705 MPa). In order to achieve consistent overmatching, the lower bound of the weld strength would have to be higher than the upper-bound pipe strength. For X80 pipes this implies that the yield strength of the weld has to be greater than 102 ksi (705 MPa) and the UTS greater than 120 ksi (825 MPa). The control of the welding processes will have to be very precise to have the weld metal at this strength level while maintaining adequate toughness and ductility. Such requirements are achievable with well-controlled mechanized GMAW processes. However achieving the same strength and toughness level for FCAW and SMAW processes can be a challenge. For pipes of grades greater than X80, achieving consistent weld strength overmatching can become even more challenging for most of the welding processes on the market.

From the viewpoint of pipe performance, there is no good reason to have the upper limit of UTS for pipe grades X52 to X70 at 110 ksi (758 MPa). Such a limit does offer the flexibility of marketing pipes of the same strength level in multiple grades. For instance, pipes meeting X70 strength requirements may be sold as X60 or even lower grades. It should be noted that welding procedure qualifications are often performed by pipe grade. If a procedure qualified on X52 is applied to pipes with an actual strength level of X70, there could be a high possibility of weld strength undermatching. The undermatching condition is generally not a concern from the viewpoint of traditional pipeline design, which is based on limiting the hoop stress to a certain percentage of the SMYS. However, threats to girth weld integrity are often associated with ground movement hazards. Having undermatching girth welds can cause strain concentrations in the girth welds, thus potentially increasing the likelihood of girth weld failures.

7.4.4.3 Y/T Ratio

In API 5L and ISO 3182, the maximum permissible Y/T ratio for X80 pipes is 0.93 [72,73]. The maximum Y/T limits are incrementally increased to 0.95, 0.97, and 0.99 for X90, X100, and X120.

It is important to note that, for pipes of moderate to large diameter, the above Y/T limits are set for flattened full thickness strap specimens tested in as-manufactured conditions (without the effects of strain ageing). Round-bar specimens without flattening tend to return higher yield strength values than flattened full-thickness straps. Strain ageing from FBE coating further increases yield strength value and Y/T ratio. Therefore, it is conceivable and likely that pipes at the time of pipeline commissioning may have Y/T ratio higher than that given in mill test

reports. If pipes were manufactured to the upper limits of Y/T ratio, the pipes in service may have Y/T ratio higher than the upper limits given in the pipe manufacture standards [72,73]. CSA Z245.1 differentiates test methods, i.e., full-thickness strap vs. other specimen geometries [78].

The pipeline industry has very limited experience with linepipes having Y/T ratio greater than approximately 0.93. The allowance of higher Y/T ratio brings many unknowns. Even in the domain of traditional stress-based design, certain implicit assumptions about material's strain hardening capacity are made in various stages of operation and maintenance. For instance, corrosion assessment tools were calibrated and validated with materials not having extremely high Y/T ratios. The applicability of those tools in the context of very high Y/T ratios is unknown and should be critically evaluated. Pipelines designed by traditional stress-based principles may still experience certain displacement controlled loading after the pipelines are put in service, such as in the event of ground settlements. The extremely high Y/T is expected to have a negative impact on the tolerance to this type of loading.

7.4.4.4 Anisotropy

Modern high-strength linepipe steels can have highly anisotropic mechanical properties due to the textures created in the plate/coil rolling processes and the deformation induced by the pipe forming and expansion processes. The degree of anisotropy can vary, depending on the steel rolling practice and pipe forming processes. The anisotropy can manifest itself as differences between the properties in the longitudinal and hoop directions in (1) yield strength, (2) UTS, and/or (3) shape of the stress-strain curves. In most cases, the difference in UTS is less than that in yield strength. The shape of the stress-strain curves can be quite different in the two directions. Strain ageing may increase the differences between the longitudinal and hoop properties and thus further exacerbating the anisotropy.

Anisotropy can have strong impact on the strength and strain capacity of pipelines [79]. One immediate impact is on the girth weld procedure qualification. One of the required tests in the weld procedure qualification is the cross-weld tensile test. The UTS from test specimens is required to be equal to or higher than the specified ultimate tensile strength of the pipe. For large diameter welded pipes, the pipe strength is qualified on the basis of hoop tensile properties. Current linepipe standards, API 5L and ISO 3183, do not require testing of longitudinal tensile specimens. Some have argued that the minimum tensile property requirement in the cross-weld tensile tests should be lower, as the longitudinal strength of the pipes could be lower than the hoop strength. Pipes with longitudinal UTS lower than the specified minimum UTS (hoop direction) could meet the API 5L and ISO 3183 requirements, as no longitudinal property is required. Published test data have shown that the tensile strength in the longitudinal direction can be either lower or higher than that in the hoop direction, depending on the type of pipes (UOE vs. spiral) and the plate/coil manufacturing practice. Without a complete picture of the anisotropy, it is difficult to form a consensus on the requirements of the weld procedure qualification.

7.4.4.5 Tensile Property Variation

The need for weld strength overmatch for strain-based design would require tight control of the spread (standard deviation) of pipe tensile properties. At the same time, any specifications aimed at achieving such tight control need to incorporate the natural variation of pipe tensile properties in the normal production environment. A ~2005-vintage 36-inch OD and ¾-inch wall thickness X100 pipe was tested at CANMET. The room-temperature stress-strain curves from round and strap specimens cut from different clock positions are shown in Figure 7-2 and Figure 7-3, respectively. The variation in yield strength is in the range of 80-90 MPa. This variation is higher than the estimated yield strength variation of 50-60 MPa (at 0.5% total strain) from published data by Tsuru, et al. [80]. Data published by Ishikawa, et al., seem to suggest much smaller variation [72].

7.4.4.6 Dependence on Specimen Type

The stress-strain curves from the round bar and square cross-section strap in Figure 7-2 and Figure 7-3 are compared in Figure 7-4 using the highest and lowest curve from each specimen type. There are some differences between the curves of the different specimen types; however there is a general agreement up to UTS. The total elongation from the strap specimens is much greater than that from the round bar specimens. The difference is attributable to the different specimen cross-section (round versus square) and the ratio of gage width (diameter) to gage length. Both types of specimen had the same gage length of 2 inches while the cross-sectional areas were different. These results show that the specification for the total elongation has to be defined in the context of a consistent specimen type and dimensions.

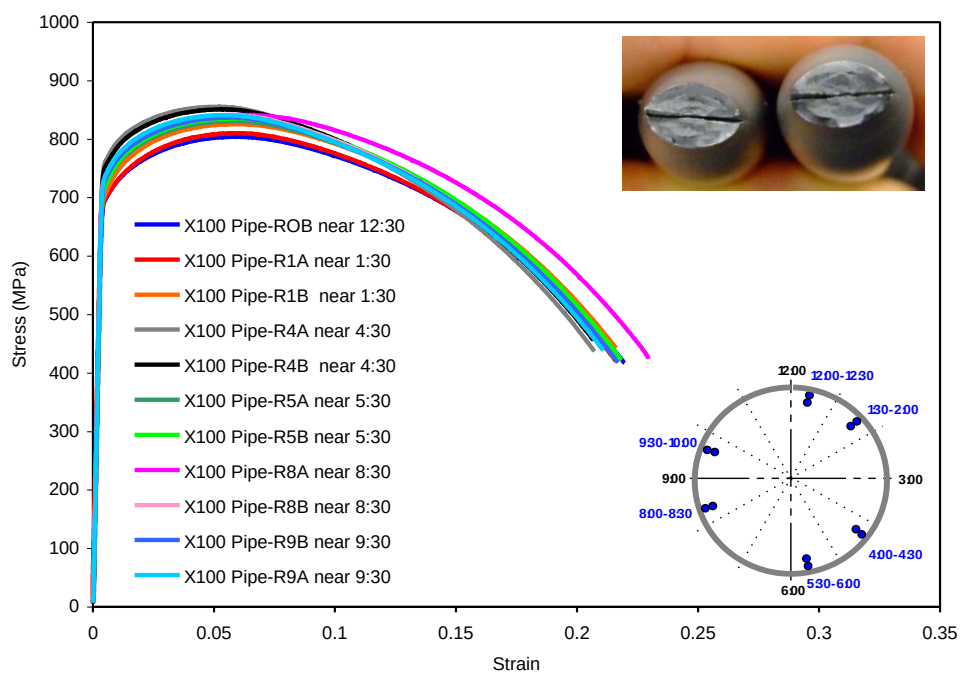

Figure 7-2 Stress-strain curves for tests using large diameter round specimens cut longitudinal to the pipe axis (LPA) at the different clock positions. Insert: image of fracture surfaces

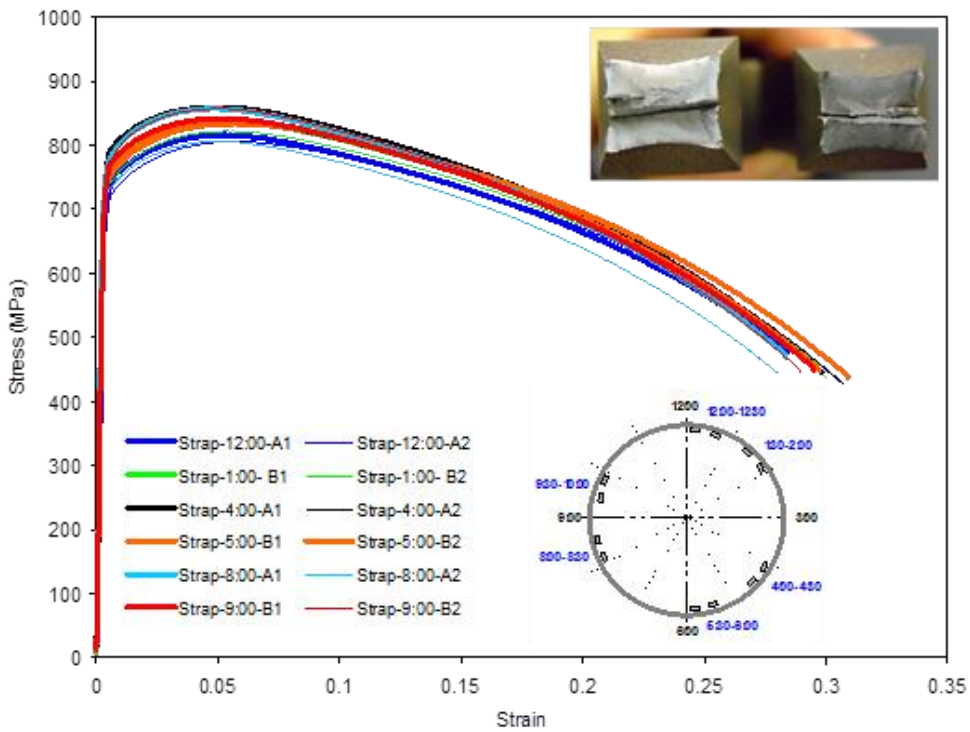

Figure 7-3 Stress-strain curves for tests using square strap tensile specimens cut longitudinal to the pipe axis (LPA) at different clock positions. Insert: image of fracture surfaces

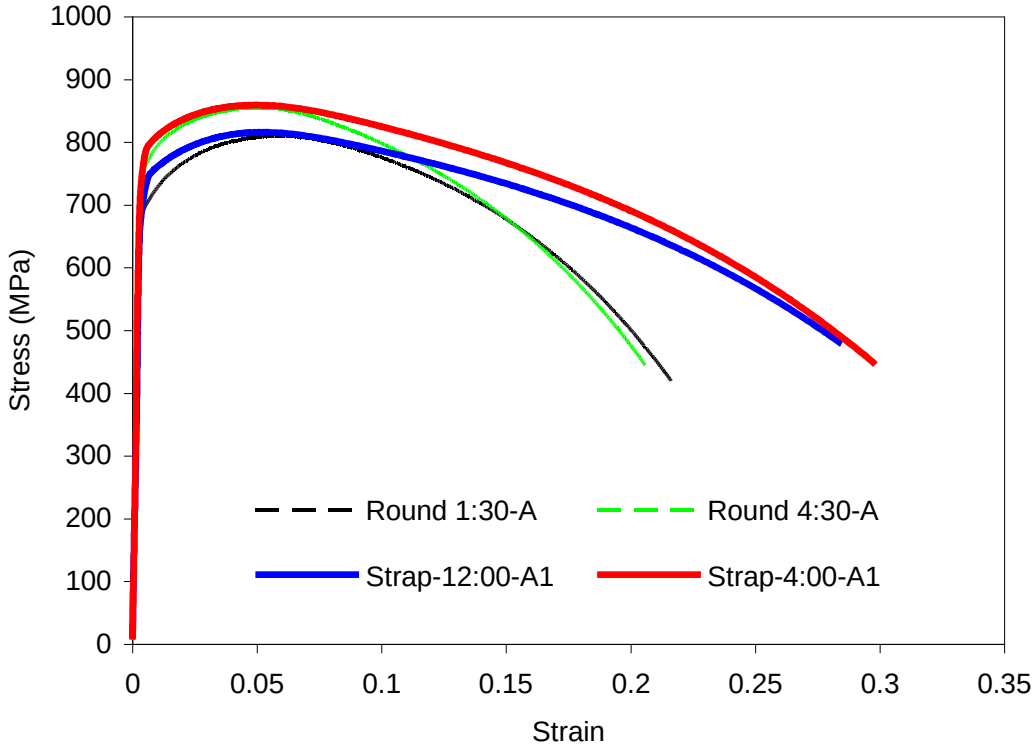

Figure 7-4 Comparison of stress-strain curves between the round bar and square cross-section strap

7.5 Girth Weld Specifications / Qualification

7.5.1 Girth Welding Procedure Qualification

Girth weld procedure qualification is usually completed in several steps.

1. Determine groups of welds for fabrication and testing. The grouping is done by referencing to essential welding variables.
2. Fabricate welds with predetermined weld processes and parameters.
3. Conduct mechanical testing of fabricated welds.
4. Compare the mechanical properties with preset requirements.
5. If the requirements are not met, re-test may be conducted when permitted. If re-test is not permitted, new welds must be made.

This section covers essential variables, mechanical tests, and requirements for weld properties.

7.5.1.1 Essential Variables

There is no separate list of essential variables for welds made for strain-based design vs. the traditional strain-based design. However, a significant amount of work has been done on essential variables related to girth welds of modern high-strength steels [81,82]. Users are encouraged to consult the publications of the work in development the grouping for welding procedure qualification.

7.5.1.2 Weld Tensile Properties and Strength Mismatch

7.5.1.2.1 *Recommendation and Requirements*

1. All weld-metal tensile tests shall be conducted using established and verified procedures such as that developed by CANMET [83].
2. The test specimens shall sample as much as-deposited weld metal as possible.
3. Full stress-strain curves shall be produced.
4. Weld strength mismatch requirement shall use ultimate tensile strength.
5. Weld strength overmatching is preferred.
6. The degree of weld strength mismatch shall be considered in conjunction with other relevant specifications, such as maximum high-low misalignment and acceptable flaw size.
7. The tensile property variations of pipe and weld metal shall be considered in specifying the mismatch level.
8. All requirements shall be made in conjunction with specific test specimen form and dimensions.

7.5.1.2.2 *Rationales for the Recommendations*

In the broad context of weld metal strength or weld metal mismatch requirement, a number of issues need to be considered, including (1) “natural” variation of pipe and weld properties, (2) proper parameter(s) with which the mismatch may be defined, and (3) appropriate level of mismatch.

Some practical challenges in implementing weld mismatch requirements are highlighted by the ranges of stress-strain curves shown in Figure 7-5 [84]. Depending on the "pairing" of the stress-strain curves, the yield strength of the weld metal can be as much as 150 MPa higher than that of the base pipe (880 MPa vs. 730 MPa) or as low as slightly below that of the base pipe. The mismatch level could therefore range from 0% to 20% overmatching. This range shown in Figure 7-5, from the same pipe and girth weld, is entirely from the natural variation of the pipe properties and differences in the type of all-weld-metal tensile specimens. Other possible contributing factors to strength variations, but not included in Figure 7-5, are (1) strain aging effects, (2) variability from the non-linear stress-strain response prior to yielding (e.g. Figure 7-1), (3) joint-to-joint variation and (4) heat-to-heat variations.

While the natural variations of pipe and weld properties are inevitable, it is clear from Figure 7-5 that using UTS as the parameter for defining weld strength mismatch would reduce the range of reported values. The variations in UTS are smaller than those in yield strength for both pipe and weld metal.

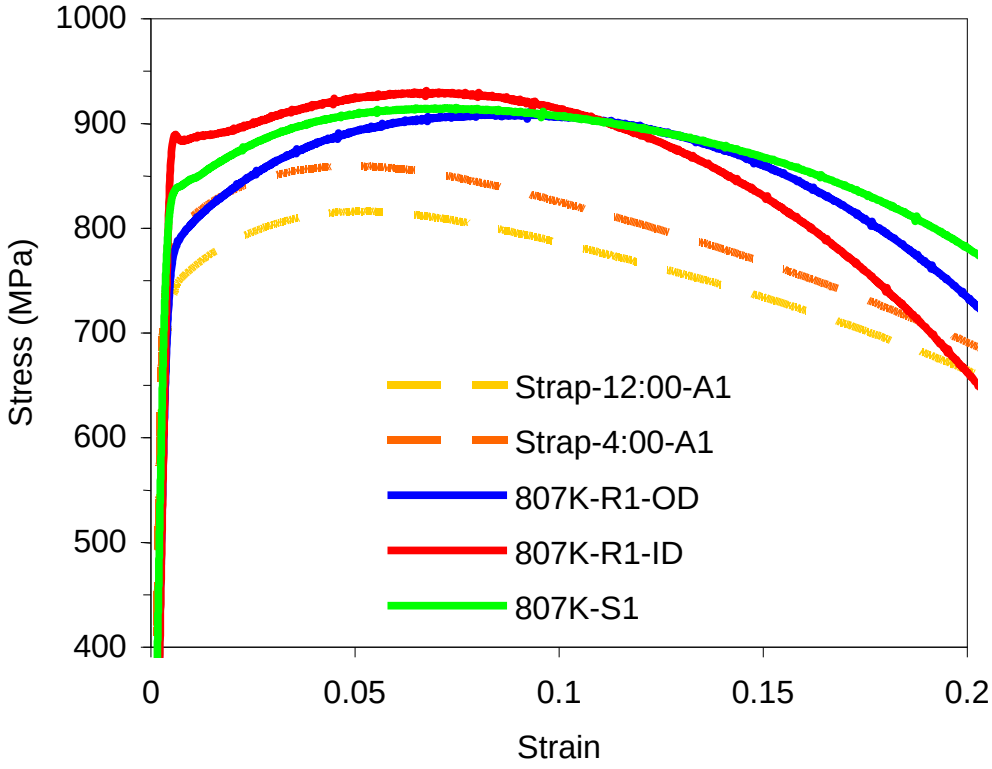

Figure 7-5 Comparison of AWM stress-strain curves (round bar biased to OD and ID and strip specimens) with longitudinal stress-strain curves of the X100 pipe (strap tensile specimens in dashed curves) [84]

It is generally agreed that weld strength overmatching is highly desirable for strain-based design as the overmatching weld metal prevents strain localization and shields the weld from overall deformation in the presence of hoop stress (from internal pressure). However, when the natural variation of the pipe properties and the large range of upper bound and minimum specified values are considered, achieving weld strength overmatching can push the minimum required weld properties very high. Meeting an overly high strength requirement may lead to

low toughness and ductility.

The minimum weld mismatch requirement (MWMR) may be set as a function of other material and girth weld parameters so some trade-off can be worked out to satisfy an intended service condition [85]. For instance, the MWMR is given as a function of flaw length and weld toughness in Figure 7-6 for a target strain capacity of 1.0%. It is evident that some degree of weld strength undermatching is permissible for cases with short flaw length and high toughness. Similar relationships can be developed with respect to other parameters using the PRCI-CRES tensile strain models.

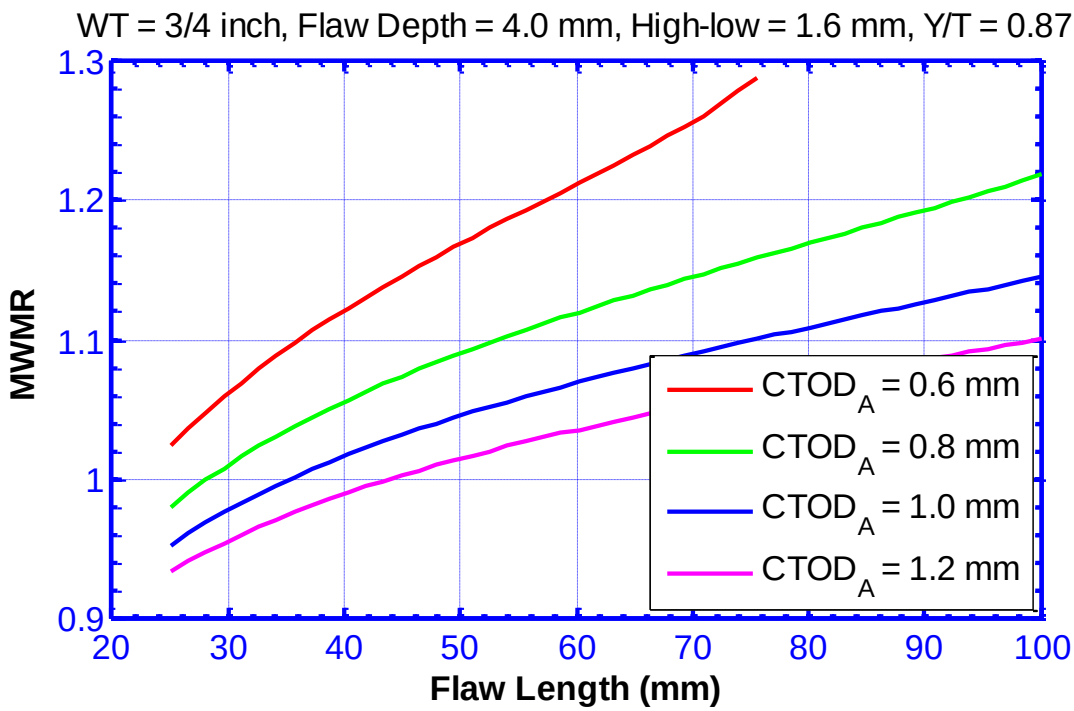

Figure 7-6 A sample relationship among MWMR, flaw length, and toughness for a target strain capacity of 1.0% from the PRCI-CRES tensile strain models

All-weld-metal-round bars are usually tested to obtain all-weld metal tensile properties. Systematic investigation has been performed at CANMET to determine, in part, the variation of weld metal tensile properties with respect to test specimen geometry and location within a weld [86,87]. One such example from a 36-inch (914-mm) diameter and 0.75-inch (19-mm) wall thickness X100 single-torch girth weld is shown in Figure 7-7 [86]. The specimens from the ID show much higher yield strength (910-920 MPa) than those from the OD (750-780 MPa). The ultimate tensile strengths of the ID and OD specimens are very close at approximately 940 MPa.

Stress-stress curves of the two round bars and one rectangular strip from a single-torch weld are compared in Figure 7-8. The three curves exhibit the highest degree of difference at the region around the yield points. The ID-biased round bar specimen gives the highest yield strength, whereas the OD-biased round bar gives the lowest yield strength. The strength of rectangular strip specimens generally falls between those of ID and OD round bar specimens. These results follow the same trend observed previously for similar X100 pipeline welds [87].

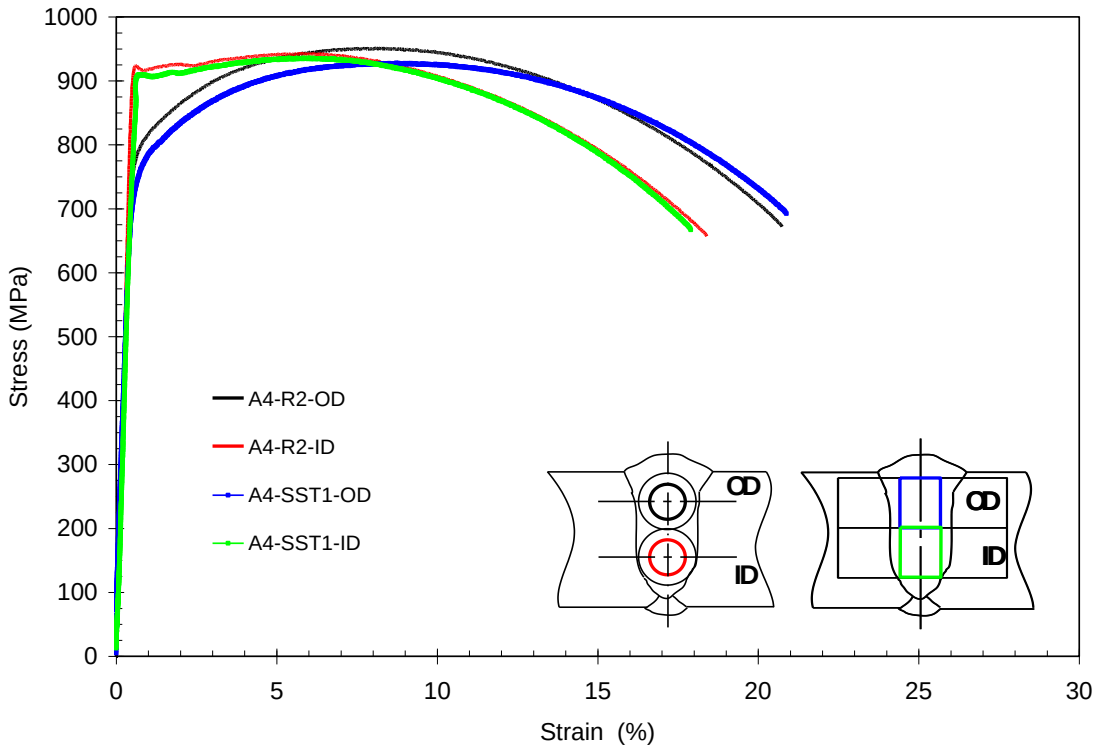

Figure 7-7 All-weld-metal tensile properties from round bar (R1) and split strip (SS) specimens [86]

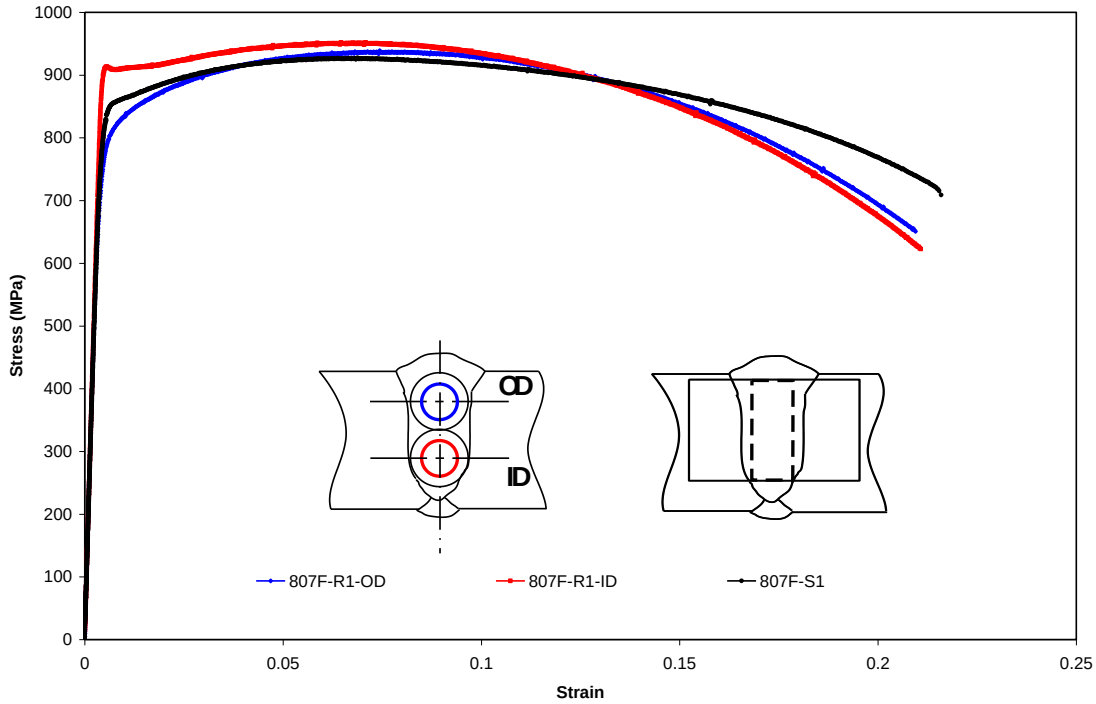

Figure 7-8 Stress-strain curves of weld metal from three specimens of different location and type

7.5.1.3 Weld Toughness

7.5.1.3.1 *Recommendations and Requirements*

1. To understand the overall material behavior and the significance of occasional low CTOD toughness, more emphasis should be placed on the generation and use of toughness transition curves. Furthermore, single minimum values defined at a set test temperature may not be adequate to reflect material's toughness behavior. For instance, the often used 0.004 in (0.1 mm) CTOD toughness is sufficient to ensure ductile behavior for SMAW welds, but can be insufficient for mechanized GMAW welds. Transition temperature from transition curves is a better indicator of material's toughness behavior.
2. Typical triplicate CTOD tests for HAZ toughness may not be sufficient for strain-based design due to the possible large variations of toughness values, particularly for flaws located in HAZ. The CTOD tests should be supplemented by Charpy transition curves which can be generated quickly and inexpensively. The transition curves provide clearer picture of overall material behavior, i.e., upper shelf vs. lower shelf behavior, than toughness values at a single temperature when these toughness values have large variations.
3. Strain-based design on the basis of overall upper shelf toughness is more representative of the expected large-scale behavior than the lowest value at a given temperature when the scatter of the toughness values is considered. A low risk of brittle (cleavage) fracture requires adequate demonstration by toughness testing. If high-constraint tests do not present evidence of cleavage, the risk of brittle fracture is low. However, if such specimens fail in a brittle manner then enough low-constraint tests must be done to ensure that the risk of brittle fracture is acceptably low.
4. To achieve the overall high tensile strain capacity, the benefits of weld strength overmatch should be considered in conjunction with toughness considerations.
5. Occasional low CTOD toughness, particularly those from pop-in events, likely exists in many girth welds. It is suggested that the occasional low values should be analyzed on a case-by-case basis. Requirements of weld integrity on the basis of the occasional low toughness could be counter-productive for overall pipeline safety.

7.5.1.3.2 *Rationales of the Recommendations*

A set of sample Charpy transition curves of a mechanized GMAW weld is given in Figure 7-9. The upper shelf energy is very high, nearly 300 ft-lbf or 400 J. The upper shelf energy of HAZ is also quite high. The upper shelf energy of the weld metal is lower than HAZ. The weld metals also have higher transition temperatures than the HAZ. The Charpy transition curves of a SMAW weld made in the early 1950's are shown in Figure 7-10. The transition temperature of the manual SMAW weld is much higher than the mechanized GMAW weld. The upper shelf energy of the SMAW weld is in the range of 50-60 ft-lbf. However, the same energy level would put the GMAW weld on the lower transition. The upper shelf energy of the GMAW weld is in the range of 160-180 ft-lbf. This comparison clearly demonstrates the need to understand the transition behavior in addition to the energy level at a given test temperature

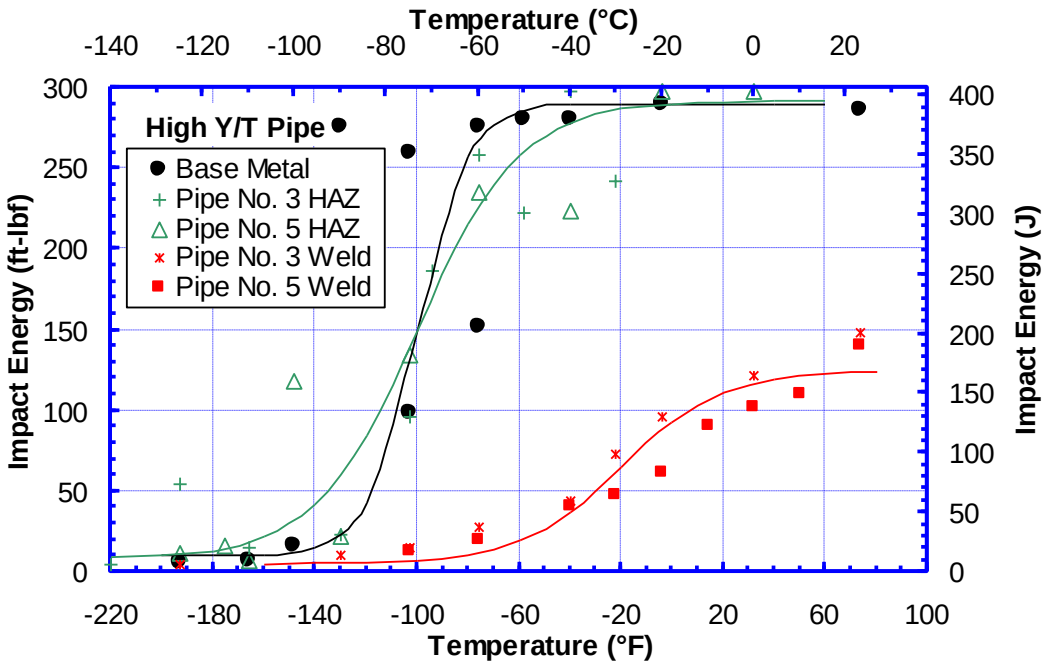

Figure 7-9 Charpy transition curves of the pipe and evenmatch weld of the high Y/T X65 pipe

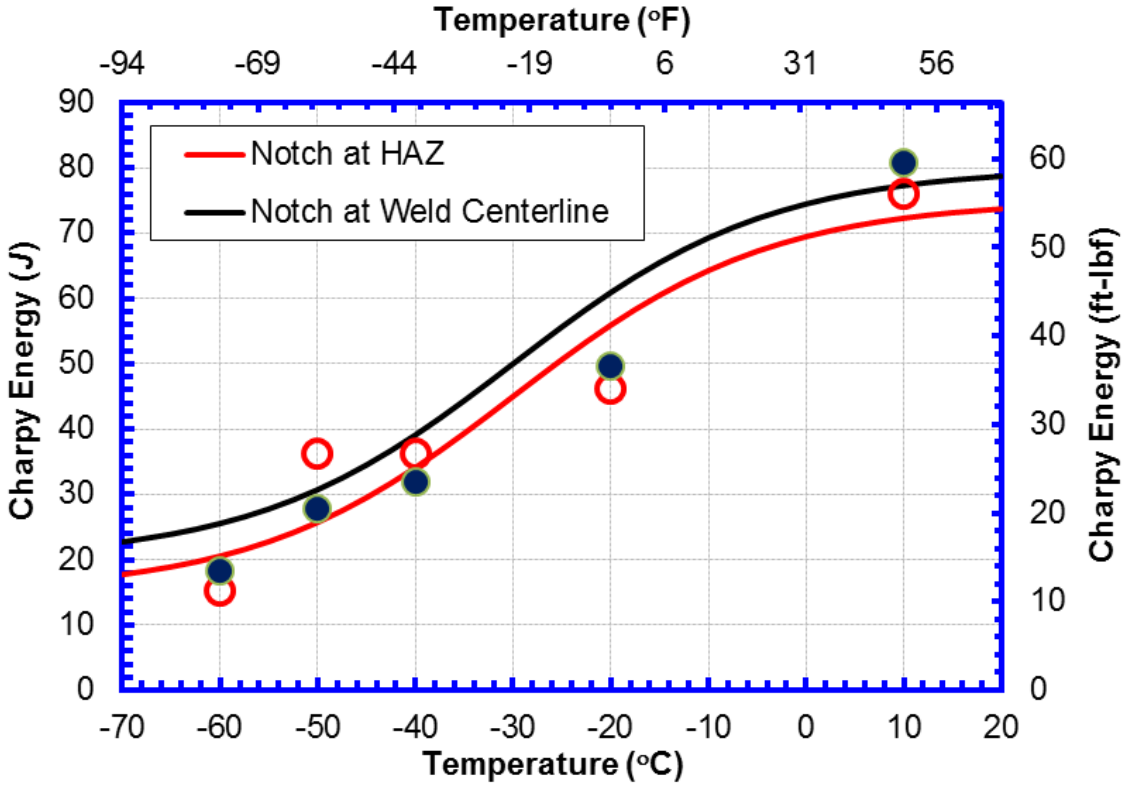

Figure 7-10 Charpy transition curves of a SMAW girth weld made in early 1950's on an X52 pipe. Each data point represents the averaged value of three individual test specimens.

The importance of transition temperature, as opposed to a single value at a given temperature, can be demonstrated in the CTOD transition curves in Figure 7-11 and Figure 7-12. All CTOD tests were conducted in BX2B deeply-notched SENB configurations following test standard BS 7448. In general there is greater scatter at the same test temperature in the HAZ transition curves than that in the weld metal transition curves.

The data scatter, particularly in the HAZ specimens, makes it difficult to precisely draw transition curves. However, it is clear that a CTOD value as high as 0.008 in (0.2 mm) could still indicate lower shelf behavior.

7.5.1.4 Cautionary Notes on New Toughness Tests

Small-scale toughness tests in the form of Charpy and three-point-bend CTOD have been practiced over many decades. There are well established standards governing all aspects of the tests, from specimen preparation, data acquisition, data processing, validity criteria, and reporting.

Single-edge notched tension, or SENT, specimens are being increasingly used to derive resistance curves under low constraint conditions. DNV F108 has a multi-specimen test procedure [88]. A single specimen procedure has been developed by CANMET [89]. ExxonMobil has its own procedure using a double-clip gage method [90]. Until proven otherwise, it is expected that those procedures would produce different results even for the same material behavior as the test procedures, including raw data acquisition and data processing, are different. A project supported by PRCI includes a round-robin effort to examine the consistency of test results from different labs [91].

There are a number of outstanding issues related to the use of SENT test results. There has been argument that SENT test specimens don't need to be fatigue precracked as the test is supposed to capture upper shelf behavior. EDM notch has been proposed as an alternative. Existing fracture toughness test standards have not sanctioned EDM-notched specimens without fatigue pre-cracking. While the EDM notch radius can be controlled in research projects, the radius used among variety of commercial labs should be evaluated carefully. At a minimum, a test procedure should include provisions on the validation and confirmation of EDM notching procedures. Work by Shih, et al., has shown that the blunting of the crack tip needs to be at least 2-3 times of the initial notch radius to minimize the effects of initial notch radius on the toughness test results [92]. For a weld with initiation toughness of 0.024 in (0.60 mm), the radius of the EDM notch should be 0.040 -0.060 in (0.10-0.15 mm) or less for the notch radius not affecting the test results. This is a very tight requirement.

The second issue is the transferability of SENT and full-scale resistance curve. Cheng et. al. has shown that SENT and full-scale specimens provide the same resistance curve [90]. Our analysis and experimental tests have shown that the resistance curves from SENT should be lower than those from full-scale pipe specimens.

The third issue is premature fracture in some SENT specimens. In some cases, SENT specimens would fracture prior or immediately after maximum load. The treatment for such specimens is still an open issue.

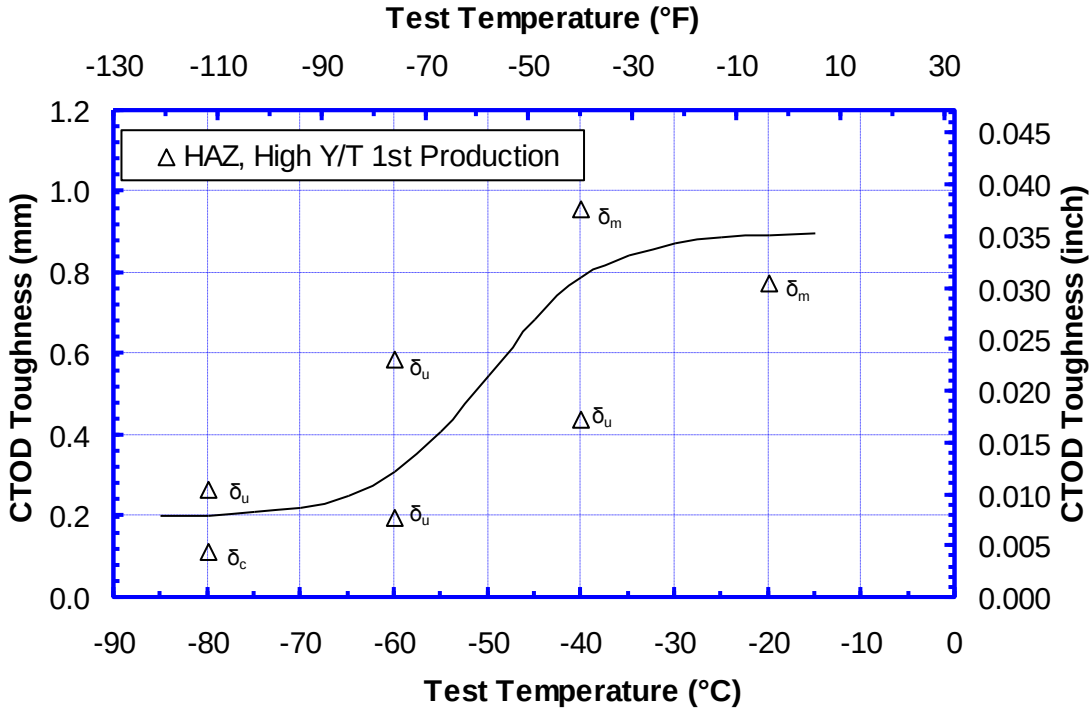

Figure 7-11 HAZ CTOD transition curve of the evenmatch weld of high Y/T X65 pipe

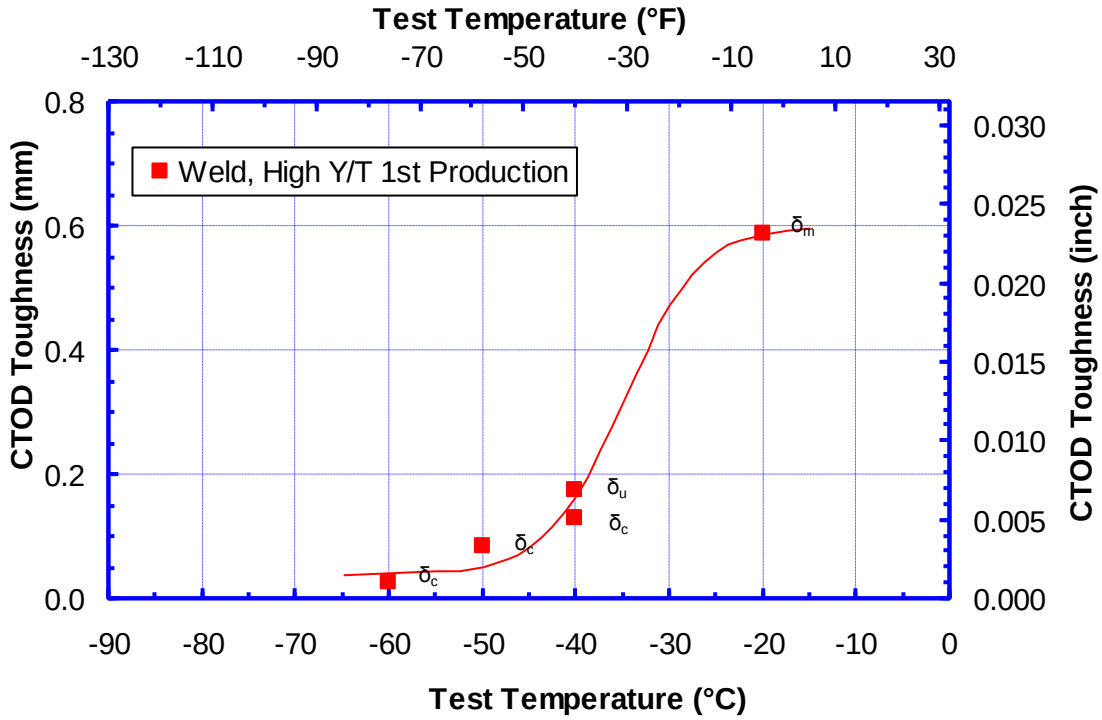

Figure 7-12 Weld metal CTOD transition curve of the evenmatch weld of high Y/T X65 pipe

8 Gaps for Further Studies

8.1 Introduction

The existing tensile and compressive strain models were developed for plain pipes and pipes with regular girth welds which join pipes of equal wall thickness. The imperfections or defects covered in the tensile strain models are the girth weld flaws. The imperfections/defects covered by the compressive strain models are the geometry imperfections due to pipe manufacturing and welding.

Although the existing models covered a large number of influencing factors, some important factors were not considered. The most critical factors needed for further investigations are given in Sections 8.2 and 8.3 for tensile and compressive strain models, respectively.

Transition welds are those which join pipes with pipes and fittings (such as hot bends, elbows, tees, and valves) of unequal wall thickness. The discontinuity of the wall thickness at the weld introduces additional stress/strain concentrations and affects the compressive and tensile strain capacity. In addition, corrosion defects and mechanical damages such as dents are often found in the pipelines. The corrosion defects and mechanical damages can also affect the tensile and compressive strain capacity.

The existing integrity assessment models for the transition welds, corrosion defects, and mechanical damages are not valid for pipelines under high longitudinal strains. In this section, the preliminary studies on the integrity of the pipelines with transition welds, corrosion defects, and mechanical damages under strain-based design conditions are presented.

The results related to the transition welds are presented in Section 8.4. The results on the corrosion defects are given in Section 8.5 and the results on the mechanical damages (dents) are given in Section 8.6.

8.2 Tensile Strain Models for Girth Welds of Equal Wall Thickness

8.2.1 Flaw Interactions

The focus of the tensile strain models is the defects in the girth welds. In all existing models, a single flaw was assumed in a girth weld. However, in general, the girth weld contains multiple flaws. The adjacent flaws may interact with one and another if they are close enough.

In the traditional stress-based design methods, the flaws within a given distance (i.e., spacing limit) must be combined and treated as one big flaw. The spacing limit is usually obtained from historical experiences without sound engineering basis. The spacing limit is often proportional to the flaw sizes.

Under the strain-based design conditions, due to the potential large longitudinal loadings, the spacing limit for potential flaw interactions may be significantly larger than that for the stress-based design conditions. Therefore, the rules for treating the interacting flaws in the stress-based methods may become unrealistic. New rules of the flaw interactions for strain-based designs are needed.

8.2.2 Applicable Strain Ranges

The existing tensile strain models are targeted for strains greater than 1.0%. At the same

time, the traditional stress-based design methods are for the stresses within the elastic limit, i.e., for strains up to 0.2% - 0.5%. Therefore there is a gap for strains between 0.2% to 1.0%. However, in many field conditions, the strains experienced by a pipeline can be between 0.2% and 1.0%. There is a need to extend the current tensile strain models to strains between 0.2% and 1.0%.

8.3 Compressive Strain Models for Girth Welds of Equal Wall Thickness and Plain Pipes

8.3.1 Effect of Net-Section Axial Compressive Force

The refined compressive strain models incorporated the beneficial effect of the longitudinal tensile forces (or stresses). It is known that the compressive stress in the longitudinal direction is detrimental the CSC. The recent research shows that the CSC under pure compressive force is half of the CSC under bending [11]. The reduction of the CSC due to the compressive stress (or strain) in the longitudinal direction could be significant depending on the relative component of the strains from bending and compression. The effect of the compressive stress (or strain) on the CSC needs to be investigated.

8.3.2 Effect of Compression Induced Hoop Strain

Under bending and/or compression, small wrinkles are often developed before the CSC is reached. Although the magnitude of the wrinkles is typically very small, compressive strains of high magnitude can be induced near the wrinkle in the longitudinal directions. The local strains near the wrinkle can often be three times as much as the reported CSC (Figure 3-17). Due to the high longitudinal compressive strain, high tension strains of similar magnitude can be induced in the pipe's hoop direction. The local tensile strain may negatively affect the integrity of a seam weld if the seam weld passes through the wrinkle. The effect of the large hoop strain induced by the longitudinal compression and/or bending on the seam weld integrity needs to be studied.

8.4 Tensile and Compressive Strain Models for Transition Welds

The tensile and compressive strain models discussed in the previous sections are targeted for the regular girth welds for joining pipes of equal wall thickness. The girth welds joining pipes of unequal wall thickness are transition welds. For the transition weld, the pipe with the thicker wall is typically of lower grade (i.e., strength) than the pipe with the thinner wall. The ratio of the wall thickness is determined by the ratio of the strengths of the two pipes. For example, in ASME B31.8 [69], the maximum allowed ratio between the SMYS of the higher grade pipe and the lower grade pipe is 1.5. The minimum required wall thickness ratio between the thicker and thinner pipes equals to the ratio between the SMYS of the higher and lower grade pipes.

To facilitate the fabrication of the welds, the edge of the pipe with the thicker wall is tapered as shown in Figure 8-1. The tapered angle typically ranges between 14° to 30°. The transition welds may often become the weakest link of the pipeline under the strain-based design due to the following factors:

(1) Transition welds are often used to connect elbows, induction bends, Tees, etc. Those connections often behave as anchor points of the pipeline which may see high stress/strain demands.

(2) It tends to generate girth weld defects due to the complicated weld geometries.

(3) The geometrical discontinuity at the transition weld often induces additional stress/strain concentrations.

(4) The segment of the pipe in the tapered area has the reduced load carrying capacity due to the low strength and reduced wall thickness.

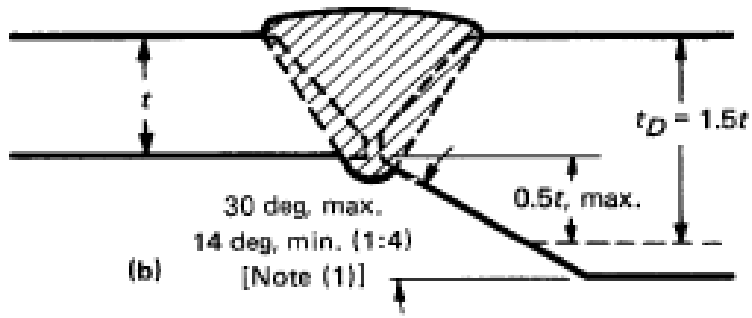

Figure 8-1 Acceptable design of unequal wall thickness [69]

To demonstrate the tensile strain capacity of the transition welds, a couple of sample cases were analyzed with FEA. A typical FEA model is shown in Figure 8-2 where the thicker wall pipe with lower strength is referred to as 'fitting' and the thinner wall pipe with higher strength is referred to as 'pipe'. Due to symmetry conditions, only half of the pipe in the hoop direction was modeled. The parameters used in the analyses are summarized in Table 8-1. In sample case A (Table 8-1), the ratio between the wall thickness is close to the ratio between the strength of the fitting and the pipe (i.e., $t_{fitting}/t_{pipe} \approx YS_{pipe}/YS_{fitting}$) which represents the conditions which satisfy the minimum design requirement. In sample case B, the wall thickness ratio is greater than the strength ratio (i.e., $t_{fitting}/t_{pipe} > YS_{pipe}/YS_{fitting}$). In each case (A and B), the transition welds with two thickness (strength) ratios were investigated. The regular welds of equal wall thickness (i.e., equal strength) were also analyzed for reference. The TSC from the FEA is shown in Figure 8-3 and Figure 8-4 for the sample cases A and B, respectively, where the TSC was measured on the pipe with the thinner wall. For the case A where the wall thickness ratios satisfied the minimum design requirement, the TSC of the transition welds is significantly smaller than that of the regular welds. For case B, the TSC of the transition welds is smaller than that of the regular welds. The higher the thickness (strength) ratio, the higher the reduction of the TSC.

Table 8-1 Parameters used for transition weld analyses

Sample Case	YS (ksi)		Y/T		Wall Thickness (inch)		Thickness Ratio	YS Ratio
	Pipe	Fitting	Pipe	Fitting	Pipe	Fitting	$t_{fitting}/t_{pipe}$	$YS_{pipe}/YS_{fitting}$
A	80	65	0.88	0.84	0.5	0.625	1.25	1.23
		56		0.84		0.750	1.50	1.43
B	95	85	0.91	0.87	0.5	0.625	1.25	1.12
		75		0.82		0.688	1.38	1.27
Flaw depth = 3.0 mm, Flaw length = 50.0 mm, Pressure factor = 0.60, Weld strength overmatch = 10%, CTODA = 1.0 mm								

The results indicated that for the strain-based design, more stringent requirements on the minimum wall thickness ratio and maximum allowed strength ratio need to be developed. For example, the maximum allowed strength ratio may need to be reduced and the minimum wall thickness ratio needs to be increased. Tensile strain models are needed for transition welds.

In addition to the tensile strain capacity, the compressive strain capacity may also be affected by the transition welds. The compressive strain models for the transition welds are needed.

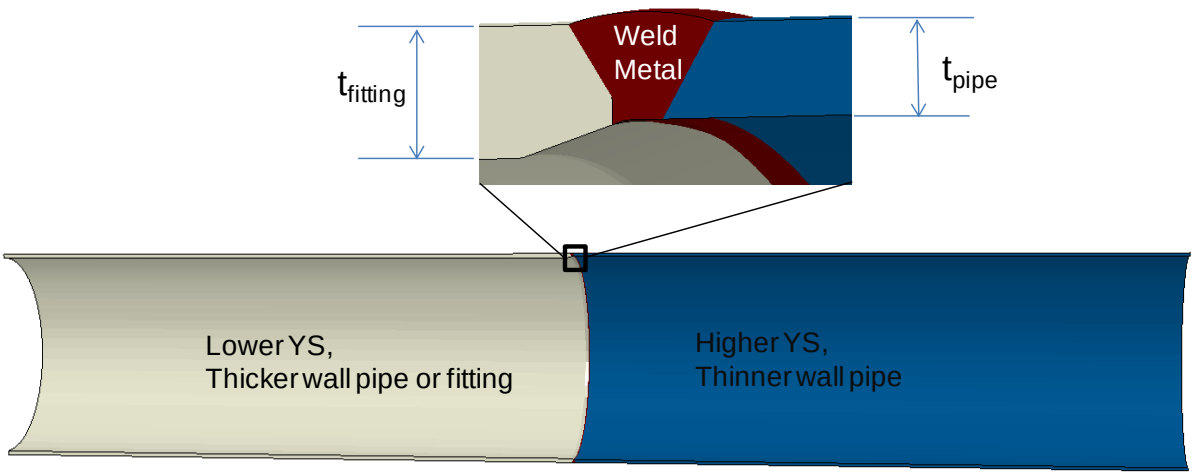

Figure 8-2 FEA model for transition welds

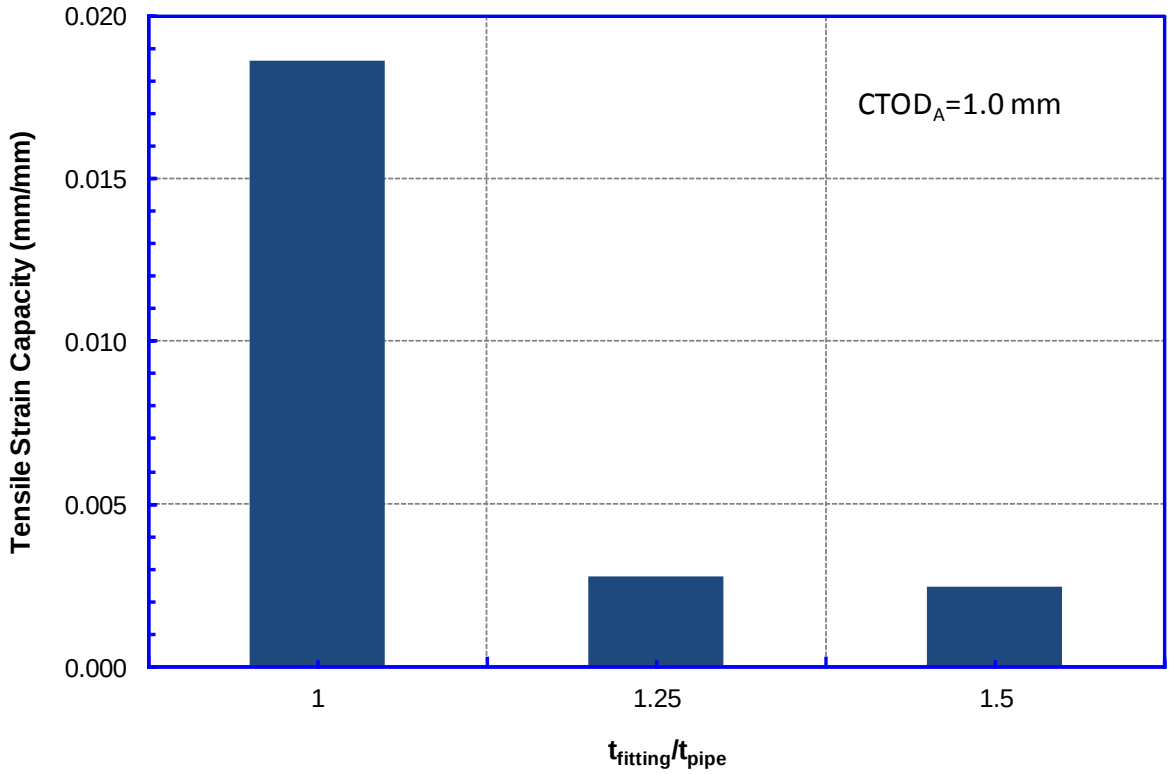

Figure 8-3 TSC for sample case A (minimum design requirement)

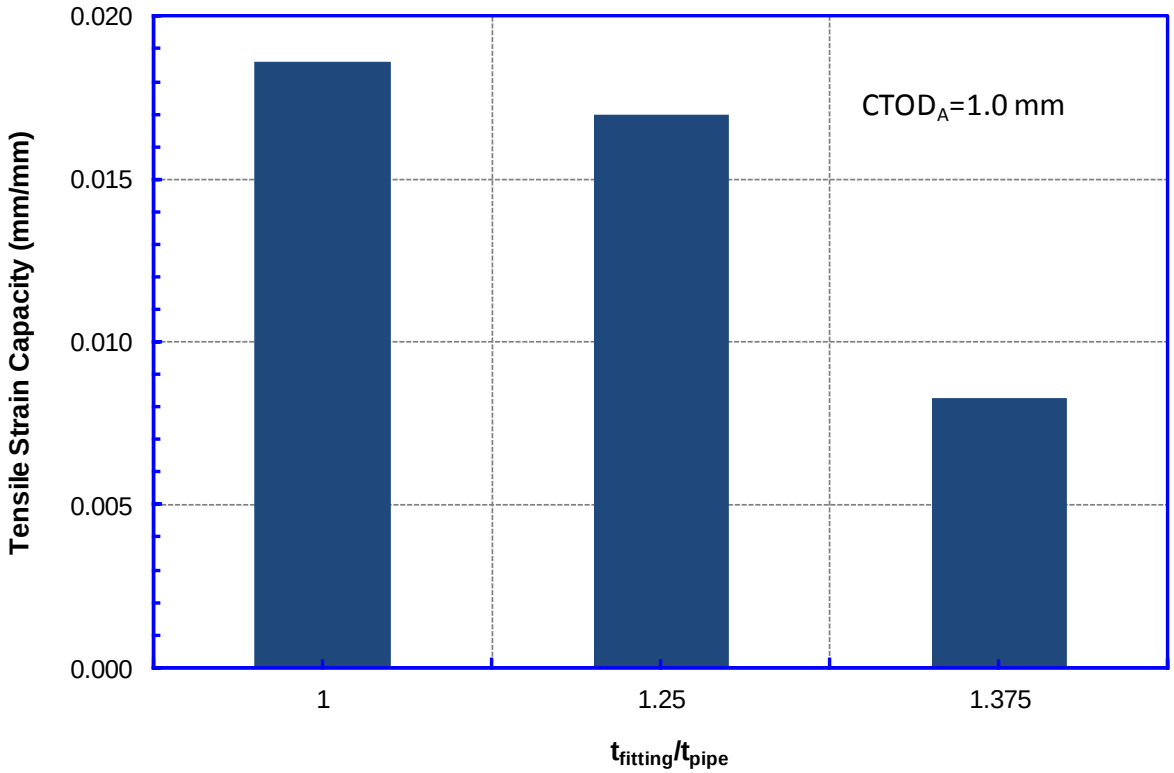

Figure 8-4 TSC for sample case B (more stringent design requirement)

8.5 Burst Pressure and Tensile/Compressive Strain Models for Corroded Pipes

8.5.1 Burst Pressure

The pipelines in service contain corrosion defects. Under strain-based design conditions, the following limit states need to be considered for the pipes with corrosion defects.

(1) Burst pressure under high longitudinal strains,

(2) Tensile strain capacity,

(3) Compressive strain capacity.

Many limit state equations for the burst pressure of corroded pipes currently exist. However, the existing equations have not considered the situations where large longitudinal strains are present. The longitudinal strains, especially the compressive strains, may be detrimental to the burst pressure. A sample FEA was performed to study the effect the longitudinal strains on the burst pressure. The finite element model is shown in Figure 8-5. Due to symmetry conditions, only half of the pipe was modeled. The parameters used in the FEA are given in the following:

- Materials: Yield Strength (YS) = 69 ksi and Y/T = 0.76,
- Pipe size: OD = 30 in (762 mm), t = 0.5 in (12.7 mm),
- Corrosion defect: d = 50%t, L_{axial} = 23.6 in (600 mm), L_{hoop} = 23.6 in (600 mm).

The calculated burst pressure for different longitudinal strains is shown in Figure 8-6. The calculated burst pressure was normalized by the burst pressure calculated from the modified B31G equations. The results indicate that the longitudinal strains have limited effect on the burst pressure. The tensile strains slightly increase the burst pressure while the compressive strains

slightly decrease the burst pressure. The modified B31G equations give conservative burst pressure for all situations.

8.5.2 Tensile and Compressive Strains

The tensile and compressive strain capacity of the corroded pipes was also analyzed with sample FEA. The FEA model in Figure 8-5 was used in the analyses. In the simulations of the compressive strain capacity, the corrosion defects were located on the compressive side of the pipe. The parameters used in the analyses are given in the following:

- Materials: Yield Strength (YS) = 69 ksi and Y/T = 0.76,
- Pipe size: OD = 30 in (762 mm), t = 0.5 in (12.7 mm),
- Corrosion defect: d = 50%t, L_{axial} = variable, L_{hoop} = variable,
- Internal pressure: pressure factor = 0.60.

The calculated tensile (TSC) and compressive (CSC) strain capacity for various corrosion defects is shown in Figure 8-7 and Figure 8-8, respectively. The results indicated that the TSC can be greatly reduced by increasing the defect size in the circumferential direction. The TSC is reduced from about 5% to 1% when the width of the corrosion defects in the pipe circumference increases from 3.9 to 23.6 in (100 to 600 mm), i.e., from 4.1% to 25% of the pipe's perimeter. Compared with the girth weld flaws, the corrosion defects may become the weakest link in terms of the TSC. It is expected that the defect size in the longitudinal direction can also affect the tensile strain capacity.

The compressive strain capacity can be affected by the defect size in both the longitudinal and hoop directions. Increasing the defect size in the circumferential direction from 3.9 to 23.6 in (100 to 600 mm) decreases the compressive strain capacity. However, it is found that the compressive strain capacity is increased by increasing the defect size in the longitudinal direction from 7.8 to 23.6 in (200 to 600 mm). In Section 3.6.2 of the report, it is shown that the geometry imperfections of the critical wavelength are the most detrimental to the compressive strain capacity. The corrosion defects are also a type of geometry imperfections. Therefore, the corrosion defects of certain lengths in the longitudinal direction may be the most detrimental to the compressive strain capacity.

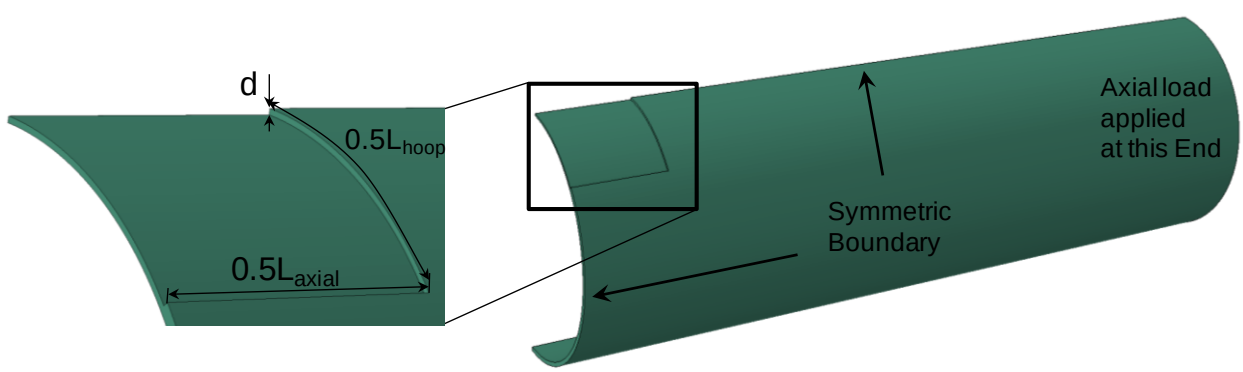

Figure 8-5 FEA model for corroded pipes

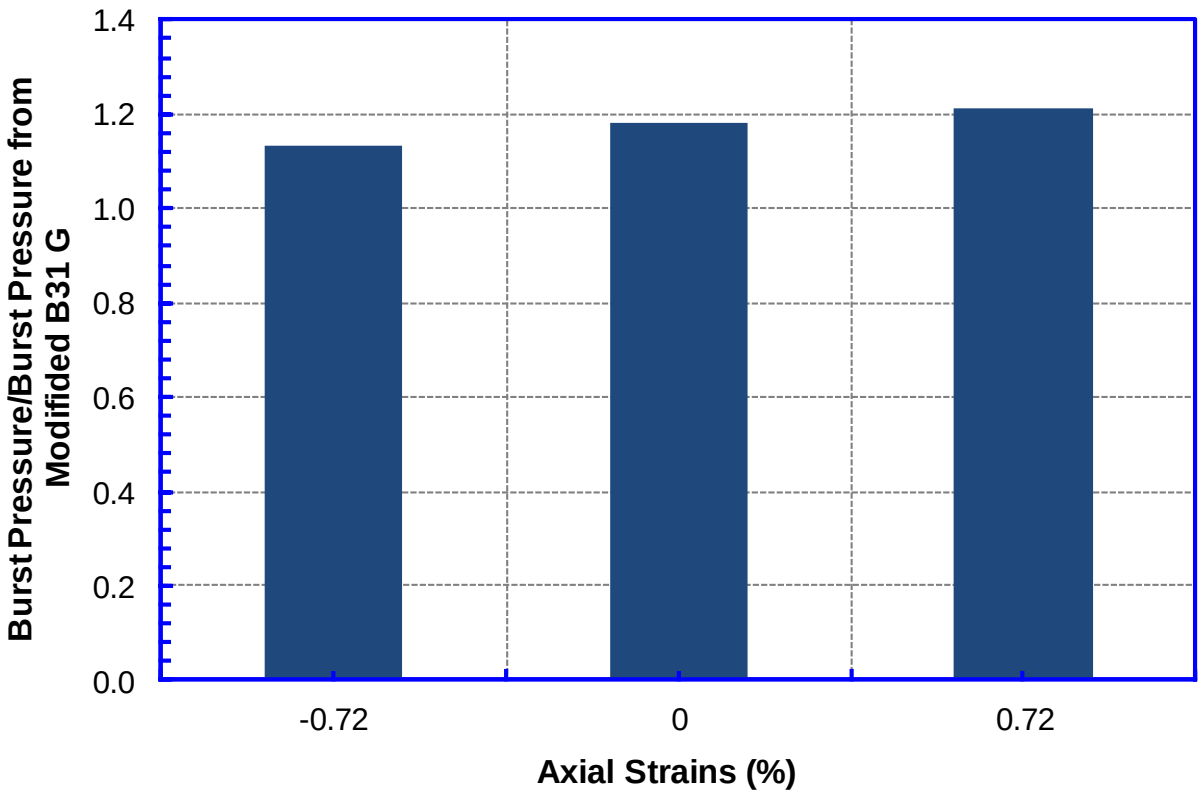

Figure 8-6 Burst pressure of corroded pipes at different axial/longitudinal strains

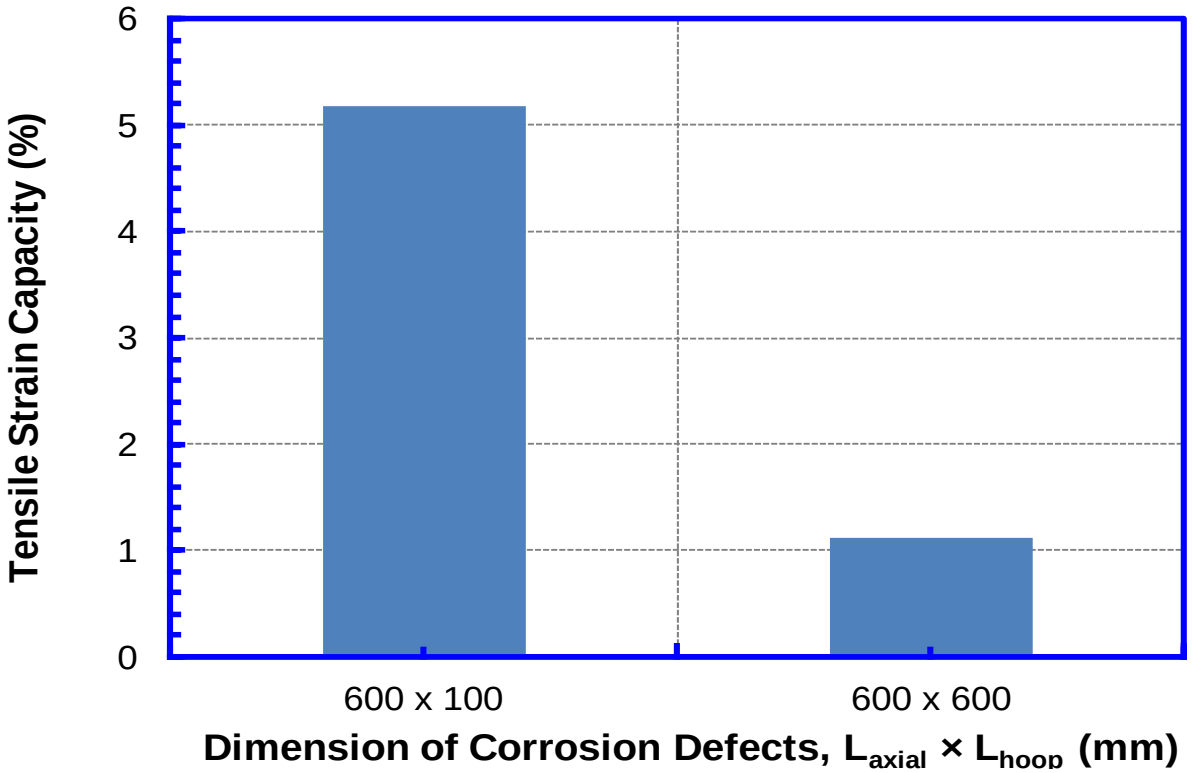

Figure 8-7 Tensile strain capacity of corroded pipes

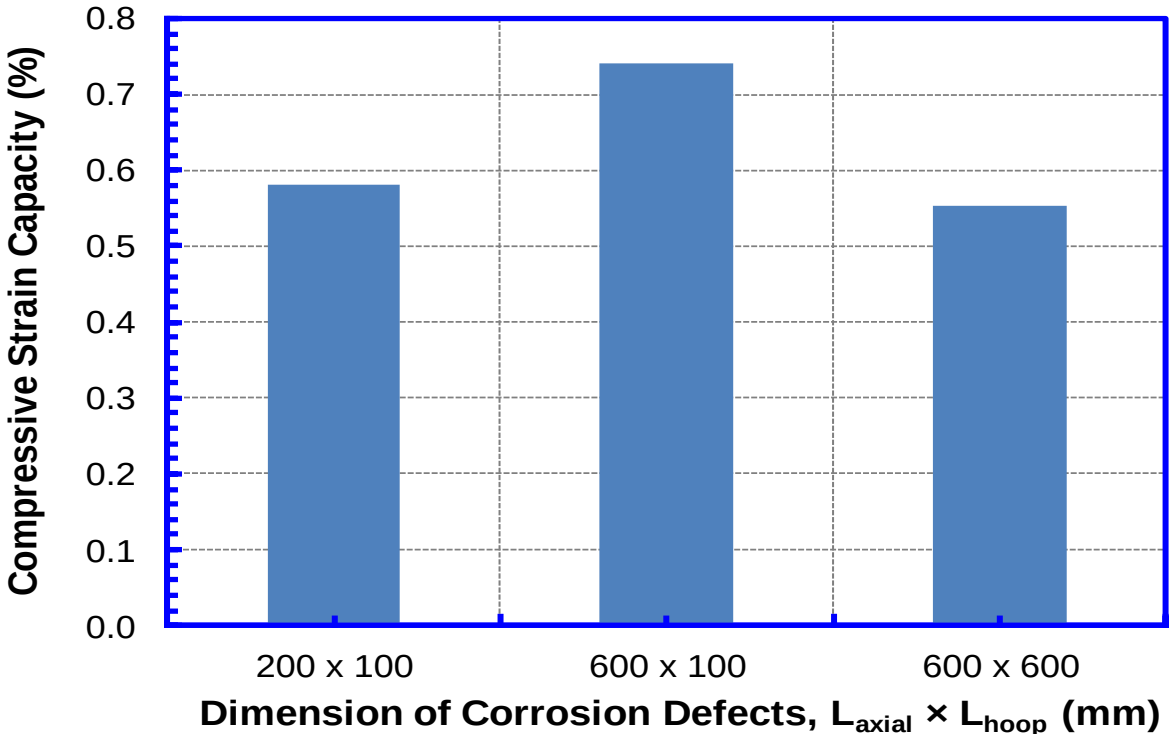

Figure 8-8 Compressive strain capacity of corroded pipes

8.6 Compressive Strain Models for Dented Pipes

Mechanical damages such as dents are common threats to the in-service pipelines. The dents can be formed due to the contact of the pipeline with other hard objects such as rocks, excavation equipments, etc. The dents often come with other defects such as gauges and cracks. The focus of this study is the plain dents (the ones without gauges and other defects).

Similar to the corroded pipes, three limit states also exist for the pipes with dents: (1) burst pressure, (2) tensile strain capacity, and (3) compressive strain capacity. It has been found that the plain dents don't show significant effects on the burst pressure. It is also expected that the plain dents will have limited effects on the tensile strain capacity. However, since the dents can be considered a type of geometry imperfections, the dents can affect the compressive strain capacity of the pipe. Sample FEA were conducted to study the effect of the dents on the compressive strain capacity of pipes. The variables used in the sample analyses are given in the following:

- Materials: X52,
- Pipe size: OD = 24 in (609.6 mm), WT = 0.31 in (7.9 mm),
- Spherical indenter radius = 4.5 in (114.0 mm).

The typical FEA model used in the FEA of the dented pipes is shown in Figure 8-9. It is well known that the shape of a dent can change due to the pressurization of the pipe. To simulate the change of a dent at different stages of the pipeline service, five steps representing various loading conditions were used as shown in Table 8-2. Step 1 simulates the dent formation during the transportation or construction of the pipes or pipeline. Step 2 simulates the elastic rerounding of

the dent due to the removal of the hard object. Step 3 simulates the plastic rerounding of the dent during the hydrotesting. Step 4 simulates the rerounding and stabilization of the dent shape under operating pressure cycles. Step 5 simulate the bending of the dented pipe due to ground deformation.

The calculated compressive strain capacity and maximum bending moment for various dent depths are shown in Figure 8-10. The results show that both the compressive strain capacity and bending moment are reduced by the dents. The larger the depths of the dents, the larger the reduction of the compressive strain capacity and maximum bending moment.

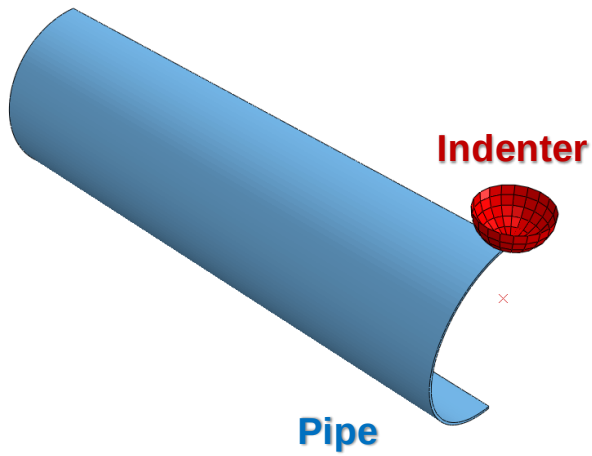

Figure 8-9 FEA model for dented pipes

Table 8-2 FEA procedures for dented pipes

Step number	Simulation in FEA	Related field situation
1 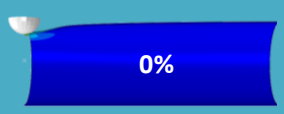	Indentation, zero internal pressure	A pipe is dented during transportation/construction
2 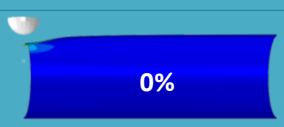	Remove indenter, zero internal pressure (Elastic rerounding)	The object that caused dent is no longer in contact with the pipe.
3 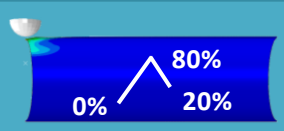	First pressure cycle Hoop stress/SMYS: 0% → 80% → 20% (Plastic rerounding)	Hydrostatic test.
4 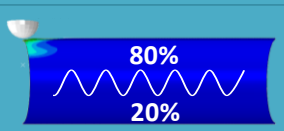	Additional five pressure cycles 20% ≤ Hoop stress/SMYS ≤ 80%	Dent depth is stabilized under normal pressure cycles during operation .
5 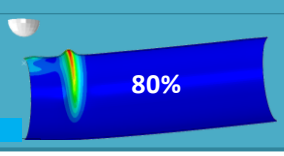	Bending with internal pressure Hoop stress/SMYS = 80%	Large deformation hazard (e.g., ground movement) is encountered.

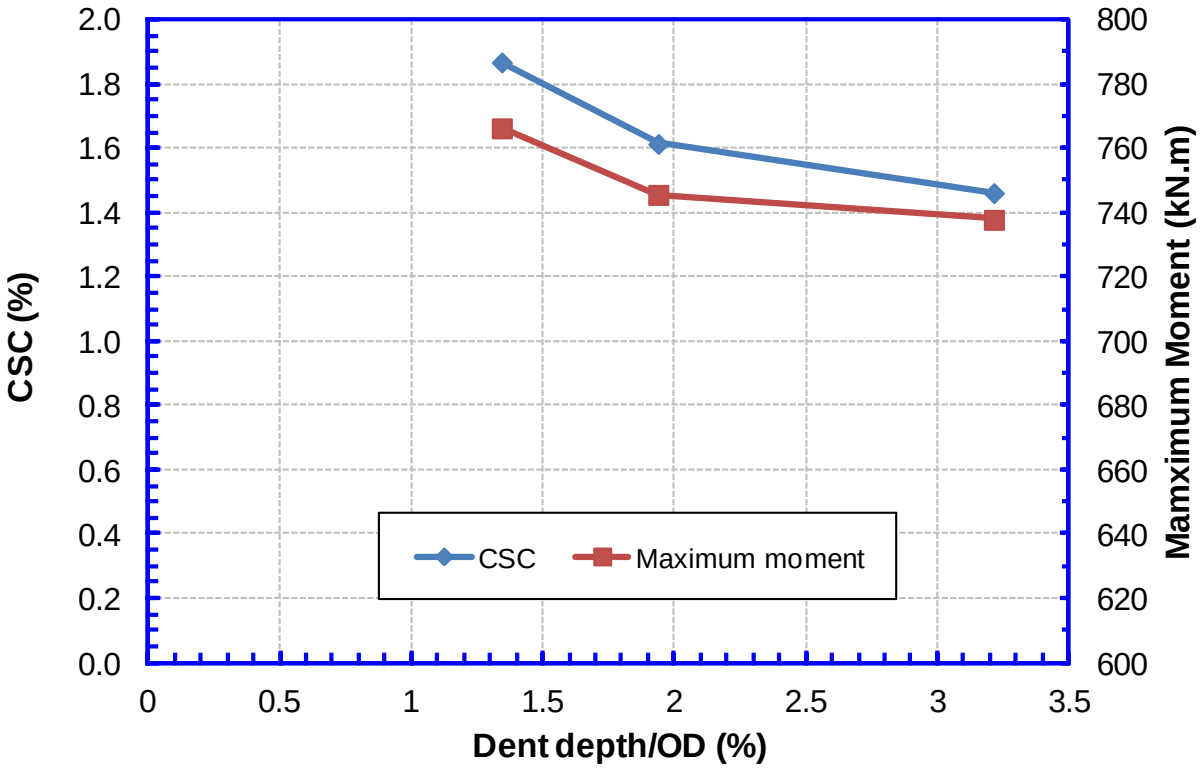

Figure 8-10 Effect of dents on the compressive strain capacity

9 Concluding Remarks

Pipeline design against longitudinal load/stress/strain has been around for many decades. However the development and application of modern quantitative strain-based design methodology are very new. Significant progress has been made in the last decade in strain-based design models which correlate the strain capacity with various influencing parameters. These models are only a part of an overall strain-based design approach. Parallel developments, particularly tools and procedures that enable the effective use of those models are still needed.

One of the major contributions of this project is the development of refined compressive strain models. The refined compressive strain models developed in this project will lead to more accurate prediction of the compressive strain capacity in realistic pipeline environments. When combined with the tensile strain models developed previously, these models allow effective use of strain-based design for new pipelines and strain-based assessment for existing pipelines. The implementation of the ranking system for SBD will allow the prioritization of resources in all phases of a pipeline's service life, including material procurement, welding, construction, and post-construction integrity management. The outputs of this project provide effective tools in mitigating threats that cause high longitudinal strains in pipelines.

The status of the tensile and compressive strain models are briefly summarized below. This summary is followed by a gap analysis and thoughts on future research directions.

9.1 Tensile Strain Models

Various tensile strain models have been developed in recent years. In-depth analysis and comparison of model predictions and experimental test data have led to the following general observations.

1. Pipelines subjected to strain-based design are expected to operate when the material is under fully plastic conditions. Under these conditions, a small variation in material's strength, either within a single joint or among multiple joints, can lead to large spatial variations in strains. Such variations should be accounted for in pipeline designs and maintenance.
2. The potential large spatial variations of strains should be considered in setting up the instrumentation plan in large scale testing. The test procedure, data acquisition, and post-test data analysis should be fully documented and open for review. Furthermore such variations shall be considered in model evaluations.
3. While there are some important differences among various tensile strain models, the impact of uncertainties in material properties introduced by current material testing procedures should not be underestimated. Improvements are needed in almost all test procedures in order to capture material properties at the level of accuracy that is commensurate with the requirements of strain-based design.
4. There can be large variations in the measured TSC, particularly when the measured TSC is high. In some cases, strains measured on either side of a girth weld can differ by a factor of two or more even when both sides were taken from the same joint of pipe.

5. The PRCI-CRES tensile strain models provide similarly consistent prediction from girth welds of pipes from Grade X56 to X100. There is an overall good agreement between the experimentally measured and predicted TSC.
6. There is no obvious improvement in the accuracy of the predicted TSC by using ductile instability limit state than initiation limit state.
7. Although ductile instability is a valid limit state for tensile strain design, limit state on the basis of initiation control is preferred for tensile strain design.
   (a) It is demonstrated that the remaining strain capacity is limited after the initiation of a macroscopic flaw growth. Consequently, sufficiently accurate strain capacity can be determined from the initiation limit state.
   (b) Repeated application of strains on pipeline girth welds is possible in offshore installation by reeling, in in-service pipelines under frost heave and thaw settlement (due to seasonable temperature variations), and in the events of earthquake. Designs on the basis of instability limit state, which allows flaw growth to a point of instability in the first application of strain, does not have reserve for subsequent applications of strains. Design on the basis of initiation control does not permit flaw growth thus has reserve for multiple cycles of strain application.
   (c) Tensile strain design on the basis of ductile instability assumes greater risks in comparison to initiation control without appreciably additional benefits.

9.2 Compressive Strain Models

The following existing CSC models were reviewed in details:

- CSA Z662;
- DNV OS F101;
- API RP 1111;
- University of Alberta (UOA);
- JFE; and
- C-FER.

The comprehensive review demonstrates that the existing CSC models have:

- large differences in input parameters and their applicable ranges;
- large differences in computed CSC, especially for pressurized conditions;
- large differences in recommended safety factors; and
- inconsistent trends on the conservatism of CSC.

The differences in the CSC models are partially due to the differences in the modeling processes used to develop those CSC models. Improved modeling processes were established through systematic studies on various (experimental and/or numerical) modeling factors including:

- the representation of material properties;

- the representation of field conditions;
- the definition/measurement of the compressive strain and strain capacity;
- the construction of the finite element models.

Refined compressive strain models are developed using the improved modeling processes. The models recognize the following parameters:

- Pipe *D*/*t* ratio;
- Internal pressure;
- Pipe Y/T ratio;
- Geometry imperfection, specifically the height (from peak to valley) of pipe surface undulation;
- Pipe uniform strain;
- Pipe Lüder's strain; and
- Net-section stress (only tension currently).

Since the geometry imperfections which are critical to the CSC are often not easily available, recommendations on the size of the geometry imperfections are provided. The refined models are evaluated with 40 full-scale bending tests in the public domain.

Compared with the other existing compressive strain models, the refined compressive strain models provide the following key improvements:

- The refined models are developed using a set of modeling procedures that provide realistic representation of field conditions;
- The refined models recognize an increased number of key controlling parameters compared with the existing models;
- The applicable range of each controlling parameter is extended or similar to the largest range of the existing models;
- The effects of the pipe *D*/*t* ratio and internal pressure are more precisely captured than the existing models;
- The compressive strain capacity (CSC) can be greatly affected by geometry imperfections. The magnitude of geometry imperfections is usually not available. Recommendations on the median, lower, and upper bound levels of geometry imperfections are provided. The upper bound geometry imperfections can lead to reasonably conservative CSC. The median and upper/lower geometry imperfections can lead to more realistic range of CSC with balanced conservatism.
- The effect of the girth weld, especially the effect of the high-low misalignment, is more properly accounted for than the existing models.

9.3 Gaps in Strain-Based Design and Future Directions

Strain-based design is an evolving engineering discipline. Although there has been significant progress in models for strain-based design, there is no generally agreed framework at

the regulatory and standards level. Furthermore, methodologies for strain-based design need to be robust yet flexible for pipeline projects of various scales.

A few gaps and recommended future direction are summarized below.

9.3.1 Regulatory Requirements

Until recently, there has been no practically actionable regulatory approach towards strain-based design. It is in the interest of all stakeholders that a regulatory framework be developed. Recently published possible conditions for strain-based design is a good starting point for such framework [93]. The possible conditions in the recent publication include

- Requirement for SBD plans before, during, and after pipeline construction,
- Requirements for design and materials, including linepipe specifications, engineering critical assessment, testing procedures, fracture control, etc.
- Requirements for construction, including welding procedure qualification, construction quality control, girth weld testing and identification during construction, use of high resolution caliper tools soon after construction to establish baseline conditions, cathodic protection, and right-of-way monitoring,
- Requirements for Operations and Maintenance (O&M), including O&M procedures, strain demand monitoring, geospatial pipeline mapping, and corrosion control, and
- Levels of remediation action based on the strain demand limit and the range of actual strain demand.

In addition to the specific requirements, common terms in strain-based design are defined in the document. Examples of pipe specifications and steel pre-production qualification are given.

The possible conditions cover a wide range of subject areas. As in many regulatory documents, striking a proper balance between performance and prescriptive requirements can be a challenge. As there are still many gaps in the application of strain-based design and no standardized SBD procedures, certain level of prescriptive requirements are necessary. Furthermore, test data used to facilitate and justify designs should be fully documented and subjected to review by qualified personnel.

It is expected that the possible conditions be updated when more knowledge and experience are gained in practice. The application of these conditions in small pipeline projects may be reviewed and updated as needed. For small projects, different strategies may be taken to achieve the necessary strain capacity. For instance lower grade and heavy wall pipes may be used to increase the weld metal overmatching level and compressive strain capacity. Furthermore, pipes with tight range of properties may be procured. Sufficient margins may be built into the design and fabrication so possible girth weld failures in tension may be prevented. In other words, girth welds may be fabricated with sufficient robustness that plastic tensile straining may only occur in the pipe body. Such a goal is achievable for a pipeline segment of short length when the properties of the pipe and weld can be controlled in tight ranges and flaw acceptance criteria are set to small values without affecting the overall construction speed. Adopting this strategy would reduce or even eliminate the need for full-scale testing which can be a large burden on a small project.

9.3.2 Strain Demand

The determination of strain demand typically involves three key steps:

1. *Route hazards*. In the case of ground movement, the propensity and magnitude of the ground movement need to be established. Site-specific investigations may be necessary.
2. *Pipe-soil interaction.* The soil response to the ground movement and its interaction with the pipe depend on soil properties which in turn may be affected by soil type and moisture content.
3. *Pipe properties.* The strain demand generated by the soil surrounding the pipe is affected by the tensile properties of the pipe, including strength distribution, strain hardening capacity, and anisotropy (property difference in different directions, such as hoop vs. longitudinal direction). Furthermore, the value of strain demand can be affected by the magnitude of internal pressure.

In North America, strain demand analysis is often performed by a limited number of specialists. Procedures to ensure consistent outcome should be explored. Guidelines on the data collection, data processing, and usage of the processed data in the strain demand calculation in all three key steps would be helpful in ensuring consistent outcome.

9.3.3 Strain Capacity under Realistic Conditions

9.3.3.1 Interaction of Anomalies and High Longitudinal Strain

Most pipelines would be subjected to corrosion and mechanical damage of various degrees in their lifetime. The current methodologies for assessing and mitigating those anomalies were developed under the conditions of high hoop stress and low longitudinal stress. Under strain-based design, the stress and strain in the longitudinal direction are much higher than those assumed in the development of the anomaly assessment methodology. There are essentially two issues here: (1) the validity and conservatism of the assessment models under the conditions of high longitudinal strain and (2) impact of the anomalies on the strain capacity of the pipelines. Those two issues should be resolved for pipelines using strain-based design.

9.3.3.2 Strain Capacity of Manual Welds and Pipe Segments with Fittings

Almost all strain-based design models were developed for and are applicable to nominally straight sections of pipelines with nominally the same geometric and material properties. In the case of tensile strain models, most of the work has focused on mechanized GMAW welds. Most pipelines contain fittings such as hot bends, elbows, tees, and valves. The manual welds connecting those fittings to the adjacent linepipes usually have lower strength and toughness than mechanized GMAW welds. Some of these fittings, such as hot bends and elbows, may be located in the areas of high strain demand due to the topography of the right-of-way. The geometry of the fitting welds introduces strain concentrations due to wall thickness transitions and/or high-low misalignment. Fitting welds are potentially subjected to higher longitudinal strains and have less desirable properties than mainline welds. The strain capacity of these welds is largely unknown and a corresponding assessment methodology has not yet been developed.

9.3.3.3 Multiple Flaws and Flaw Interaction Rules

Almost all tensile strain models to date assume only one flaw in one girth weld. In production welds, multiple indications may exist in a single girth weld during NDT. Tensile strain models capable of dealing with multiple flaws and/or flaw interaction rules need to be developed to effectively deal with the welds with multiple indications.

9.3.3.4 Effect of Net-Section Compressive Force on Compressive Strain Capacity

Many compressive strain models are established on models and/or experimental test data by assuming pipes are under lateral bending. The refined compressive strain models developed in this project incorporate the beneficial effects of the longitudinal tensile forces. It is known that the addition of net-section longitudinal compressive force would reduce the CSC to levels below those of pure lateral bending. The net-section compressive force is often a contributor to field wrinkles/buckles. Therefore the effects of the net-section compressive force on the CSC need to be investigated.

9.3.3.5 Effect of Compression Induced Hoop Strain

Under bending and/or compression, small wrinkles are often developed before the CSC is reached. Although the magnitude of the wrinkles is typically small, local compressive strains of high magnitude can be induced near the wrinkle in the longitudinal directions. Similarly high magnitude of local tension strains can be induced in the pipe's hoop direction. The local tensile strain may negatively affect the integrity of a seam weld if the locations of the seam weld and the wrinkle coincide. The effect of the high tensile hoop strain in the vicinity of a wrinkle should be investigated.

9.3.3.6 Role of High-Low Misalignment

The effects of high-low misalignment are incorporated in the PRCI-CRES tensile strain models and CRES compressive strain models. Some other tensile strain models also include the effects of high-low misalignment. There is some indication that the effects of misalignment in those models may be overly pessimistic. The width of weld cap reinforcement in actual production welds tends to be wider than that assumed in the finite element models from which the tensile strain models were developed. Wide weld cap reduce the negative impact of high-low misalignment. The effects of high-low misalignment may be further analyzed and refined.

Field implementation of tensile strain design models would require accurate measurement and documentation of weld high-low misalignment values on every weld subjected to strain-based design. Furthermore, mitigation options are needed if the misalignment is found to exceed the target limit.

9.3.3.7 Consistency of Field Weld Quality vs. Property Variations

Some monitoring procedures may be necessary to ensure the field production welds are made to specifications and the properties are nominally equivalent to the qualification welds. At the same time, certain property variations are unavoidable. Strategies would be developed to account for the variations.

9.3.4 Testing Procedures and Material Qualification

Tensile strain capacity is very sensitive to a number of material parameters, such as strain hardening, toughness, and weld strength mismatch. Test procedures necessary to characterize those parameters either do not exist or do not have sufficient details and rigor to ensure the generation of consistent and representative data. Some of these issues are covered in Section 7. The possible conditions for strain-based design from PHMSA have a detailed list of elements that should be considered/included in test procedures [93].

9.3.5 Codes and Standards

Based on the current scope of various codes and standards, additional requirements targeted for strain-based design may be included in the following US standards and their equivalent standards in other countries.

- ASME B31.4 and B31.8
  - Conditions that require strain-based design
  - Overall design protocols
  - Strain capacity models
- API 5L
  - Linepipe specifications
  - Pipe mill test requirements
  - Pipe dimensional control
  - Calibration and possible refinement of test procedures
  - Additional reporting requirements
- API 1104
  - Welding procedure qualification
    - Confirmation and/or refinement of the list of essential variables
    - Test procedures for non-standardized tests
  - Flaw acceptance criteria, including flaw interaction rules
  - Repair procedures and proper account for property changes due to repair welding
- ASME B31.8S
  - Evaluation and prioritization of high-strain events
  - Evaluation of anomalies under high longitudinal strain conditions

In addition to the elements that may be covered by those standards, the following guidelines/tools are necessary or helpful for strain-based design:

- Guideline or protocol on strain demand evaluation,
- Project QA/QC procedures, and
- Minimum requirements for the confirmation of strain capacity.

It may be noted that the incorporate of the suggested additions to the relevant standards is still many years away. However, working group may be formed to start moving the process forward.

9.4 Summary

There has been remarkable progress in some areas of strain-based design through the joint efforts of the pipeline industry and government entities. There are still many unknowns and gaps. It is crucial that open communications be maintained among all stakeholders. Due to the lack of sufficiently refined and standardized test procedures, all test data shall be provided along with full test details, from specimen extraction to final presentation of the data, when they are used to support strain-based design. Efforts should be made to develop and implement standard test procedures when appropriate. Only with sufficiently robust test procedures can material properties variations be properly characterized and incorporated into strain-based design.

10 References

1 Wang, Y.-Y., Liu, M., Stephens, M., Petersen, R., and Horsley, D., 2009, "Recent development in strain-based design in North America," *Proceedings of the 19th International Offshore and Polar Engineering Conference*, Osaka, Japan, July 21-26.

2 Sandivk, A., Østby, E, Naess A., Sigurdsson G., and Thaulow, C., 2005, "Fracture control – offshore pipelines: probabilistic fracture assessment of surface cracked ductile pipelines using analytical equations", *Proceeding of the 24th Internal Conference on Offshore Mechanics and Arctic Engineering*, Halkidiki, Greece, June 12-17.

3 Kibey, S.A., Minnaar, K., Cheng, W., and Wang, X., 2009, "Development of a physics-based approach for the predictions of strain capacity of welded pipelines", *Proceedings of the 19th International Offshore and Polar Engineering Conference*, p132, Osaka, Japan, June 21-26.

4 Wang, Y.-Y., Liu, M., Long, X., Stephens, M., Petersen, R., and Gordon, R., 2011, "Validation & Documentation of Tensile Strain Limit Design Models for Pipelines," US DOT Contract No. DTPH56-06-T000014, final report. http://primis.phmsa.dot.gov/matrix/PrjHome.rdm?prj=200

5 Wang, Y.-Y., Liu, M., and Song, Y., 2011, "Second Generation Models for Strain-Based Design," US DOT Contract No. DTPH56-06-T000014, final report.

http://primis.phmsa.dot.gov/matrix/PrjHome.rdm?prj=201

6 Zimmerman, T., Timms, C., Xie, J., and Asante, J., 2004, "Buckling resistance of large diameter spiral welded linepipe," *Proceedings of the 5th International Pipeline Conference*, Calgary, Alberta, Canada, October 4 – 8.

7 Det Norske Veritas, 2010, "Submarine pipeline systems", DNV-OS-F101.

8 Canadian Standard Association, 2011, "Oil and gas pipeline systems", CSA Z662.

9 American Petroleum Institute, 1999, "Design, construction, operation, and maintenance of offshore hydrocarbon pipelines (limit state design)", API RP 1111.

10 Dorey, A.B., Murray, D.W., and Cheng, J.J.R., 2006, "Critical buckling strain equations for energy pipelines - a parametric study", *Journal of Offshore Mechanics and Arctic Engineering*, v128, p248-255.

11 Suzuki, N., Zhou, J., and Toyoda, M., 2008, "Compressive strain limits of high-strength linepipes", *Proceedings of 7th International Pipeline Conference*, Calgary, Alberta, Canada, Sep. 29 - Oct. 3.

12 Suzuki, N., and Toyoda, M., 2002, "Critical compressive strain of linepipes related to work hardening parameters," *Proceedings of 21st International Conference on Offshore Mechanics and Arctic Engineering*, Oslo, Norway, June 23 - 28.

13 Suzuki, N. and Igi, S., 2007, "Compressive strain limits of X80 high-strain line pipes", *Proceedings of 17th International Offshore and Polar Engineering Conference*, p3246, Lisbon, Portugal, July 1 - 6.

14 DeGeer, D., Timms, C., Wolodko, J., Yarmuch, M., Preston, R., and MacKinnon, D., 2007, "Local buckling assessments for the Medgaz pipeline", *Proceedings of the 26th International Conference on Offshore Mechanics and Arctic Engineering*, San Diego, California, June 10 - 15.

15 Timms, C.M.J., DeGeer, D., Chebaro, M.R., and Tsuru, E., 2009, "Compressive strain limits of large diameter X80 UOE linepipe", *Proceedings of the 19th International Offshore and Polar Engineering Conference*, p181, Osaka, Japan, June 21 - 26.

16 Carr, M., MacRae, I., and Bruton, D., 2009, "Local buckling of pressurized seamless linepipe: results of the SAFEBUCK JIP", *Proceedings of the Pipeline Technology Conference*, Ostend, Belgium, October 12 - 14.

17 Stephens, D.R., Olson, R.J., and Rosenfeld, M.J., 1991, "Topical report on pipeline monitoring – limit state criteria ", *NG-18 report No. 188*, Battelle, Columbus, OH.

18 Liu, B., Liu, X.J., and Zhang, H., 2008, "Compressive strain capacity of pipelines for strain-based design", *Proceedings of 7th International Pipeline Conference*, Calgary, Alberta, Canada, Sep. 29 - Oct. 3.

19 Yoosef-Ghodsi, N., Kulak, G.L., and Murray, D.W., 1994, "Behavior of girth-welded line pipe", *Structural Engineering Report No. 203*, Department of Civil Engineering, University of Alberta.

20 Gresnigt, A.M., 1986, "Plastic design of buried steel pipelines in settlement areas", *HERON*, v31(4).

21 Dorey, A.B, Murray, D.W., and Cheng, J.J.R., 2006, "Initial imperfection models for segments of line pipe," *Transactions of the ASME*, v128, p322 -329.

22 Dorey, A.B, Murray, D.W., and Cheng, J.J.R., 2002, "Material property effects on critical buckling strains in energy pipelines, " *Proceedings of the 4th International Pipeline Conference*, Calgary, Alberta, Canada, Sep. 29 - Oct. 3.

23 Gerard, G., 1956, "Compressive and tortional buckling of thin wall cylinders in yielded region," NACA, TN-No. 3726.

24 Suzuki, N., Kondo, J., Endo, S., Ishikawa, N, Okastu, M., and Shimamura, J., 2006, "Effect of geometry imperfection on bending capacity of X80 linepipe," *Proceedings of 6th International Pipeline Conference*, Calgary, Alberta, Canada, September 25-29.

25 Suzuki, N., Kondo, J., Ishikawa, N, Okastu, M., and Shimamura, J., 2007, "Strain capacity of X80 high strain line pipes," *Proceedings of the 26th International Conference on Offshore Mechanics and Arctic Engineering*, San Diego, California, June 10 - 15.

26 Sato T., Mikami, Y., Mochizuki, M., Suzuki, N., and Toyota, M., 2008, "Parametric study on the effect of geometric imperfections on the bending capacity of high strength linepipes", *Proceedings of the 7th International Pipeline Conference*, September 29 - October 3, Calgary, Alberta, Canada

27 Liu, M., and Wang, Y.Y., 2006, "Modeling of Anisotropy of TMCP and UOE Linepipes," *Proceedings of the 16th (2006) International Offshore and Polar Engineering Conference* San Francisco, California, USA, May 28-June 2.

28 Adeeb, S., Zhou, J., and Horsley, D., 2006, "Investigating the effect of UOE forming process on the buckling of line pipes using finite element modeling," *Proceedings of the 6th International Pipeline Conference*, Calgary, Alberta, Canada, September 25-29.

29 Fathi, A., Cheng, J.J.R., Adeeb, S., and Zhou, J., 2010, "Critical buckling strain in high strength steel pipes using isotropic-kinematic hardening," *Proceedings of the 8th International Pipeline Conference*, Calgary, Alberta, Canada, September 27 - October 1.

30 Hilgert, O., Zimmermann, S., and Kalwa, C., 2012, "Anisotropy - benefits for UOE line pipe," *Proceedings of the 9th International Pipeline Conference*, Calgary, Alberta, Canada, September 24 - 28.

31 Tsuru, E., Agata, J., and Nagata, Y., 2010, "Analytical approach for bucking resistance of UOE linepipe with orthogonal anisotropy under combined loading," *Proceedings of the 8th International Pipeline Conference*, Calgary, Alberta, Canada, September 27 – October 1.

32 Wang, Y.-Y., Liu, M., Zhang, F., Horsley, D., and Nanney, S., 2012, "Multi-tier tensile strain design models for strain-based design Part I - fundamental basis," *Proceedings of the 9th International Pipeline Conference*, Calgary, Alberta, Canada, September 24-28.

33 Liu, M., Wang, Y.-Y., Song, Y., Horsley, D., and Nanney, S., 2012, "Multi-tier Tensile Strain Models for Strain-Based Design Part II - Development and Formulation of Tensile Strain Capacity Models," *Proceedings of the 9th International Pipeline Conference*, Calgary, Alberta, Canada, September 24-28.

34 Liu, M., Wang, Y.-Y., Horsley, D., and Nanney, S., 2012, "Multi-tier tensile strain design models for strain-based design Part III - model evaluation against experimental data," *Proceedings of the 2012 9th International Pipeline Conference*, Calgary, Alberta, Canada, September 24-28.

35 Suzuki, N., Tajika, H., Igi, S., Okatsu, M., Kondo, J., and Arakawa, T., 2010, "Local buckling behavior of 48", X80 high-strain line pipes" *Proceedings of the 8th International Pipeline Conference*, Calgary, Alberta, Canada, September 27 - October 1.

36 Souza, L.T., and Murray, D.W., 1999, "Analysis for wrinkling behavior of girth-welded line pipe," *Journal of Offshore Mechanics and Arctic Engineering*, v121, p53-61.

37 Souza, L.T. and Murray, D.W., 1994, "Prediction of wrinkle behavior of girth-welded line pipe," *Structural Engineering Report No. 197*, University of Alberta, Department of Civil and Environmental Engineering.

38 Shitamoto, H., 2013, "Welded steel pipe fabrication method and welded steel pipe," World Intellectual Property Organization, Pub. No. WO/2013/031879.

39 Tsuru, E., Shinohara, Y., Asahi, H., and Terada, Y., 2005, "Strain capacity of line pipe with yield point elongation," *Proceedings of the 2005 15th International Offshore and Polar Engineering Conference*, Seoul, Korea, June 19-24.

40 Al-Showaiter, A., Taheri, F., and Kenny, S., 2008, "Influencing of pipeline misalignment on the local buckling response," *Proceedings of the 7th International Pipeline Conference*, September 29 – October 3, Calgary, Alberta, Canada.

41 Fatemi, A., Kenny, S., Sen, M., Zhou, J., Taheri, F., and Paulin, M., 2009, "Parameters affecting the buckling and post-buckling behavior of high strength pipelines," *Proceedings of the 28th International Conference on Ocean, Offshore and Arctic Engineering*, Honolulu, Hawaii, USA, May 31 - June 5.

42 Ken, L.,2012, PHMSA presentation at the API-AGA Joint Committee meeting on Oil & Gas Pipeline Welding Practices.

43 Igi, S., Sakimoto, T., Suzuki, N., Muraoka, R., and Arakawa, T., 2010, "Tensile strain capacity of X80 pipeline under tensile loading with internal pressure," *Proceedings of the 8th International Pipeline Conference*, Calgary, Alberta, Canada, September 27 – October 1.

44 Wang, Y.-Y., Rudland, D., Denys, R., and Horsley, D. J., 2002, "A preliminary strain-based design criterion for pipeline girth welds," *Proceedings of the International Pipeline Conference*, Calgary, Alberta, Canada, September 29 - October 3.

45 Wang, Y.-Y., Cheng, W., McLamb, M., Horsley, D., Zhou, J., and Glover, A., 2004, "Tensile strain limits of girth welds with surface-breaking defects Part I an analytical framework," in Pipeline Technology, *Proceedings of the 4th International Conference on Pipeline Technology*, Ostend, Belgium, May 9-13.

46 Wang, Y.-Y., Horsley, D., Cheng, W., Glover, A., McLamb, M., and Zhou, J., 2004, "Tensile strain limits of girth welds with surface-breaking defects Part II experimental correlation and validation," in Pipeline Technology, *Proceedings of the 4th International Conference on Pipeline Technology*, Ostend, Belgium, May 9-13.

47 Wang, Y.-Y., Cheng, W., and Horsley, D., 2004, "Tensile strain limits of buried defects in pipeline girth welds," *Proceedings of the International Pipeline Conference*, Calgary, Alberta, Canada, October 4-8.

48 Wang, Y.-Y., 2005, "Tensile strain limits and material specifications for strain-based design of pipelines," *International Forum on X100/X120 High Performance Pipe Steels*, Beijing, China, July 28-29.

49 Canadian Standard Association, 2007, "Oil and gas pipeline systems", CSA Z662.

50 Verstraete, M., Waele, W., Denys, R., Hertele, S., 2012, "Pressure correction factor for strain capacity predictions based on curved wide plate testing," *Proceedings of the 9th International Pipeline Conference*, Calgary, Alberta, Canada, September 24-28.

51 Smith, S., 2012, "Development of the BS 7910 failure assessment diagram for strain based design with application to pipelines,", *Proceeding of the ASME 2012 31st International Conference on Ocean, Offshore, and Arctic Engineering*, OMAE2012-83527, Rio de Janeiro, Brazil, July 1–6.

52 Horsley, D. and Wang, Y.-Y., 2004, "Weld mismatch effects on the strain limits of X100 girth welds," in Pipeline Technology, *Proceedings of the 4th International Conference on Pipeline Technology*, Edited by Rudi Denys, Oostende, Belgium, May 9-12.

53 Østby, E, 2005, "New strain-based fracture mechanics equations including the effects of biaxial loading, mismatch and misalignment", *Proceeding of the 24th International Conference on Offshore Mechanics and Arctic Engineering*, Halkidiki, Greece, June 12-17.

54 Nyhus, B., Østby, E, Knagenhjelm, H.O., Black, S., and RØstadsand, P.A., 2005, "Fracture control – offshore pipelines: experimental studies on the effect of crack depth and asymmetric geometries on the ductile tearing resistance", *Proceeding of the 24th International Conference on Offshore Mechanics and Arctic Engineering*, Halkidiki, Greece, June 12-17.

55 Minnaar, K. Gioielli, P.C., Macia, M.L., Bardi, F., Biery, N.E., and Kan, W.C., 2007, "Predictive FEA modeling of pressurized full-scale tests", *Proceedings of the 17th International Offshore and Polar Engineering Conference*, p3114, Lisbon, Portugal, Jul 1-6.

56 Fairchild, D.P., Cheng, W., Ford, S.J., Minnaar, K., Biery, N.E., Kumar, A., and Nissley, N.E., 2007, "Recent advances in curved wide plate testing and implications for strain-based design", *Proceedings of the 17th International Offshore and Polar Engineering Conference*, p3013, Lisbon, Portugal, July 1-6.

57 Kibey, S., Issa, J.A., Wang, X., and Minnaar, K., 2009, "A simplified, parametric equation for prediction of tensile strain capacity of welded pipelines", *Pipeline Technology Conference*, Ostend, Belgium, October 12-14.

58 Fairchild, D., Kibey, S., Tang, H., Krishnan, V., Macia, M., Chen, W., and Wang, X., 2012, "Continued advancements regarding capacity prediction of strain-based pipelines," *Proceedings of the 9th International Pipeline Conference*, Calgary, Alberta, Canada, September 24-28.

59 Igi, S. and Suzuki, N., 2007, "Tensile strain limits of X80 high-strain pipelines," *Proceedings of the 17th International Offshore and Polar Engineering Conference*, Lisbon, Portugal, July 1-6.

60 Igi, S., Sakimoto, T., Suzuki, N., Muraoka, R., and Arakawa, T., 2010, "Tensile strain capacity of X80 pipeline under tensile loading with internal pressure," *Proceedings of the 8th International Pipeline Conference*, Calgary, Alberta, Canada, September 27 – October 1.

61 Tajika, H., Igi, S., Sakimoto, T., Muraoka, R., Endo, S., Tsuyama, S., Arakawa, T. and Suzuki, N., 2012, "Compressive and tensile strain capacities of 48" X80 line pipes," *Proceedings of the 9th International Pipeline Conference*, Calgary, Alberta, Canada, September 24-28.

62 Wang, Y.-Y., Liu, M., and Song, Y., 2012, "Tensile strain models for strain-based design of pipelines," *Proceedings of the ASME 2012 31st International Conference on Ocean, Offshore and Arctic Engineering*, Rio de Janeiro, Brazil, July 1-6.

63 Wang, Y.-Y., Zhang, F., Liu, M., Cho, W., and Seo, D., 2012, "Tensile strain capacity of X80 and X100 welds," *Proceedings of the ASME 2012 31st International Conference on Ocean, Offshore and Arctic Engineering*, Rio de Janeiro, Brazil, July 1-6.

64 Zhang, F., Liu, M., and Wang, Y.-Y., Yu Z., and Tong, L., 2012, "Strain demand in areas of mine subsidence", *Proceedings of the 9th International Pipeline Conference*, Calgary, Alberta, Canada, September 24-28.

65 Zhang, F., Liu, M., Wang, Y.-Y., Yu Z., and Tong, L., 2012, "Integrity of pipeline in area of mine subsidence", *Proceedings of the 9th International Pipeline Conference*, Calgary, Alberta, Canada, September 24-28.

66 Otsuka, A., et al., 1980, "Effect of stress triaxiality on ductile fracture initiation of low strength steel," *J. of the Society of Material Science*, Japan, Vol. 29, No. 322, pp. 717-723.

67 Toyoda, M., et al., 2001, "Criterion for ductile cracking for the evaluation of steel structure under large scale cyclic loading," *Proc. Of 20th International Conference on Offshore Mechanics and Arctic Engineering*.

68 American Society of Mechanical Engineers, 2012, "Pipeline transportation systems for liquid hydrocarbons and other liquids," ASME code for pressure piping, ASME B31.4.

69 American Society of Mechanical Engineers, 2012, "Gas transmission and distribution piping systems," ASME code for pressure piping, ASME B31.8.

70 Wang, Y.Y., Liu, M., Tyson, B., Gianetto, J., Quintana, M., and Weeks, T., 2011, "Background of linepipe specifications," Topical Report 277-T-01, DOT Contract No. DTHP56-07-000005, November, 28.

71 "Yield Strength Determination for Large Diameter Pipelines," a JIP led by DNV, Microalloyed Steel Institute, and Spectra Energy.

72 American Petroleum Institute, 2013, "Specification for Line Pipe," API Specification 5L, 45th Edition.

73 International Organization for Standardization, 2012, "Petroleum and Natural Gas Industries – Steel Pipe for Pipeline Transportation System," ISO 3183.

74 Ishikawa, N., Okatsu, M., Shimamura, J., Endo, S., Shikanai, N., Muraoka, R., Kondo, J., and Suzuki, N., 2008, "Material development and strain capacity of grade X100 high strain linepipe produced by heat treatment online process," *Proceedings of the 7th International Pipeline Conference*, Calgary, Alberta, Canada, September 29-October 3.

75 Hara, T., Terada, Y., Shinohara, Y., Hitoshi, A. and Doi, N., 2008, "Metallurgical design and development of high deformable X100 line pipe steels suitable for strain based design," *Proceedings of the 7th International Pipeline Conference*, Calgary, Alberta, Canada, September 29-October 3.

76 Seo, D., Yoo, J., Song, W. and Kang, K., 2008, "Development of X100 linepipe steel with high deformation capacity," *Proceedings of the 7th International Pipeline Conference*, Calgary, Alberta, Canada, September 29-October 3.

77 Denys, R., Lefevre, A., De Baets, P., and Degrieck, J., 2000, "Effects of stable ductile crack growth on plastic collapse defect assessment," *Proceedings of the 3rd International Pipeline Technology Conference*, Vol. 1 pp.169-189, Brugge, Belgium, May 21-24.

78 Canadian Standard Association, 2007, "Steel line pipe," CSA Standard 245.1.

79 Wang, Y. Y., Liu, M., Tyson, W.R., Gianetto, J.A., Quintana, M.A. and Weeks, T.S., 2011, "Background of linepipe specifications", Final Report 277 T 01 to PHMSA per Agreement # DTPH56 07 T 000005, September.

80 Tsuru, E., Shinohara, Y., and Asahi, H., 2007, "Evaluation of precept of strain capacity of high strength UOE line pipes used in strain-based design applications," *Proceedings of the 17th International Offshore and Polar Engineering Conference*, Lisbon, Portugal, July 1-6.

81 Quintanan, M., "Summary report 278-S-01," Topical Report 278-S-01, DOT Contract No. DTHP56-07-T-000005, September.

82 Rajan, V.B., 2011, "Essential welding variables," Topical Report 278-T-06, DOT Contract No. DTHP56-07-T-000005, September.

83 Quintana, M. and Gianetto, J.A., 2011, "Background of all-weld metal tensile test protocol," Topical Report 277-T-02, DOT Contract No. DTHP56-07-0001, September.

84 Gianetto, J., Tyson, W., Wang, Y-Y., Park, D-Y, Bowker, J., and Shen, G., 2010, "Mechanical properties and microstructure of weld metal and HAZ regions in X100 single and dual torch girth welds," *Proceedings of 8th International Pipeline Conference*, Calgary, Alberta, Canada, October.

85 Wang, Y.Y., Wu, X., and Liu, M., 2011, "Weld strength mismatch requirements," Topical Report 277-T-10, DOT Contract No. DTHP56-07-0001, November, 30.

86 Gianetto, J.A., Bowker, J.T., Bouchard, R., Dorling, D.V. and Horsley, 2007, "Tensile and toughness properties of pipeline girth welds," *Welding in the World*, Vol. 51, No. 5/6.

87 Gianetto, J.A., Bowker, J.T., Dorling, D.V., Taylor, D., Horsley, D. and Fiore, S.R., 2008, "Overview of tensile and toughness testing protocols for assessment of X100 pipeline girth welds," *Proceedings of 7th International Pipeline Conference*, Calgary, Alberta, Canada, October.

88 Det Norske Veritas, 2006, "Fracture control for pipeline installation methods introducing cyclic plastic strain", DNV-RP-F108.

89 Shen, G., Gianetto, J.A., and Tyson, W.R.., 2011, "Development of procedure for low-constraint toughness testing using a single-specimen technique," Topical Report 277-T-03, DOT Contract No. DTHP56-07-000005, November 30.

90 Cheng, W., Tang, H., Gioielli, P.C., Minnaar, K., and Macia, M.L., 2009, "Test methods for characterization of strain capacity: comparison of R-curves from SENT/CWP/FS tests", *Pipeline Technology Conference*, Ostend, Belgium, October 12-14.

91 Pipeline Research Council International (PRCI), 2013,"Standardization of Weld Testing Methods - Phase I", an ongoing PRCI project, http://prci.org/index.php/site/projects_single/standardization_of_weld_testing_methods_-_phase_i/.

92 Shih, C. F., DeLorenzi, H. G., and Andrews, W. R., 1979, "Studies on crack initiation and stable crack growth," in *Elastic-Plastic Fracture*, ASTM STP 668, American Society for Testing and Materials, Philadelphia, pp. 65-120.

93 Department of Transportation (DOT), 2013, "Strain-Based Design – Possible Conditions," U.S. DOT PHMSA, February 6, 2013.

Appendix A **Construction of Pipe and Weld Stress-Strain Curves**

A.1 Background

The tensile and compressive strain capacity is affected by the shape of the material's full stress-strain curves. However, it is difficult to use a full stress-strain curve as an input parameter for equation-based assessment models. Therefore, the full stress-strain curve is often simplified and represented by key material parameters such as yield strength (YS), ultimate tensile strength (UTS), Y/T ratio, uniform strain (uEL), and strain hardening exponent (*n*).

Although the key material parameters are shown as the input to those equation-based models, full stress-strain curves were indeed used in the development of those models. Model specific procedures were used to construct the full stress-strain curves with the key material parameters. However, those model specific procedures for constructing the full stress-strain curves were in general not the focus of the studies and not given in details.

Since the material parameters, i.e., YS, UTS (or Y/T), and uEL, cannot uniquely determine a full stress-strain curve (as shown in Figure A - 1), even for the same material parameters, the full stress-strain curves used by different models from their specific procedures can be different. As a result, the strain capacity is affected.

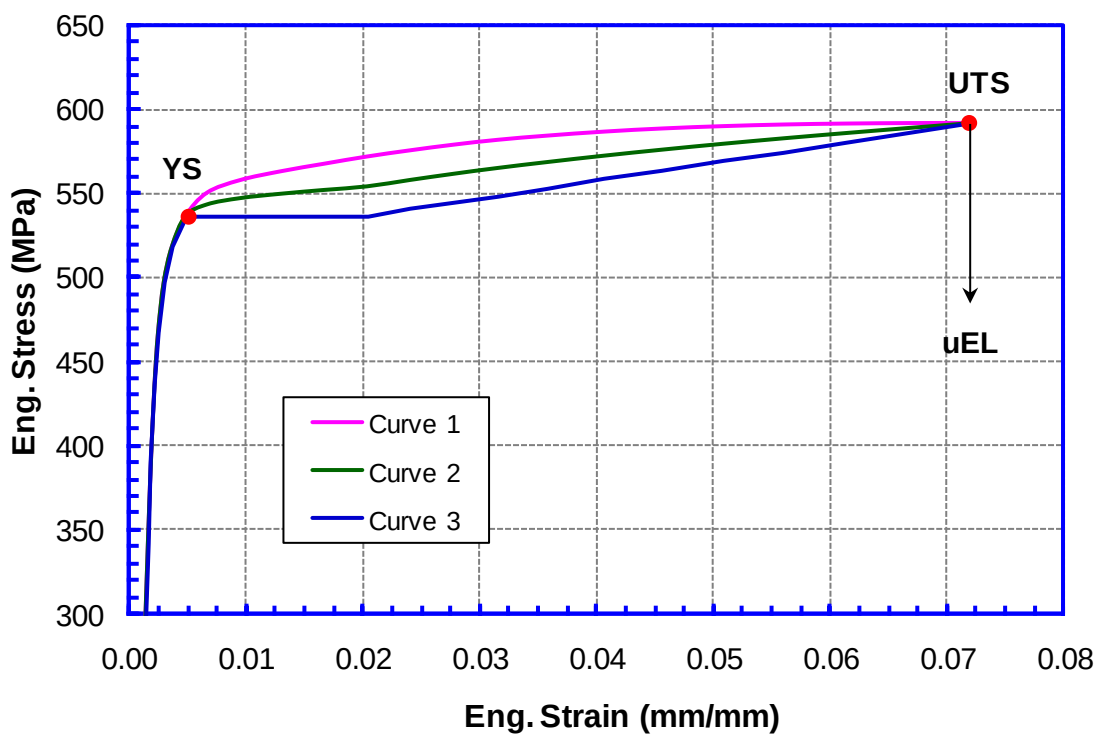

Figure A - 1 Stress-strain curves of same YS, UTS, and uEL

Based on comprehensive statistic studies, a set of mathematic equations for constructing full stress-strain curves with selected key material parameters were developed in [1, 2]. Those equations were used in the development of the tensile and compressive strain models presented in this report. The details on the development of those equations are presented in this appendix.

The mathematical equations are designed to capture the shape of the stress-strain curves in actual materials. The equations can (1) uniquely determine a full stress-strain curve using the three material parameters, i.e., YS, UTS (or Y/T), and uEL; and (2) statistically give a reasonable representation of the stress-strain curves of actual pipe and weld materials.

A.2 Ramberg-Osgood vs. CSA Stress-Strain Curve Equations

Two widely used stress-strain curve equations, i.e., the Ramberg-Osgood (RO) equation and the CSA Z662 equation are examined in this section. Both equations create smooth stress-strain curves (i.e., the round-house shape). The discontinuities in the stress-strain curve, such as the Lüder's strain, are not created. The Lüder's strain of the pipe material may increase or decrease the tensile or compressive strain capacity. The effects of the Lüder's strain on the tensile and compressive strain capacity are discussed in [1] and Section B.6.

The RO equation shows the relationship between the true stress (σ_T) and true strain (ε_T) as in the following,

$$\varepsilon_T = \frac{\sigma_T}{E} + 0.002\left(\frac{\sigma_T}{\sigma_0}\right)^m , \tag{A.1}$$

where E and σ_0 are the Young's modulus and reference stress, respectively. The m is the strain hardening exponent of the RO equation. By definition, the reference stress σ_0 is the true stress corresponding to a plastic strain of 0.2% and therefore is usually very close to the YS at 0.5% strain. The engineering stress-strain curve calculated from the RO equation consists of a natural peak, i.e., UTS and uEL. By calibrating σ_0 and m, the RO equation can generate a stress-strain curve for given YS and UTS. The uEL, however, is an outcome of the equation and cannot be independently varied.

In Figure A - 2, the relationship between the measured uEL and Y/T ratio is shown for some pipe materials with YS in the 56-ksi and 70-ksi range. The experimental data show that the uEL is affected by both YS and Y/T ratio. In general, the uEL decreases as the increase of the Y/T and YS. For comparison, the uEL from the stress-strain curves generated by the RO equations are also included for a large range of YS and Y/T ratio. It is shown that the uEL created by the RO equation is almost independent of the YS and only depends on the Y/T. The uEL calculated from a stress-strain curve generated by a RO equation can be significantly lower than the uEL measured from an actual stress-strain curve of the same YS and UTS (or Y/T). It is especially true for the pipe materials with low YS.

In contrast to the RO equation, the equation given in CSA Z662 [3] defines the relationship between the engineering stress (σ) and engineering strain (ε) as in the following:

$$\varepsilon = \frac{\sigma}{E} + \left(0.005 - \frac{\sigma_y}{E}\right)\left(\frac{\sigma}{\sigma_y}\right)^n , \tag{A.2}$$

where σ_y is the YS at 0.5% strain and n is the strain hardening exponent of the CSA equation. For any given set of YS, UTS, and uEL, a unique n can be determined by Eq. (A.3). Therefore,

the CSA equation can uniquely determine a full stress-strain curve for a given set of YS, UTS (or Y/T), and uEL.

$$n = \ln\left(\frac{\text{uEL} - \text{UTS}/E}{0.005 - \text{YS}/E}\right) / \ln\left(\frac{1}{\text{Y/T}}\right) \tag{A.3}$$

Based on the observations, the CSA Z662 equation is selected to generate the full stress-strain curves.

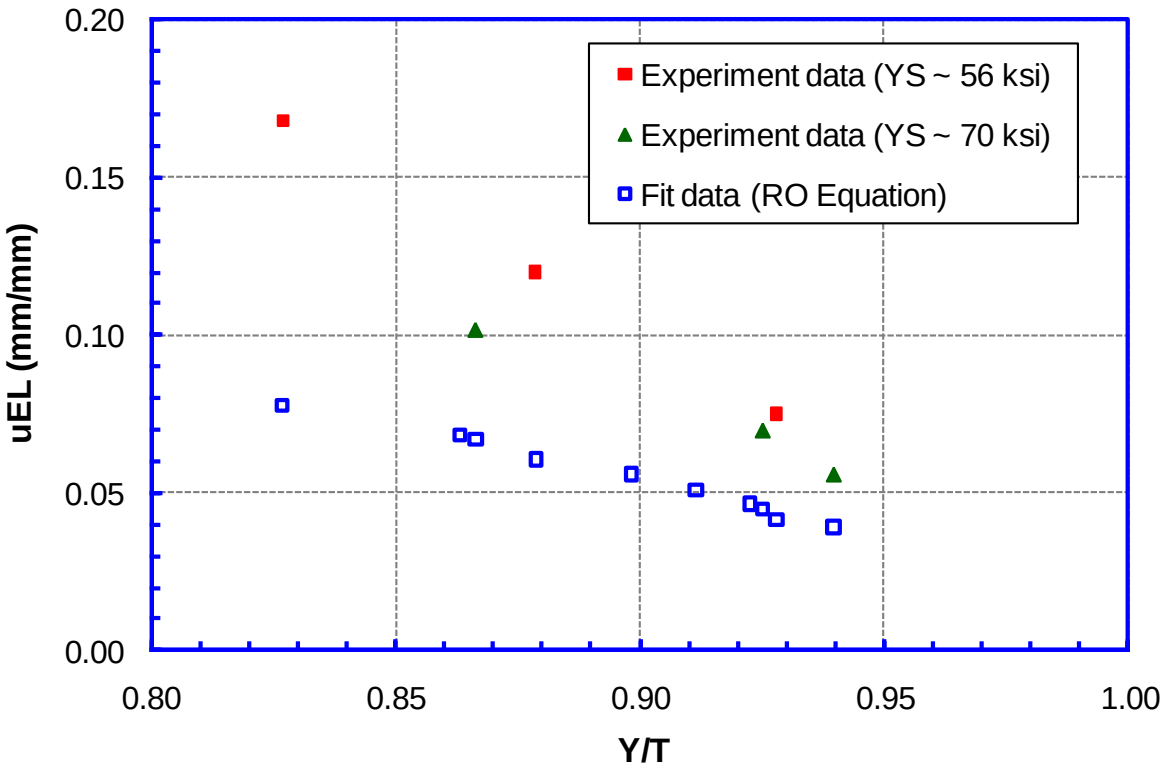

Figure A - 2 Correlation between uEL and Y/T (experiment data: obtained from measured stress-strain curves; Fit data: obtained from fitted stress-strain curves of the measured ones using the RO equation)

A.3 Representation of Pipe Stress-Strain Curves

A representative pipe stress-strain curve is shown in Figure A - 3. The curve is of round-house shape but becomes very flat near the UTS/uEL. The flat part near the UTS is typical for modern linepipe steels which can raise some challenges in representing the stress-strain curve, especially for determining the uEL. For example, the uEL of the same curve can be measured quite differently due to slightly different interpretations (or processing) of the experiment data. In addition, a trivial difference in the slope of the flat part of the curve, may not affect the strain capacity, but can result in a significant difference in the uEL.

To better understand the linepipe properties (especially the uEL), the material parameters were analyzed using a collected material database. The database contains 76 pipe longitudinal stress-strain curves. The range of the material properties in the database is summarized in Table A - 1. The YS (in longitudinal direction) ranges from 56 ksi to 114 ksi and the uEL varies from

5% to 17%.

The key material parameters, i.e., the YS, UTS, and uEL, were directly measured from the stress-strain curves and used to calculate the Y/T and the strain hardening exponent *n* of the CSA equation (with Eq. A-3). The relationship between the strain hardening exponent *n* and the Y/T ratio was shown in Figure A - 4, where a clear correlation can be observed. A fitting equation for the correlation was developed and given in the following:

$$n = \frac{3.14}{1 - \mathrm{Y/T}}. \tag{A.4}$$

The correlation observed in Figure A - 4 indicates that the linepipe properties, i.e., YS, UTS (or Y/T), and uEL are interrelated to a certain degree. The uEL of the material can be dismissed as an independent material parameter. In an average sense, the uEL can be estimated from the YS and UTS with satisfactory accuracy.

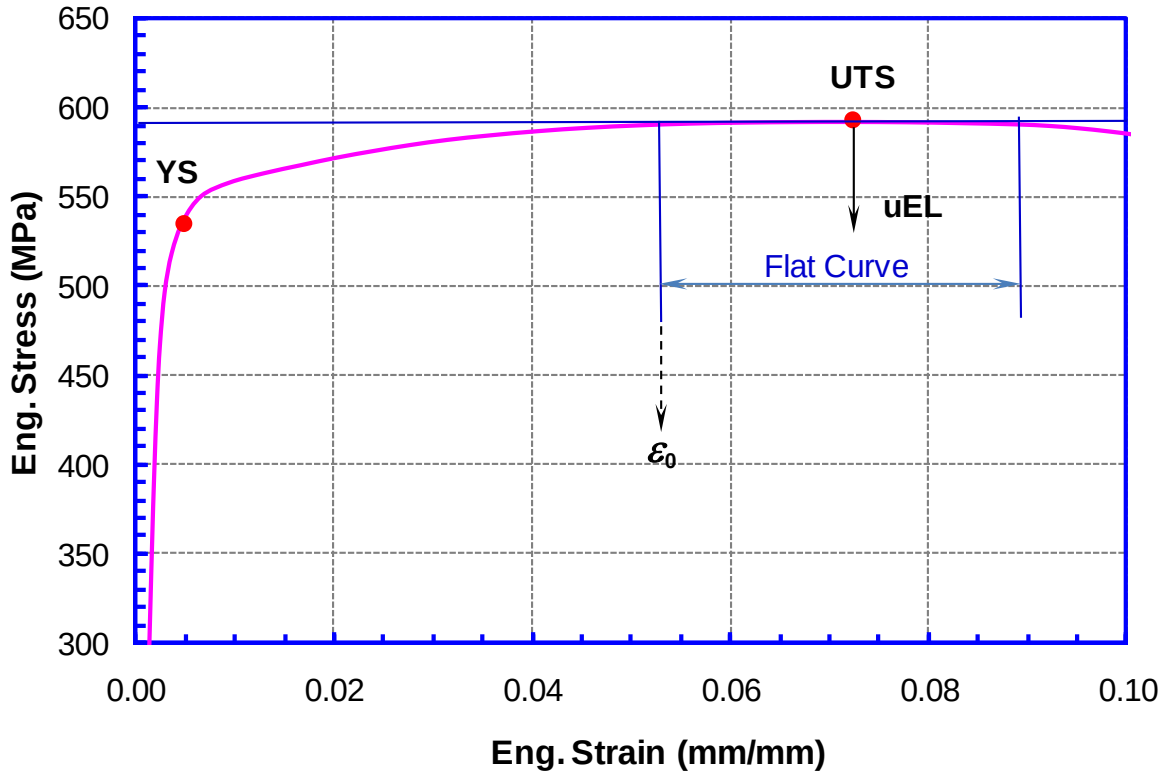

Figure A - 3 Sample pipe stress-strain curves

Table A - 1 Summary of the material database (pipe) - longitudinal tensile properties

	YS-0.5%	UTS	uEL	YT	*n* (CSA)
	ksi	ksi	mm/mm		
Minimum	56	68	0.05	0.74	11.9
Maximum	114	125	0.17	0.95	75.3
Median	84	100	0.07	0.88	29.8

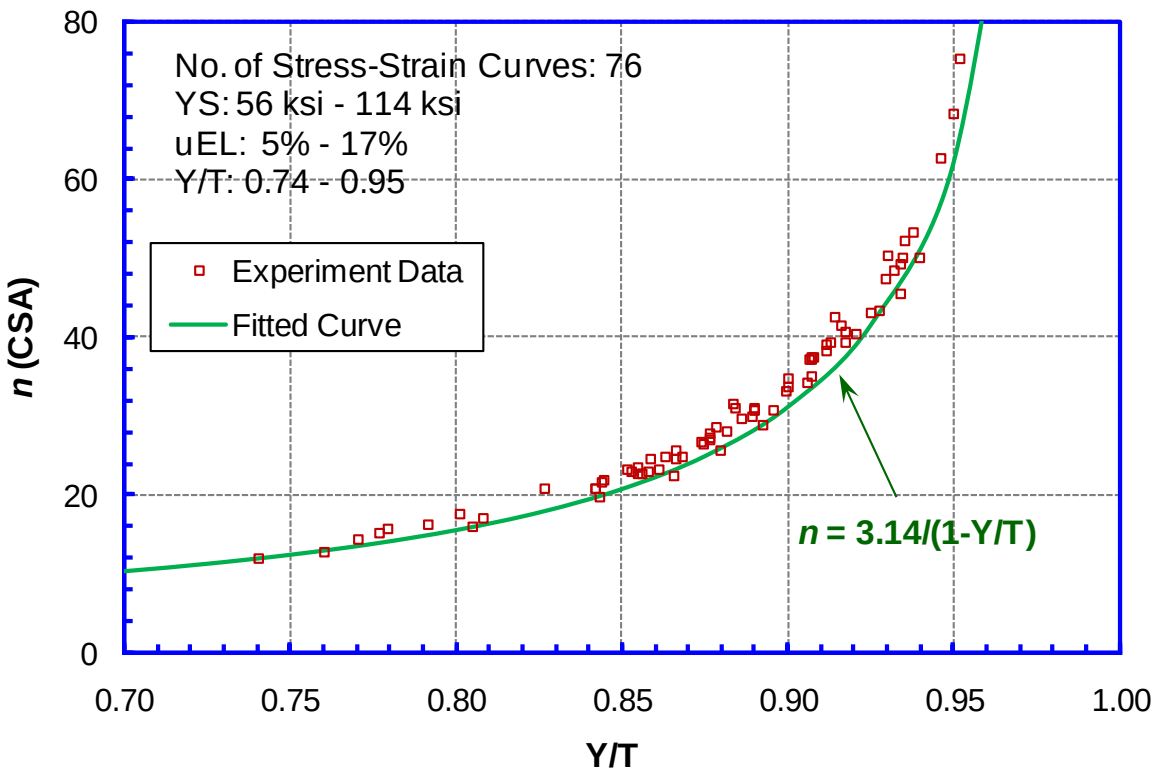

Figure A - 4 Correlation between strain hardening exponent and Y/T (pipe)

The flat part of the stress-strain curve also makes the representation of the curve with a single mathematical equation difficult. To obtain a better representation of the stress-strain curves, the curve is divided into two parts and represented by two different equations, respectively. The first part of the curve ($\varepsilon \leq \varepsilon_0$) in Figure A - 3 is represented by the CSA equation, i.e., Eq. (A.2), and the second part of the curve ($\varepsilon_0 \leq \varepsilon \leq$ uEL) is represented as a horizontal line (i.e., constant stress at UTS). The ε_0 is the strain calculated from Eqs. (A.2) and (A.4) when σ = UTS, i.e.,

$$\varepsilon_0 = \frac{\text{UTS}}{E} + \left(0.005 - \frac{\text{YS}}{E}\right)\left(\frac{1}{\text{Y/T}}\right)^n \quad \text{and} \quad n = \frac{3.14}{1 - \text{Y/T}}. \tag{A.5}$$

The uEL is the strain at the end of the curve, which is calculated from the following equation:

$$\text{uEL} = 1.25\varepsilon_0 \tag{A.6}$$

The uEL was calculated using Eqs. (A.5) and (A.6) for all the stress-strain curves given in the material database and is compared with the original values. As shown in Figure A - 5, on average, the calculated uEL matches the original values fairly well.

In summary, the following steps are recommended to create a full pipe stress-strain curve for given YS and UTS:

(1) Determine YS and UTS,

(2) Calculate Y/T using YS and UTS,

(3) Calculate n using Eq. (A.4),

(4) Calculate ε_0 using Eq. (A.5),

(5) Calculate uEL using Eq. (A.6),

(6) Construct the 1st part of the stress-strain curve using Eq. (A.2) for strains up to ε_0,

(7) Construct the 2nd part of the stress-strain curve by extending a horizontal line of constant stress from ε_0 to uEL.

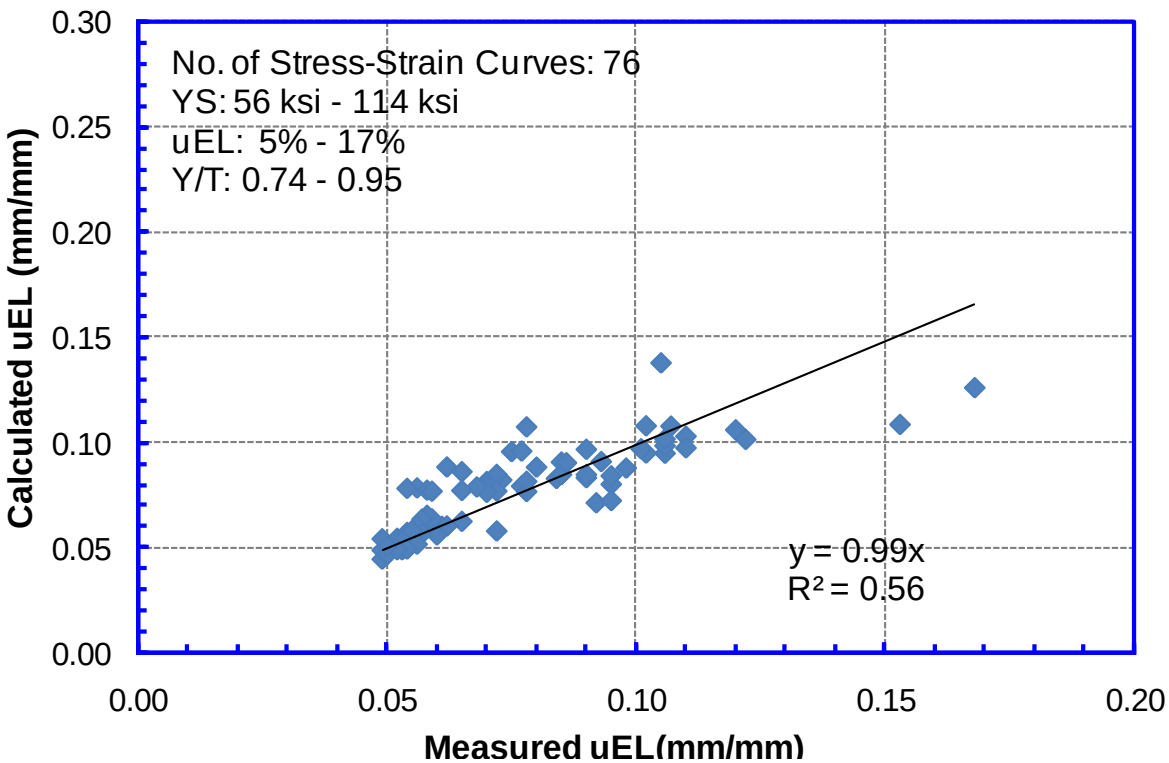

Figure A - 5 Calculated uEL vs. measured uEL

A.4 Representation of the Weld Metal Stress-Strain Curves

Two sample weld stress-strain curves are shown in Figure A - 6, one for an X65 pipe and the other for an X100 pipe. Different from the round-house type of pipe stress-strain curves, the weld metal curves usually show a discontinuous yielding point, and before reaching the yielding point, the curves are almost a straight line.

In addition, it has been frequently observed that the weld stress-strain curves sometimes contain a Lüder's strain as high as 2%, but sometimes do not. The most recent data suggest that the existence of the Lüder's strain is closely related to specimen locations. The Lüder's strain usually exists in specimens extracted near pipe ID, while OD specimens usually do not show the Lüder's strain. The difference is believed to be due to the different thermal histories experienced by the ID and OD weld materials. When the full thickness specimens are tested, the weld stress-strain curves usually do not show an obvious Lüder's strain. For conservative purposes, it was decided to include a 1% Lüder's strain in the weld stress-strain curve equations.

Based on the above observations, it was decided to divide the weld stress-strain curves into three parts. The first part is represented by a straight line with a slope E (the Young's modulus). The second part represents the Lüder's extension, which is of constant stress at σ_y (the YS). The third part characterizes the strain hardening of the curve and is in the form of a modified CSA

equation. The equations are shown in the following:

$$\varepsilon = \frac{\sigma}{E} \qquad \text{if } \varepsilon \le \sigma_y / E$$

$$\sigma = \sigma_y \qquad \text{if } \sigma_y / E < \varepsilon \le 1\% \tag{A.7}$$

$$\varepsilon = \frac{\sigma}{E} + \left(0.005 - \frac{\sigma_y}{E}\right)\left(\frac{\sigma}{\sigma_y}\right)^n + 0.005 \quad \text{if } 1\% < \varepsilon \le \text{uEL}$$

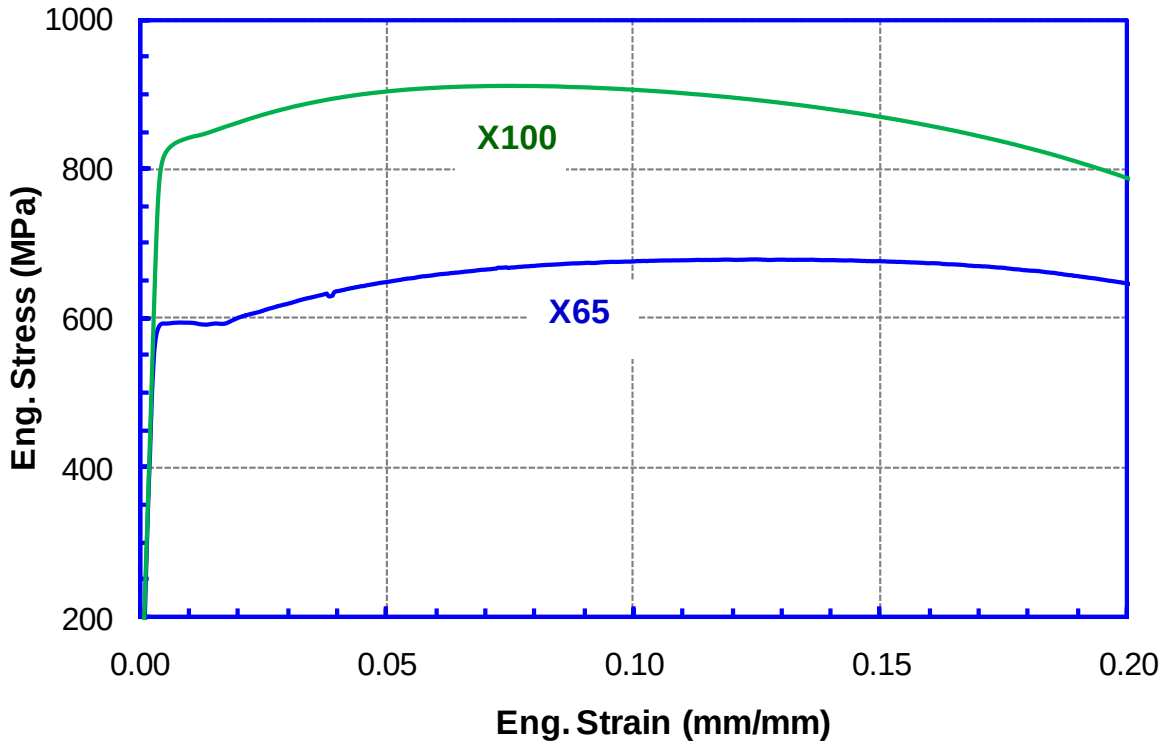

Figure A - 6 Sample weld metal stress-strain curves

A material database of weld stress-strain curves was also collected. The database contains approximately 64 weld stress-strain curves with YS ranging from 66 ksi to 132 ksi. The range of the weld material properties is summarized in Table A - 2. Specimens, of different types and extracted at different locations, are not distinguished in the database. By examining the database, a similar correlation equation for the strain hardening exponent *n* and Y/T ratio was found for weld metal stress-strain curves. As shown in Figure A - 7, the correlation equation is given as:

$$n = \frac{2.58}{(1 - \mathrm{Y/T})^{1.17}} \,. \tag{A.8}$$

With the correlation equation (Eq. A.8), the uEL of the weld materials can be determined from the YS and the UTS, and is not an independent parameter.

To further reduce the number of independent parameters for generating a weld stress-strain curve, a correlation equation for the YS and UTS of the weld was established based on the weld material database. As shown in Figure A - 8, the correlation equation is given as:

$$YS = UTS - 13.2, \tag{A.9}$$

where the unit of YS and UTS is ksi. Using Eqs. (A.7), (A.8), and (A.9), a unique weld metal stress-strain curve can be generated for a given UTS.

In summary, the following steps are recommended to create a full weld stress-strain curve for given UTS:

(1) Determine UTS,

(2) Calculate YS using Eq. (A.9),

(3) Calculate Y/T using YS and UTS,

(4) Calculate *n* using Eq. (A.8),

(5) Construct the stress-strain curve using Eq. (A.7).

Table A - 2 Summary of the material database (weld)

	YS	UTS	uEL	YT	*n* (CSA)
	ksi	ksi	mm/mm		
Minimum	66	82	0.04	0.81	15.9
Maximum	132	138	0.13	0.96	96.9
Median	112	127	0.08	0.89	34.2

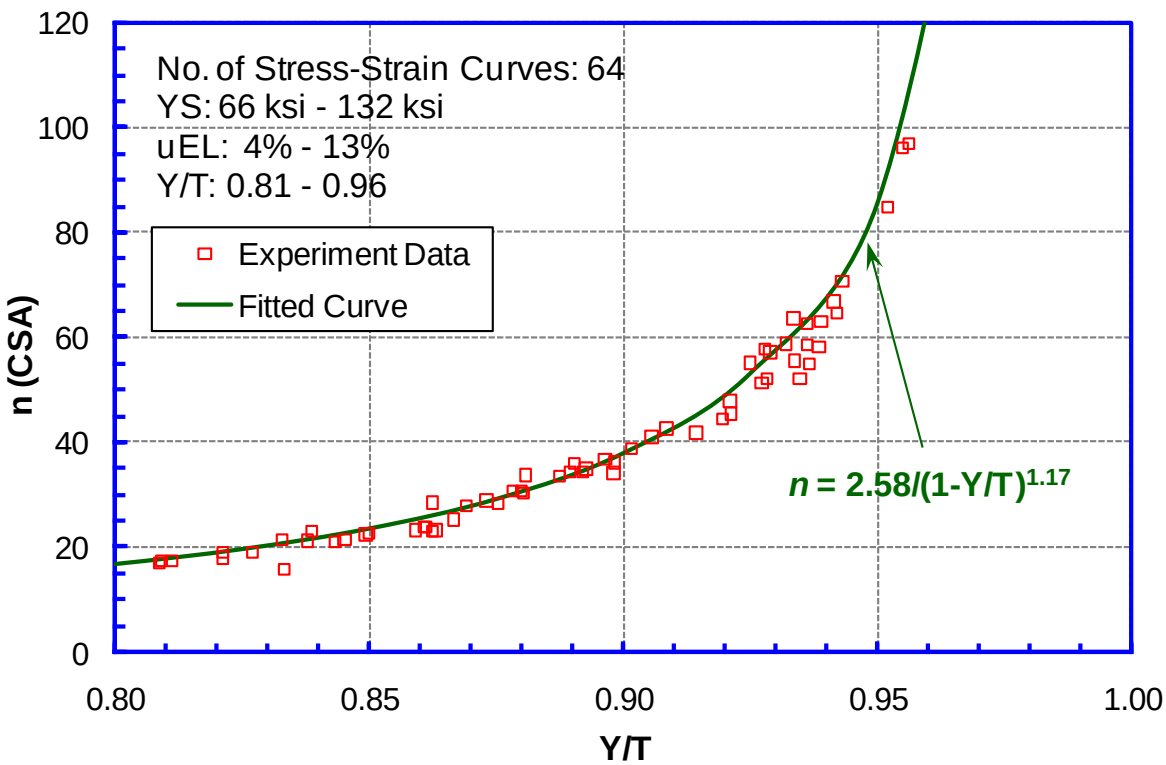

Figure A - 7 Correlation between strain hardening exponent and Y/T (weld)

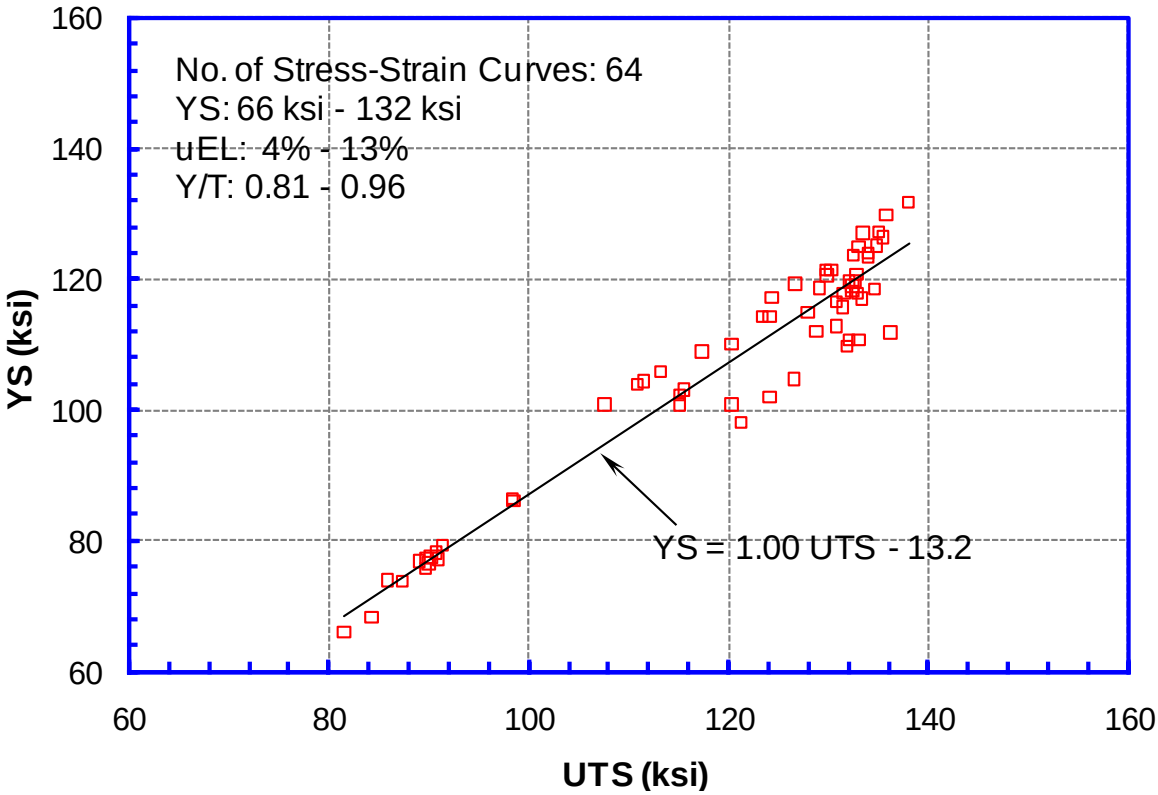

Figure A - 8 Correlation between YS and UTS (weld)

A.5 Evaluation of the Constructed Stress-Strain Curves

The constructed stress-strain curves using the equations in this section are compared with some measured stress-strain curves for pipe grades X65 to X100. The results for weld and pipe materials are given in Figure A - 9 and Figure A - 10, respectively. It is seen that on the average, the constructed stress-strain curves match the measured ones fairly well.

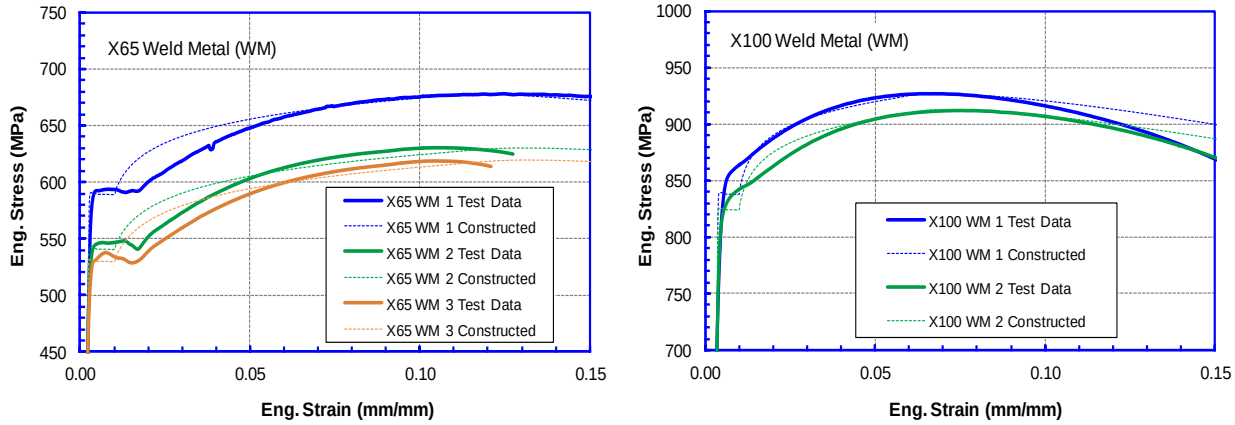

Figure A - 9 Comparison of constructed and measured full stress-strain curves (weld)

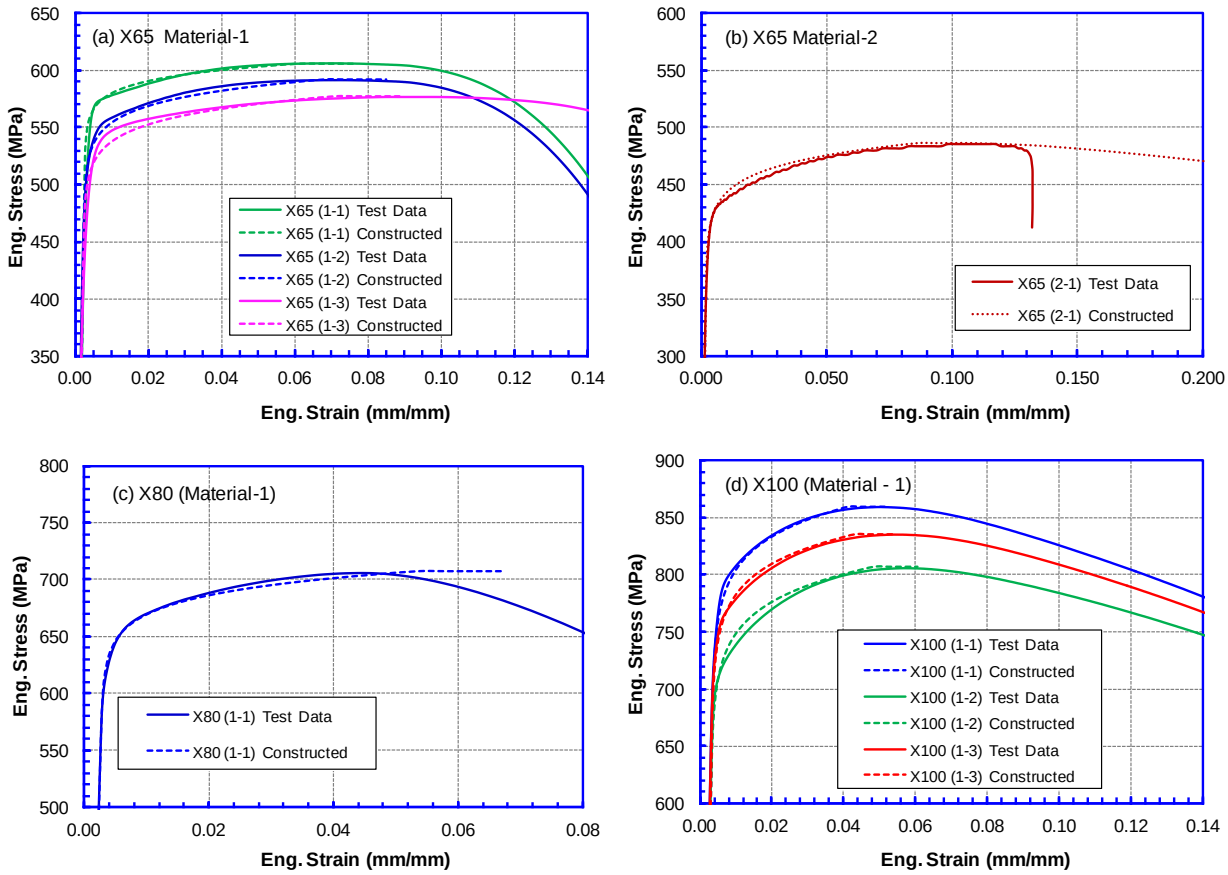

Figure A - 10 Comparison of constructed and measured full stress-strain curves (pipe)

A.6 References for Appendix A

1 Wang, Y.-Y., Liu, M., and Song, Y., 2011, "Second Generation Models for Strain-Based Design," US DOT Contract No. DTPH56-06-T000014, final report. http://primis.phmsa.dot.gov/matrix/PrjHome.rdm?prj=201

2 Liu, M., Wang, Y.-Y., Song, Y., Horsley, D., and Nanney, S., 2012, "Multi-tier Tensile Strain Models for Strain-Based Design Part II - Development and Formulation of Tensile Strain Capacity Models," *Proceedings of the 9th International Pipeline Conference*, Calgary, Alberta, Canada, September 24-28

3 Canadian Standard Association, 2011, "Oil and gas pipeline systems", CSA Z662.

Appendix B **Influencing Parameters for CSC**

B.1 Overview of Influencing Parameters

It has been recognized that the CSC can be affected by many influencing factors/parameters. The influencing factors/parameters recognized in the existing models and relevant research work are listed in the following:

- Pipe's geometries: pipe's *D*/*t* ratio;
- Loading conditions: pressure and longitudinal net-section force;
- Pipe's properties: yield strength, strain hardening exponent, pipe's Y/T ratio, Lüder's strain, and material anisotropy (anisotropic strength or strain hardening capacity);
- Geometry imperfections: cross section ovality and longitudinal surface undulation;
- Girth welds: high-low misalignment.

All the existing CSC models adopt the pipe's *D*/*t* ratios and the pressure. The recognition of other factors in the existing models varies greatly.

For example, as for the material properties, the DNV, C-FER, and JFE equations all use the strain hardening capacity of the pipe materials. The DNV equation adopts the Y/T ratio, and the C-FER and JFE equations adopt the strain hardening exponent (*n*). On the other hand, the UOA equations adopt the yield strength of the pipe materials.

As for the geometry imperfection, in the API and the C-FER equations, the ovality (i.e., the out of roundness of the pipe cross section) is recognized. The API equation explicitly takes the ovality as an input parameter, while in the C-FER equation, a constant ovality of 0.6% is used. The JFE and UOA equations, on the other hand, recognize the undulation of the pipe's outside surface. In the UOA equation, the surface undulation is an input parameter. In the JFE model, the surface undulation measured in typical JFE pipes (4% - 8% of wall thickness) is used.

As for the girth weld, the UOA equations recognize the high-low misalignment. The DNV equation adopts a reduction factor for the existence of the girth weld regardless of the high-low misalignment.

The inconsistence in selecting the influencing factors among the existing equations is mainly due to the lack of the comprehensive understanding on how those factors affect the CSC. In this section, the various factors which may affect the pipe's CSC are investigated systematically. The predicted CSC with various models are compared with the results from systematic finite element analyses (FEA). The details of the finite element models used in the FEA are given in Section 3.

The main objective of the investigation is to understand the influencing mechanisms and identify the key influencing factors.

B.2 Pipe *D*/*t* Ratios and Internal Pressure

All the existing compressive strain equations recognize the *D*/*t* ratio and the internal pressure. The CSC increases as the *D*/*t* ratio decreases and/or the internal pressure increases.

Figure B - 1 shows the relationship between the normalized CSC and the *D*/*t* ratio calculated by different models where the CSC is normalized by the CSC of *D*/*t* = 44. Except for the CSA

models, the other models adopt a multiplying form where individual equations of single variables are established for each input parameter and the single-variable equations are multiplied together (see Section 2.3). As a result, the normalized CSC - D/t relationship is independent of the other input parameters. In the CSA model, the single-variable equations of the D/t ratio and pressure are added together. The CSC - D/t relationship of the CSA model depends on the pressure. In Figure B - 1, the CSC - D/t relationship of the CSA model is calculated without pressure. In this section, the UOA model for plain pipes with round-house stress-strain curves is used.

Figure B - 1 shows the relative sensitivity of the CSC to the D/t ratio predicted by the different models and does not indicate the relative conservatism of those models. The UOA and the CSA models show very similar results for $D/t \geq 40$. For $D/t < 40$: (1) the DNV and the UOA models show similar results while the CSA and the API models show similar results; (2) the DNV and the UOA models show faster decease of the CSC as the D/t ratio increases than the CSA and API models show. For $20 < D/t < 100$, the FEA results match the CSA model very well.

The internal pressure is known to increase the CSC. Figure B - 2 shows the normalized CSC - f_p relationship calculated by different models, where the CSC is normalized by the CSC of zero pressure. Similar to the CSC - D/t relationship, the CSC - f_p relationship of the DNV and UOA models are independent of other parameters. Figure B - 2 shows that the increase of the CSC due to the internal pressure given by the DNV model is much larger than those predicted by the other models, e.g., about two times of the amount given by the UOA models. The API model is not applicable when the internal pressure is higher than the external pressure and is not shown in Figure B - 2.

The FEA results indicate that the increase of the CSC due to the internal pressure depends on the pipe's D/t ratio. The smaller the D/t ratio, the larger the increase of the CSC at the same level of the internal pressure. The result of the UOA model is close to the FEA results of the small D/t pipes ($D/t \leq 30$).

Although the CSC - f_p relationship given by the CSA model depends on the pipe's D/t ratio, the CSC model generates an opposite trend to the FEA results, i.e., the increase of the CSC is smaller as the D/t ratio decreases. As a result, the CSA model may overestimate the increase of the CSC due to the internal pressure for large D/t-ratio pipes but underestimate the increase of the CSC due to the internal pressure for small D/t-ratio pipes.

The UOA models were also developed based on FEA. The causes for the difference between the FEA results shown in this project and the UOA models are further examined. The difference can be mainly attributed to two factors: (1) the loading condition or the net-section force and (2) the shape of the geometry imperfection as shown in Figure B - 3.

The loading conditions used in the FEA of this Appendix are ER-NLF$_0$ (Section 3.3), if not mentioned otherwise. The FEA in developing the UOA equations assume the ER-NLF$_p$. As a result, the net tensile force induced by the ER-NLF$_p$ tends to further increase the CSC under high internal pressure. As shown in Figure B - 3, the increase of the CSC due to the internal pressure under ER-NLF$_p$ is higher than that under ER-NLF$_0$ (empty vs. solid triangles).

The details on the effect of the geometry imperfection on the CSC are given in the following section (Section B.3). In a summary, for the surface-undulation type of geometry imperfection, the CSC is affected by its size and shape (see Figure 2-2). The surface undulation of the critical wavelength is the most detrimental to the CSC. The critical wavelength varies with the loading condition. In general, the critical wavelength increases with the increase of the internal pressure. The surface undulation of the critical wavelength at different pressure levels was used in Figure B - 2. The results of the case with D/t = 80 in Figure B - 2 are given in Figure B - 3 as the solid blue squares. The rest of the FEA in Figure B - 3 assume the undulation of constant wavelength (i.e., 0.20D). It is seen that using the constant wavelength of 0.20D at different pressure levels shows larger increase of the CSC due to internal pressure compared with that using the critical wavelength of different pressure levels.

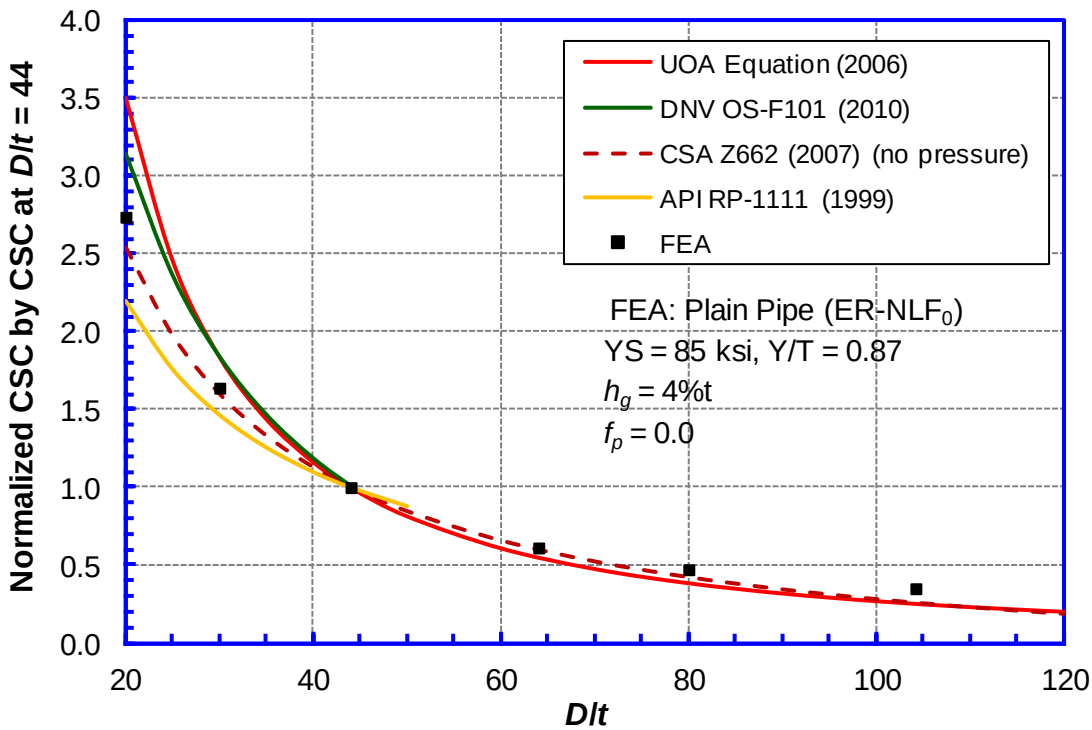

Figure B - 1 Normalized CSC vs. D/t ratio (models vs. FEA)

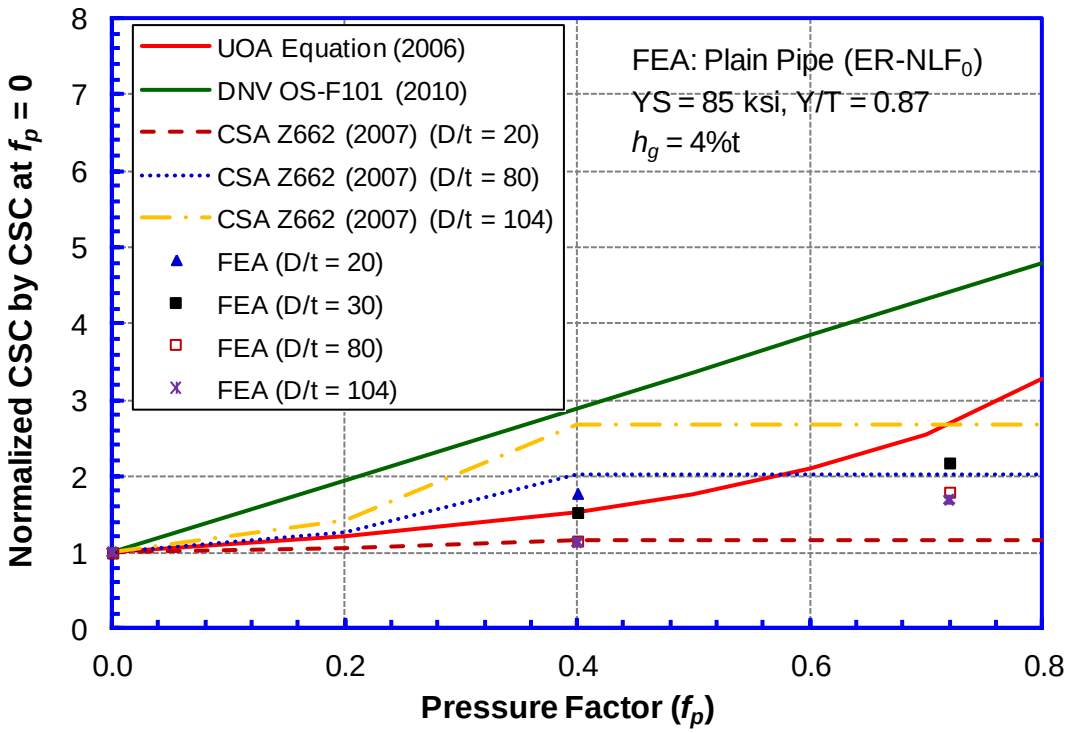

Figure B - 2 Normalized CSC vs. pressure factor (models vs. FEA)

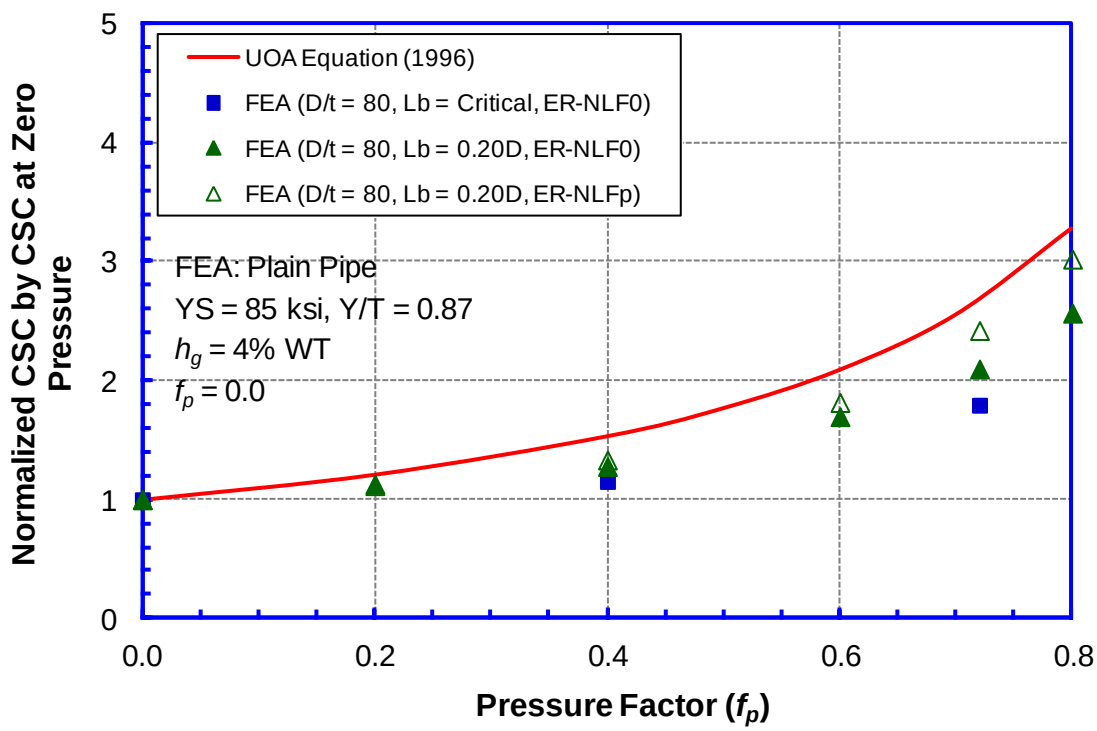

Figure B - 3 Normalized CSC vs. pressure factor (effect of loading and shape of geometry imperfection)

B.3 Geometry Imperfections

B.3.1 Shape of Geometry Imperfections

The geometry imperfections discussed herein are those generated during pipe manufacturing. The imperfections due to mechanical damages (such as dents and gauges) and corrosion defects are not considered here.

The out of roundness of a pipe's cross section, i.e., ovality, can reduce the pipe's CSC, where the oval cross section is assumed to be uniform along the length of the pipe. The effect of the ovality on a pipe's CSC is recognized in API RP-1111. According to the model calculation, the CSC of a pipe with the ovality up to 1% is about 17% smaller than the CSC of a pipe without ovality. Therefore, due to its limited size, the typical ovality from pipe manufacturing could have very limited effect on the CSC.

In recent studies, the geometry imperfection in a form of a wave-like variation of the pipe's outside surface along the length of the pipe (referred to as surface undulations), was found to be critical for the pipe's CSC [1,2,3,4,5,6,7,8]. The profile of the OD surface of a sample UOE pipe is shown in Figure B - 4 [8]. The *y*-axis of the plot shows the pipe's outside radius and the *x*-axis shows the location along the length of the pipe. The different curves show the radius measured at different clock positions along the pipe's circumference. The difference among those curves indicates the out of roundness of the cross section.

The variation of the OD surface along the length of the pipe shows a wave-like pattern with a dominant wavelength. But, the surface variation does contain waves with multiple wavelengths of different amplitudes (or heights). A similar pattern is found for the pipe's wall thickness as shown in Figure B - 5 [8]. The observed wavelength varies from pipe to pipe and may be related to the pipe's manufacturing process. However, it should be noted that the existing data on the pipe's surface undulations (e.g., shape and size), at the time of the report, are all from UOE pipes. It is not clear if the pipes of other manufacturing processes, e.g., ERW, spiral, etc., carry similar types of surface undulations.

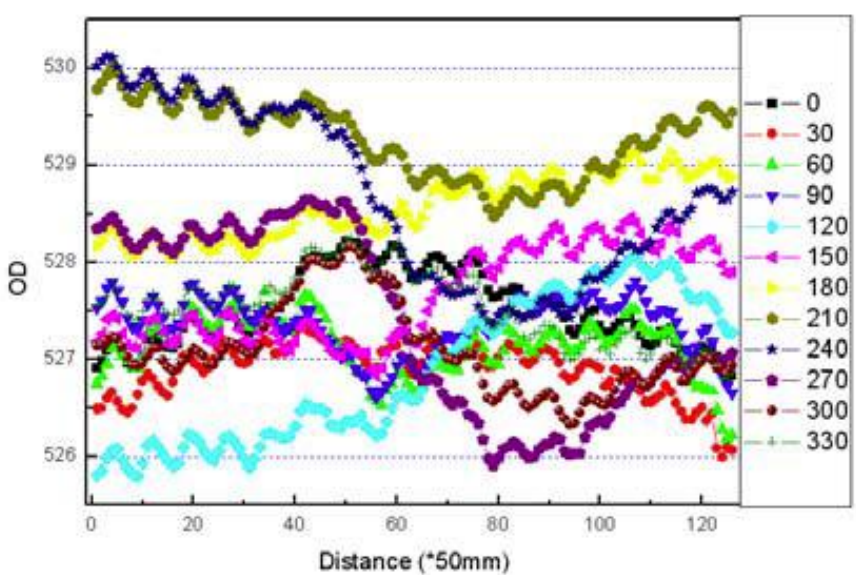

Figure B - 4 Sample profile of pipe's OD surface [8]

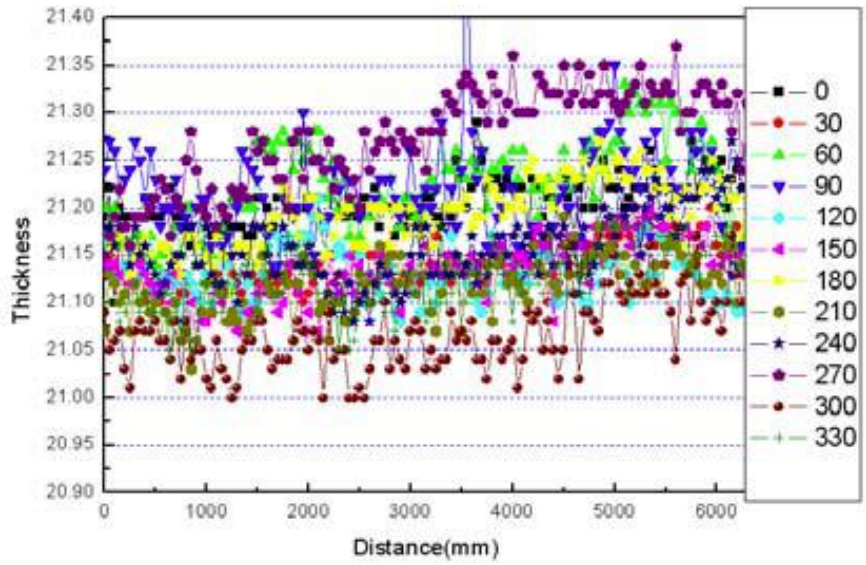

Figure B - 5 Sample profile of pipe's wall thickness variation [8]

B.3.2 Modeling of Geometry Imperfections

The surface undulation can be attributed to the variation of the pipe's diameter and/or wall thickness and the actual surface variation is often very complicated. To facility the numerical modeling and capture the effect of the surface undulation on the CSC, numerical models of the surface undulation were developed and used in the numerical simulations.

One of the representative models is the single wave model, i.e., a local outward bulge on the pipe's OD surface, developed by University of Alberta (UOA) [7] as shown in Figure B - 6. This single wave model is often referred to as a single blister model. In the original UOA model, the bulge has a wavelength of $D/2$ (i.e., $L_b = D/2$) along the length of the pipe and covers 90° (i.e., $\alpha = 90°$) in the pipe's circumference. The wavelength and angle were determined by matching the simulated CSC with the testing results. The height of the bulge was kept as a variable. It should be noted that in this model, the pipe's cross section is not perfectly round. As a result, the effect of the out of roundness of the pipe's cross section on the CSC can be partially included.

In addition to the single wave model, a multi wave model, as shown in Figure B - 7, has been used in the work by JFE [4] and Nippon Steel [5]. The modeled imperfections is also referred to as longitudinal blisters. In the original models, the surface undulation is purely generated by the variation of the pipe's OD along the length of the pipe. Therefore, the pipe's cross section is perfectly round and the wall thickness is uniform.

In this appendix, the effect of the type, height, wavelength, and angle (in the circumference) of the surface undulation is studied. Three types of the surface undulation are investigated:

(1) Single wave due to OD variation;

(2) Multi wave due to OD variation;

(3) Multi wave due to wall thickness variation.

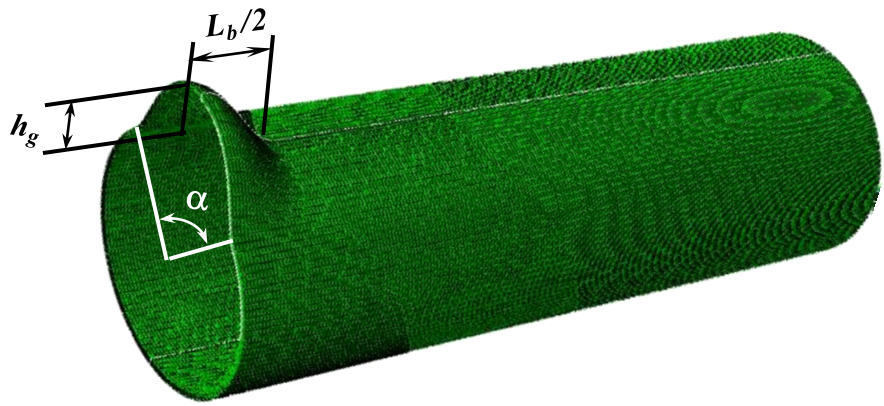

Figure B - 6 Representation of the surface undulation - single wave model

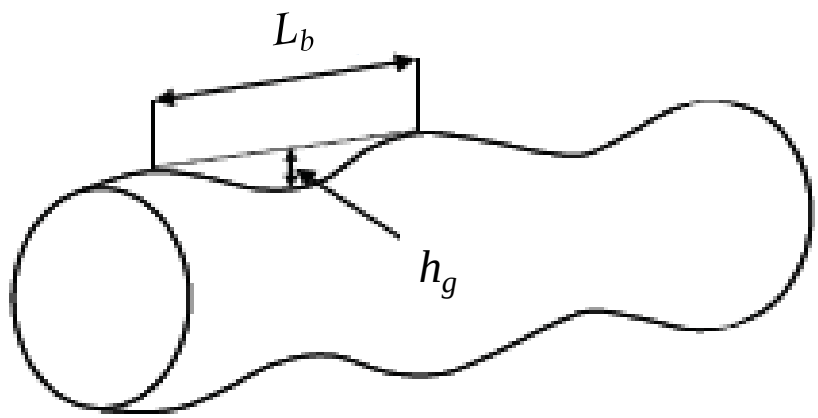

Figure B - 7 Representation of the surface undulation - multi wave model

B.3.3 Effect of the Type of Geometry Imperfections on CSC

The CSC obtained with different types of surface undulations is shown in Figure B - 8. In general, the single wave model shows the lowest CSC, especially for the surface undulations of relatively large heights ($h_g/t \geq 8\%$). The multi wave model with OD variation shows similar or slightly lower CSC than that with thickness variation. All three models produce similar CSC when $h_g/t \leq 8\%$. The actual surface undulation is often the combination of the three models as shown in Figure B - 4 and Figure B - 5. The surface undulation contains multiple waves. But, since the individual waves have different sizes, one singe wave will eventually dominate and initiate the buckling. According to the observations, the single wave model is recommended and used in the future studies in order to produce reasonably conservative results.

Compared with the multi wave model, the single wave model has an extra parameter, i.e., the angle of the single wave surface undulation in pipe's circumference (α). The effect of the angle (α) on the CSC is shown in Figure B - 9. The CSC decreases as the angle increases. The rate of the CSC reduction becomes very small when $\alpha \geq 90°$. As shown in Figure B - 4, the angle of the surface undulation can vary along the length of the pipe. In general, the angle covers the whole circumference. Therefore, the angle of 180° is recommended and used in the future studies.

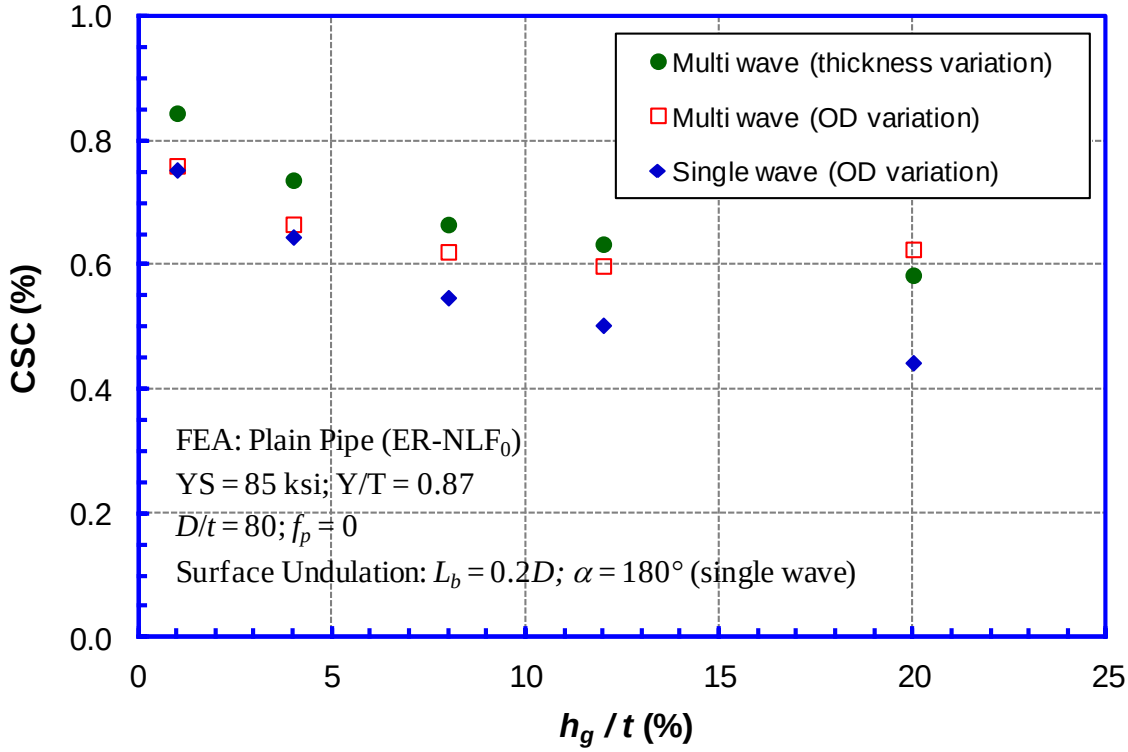

Figure B - 8 Effect of the type of the surface undulation on the CSC

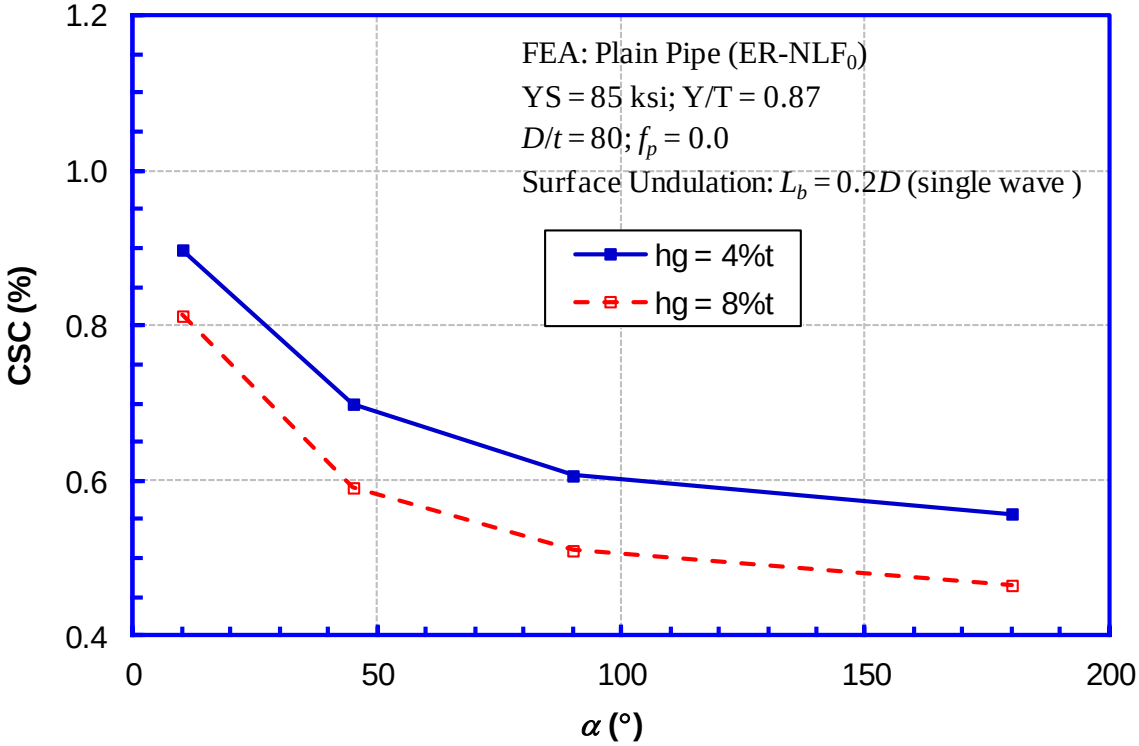

Figure B - 9 Effect of the angle (α) of the surface undulation on the CSC

B.3.4 Critical Wavelength of Geometry Imperfections

The effect of the wavelength (L_b) of the surface undulation on the CSC is shown in Figure B - 10 where the multi wave surface undulation due to the OD variation is used. The figure shows two sets of simulations: (1) the height of the surface undulation is constant, i.e., $h_g = 4\%t$ and (2) the height-to-wavelength ratio is constant, i.e., $h_g/L_b = 0.2\ t/D$. The reason of keeping a constant height-to-wavelength ratio is to maintain similar slope or sharpness for the surface undulations of different wavelengths. It should be noted that due to the constant height-to-wavelength ratio, the height of the surface undulation can be much greater than 4%t (0.04t) for large wavelength, e.g., $h_g = 0.2t$ when $L_b = D$.

The results show that as the wavelength increases, the CSC firstly rapidly decreases and then increases. A critical wavelength exists at which the CSC is the lowest, i.e., the most detrimental to the CSC. When the wavelength of the surface undulation is much smaller or larger than the critical wavelength, the surface undulation shows trivial effects on the CSC despite the height of the undulation. The critical wavelength for the case shown in the figure is about 0.2D.

Similar critical wavelength is observed in simulations using single wave surface undulations as shown in Figure B - 11 where the pressure effect is also investigated. The internal pressure increases the critical wavelength. It should be noted that under internal pressure, a net-section tensile force exists due to the applied loading condition, ER-NLF$_p$ in the analyses.

The critical wavelength of the surface undulation is similar to the wavelength of the wrinkle (L_w) formed at the maximum moment. When the maximum moment is reached, a small wrinkle, although may not be visible, is often formed (see Section 3.3.5). The wavelength of the wrinkle is found to depend on the pipe geometry and internal pressure as shown in Figure B - 12 and Figure B - 13. The wrinkle wavelength increases with the decrease of the pipe's D/t ratio and/or the increase of the internal pressure. For the large range of the D/t ratio and internal pressure studied, the wrinkle wavelength varies between 20% and 60% of the pipe's OD, a relatively tight range. The wrinkle wavelength is insensitive to the net-section force in the longitudinal direction as shown in Figure B - 13 where no net-section force exists for ER-NLF$_0$ while net-section force exists for ER-NLF$_p$.

The wrinkle wavelength is not sensitive to the size (i.e., h_g, α, and L_b) of the initial surface undulation as shown in Figure B - 14 and Figure B - 15. The results indicate that the wrinkle wavelength is a property of the pipe which is mainly determined by the stiffness of the pipe (therefore is affected by the pipe's D/t ratio and the internal pressure). The initial geometry imperfection has very limited effect on the wrinkle wavelength.

The measured wavelength of the surface undulations in the UOE pipes reported in [1, 2, 3] is found to be within similar ranges as the critical wavelength in Figure B - 12. In addition, Figure B - 10 and Figure B - 11 show that the surface undulation having wavelength twice of the critical wavelength shows similar low CSC as that of the surface undulation with critical wavelength.

As a result, the critical wavelength of the surface undulation (i.e., wrinkle wavelength) is recommended and used for future analyses. The critical wavelength depends on the pipe D/t ratio and internal pressure.

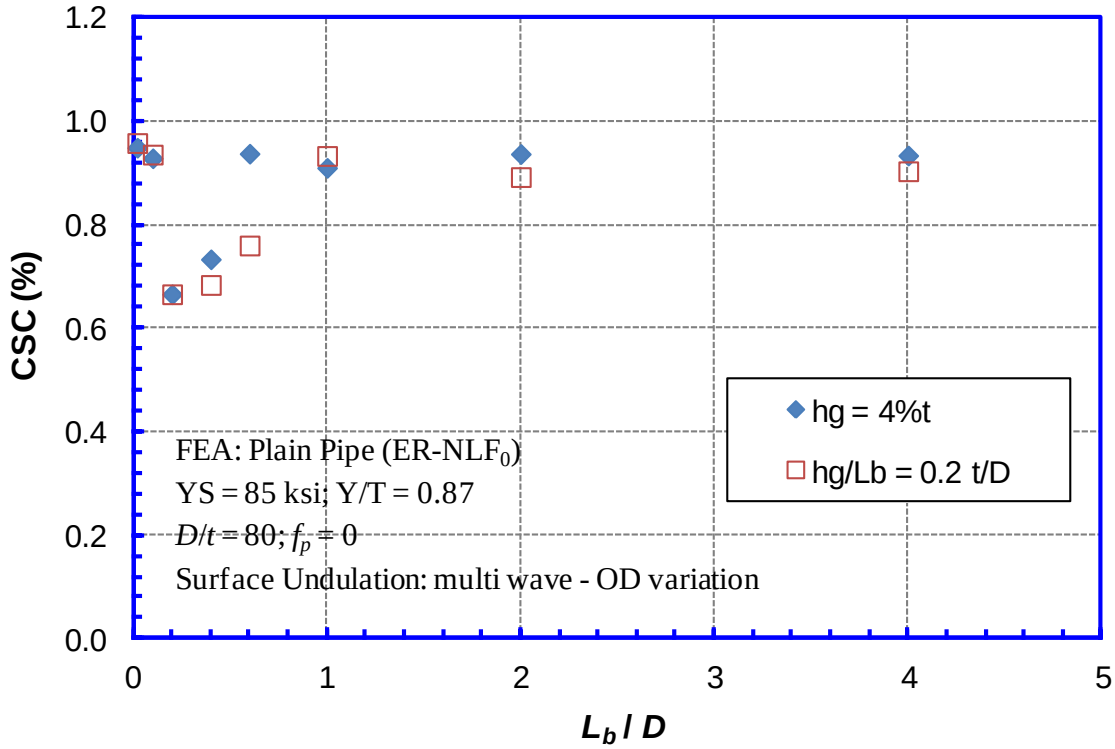

Figure B - 10 Effect of the wavelength (L_b) of the surface undulation on the CSC (multi wave)

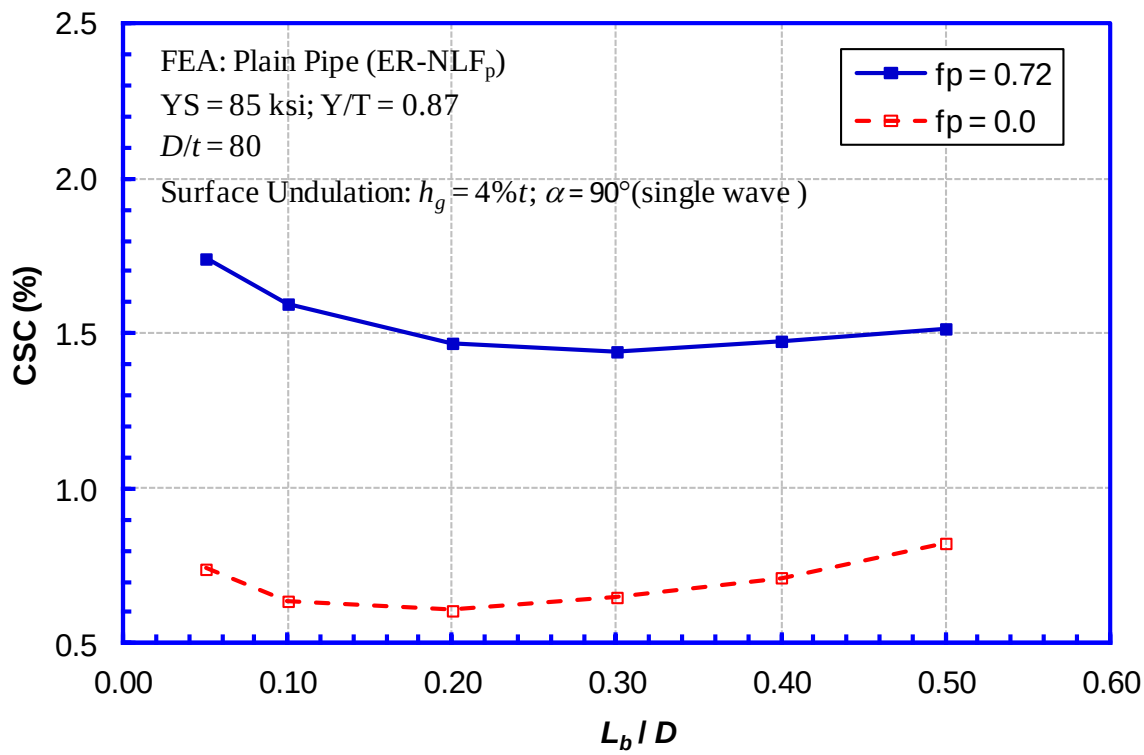

Figure B - 11 Effect of the wavelength (L_b) of the surface undulation on the CSC (single wave)

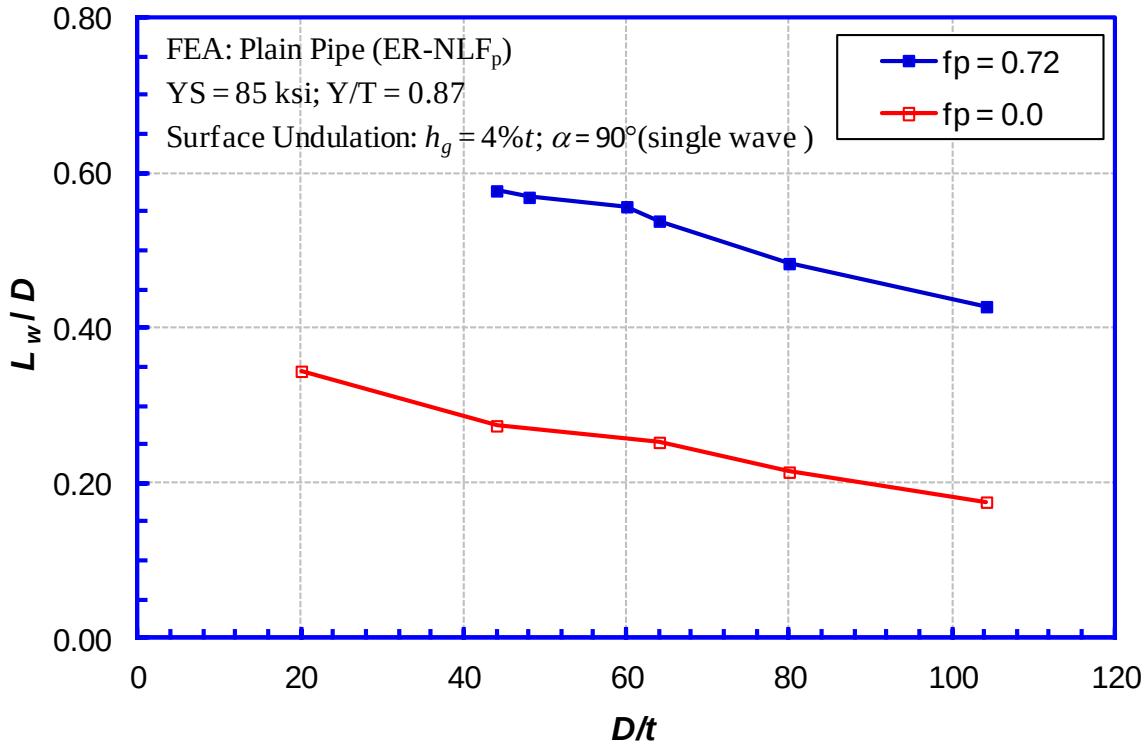

Figure B - 12 Effect of pipe *D/t* on wrinkle wavelength (L_w)

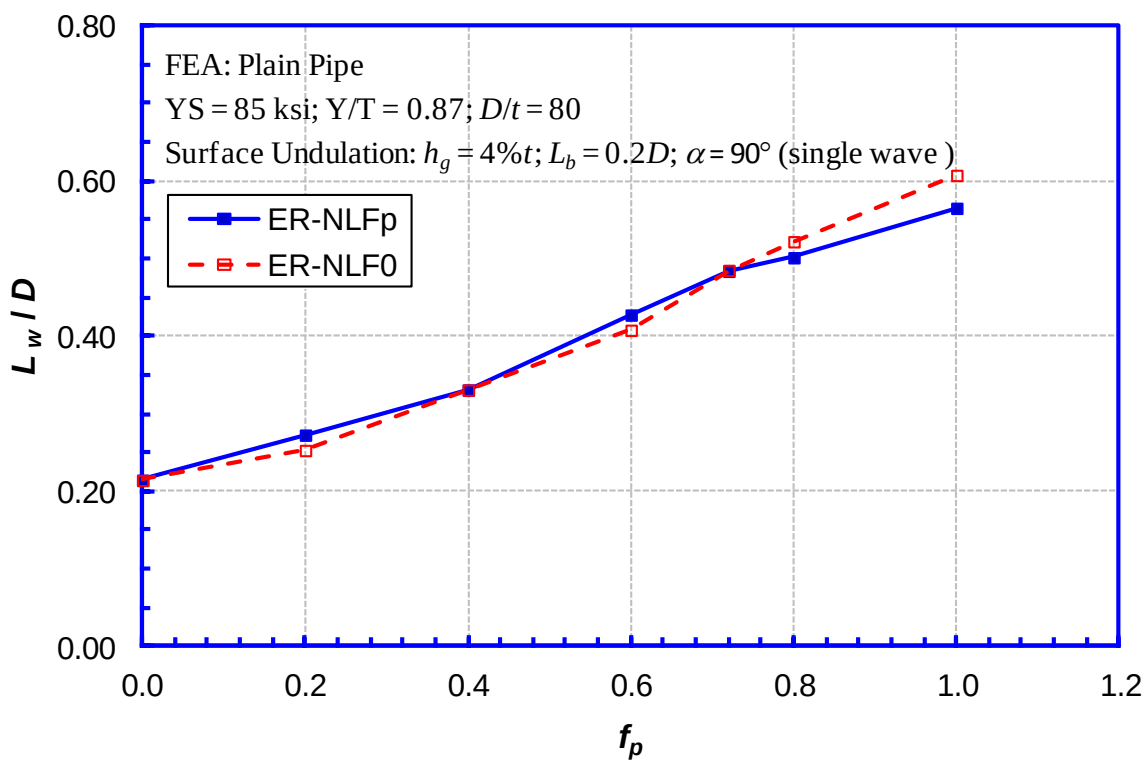

Figure B - 13 Effect of internal pressure (f_p) on wrinkle wavelength (L_w)

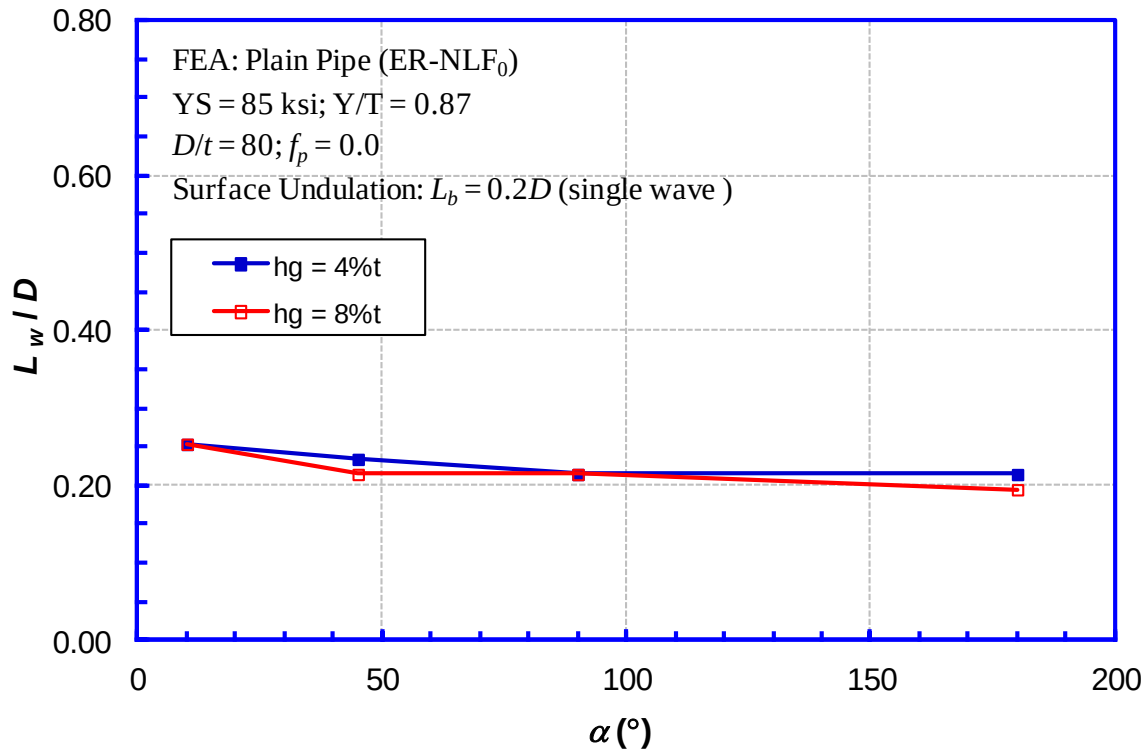

Figure B - 14 Effect of angle (α) of surface undulation on wrinkle wavelength (L_w)

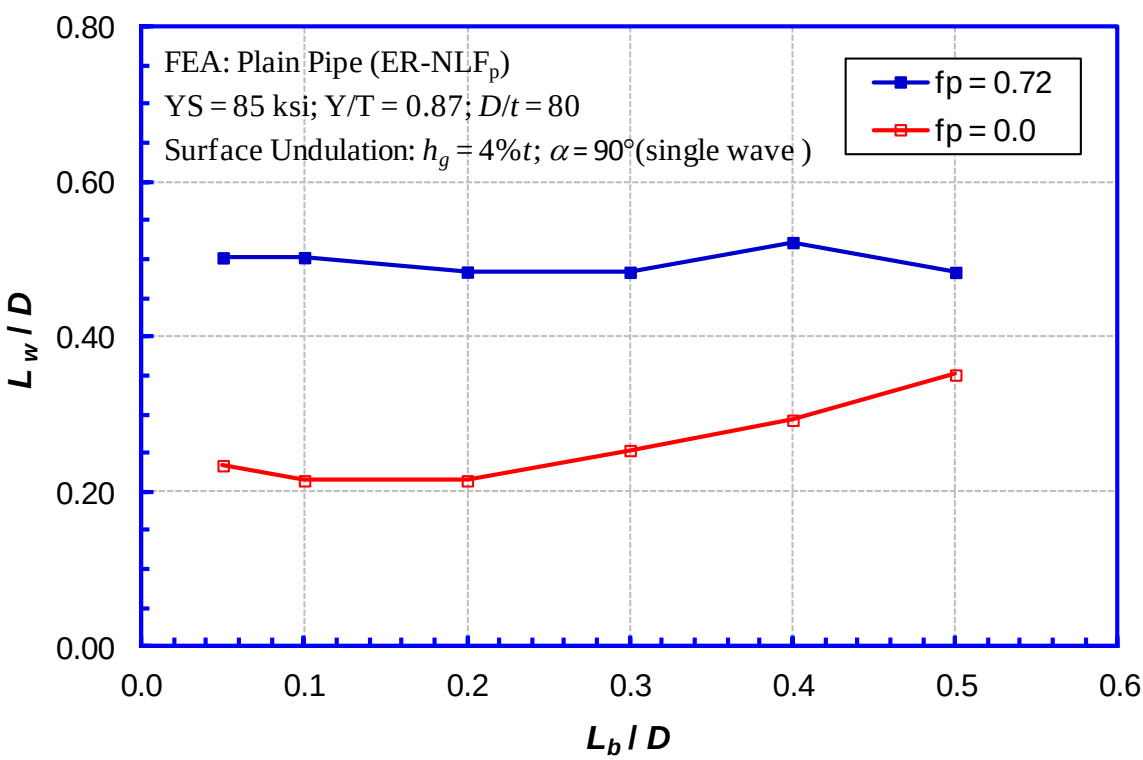

Figure B - 15 Effect of wavelength (L_b) of surface undulation on wrinkle wavelength (L_w)

B.3.5 Effect of the Height of Geometry Imperfections on CSC

The effect of the height (h_g) of the surface undulation on the CSC is shown in Figure B - 16. The CSC is normalized by the CSC at h_g = 4%t. The results of the UOA model are also included for comparison and the FEA results match the UOA results very well. It is seen that the surface undulation can be very detrimental to the CSC. For example, the CSC can be reduced by 50% as the height of the surface undulation increases from 0.1%t to 20%t. The rate of the reduction of the CSC decreases as the height increases.

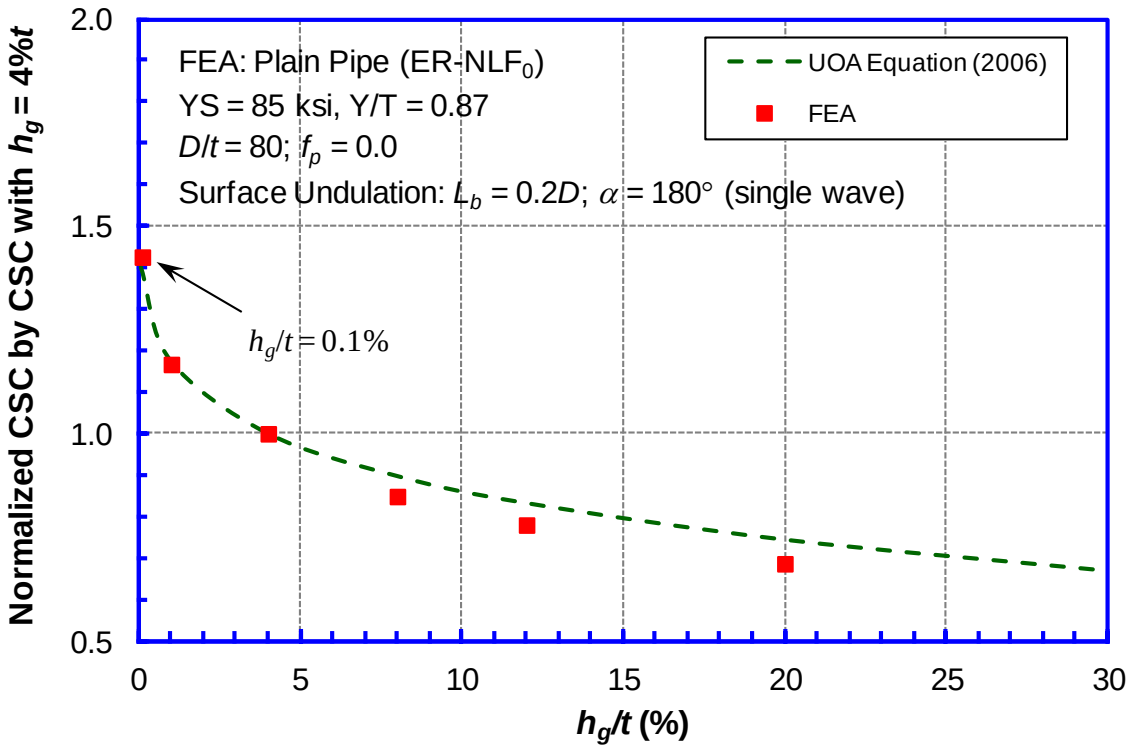

Figure B - 16 Effect of the height of the surface undulation on the CSC

B.4 Pipe Yield Strength and Strain Hardening Capacity

The strain hardening exponent (n) and Y/T ratio (i.e., the ratio between the yield and tensile strength) both measure a material's strain hardening capacity. The shape of a stress-strain curve can be uniquely determined for a given strain hardening exponent (n) but not for a given Y/T ratio. In spite of the differences between the two parameters, they are usually treated equivalent. The correlation between the Y/T ratio and n for linepipe steels has been established through a statistic analysis (see Appendix A). In the following studies of this section, the Y/T ratio is used to measure the materials' strain hardening capacity. The findings are also applicable to the strain hardening exponent (n).

The pipe's Y/T ratio and its yield strength are often related, e.g., the low grade (or strength) pipes often have lower Y/T ratios (i.e., higher strain hardening capacities) than the high grade pipes. In other words, pipes of different yield strengths often have different Y/T ratios. As a result, the difference of the CSC of the pipes with different strengths could be caused by the difference in their strain hardening capacities.

The acceptance of the pipe's yield strength and strain hardening capacity by the existing CSC models varies. The DNV, JFE, and C-FER models accept the strain hardening capacity (e.g., DNV - Y/T ratio; JFE and C-FER - strain hardening exponent, *n*). The CSA and UOA models use the pipe's yield strength. It should be noted that in the development of the UOA equations, different Y/T ratios were adopted for pipes with different strengths. Therefore, the dependence of the CSC on the yield strength recognized in the UOA equations may also be due to the Y/T ratio.

To separate the effects of the pipe's strength and strain hardening capacity on the CSC, two groups of special stress-strain curves (different from those in Section 3.2.4) were constructed. The procedures in Appendix A are used to create the stress-strain curves. In the first group, the yield strength (YS) is constant (85 ksi) while the Y/T ratio varies from 0.76 to 0.96 by changing the ultimate tensile strength (UTS). In the second group, the YS varies from 69 ksi to 115 ksi and the UTS varies from 79 ksi to 132 ksi while the Y/T ratio is constant (0.87).

The effects of the pipe's Y/T ratio and yield (and tensile) strength on the CSC are shown in Figure B - 17 and Figure B - 18, respectively. It is seen that the CSC depends on the pipe's Y/T ratio (i.e., the strain hardening capacity). Decreasing the pipe's Y/T ratio (i.e., increasing the strain hardening capacity) can increase the CSC. On the other hand, the CSC is independent on the pipe's strength (if the Y/T ratio is kept constant), similar to the early findings by [9,10].

The CSC-Y/T relationship predicted by the DNV equation is compared with the FEA results and shown in Figure B - 19 where the CSC is normalized by the CSC at Y/T = 0.87. The FEA results match the DNV results very well.

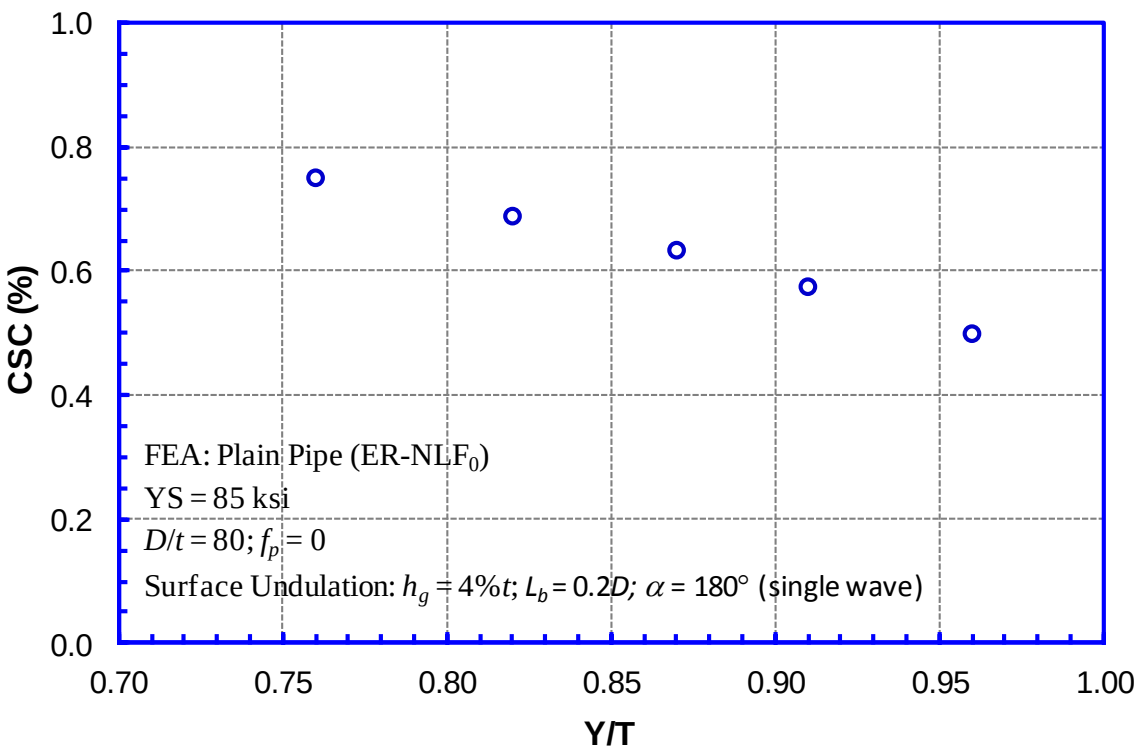

Figure B - 17 Effect of the pipe's Y/T ratios on the CSC

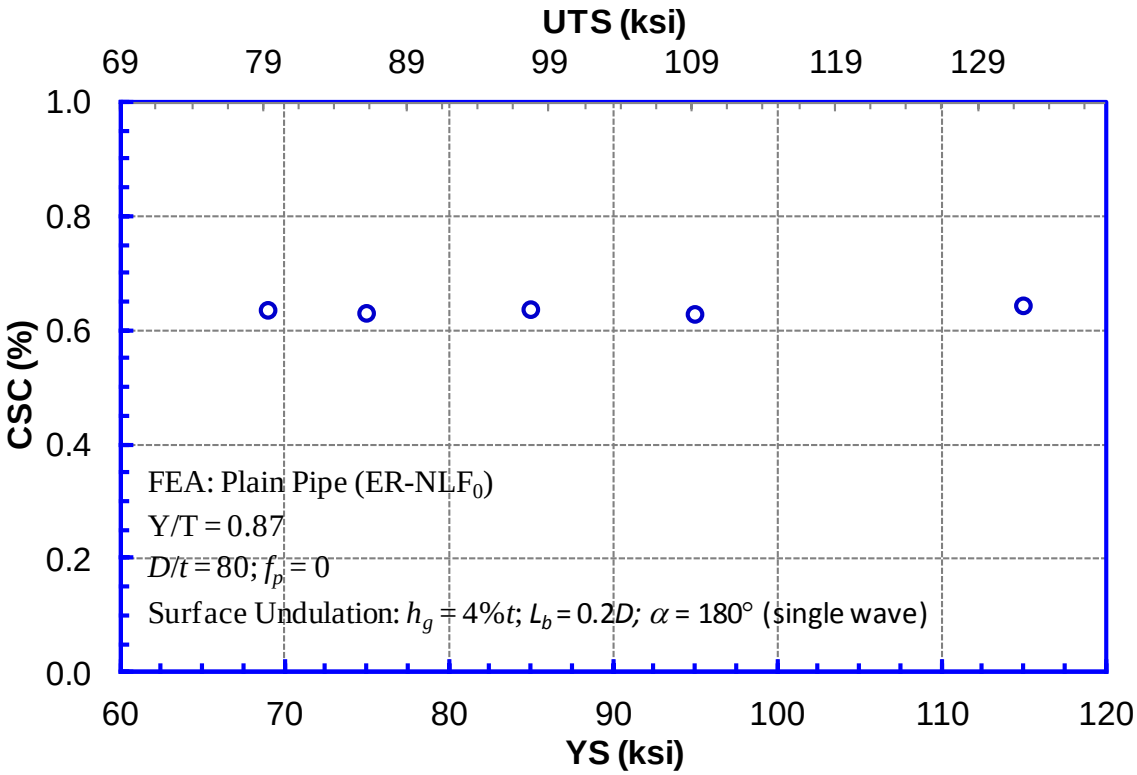

Figure B - 18 Effect of the pipe's yield strength on the CSC

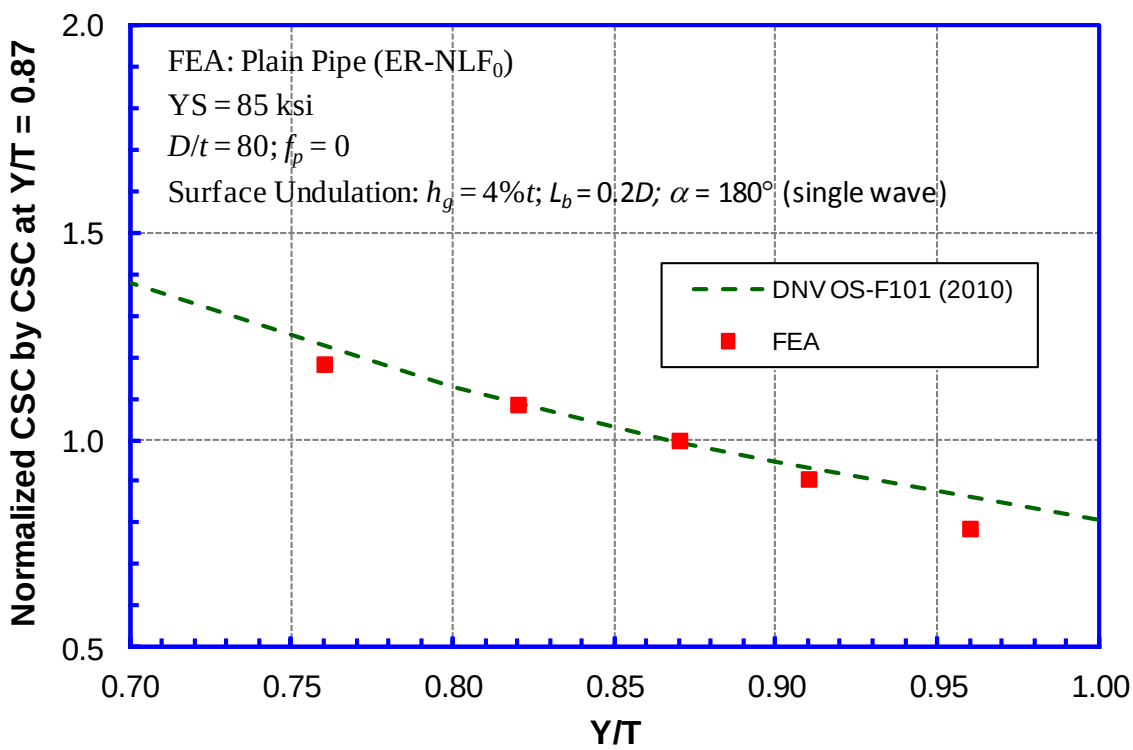

Figure B - 19 Effect of the pipe's Y/T on the CSC (comparison with DNV model)

B.5 Pipe Uniform Strains

It is known that the pipe's CSC is affected by the shape of the full stress-strain curves (SSC). In addition to the yield strength and Y/T ratio, the uniform strain (uEL) is another key parameter often used for characterizing the full stress-strain curves.

Similar to the relationship between a pipe's strength and strain hardening capacity, the pipe's uniform strain, strength, and strain hardening capacity are also related. Low strength materials often have high strain hardening capacities and large uniform strains. Therefore their effects on the CSC are often coupled. To separate the effect of the pipe's uEL on the CSC from the other factors such as the strength and strain hardening capacity, a special group of stress-strain curves were constructed as shown in Figure B - 20. All the stress-strain curves in the figure have the same yield and tensile strengths (thus the same Y/T ratio). However, the uniform strain varies from 8.2% to 4.4%. The stress-strain curve with 8.2% uEL is referred to as the baseline stress-strain curve (i.e., baseline SSC).

The effect of the uEL on the CSC is shown in Figure B - 21 for various *D*/*t* ratios and internal pressure levels. The reduction of the uniform strain shows no effect on the pipe's CSC as long as the reduced uniform strain is greater than the CSC of the material with the baseline SSC. However, if the uniform strain is reduced to be smaller than the CSC of the baseline material, the CSC will be reduced to the value of the reduced uniform strain.

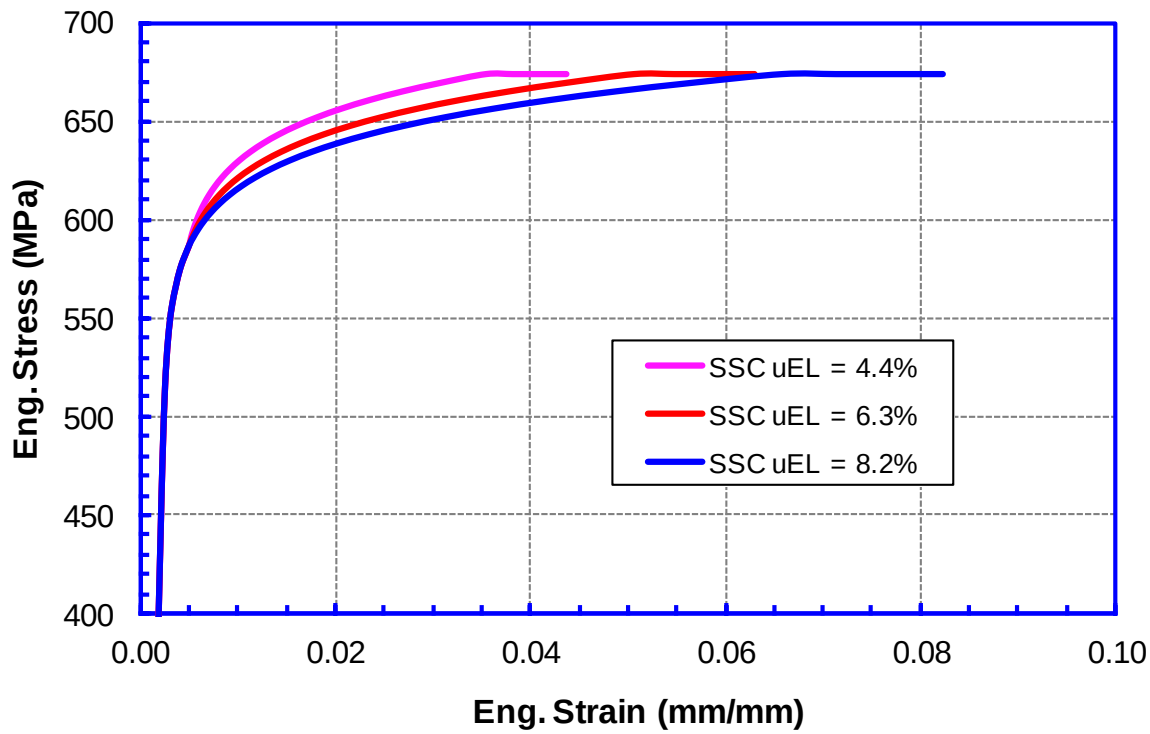

Figure B - 20 Stress-strain curves (SSC) with different uniform strains (uEL)

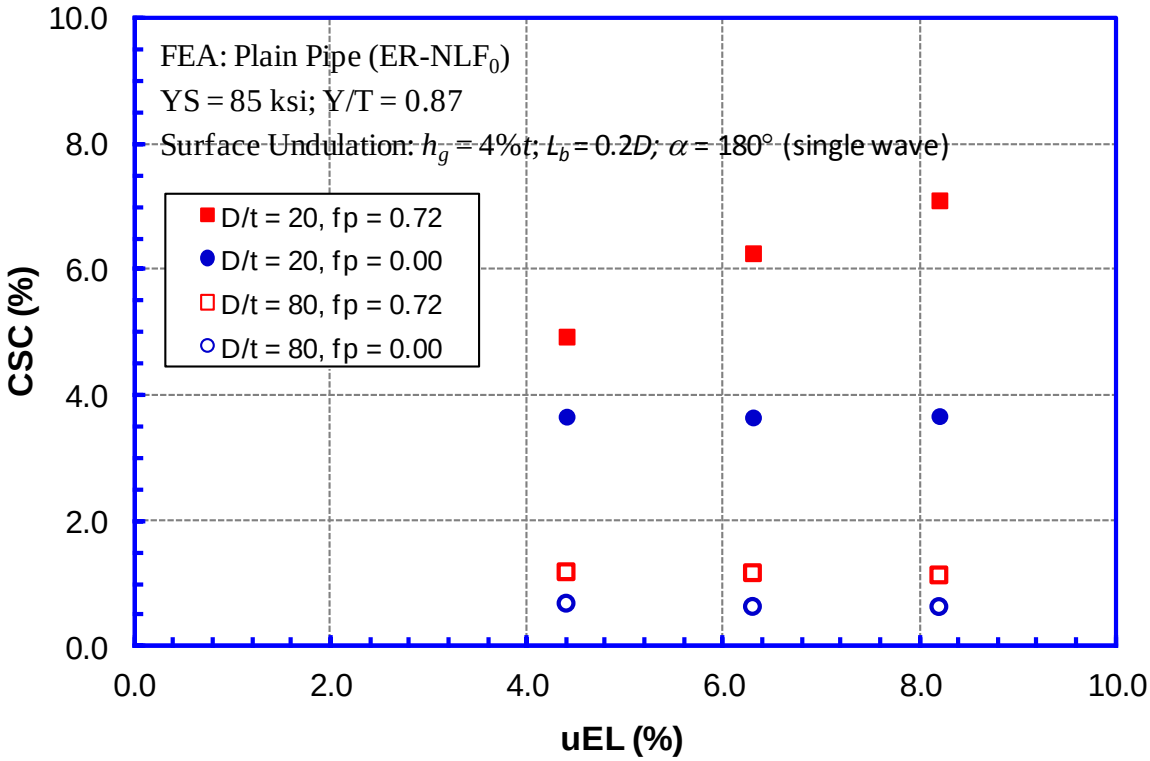

Figure B - 21 Effect of the pipe's uniform strain (uEL) on the CSC

B.6 Pipe Lüder's Strains

In addition to the uniform strain, the Lüder's strain (i.e., the plateau in the stress-strain curve after the yield point) changes the shape of the stress-strain curve and the CSC. The existence of the Lüder's strain can sometimes increase the CSC and sometimes reduce the CSC [11,12]. The UOA models use separate equations for the pipes with and without the Lüder's strain. It should be noted that the Lüder's strain always ends at 0.5% strain in the UOA models.

To study the effect of the Lüder's strain on the CSC, stress-strain curves with various Lüder's strains were created and are shown in Figure B - 22. The yield strength, tensile strength (thus the Y/T ratio), and the uniform strain of the stress-strain curves are the same. The Lüder's strain (i.e., ε_e, the strain at which the Lüder's extension ends) varies from 1.0% to 2.0%.

It is generally believed that the appearance of the Lüder's strain in a pipe's stress-strain curve can reduce its CSC. The CSC of the pipes with 2% Lüder's strains is compared with the CSC of the pipes with round-house stress strain curves (i.e., without Lüder's strains) in Figure B - 23. The pipe's yield strength, Y/T ratio, and uniform strain are kept the same for the pipes with and without Lüder's strains as shown in Figure B - 22. The results for various D/t ratios without the pressure (f_p = 0.0) are shown. For pipes of $D/t \geq 44$, as generally expected, the CSC of the pipes with round-house stress-strain curves (CSC_{RH}) is higher than the CSC of the pipes with Lüder's strains (CSC_{LD}), i.e., $CSC_{RH} > CSC_{LD}$. However, for pipes of D/t = 20, an opposite trend is seen, i.e., $CSC_{RH} < CSC_{LD}$, that is the Lüder's strain increases the CSC.

To further investigate the above observed trend, the relationship between the moment and the compressive strain from the pipes with D/t = 20 and 44 are shown in Figure B - 24 (a) and (b), respectively. In both cases, the maximum moment of the pipes with round-house stress-strain curves is higher than that with Lüder's strains. For D/t = 20, CSC_{RH} is greater than ε_e (the strain at which the Lüder's extension ends). However, for D/t = 44, CSC_{RH} is less than ε_e. Figure B - 22 shows that if the strain is greater than ε_e, the slope (or the strain hardening rate) of the stress-strain curve with the Lüder's strain is increased and is higher than the strain hardening rate of the stress-strain curve without the Lüder's strain. As a result, if the CSC_{RH} is greater than ε_e, the appearance of the Lüder's strain can further increase the CSC_{LD} due to the increase of the strain hardening rate, i.e., $CSC_{RH} < CSC_{LD}$. On the other hand, if the CSC_{RH} is smaller than ε_e, the appearance of the Lüder's strain can reduce the CSC_{LD} due to the low strain hardening rate on the Lüder's extension (or plateau), i.e., $CSC_{RH} > CSC_{LD}$.

The CSC of the pipes with 2% Lüder's strains is compared with the CSC of the pipes without Lüder's strains for pressurized conditions (f_p = 0.72) in Figure B - 25. Unlike the results for the non-pressurized conditions, for pipes of $D/t \leq 80$, the CSC_{RH} is less than CSC_{LD}, i.e., the Lüder's strain increases the CSC. Only for the pipe of D/t = 104, $CSC_{RH} > CSC_{LD}$. The pressure effect is mainly due to two reasons: (1) the internal pressure increases the CSC_{RH} and (2) the internal pressure reduces the equivalent ε_e. As shown in Figure B - 26, with internal pressure, the plateau on the moment - strain curves caused by the Lüder's strain is not as obvious as those in the non-pressurized conditions (shown in Figure B - 24). Therefore it is more likely the CSC_{RH} is higher than ε_e for pressurized conditions and thus $CSC_{RH} < CSC_{LD}$.

The effect of the magnitude of the Lüder's strain (i.e., ε_e) on the CSC is shown in Figure B - 27. It should be noted that in the plot, when ε_e = 0.5%, the stress-strain curve is in fact of round-house shape, i.e., without the Lüder's strain. Therefore, the CSC at ε_e = 0.5% is actually CSC_{RH}. Compared with the CSC_{RH}, the CSC_{LD} firstly increases as ε_e increases. Once ε_e reaches a critical value, the CSC_{LD} starts to decrease rapidly. The critical ε_e depends on the other parameters, e.g., the pipe's Y/T ratio in the case.

In Figure B - 28, the three curves in Figure B - 27 are re-plotted by normalizing the CSC and ε_e with the CSC_{RH}. The CSC_{LD}/CSC_{RH} (i.e., the y-axis) is the ratio between of the CSC of the pipes with and without the Lüder's strain. If $CSC_{LD}/CSC_{RH} < 1$, the Lüder's strain reduces the CSC. It is seen that for all three Y/T ratios, the CSC_{LD}/CSC_{RH} ratio is larger than 1 for small ε_e and less than 1 for large ε_e. The transition takes place at $\varepsilon_e / CSC_{RH} = 1$, i.e., $\varepsilon_e = CSC_{RH}$.

Similar observations to those for Figure B - 28 can be observed in Figure B - 29 and Figure B - 30 as well. In Figure B - 29, the results from different D/t ratios are given and in Figure B - 30, the results from different geometry imperfections are given.

All the above results confirm that if the CSC_{RH} is greater than ε_e, the existence of the Lüder's strain increases the CSC. However, if the CSC_{RH} is smaller than ε_e, the existence of the Lüder's strain reduces the CSC. The results in Figure B - 27 to Figure B - 30 are all for non-pressurized conditions. But those results can be conservatively applied to the pressurized conditions as indicated by Figure B - 25.

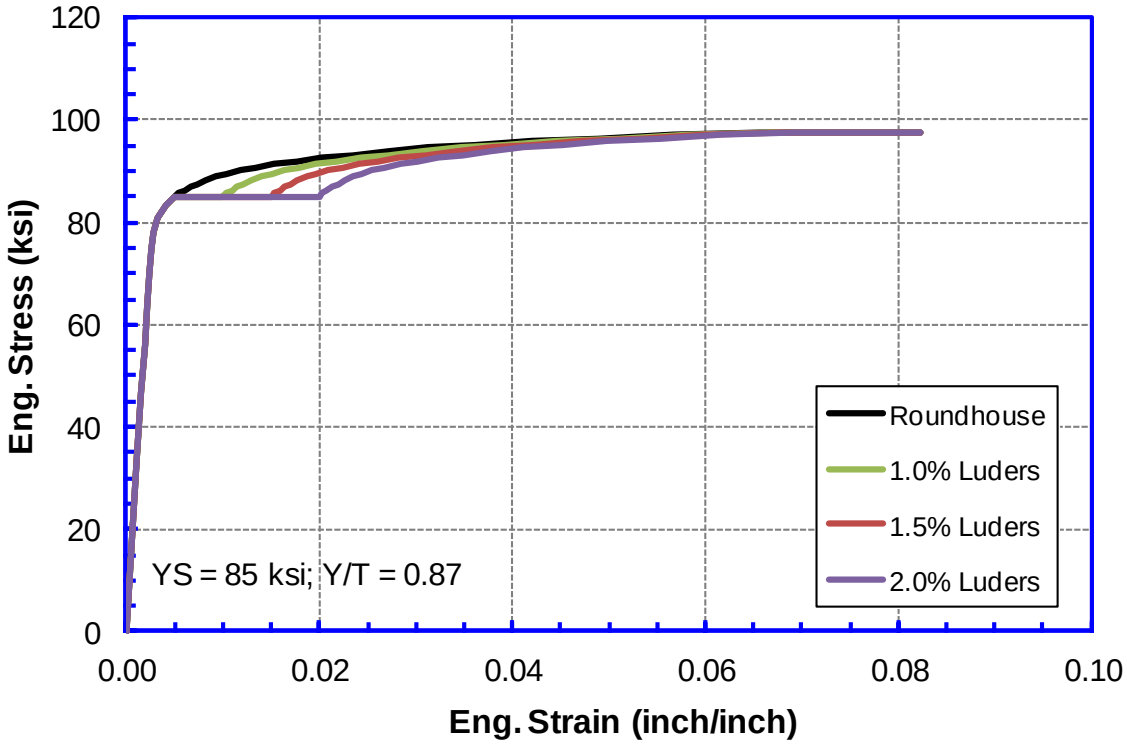

Figure B - 22 Stress-strain curves (SSC) with different Lüder's strains

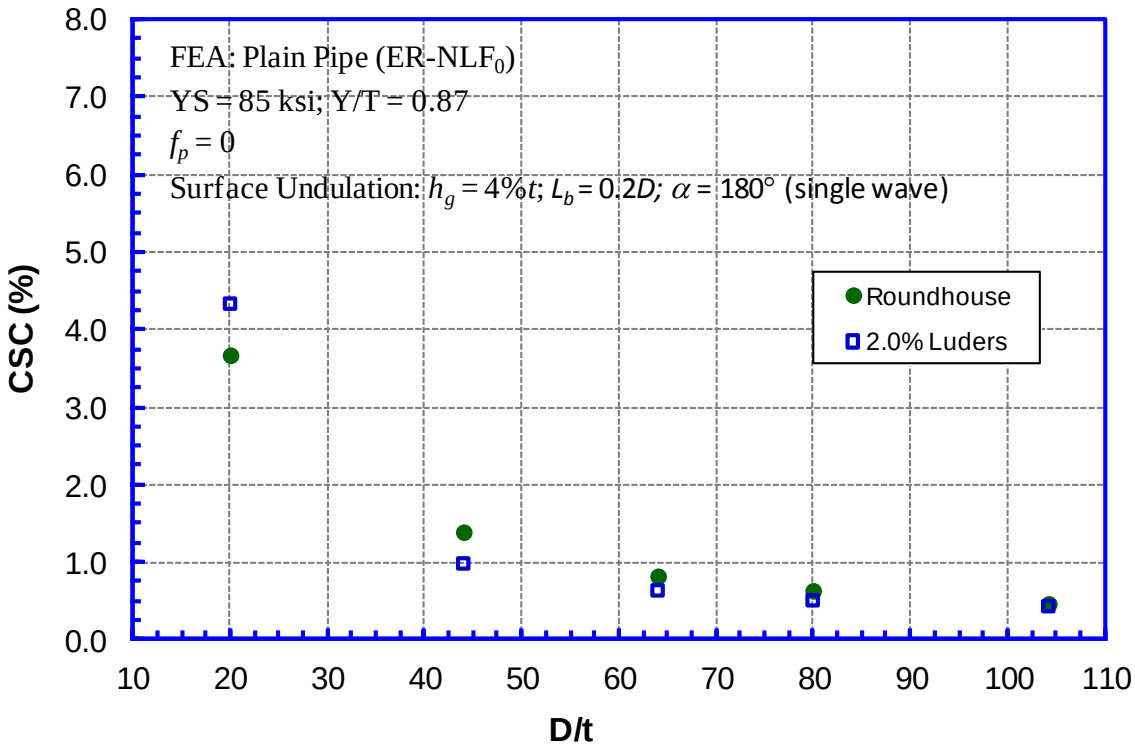

Figure B - 23 Comparison of the CSC for pipes with and without Lüder's strains (f_p = 0.0)

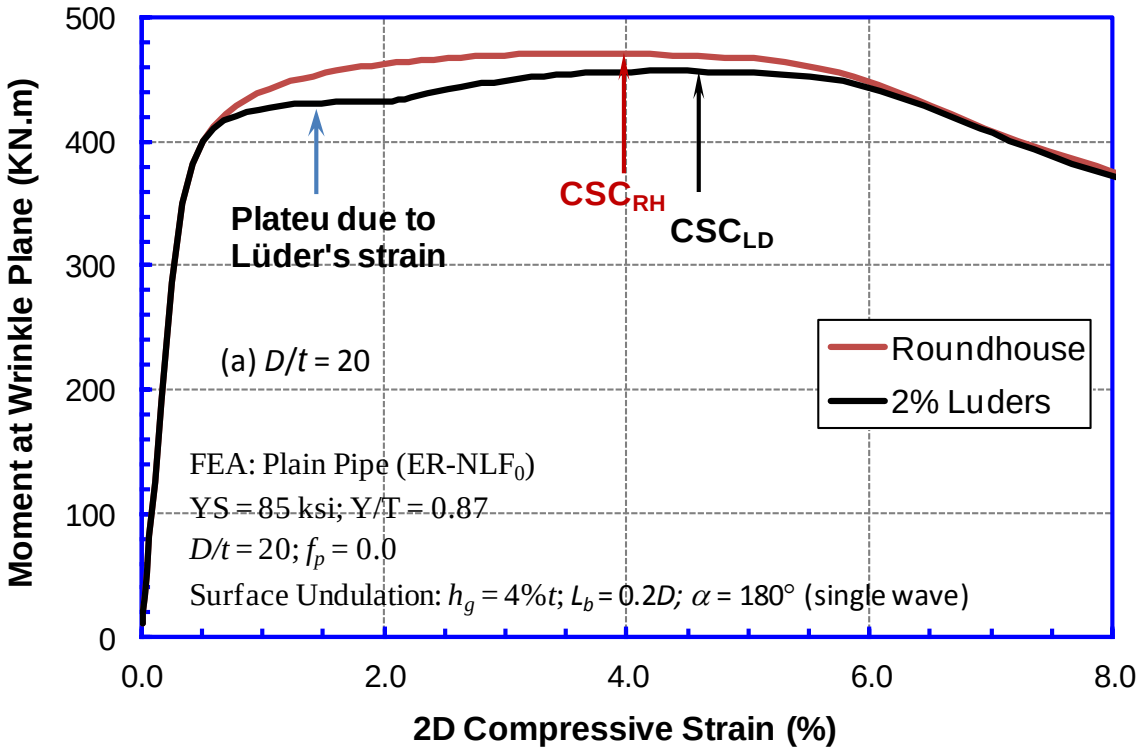

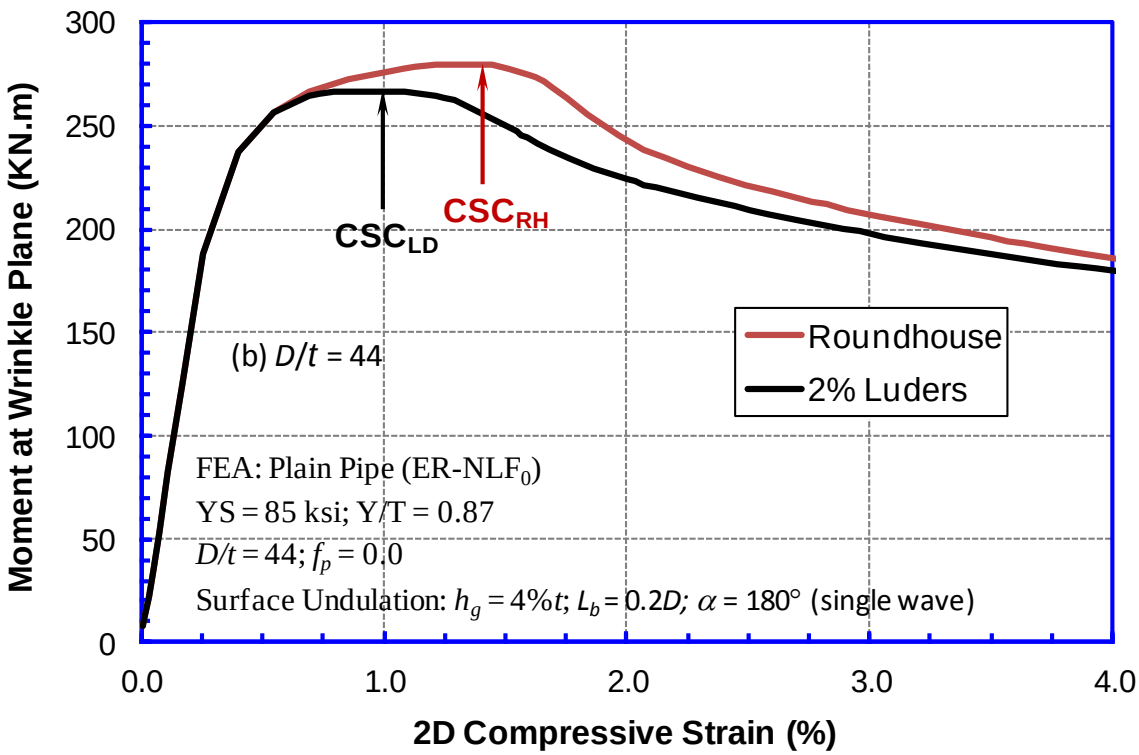

Figure B - 24 Effect of the Lüder's strain on the moment-strain curves (f_p = 0.0) (a) D/t = 20 and (b) D/t = 44

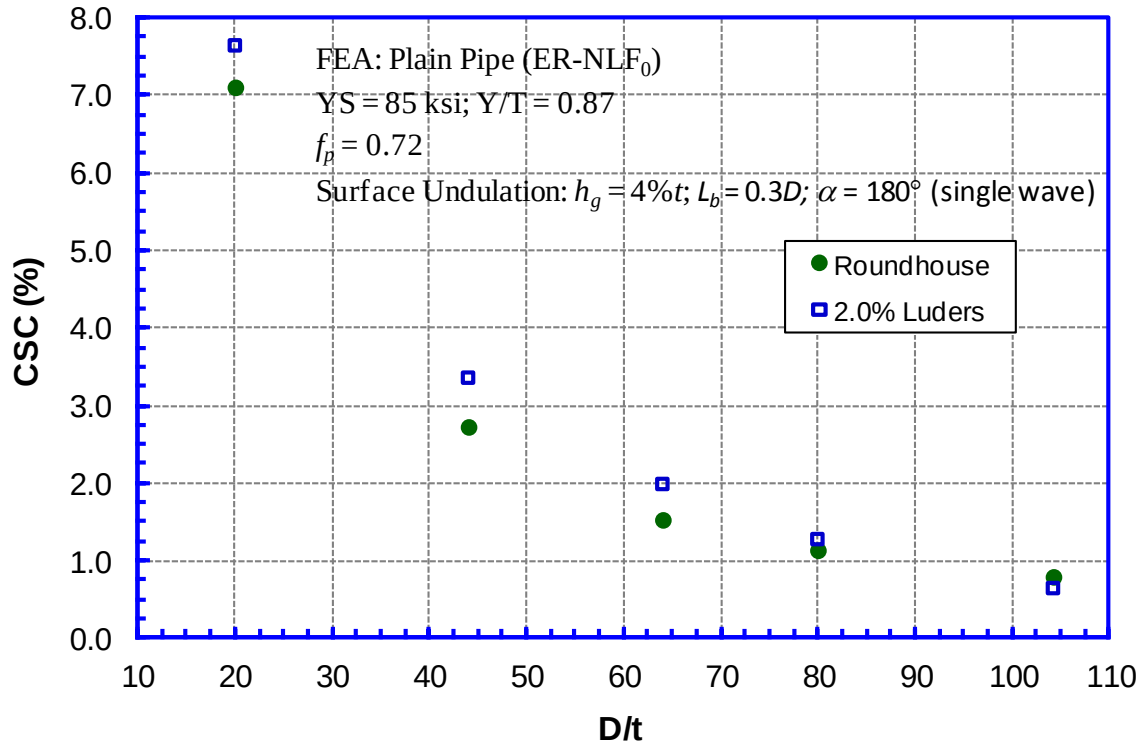

Figure B - 25 Comparison of the CSC for pipes with and without Lüder's strains (f_p = 0.72)

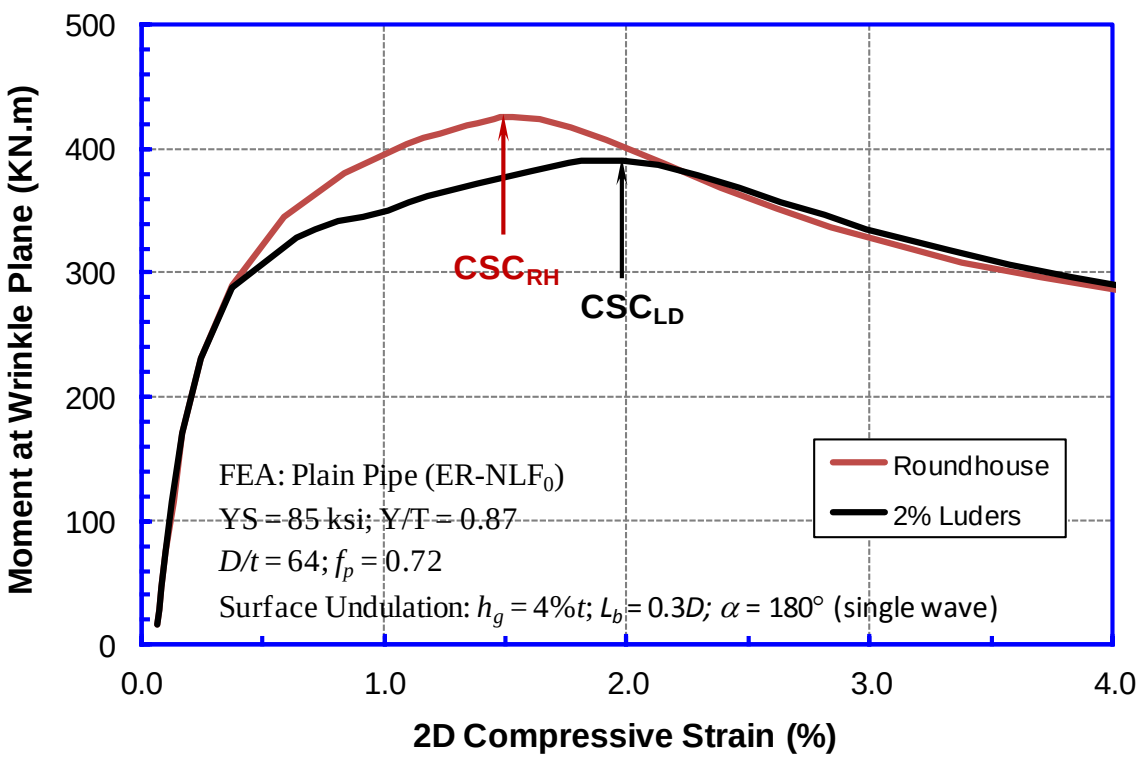

Figure B - 26 Effect of the Lüder's strain on the moment-strain curves (f_p = 0.0, D/t = 64)

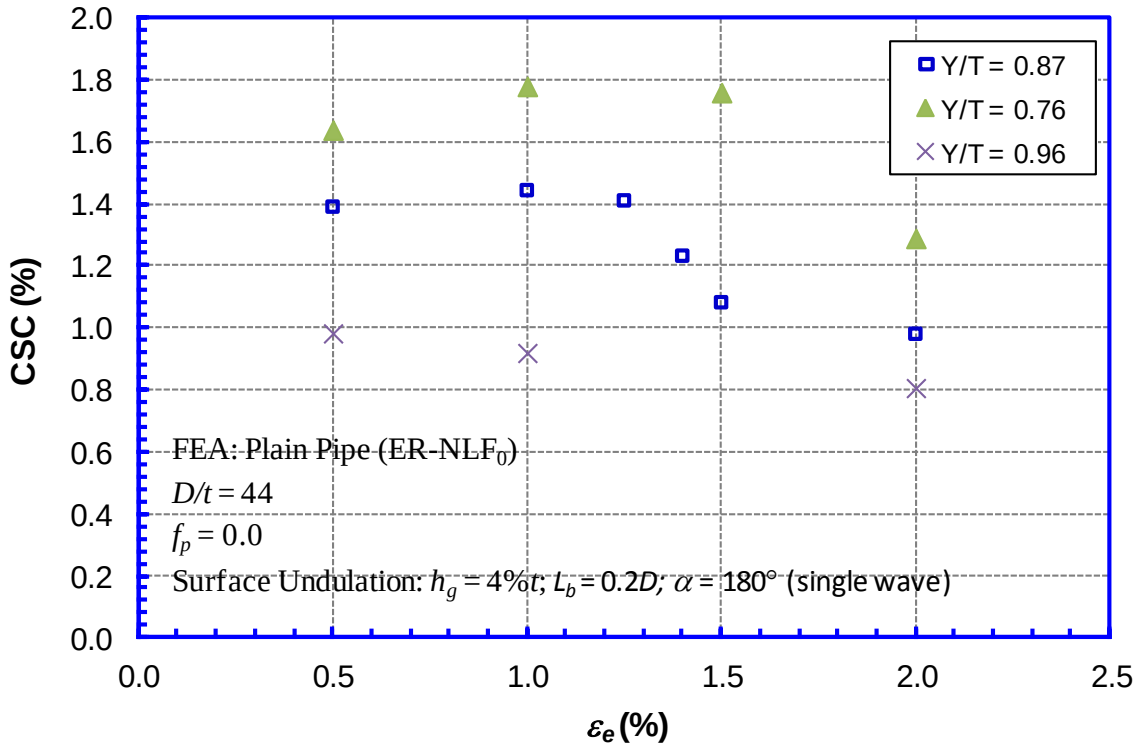

Figure B - 27 Effect of the magnitude of the Lüder's strain on the CSC (f_p = 0.0, D/t = 44)

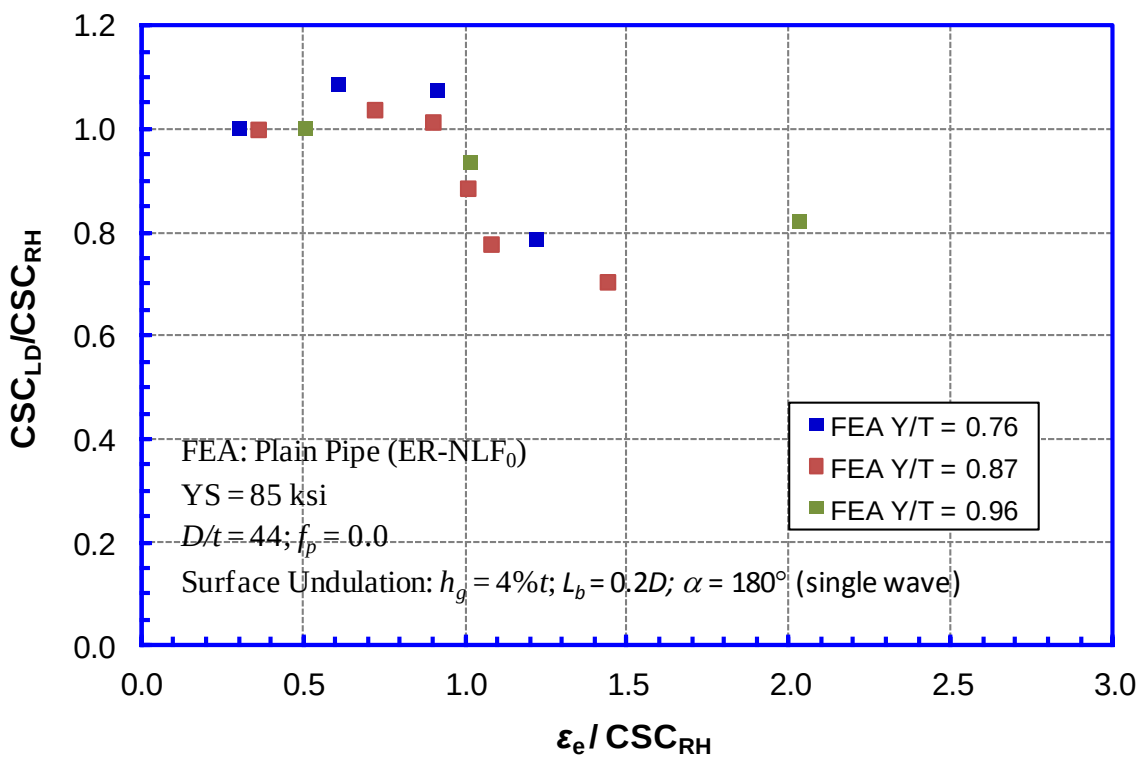

Figure B - 28 Normalized CSC vs. normalized Lüder's strain (effect of Y/T)

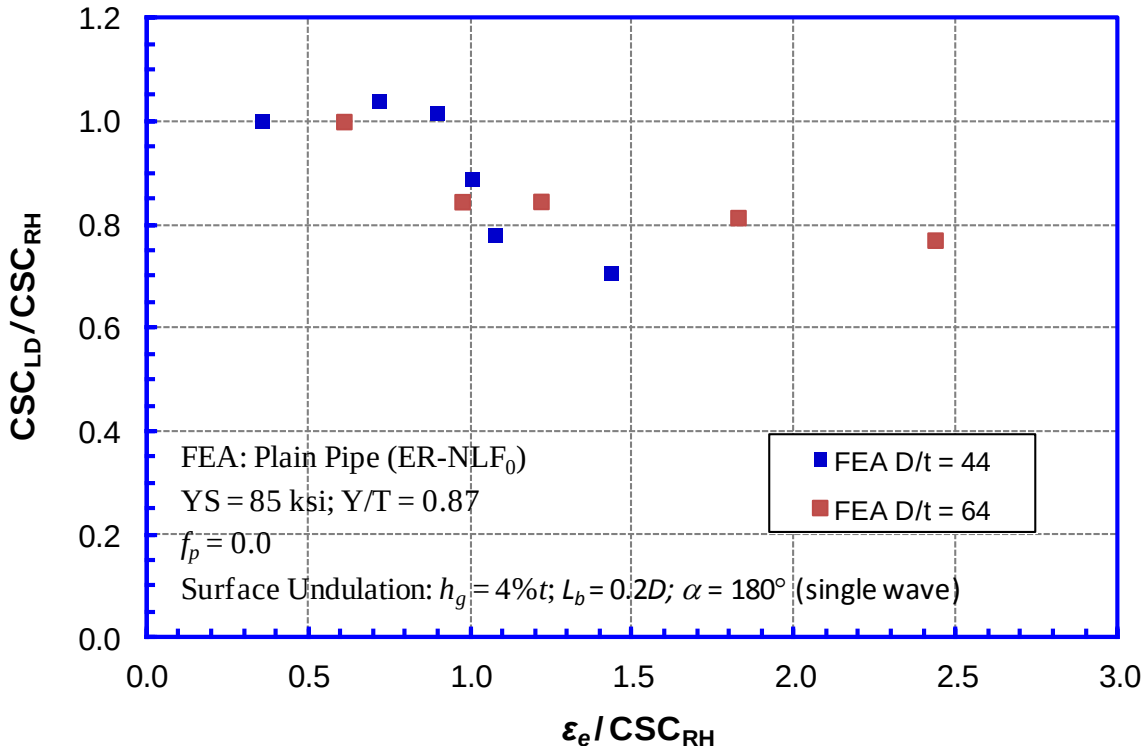

Figure B - 29 Normalized CSC vs. normalized Lüder's strain (effect of *D*/*t*)

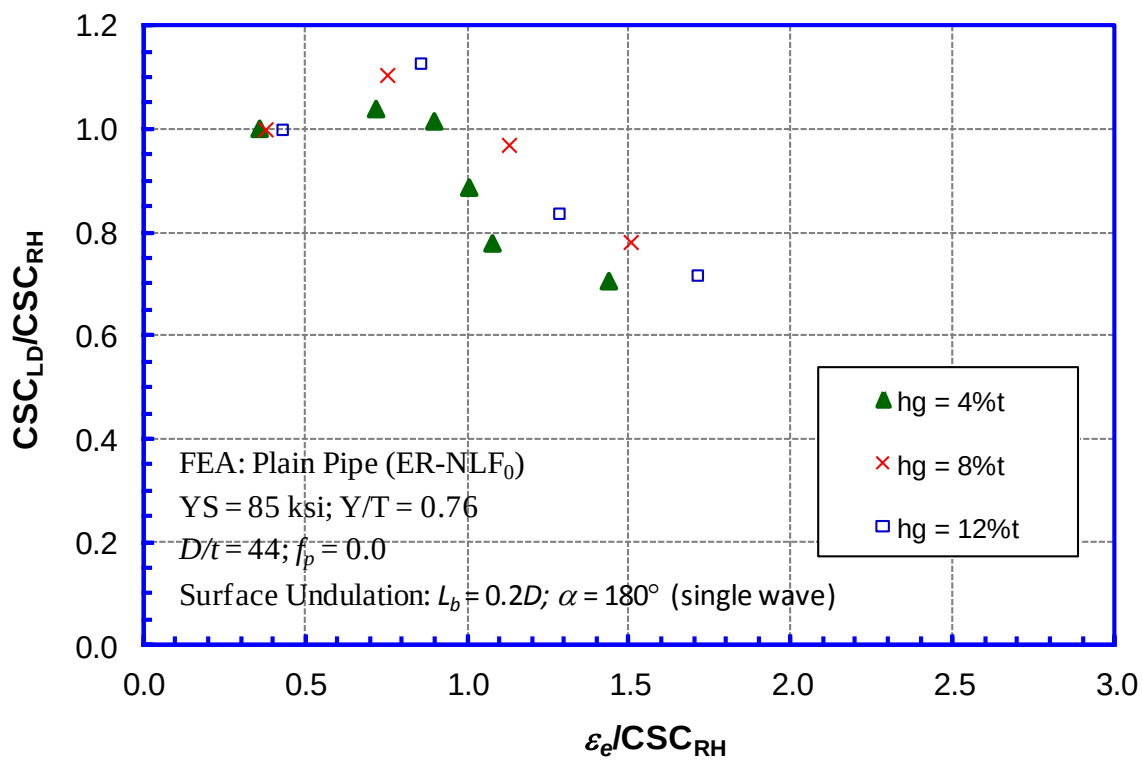

Figure B - 30 Normalized CSC vs. normalized Lüder's strain (effect of h_g)

B.7 Pipe Property Anisotropy

The linepipe steels often show anisotropic properties in the longitudinal and circumferential (i.e., hoop) directions. In addition, the linepipe steels often show different stress-strain curves for tension and compression. The material's anisotropy is mainly caused by the plate and pipe forming strains and the so-called Bauschinger effect.

The anisotropy often shows different yield/tensile strengths and strain hardening capacities. For the UOE pipes, the hoop properties often show higher yield and tensile strengths and Y/T ratios (i.e., smaller strain hardening capacities) than the longitudinal properties.

The findings on the effect of the material's anisotropy on the CSC are mixed. To some extent, the mixed findings are due to the lack of comprehensive numerical models that can capture the material's complicated anisotropic behaviors. For example, the numerical models in existing finite element software such as ABAQUS®, cannot simultaneously represent the difference in the tensile strengths and strain hardening capacities between the longitudinal and circumferential directions. For example, the kinematic hardening models can reproduce the different strain hardening capacities in the longitudinal and circumferential directions, but the tensile strength in the two directions are the same. On the other hand, the Hill's hardening models can simulate the different strengths in the longitudinal and circumferential directions, while the strain hardening capacities of the two directions are the same.

To examine the effect of the material anisotropy on the pipe's CSC, the CSC calculated with the anisotropic models is usually compared with the CSC calculated from the isotropic models using the tensile stress-strain curves of the longitudinal direction. Using the models which can capture the anisotropic strain hardening capacities of the pipe's longitudinal and circumferential directions (e.g., kinematic hardening models), the reduction of the strain hardening capacity in the hoop direction was found detrimental to the CSC [13,14,15]. However, using the numerical models which can capture the anisotropic tensile strength in the longitudinal and circumferential directions (e.g., Hill's hardening models), the increased tensile strength in the hoop direction can increase the CSC [16].

In recent work, a new numerical model based on a combined Hill's and kinematic hardening models was established to simulate the different strengths and strain hardening capacities in the pipe's longitudinal and hoop properties simultaneously [17]. The new model was used to study the CSC of a UOE pipe using measured anisotropic strengths and strain hardening capacities. The CSC is found reduced by the material's anisotropy which indicates that the anisotropic strain hardening capacities tend to play a more dominant role on the CSC than the anisotropic strengths.

Finite element analyses (FEA) were also conducted in this project to further investigate the effect of the material anisotropy on the CSC. The major objective of the analyses is to identify simplified methods which can capture the effect of the material anisotropy.

The stress-strain curves of a representative X100 linepipe steel in [15] were used in the FEA. The stress-strain curves (SSC): longitudinal tension, longitudinal compression, and hoop tension, are shown in Figure B - 31. The tensile stress-strain curve in the circumferential direction shows higher yield strength and Y/T ratio than those in the longitudinal direction. In the longitudinal direction, the compressive stress-strain curve shows higher yield strength than the tensile curve.

The OD of the pipe is 24 in (609.6 mm) and the thickness is 0.5 in (12.7 mm), thus $D/t = 48$. The length of the pipe is $6D$. The loading condition is ER-NLF$_0$, i.e., the end cap is not modeled. The single-wave surface undulation ($h_g = 4\%t$, $L_b = 0.5D$, and $\alpha = 90°$) is used in the analyses.

The following four (4) material's models were used in the finite element analyses:

(1) Kinematic: kinematic hardening model in [15] was used for the whole pipe which can simulate the tensile and compressive stress-strain curves in both the longitudinal and circumferential directions simultaneously.

(2) Iso-Com: isotropic hardening model using the compressive SSC of the longitudinal direction was used for the whole pipe.

(3) Iso-Ten: isotropic hardening model using the tensile SSC of the longitudinal direction was used for the whole pipe.

(4) Ten-Com: isotropic hardening model using the tensile SSC of the longitudinal direction was used for the half pipe on the tensile side and isotropic hardening model using the compressive SSC of the longitudinal direction was used the half pipe on the compressive side.

The Kinematic model is expected to produce the actual buckling behavior since it captures the actual anisotropic material properties. The Iso-Ten model is the mostly used models in the existing analyses.

The relationship between the moment and rotation angle simulated using the four models is shown in Figure B - 32 and Figure B - 33 for the non-pressurized ($f_p = 0.0$) and pressurized ($f_p = 0.72$) conditions, respectively. It should be noted that the rotation angle is proportional to the compressive strains. By comparing the results from the Kinematic and the Iso-Ten models, the results confirm that the reduced strain hardening capacity in the hoop direction can decrease the CSC. In another word, the CSC can be over-estimated using the longitudinal tensile SSC.

The results from the Kinematic, Iso-Com, and Ten-Com models are very similar. In all three models, the compressive SSC of the longitudinal direction is actually used for the part of the pipe under compression. The results indicate that the CSC is mainly determined by the compressive SSC of the longitudinal direction. The difference of the tensile SSC between the longitudinal and circumferential directions plays a secondary role. Therefore, the compressive SSC of the longitudinal direction is recommended for the buckling analyses under bending and the isotropic material's models are adequate.

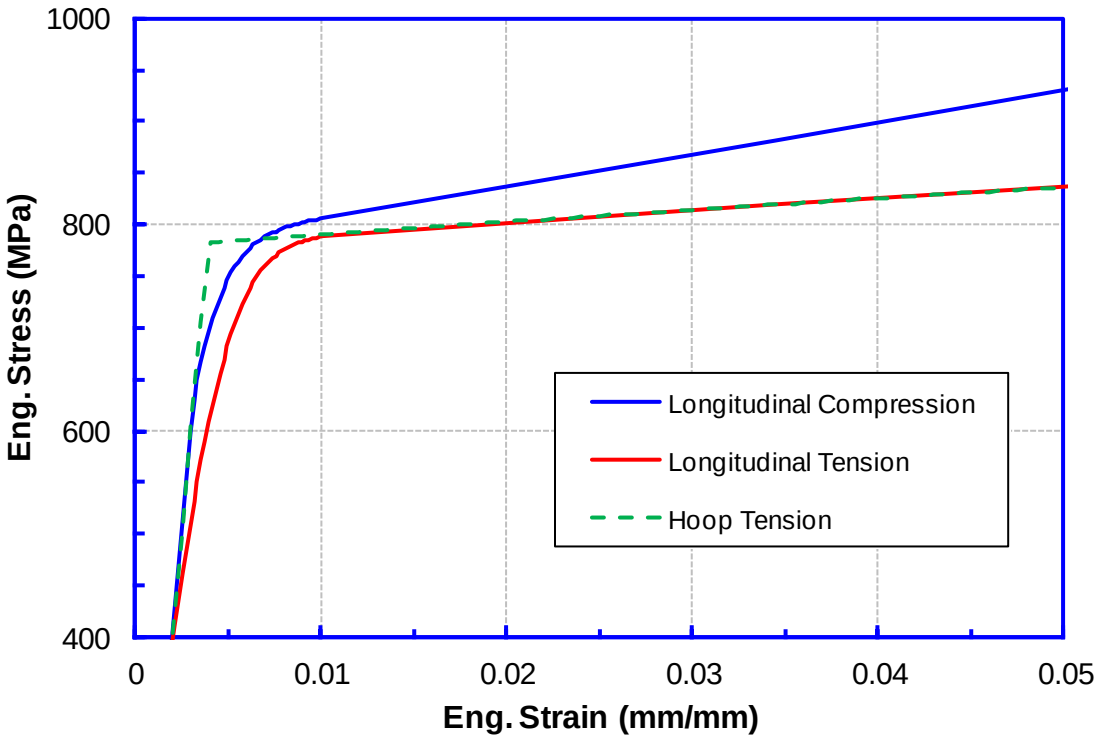

Figure B - 31 Longitudinal and circumferential stress strain curves of a representative X100 linepipe material

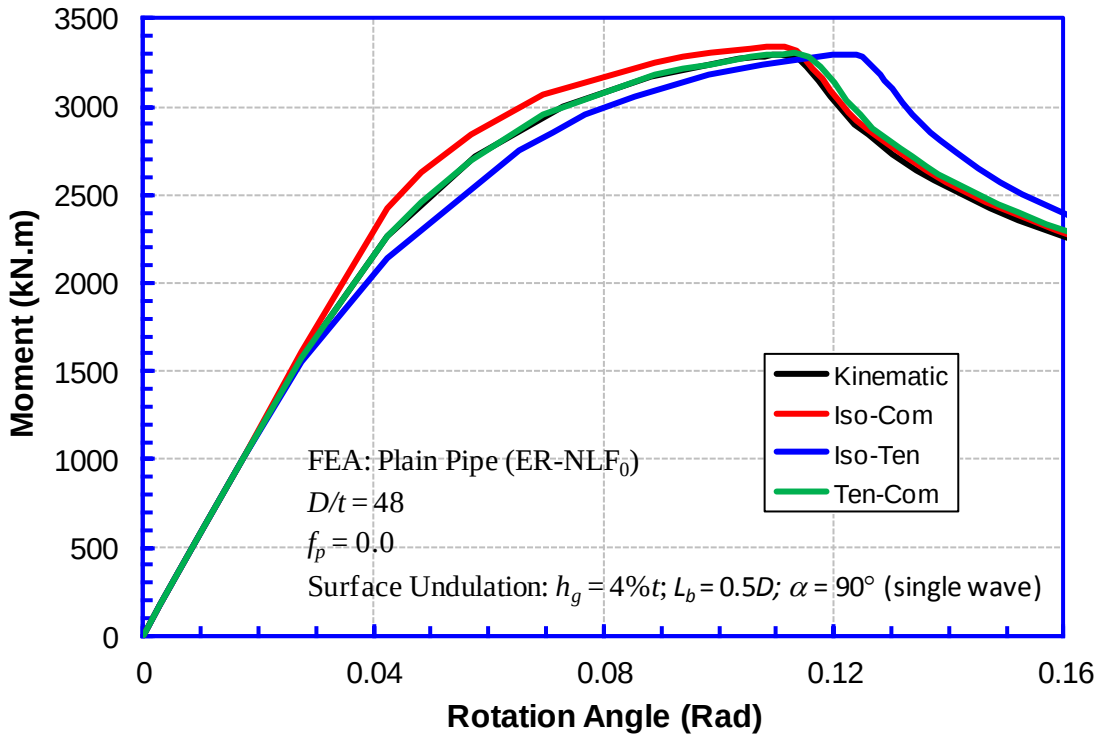

Figure B - 32 Relationship between the simulated moment and rotation angle (f_p = 0.0)

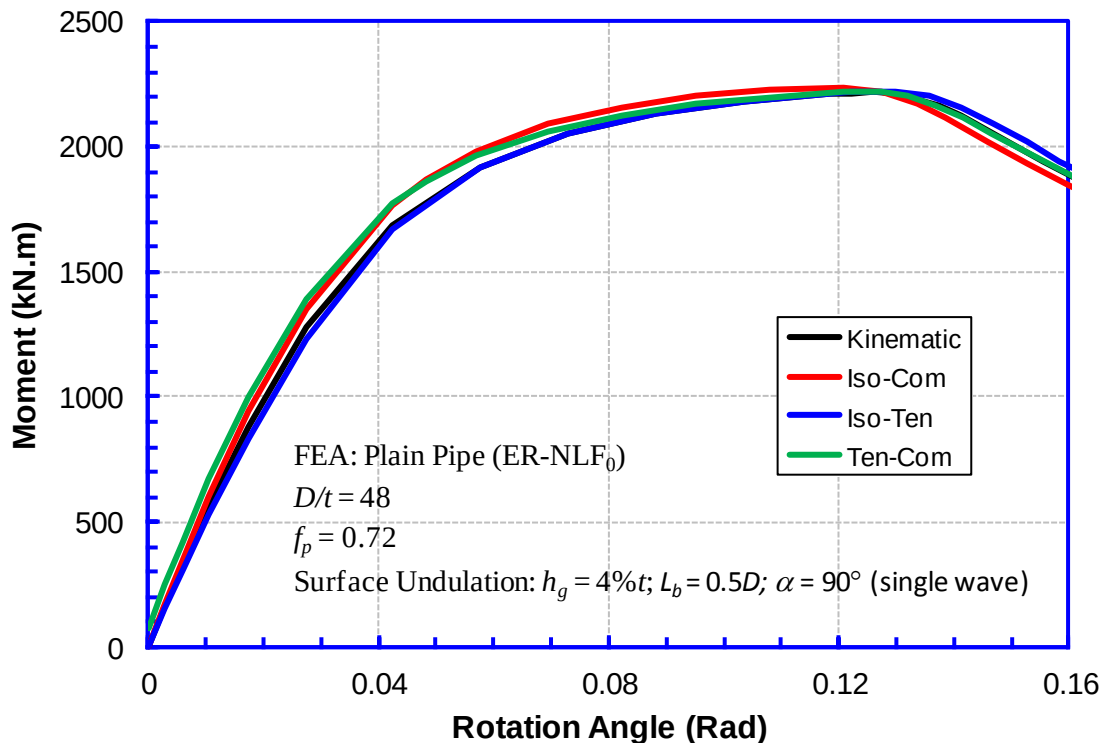

Figure B - 33 Relationship between the simulated moment and rotation angle (f_p = 0.72)

B.8 Girth Welds

B.8.1 Overview of Girth Weld Effect

Wrinkles formed due to compressive buckling are often found near girth welds. The material and geometry discontinuities at the girth welds are believed to be detrimental to the CSC. While the weld strength overmatch and cap overbuild could enhance the CSC.

The studies on the effect of the girth welds on the CSC showed mixed results. In the DNV codes [18], the existence of a girth weld was treated as detrimental. A 40% reduction of the CSC was recommended in the DNV codes for D/t = 50 based on a set of bending tests for 12-in X52 ERW pipes conducted at Univ. of Alberta (UOA) in 1994 [19]. However, the tests on a set of 20-in X56 DSAW pipes of D/t = 60 in the same UOA work [19] didn't show detrimental effects of the girth welds.

The effects of the welding residual stress [20,21] and weld high-low misalignment [20,21,22, 23] on the CSC were studied with finite element simulations. The weld high-low misalignment was identified as the key parameter that can reduce the CSC. Based on FEA, separate equations were developed for pipes with girth welds in the UOA models, where the magnitude of the high-low misalignment was used as an input parameter. However, in most existing CSC calculations related to the girth welds, shell models were used. As a result, the girth weld profile including the high-low misalignment cannot be precisely modeled.

B.8.2 Effect of Weld Profile and Strength Mismatching

The effects of the weld profile, weld/HAZ strength mismatch, and high-low misalignment on the CSC were further investigated with numerical simulations. Three dimension (3D) solid finite

element models were used to precisely simulate the girth weld profile. The representative weld profile is shown in Figure B - 34.

The key geometric characteristics of the girth weld, such as the high-low misalignment, bevel angles, caps, widths, and heat affected zones (HAZ) can be modeled. In addition, the change of the material properties in the girth welds and HAZ can be simulated. In general, the weld metal has higher strength than the pipe material, i.e., weld overmatch. For modern linepipe steels, the strength of the HAZ material is often reduced compared with the pipe material due to the heat generated during welding, often known as HAZ softening.

In the FEA of this section, the pipe's OD is 24 in (609.6 mm) and the thickness is 0.5 in (12.7 mm), thus D/t = 48. The length of the pipe is 6D. The loading condition is ER-NLF$_0$, i.e., the end cap is not modeled. The default parameters of the weld profile is: θ = 6°, w = 0.2 in (5 mm), h = 1/16 in (1.6 mm), H_C = 0.08 in (2 mm), E_C =0.08 in (2 mm), H_R = 0.08 in (2 mm), ω = 30°, and E_R = 0.04 in (1 mm). Except for the weld high-low misalignment, no other geometry imperfections were used.

The pipe's yield strength is 85 ksi and Y/T ratio is 0.87 (the SSC can be found in Section 3.2.4). The SSC of the HAZ materials was created by scaling the SSC of the pipe material. For example, the SSC of a 20% softened HAZ was created by scaling down the SSC of the pipe material by 20%. The weld strength mismatch ratio was defined as the ratio between the weld metal's UTS and the pipe material's UTS. The SSC of the weld metal was created following the procedures in Section A.4.

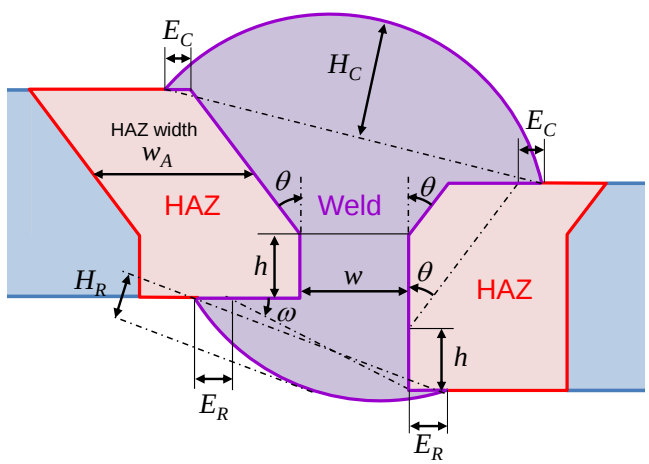

Figure B - 34 Illustration of representative girth weld profile in FE models

Figure B - 35 shows the effect of the HAZ softening and HAZ width on the CSC where the HAZ softening varies from 0% to 20%. The weld strength mismatch ratio is 1.3 (i.e., 30% weld strength overmatching). Two sets of analyses were preformed to study the effect of the internal pressure and weld high-low misalignment (h_m): (1) f_p = 0.72 and h_m = 0.0 in and (2) f_p = 0.0 and h_m = 0.19 in (4.8 mm, 36%t). The combination of f_p and h_m was selected to maximize the difference of the CSC of the two sets of analyses and to produce upper/lower bound CSC. In Figure B - 35, the solid lines with filled symbols show the CSC for a 0.18-in (4.5-mm) wide HAZ. The hollow circles at 10% HAZ softening show the CSC for a 0.31-in (8.0-mm) wide

HAZ. The results show that the CSC is nearly independent of the HAZ softening and width.

Figure B - 36 shows the effect of the weld strength mismatch on the CSC. The HAZ width is 0.18 in (4.5 mm) and the HAZ softening is 10%. The weld strength mismatch ratio varies from 1.0 to 1.3, i.e., even match to 30% overmatch. The CSC is nearly independent of the weld strength mismatch.

Figure B - 37 shows the effect of the size of the girth weld cap on the CSC. The height of the caps on both OD (H_C) and ID (H_R) surfaces is varied from 0 and 0.16 in (0.0 to 4.0 mm). The HAZ width is 0.18 in (4.5 mm) and the HAZ softening is 10%. The weld strength mismatching ratio is 1.3. The CSC decreases with the increase of the cap height for the pressurized conditions but barely varies for the non-pressurized conditions. It should be noted that the difference between the CSC for a 0.08-in and 0.16-in (2.0-mm and 4.0-mm) cap is very small. In practical conditions, a weld cap of 0.08 in (2.0 mm) and above is normal. Therefore, it is reasonable to conclude that the CSC is not sensitive to the cap height for its typical size. For the analyses conducted in the section, the weld cap height was set as 0.08 in (2.0 mm) unless otherwise mentioned.

B.8.3 Weld Residual Stresses

The influence of the weld residual stress on the CSC was studied with FEA. The pipe OD is 12.75 inch (324 mm) and the wall thickness is 1/4 inch (6.35 mm), therefore D/t = 51. The total length of the pipe is 5D. No geometry imperfections or high-low misalignments are modeled. The loading condition is ER-NLF$_p$, i.e., the end cap is modeled. The pipe's yield strength is 69 ksi and Y/T ratio is 0.76 (the SSC can be found in Section 3.2.4). The weld metal has the same SSC with the pipe material (i.e., evenmatch) and no HAZ softening is assumed.

In general, the weld residual stress not only causes local stress concentrations and affects the local material behaviors, but also changes the local geometry. The pipe diameter often shrinks at the girth weld due to the residual stress. The shrinkage can introduce the same type of geometry imperfections as the surface undulation. Under high residual stresses, the CSC can be affected by both the residual stress and the imperfection generated by the residual stress. It is believed that the geometry imperfection generated by the weld residual stress should have similar effect on the CSC with that from the surface undulation. The purpose of this study is to investigate the effect of the stress localization and material behavior change induced by the weld residual stress on the CSC. To avoid the residual stress induced shrinkage, the residual stress in the weld metal is set to be 52 psi (75% of the yield strength). The FEA results show that the shrinkage is very small.

In Figure B - 38, the simulated moment - rotation relationship for the cases with and without residual stresses are compared. The moment and rotation angle are all calculated at the end of the pipe. No pressure was applied (f_p = 0.0). It is seen that the moment - rotation curves of the two cases are almost identical, especially before reaching the maximum moment. Very similar observations are found for the simulations with the internal pressure. The results indicate that the CSC is insensitive to the weld residual stress (i.e., the stress localization and material behavior change caused by the residual stress) in the girth welds. However, the geometry changes caused by the residual stress is expected to have a large effect on the CSC.

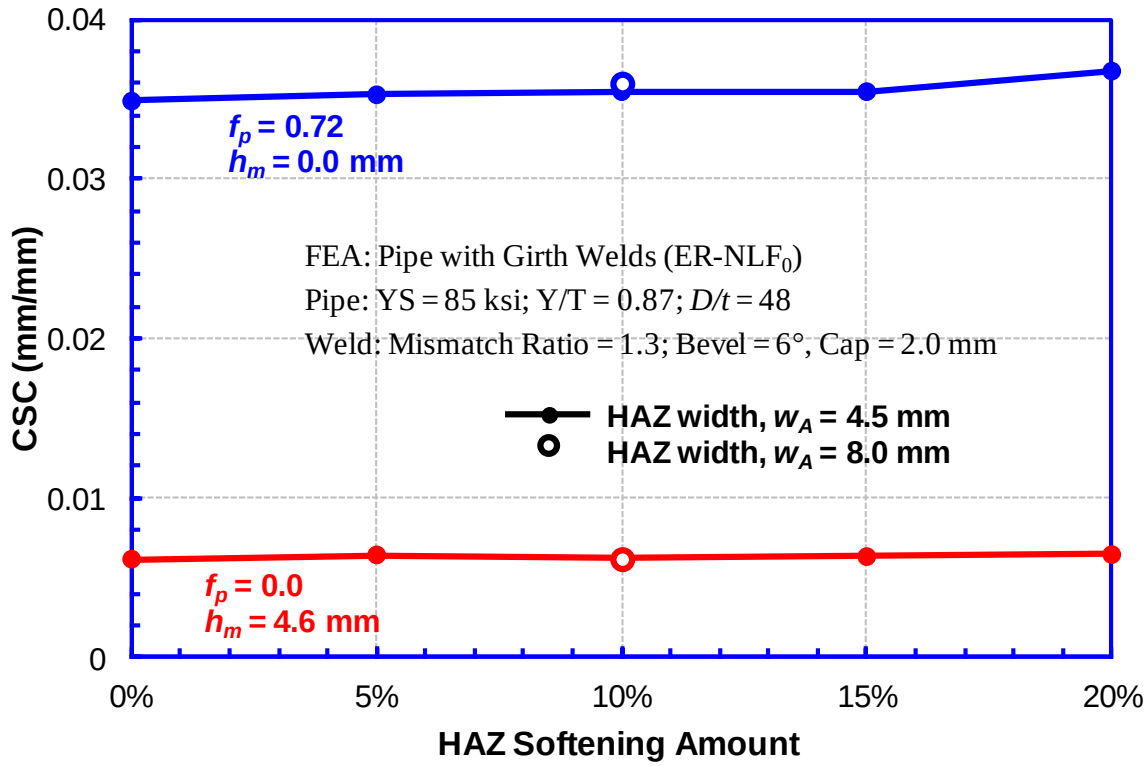

Figure B - 35 Effect of HAZ softening and width on the CSC

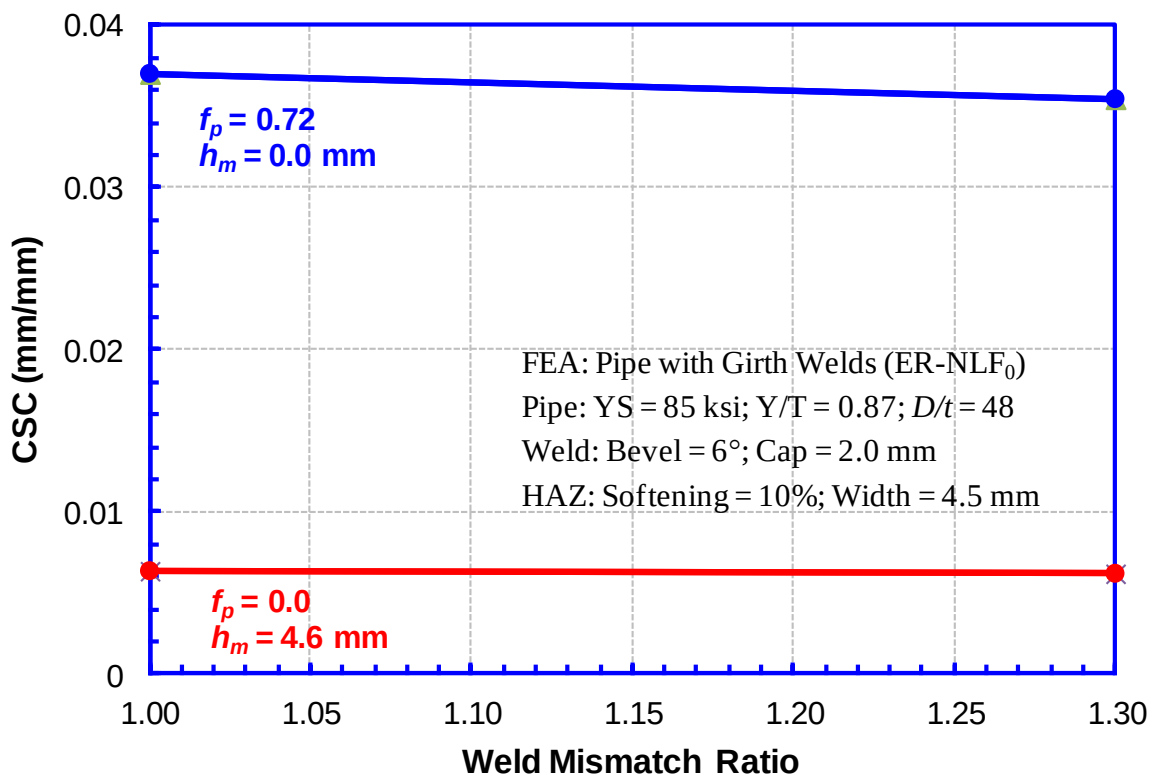

Figure B - 36 Effect of weld strength mismatch ratio (i.e., the ratio between the UTS of weld and pipe) on the CSC

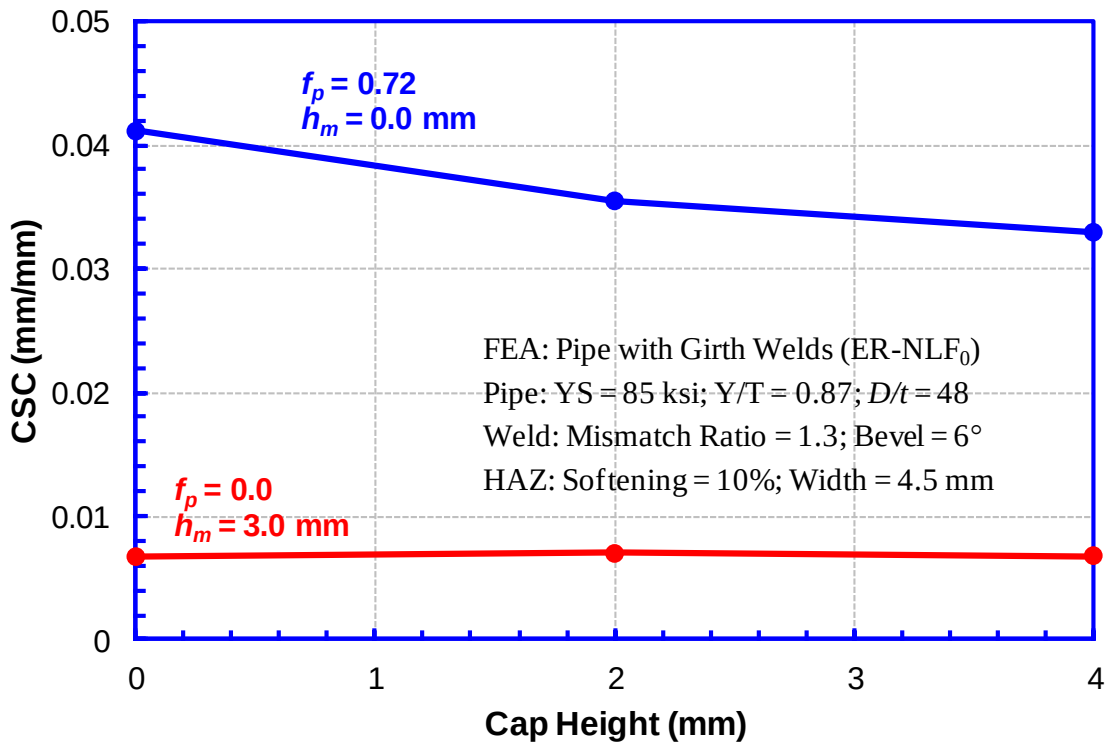

Figure B - 37 Effect of weld cap size on the CSC

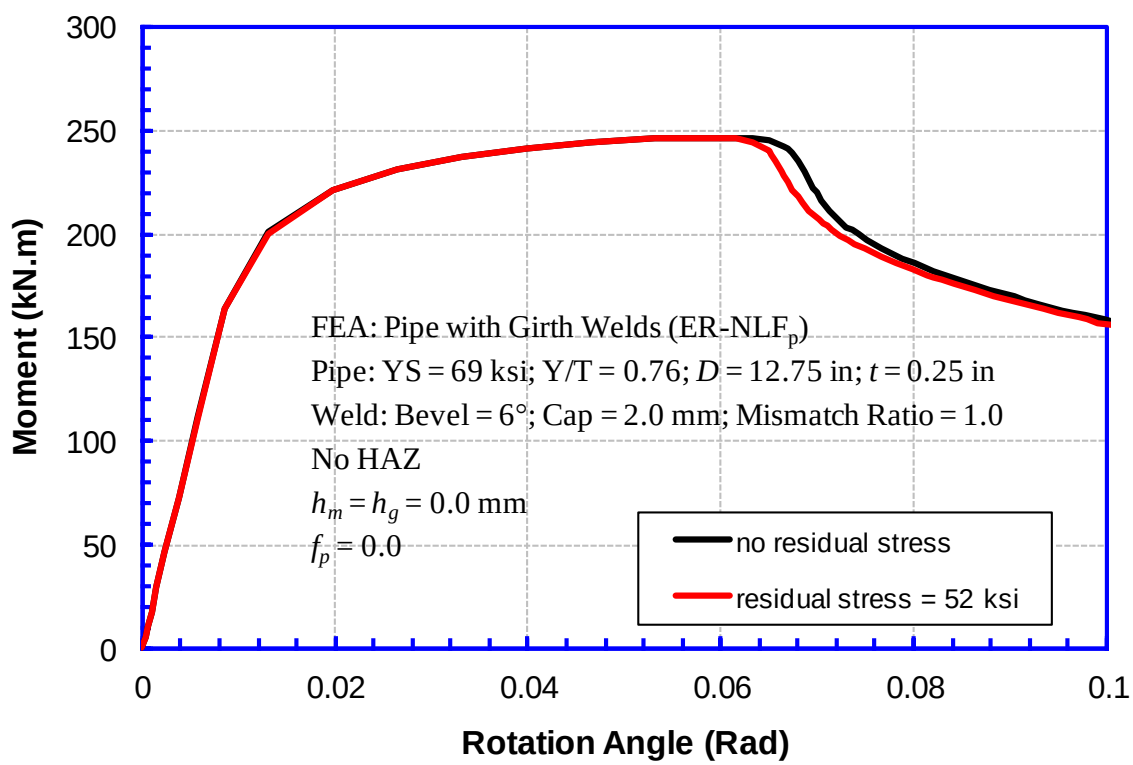

Figure B - 38 Effect of weld residual stress on the CSC

B.8.4 Weld High-Low Misalignment

Finite element analyses (FEA) were conducted to further investigate the effect of the high-low misalignment on the CSC. In the FEA, the pipe OD (D) is 30 inches (762 mm) and the wall thickness (t) is 3/8 inch (9.53 mm). The D/t ratio is 80. The total length of the model is 6D, with a 3D-long pipe joint on each side the girth weld. The weld has a 30° bevel angle and 0.08-in (2-mm) cap. The yield strength of the pipe is 85 ksi and the Y/T ration is 0.87 (see Section 3.2.4 for SSC). The weld strength mismatch ratio is 1.15. No HAZ softening is assumed.

The loading condition is ER-NLF$_0$, i.e., no end caps are modeled. The FEA are conducted for both pressurized (f_p = 0.72) and non pressurized (f_p = 0.0) conditions. The weld high-low misalignment varies from 5% to 50% of the pipe's wall thickness.

In practical conditions, the high-low misalignment is typically localized within a limited area in the circumference direction and doesn't cover the whole circumference. In the FEA, the high-low misalignment covers only the half pipe circumference on the compressive side. Excessive high-low misalignment on the tension side of the pipe can trigger the reduction of the bending moment due to necking (i.e., wall thinning by tension) even before the buckling initiates. The necking induced limit state belongs to the tensile failure and should be captured by the tensile strain models. Therefore, the adopted models (i.e., no high-low misalignment on the tensile side of the pipe) only induce the buckling failure.

In an actual pipe, other than the weld high-low misalignment, the plain pipe also contains the geometry imperfections such as the surface undulations (see Section B.3). Both the pipe surface undulation and the weld high-low misalignment can negatively affect the CSC. To separate the effect of the weld high-low misalignment from the plain pipe geometry imperfections, two sets of FEA were conducted: (1) perfect pipes without geometry imperfections except for the high-low misalignment and (2) pipes with geometry imperfections and weld high-low misalignment.

The geometry imperfection is in the form of the surface undulation with multi waves caused by OD variations. The height of the surface undulation (h_g) is set as 4%t. The wavelength of the surface undulation is 0.2D and 0.3D for non-pressurized and pressurized conditions, respectively.

Figure B - 39 shows the effect of the high-low misalignment on the CSC for pressurized (f_p = 0.72) conditions. The curve shows the CSC of the pipes with the surface undulations (h_g = 4%t) and the hollow symbols show the CSC of the pipes without the surface undulations. For the case with the surface undulation, the CSC is almost independent of the high-low misalignment for $h_m \leq$ 50%t. For the case without any surface undulation, the CSC is not negatively affected by the high-low misalignment of up to 25%t. When the misalignment (h_m) reaches 50%t, the CSC is reduced. However, the reduced CSC is equivalent to the CSC of a plain pipe with a 4%t surface undulation. The 4%t surface undulation is considered to be typical for plain pipes (Section 4.6). The results indicate that under high pressure conditions, the weld high-low misalignment does not show obvious negative effects on the CSC of the pipes with normal size surface undulations.

Figure B - 40 shows the effect of the high-low misalignment on the CSC for non-pressurized pipes. The curve shows the CSC of the pipes with the surface undulations of 4%t. The hollow symbols show the CSC of the pipes without any surface undulations. For both cases, the CSC decreases with the increase of the high-low misalignment. However, the reduction of the CSC

due to the high-low misalignment shows a step change. For example, for relatively small high-low misalignment (i.e., $h_m \leq 10\%t$), the CSC reduction due to the misalignment (h_m) is marginal. Once reaching a critical h_m, the CSC is greatly reduced. But the change of the CSC by further increasing the h_m (i.e., $25\%t \leq h_m \leq 50\%t$) becomes marginal. It should be noted that the CSC at $h_m = 50\%t$ is equivalent to the CSC of a plain pipe with a surface undulation of about 15%*t*.

The step change of the CSC due to the increase of the high-low misalignment may be tied to the change of the wrinkle location as shown in Figure B - 41. The green dashed line highlights the locations of the girth welds. The figure shows that for $h_m \leq 10\%t$, the wrinkle forms near the girth weld but not right at the girth weld. However, for $h_m \geq 25\%t$, the wrinkle forms right at the girth weld. Based on the above observations, the step reduction of the CSC is likely the result of the change of the wrinkle location.

B.8.5 Summary of the Girth Weld Effect on the CSC

When girth welds exist, the CSC of the pipe is affected by both the girth welds and geometry imperfections of the plain pipes. The results given in this section indicate that within reasonable ranges, the weld profile, welding residual stress, and strength mismatch have marginal effects on the CSC, compared with the plain pipes with reasonable geometry imperfections, e.g., a surface undulation of 4%*t*.

The high-low misalignment also shows relatively limited effect on the CSC especially under pressurized conditions. For the weld high-low misalignment (h_m) up to 50%*t*, the effect of the misalignment on the CSC is equivalent to a 4%*t* and 15%*t* surface undulation in a plain pipe under high and no pressure conditions, respectively. As shown in Section 4.6, the 15% surface undulation may fall well within the surface undulations found in plain pipes.

In the simulations, similar to what is observed in the field conditions, the wrinkles typically form near the girth weld but not right at the girth welds. When the wrinkles are not right at the girth weld, the effect of the girth weld on the CSC is marginal. However, with excessive high-low misalignment (together with low pressure), the wrinkle may form right at the girth weld and the reduction to the CSC can be equivalent to a 15%*t* surface undulation.

The shrinkage of the girth weld tends to create a surface undulation near the girth weld and reduce the CSC. The surface undulation induced by the girth weld shrinkage can be treated in the same way as those in plain pipes.

B.9 Net-Section Longitudinal Force

The net-section longitudinal force is known to affect the pipe's CSC under bending, e.g., the net-section tensile force in the longitudinal direction can increase the CSC, while the net-section compressive force can reduce the CSC. As discussed in Section 2.3.5, the JFE equations [24] indicate that the pipe's CSC under pure longitudinal compressive force is half of that under pure bending.

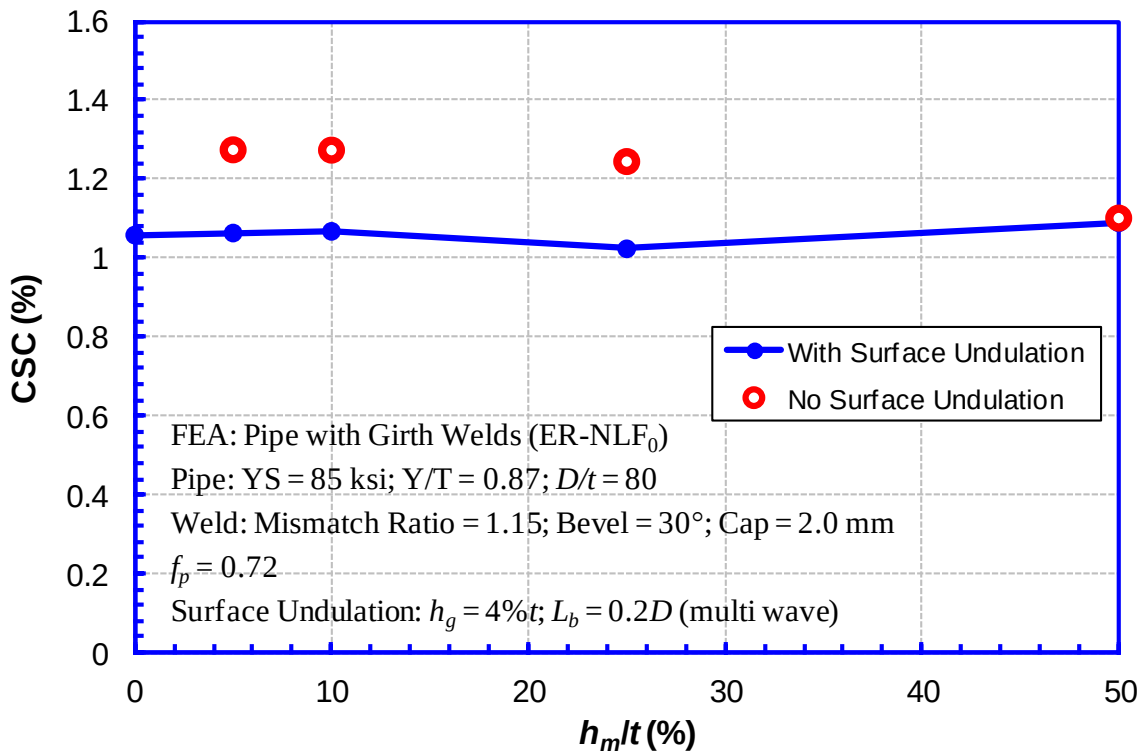

Figure B - 39 Effect of high-low misalignment on the CSC (f_p = 0.72)

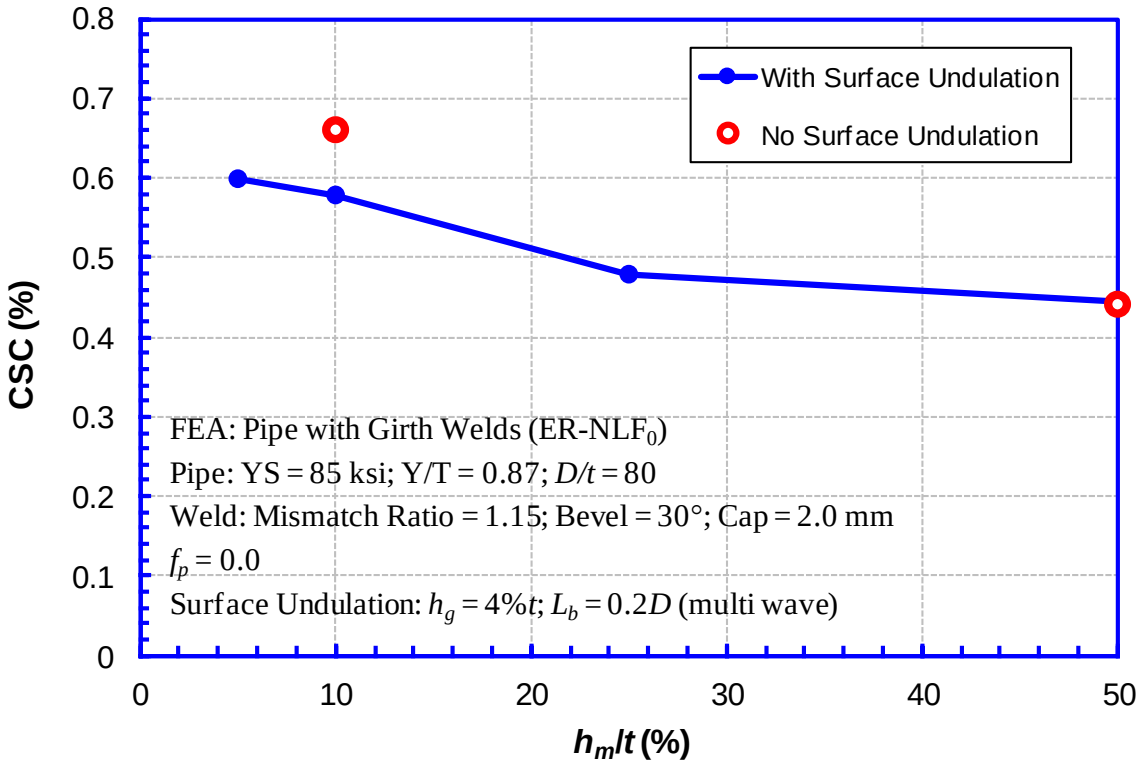

Figure B - 40 Effect of high-low misalignment on the CSC (f_p = 0.0)

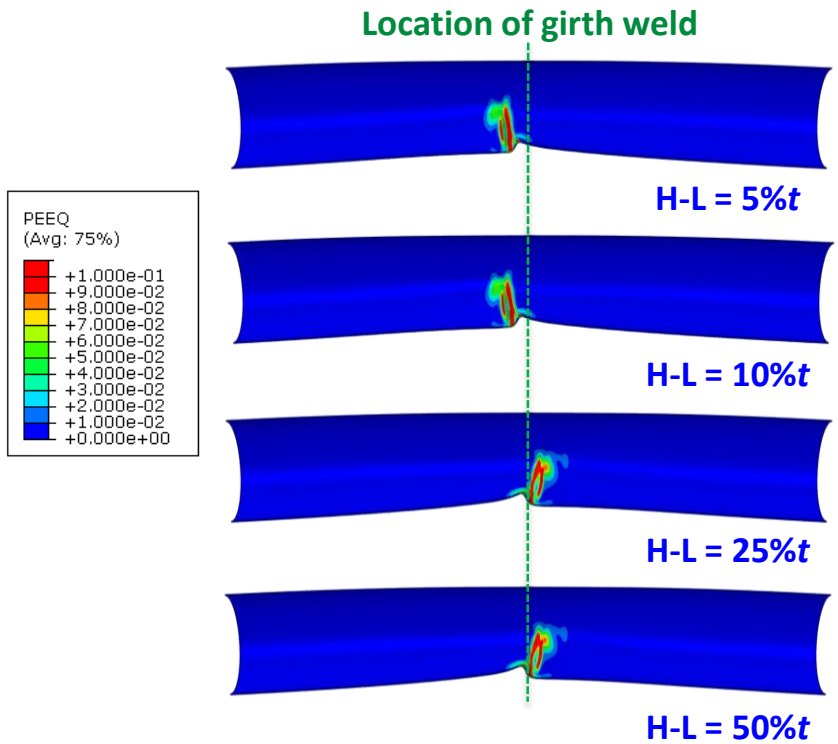

Figure B - 41 Buckling pattern of non-pressurized pipes with geometry imperfections for various high-low misalignments: the dashed line indicates the location of girth welds. The contour shows the equivalent plastic strain. (H-L means h_m)

Most existing models were developed under bending dominant conditions. Although the net-section force in the longitudinal direction is often secondary compared with the bending moment, there do exist differences on the handling of the net-section forces. For example, the DNV and UOA models were developed under the condition that the internal pressure applied to the end plates (or end caps) induces a net-section tensile force (i.e., the end cap effect). The JFE model was developed with zero net-section forces. Compressive net-section forces were not considered in the existing models.

Similarly, the net-section longitudinal forces used in different experimental tests are also different. For example, in some tests, the net-section longitudinal force generated by the internal pressure on the end cap is compensated by an externally applied longitudinal compressive force. Therefore, the tests are done with zero net-section force. In some tests, the net-section force due to the internal pressure is not or is only partially compensated. As a result, the tests are done with varying levels of net-section tensile forces in the longitudinal direction. In some tests, the tests are done with an intentionally applied net-section compressive force.

However, due to the scatters of the CSC reported in bending tests, the change of the CSC due to the net-section force is often buried within the testing scatters. As a result, the existing models are often recommended for combined bending and longitudinal forces.

There have been some studies on the effect of the net-section force on the CSC. However, no reliable correlations between the net-section force and the CSC have been established. The

effect of the net-section tensile force induced by the internal pressure (i.e., the end cap effect) on the CSC is further analyzed in this section with FEA. The objectives of the analyses are to: (1) understand the potential difference on the CSC produced by the different models due to the assumptions on the net-section forces and (2) understand and correlate the experimentally reported CSC obtained under different testing conditions (e.g., with or without the compensation of the net-section force induced by the end cap effect).

The FEA were conducted with two loading conditions, i.e., ER-NLF$_p$ and ER-NLF$_0$. In ER-NLF$_p$, the net-section tensile force resulted from the internal pressure is applied and in ER-NLF$_0$, no net-section force exists. The CSC from those two conditions at various internal pressure levels is shown in Figure B - 42. The pipe geometry and properties used in the FEA can be found in the figure. Figure B - 42 shows that the net-section tensile force increases the CSC. The higher the internal pressure, the higher the increase of the CSC.

Figure B - 43 shows the ratio between the CSC under ER-NLF$_p$ and ER-NLF$_0$ for different net-section longitudinal stress factors (f_n). The f_n is the ratio between the net-section longitudinal stress and the pipe's yield strength. Since under ER-NLF$_p$, the net-section longitudinal stress is generated by the internal pressure only, the net-section longitudinal stress is half of the hoop stress and therefore, $f_n = 1/2\ f_p$. It is seen that the increase of the CSC increases with the increase of f_n. For f_n of 0.4 (i.e., f_p of 0.8), the increase of the CSC can be 20%.

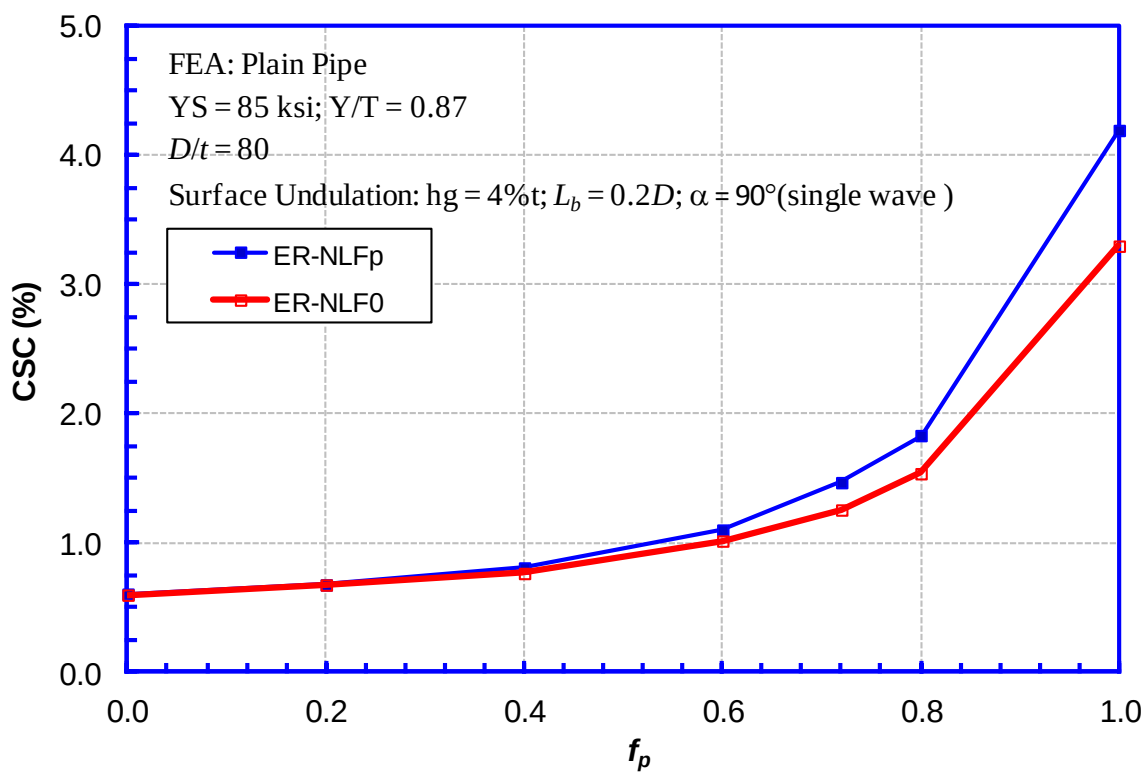

Figure B - 42 CSC of pipes with and without net-section tension

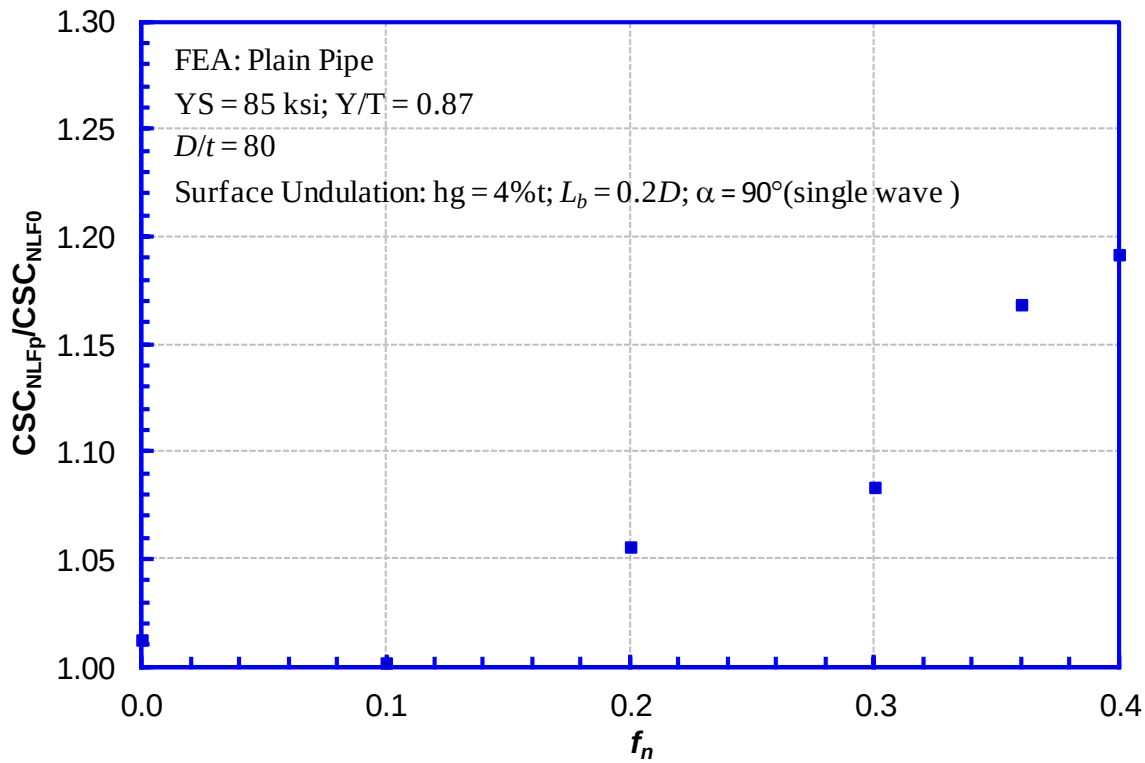

Figure B - 43 Increase of the CSC vs. net-section stress factor

B.10 Summary of Sensitivity Studies

Systematic sensitivity studies were carried out on the influencing parameters for the CSC via FEA. The key findings are summarized in the following:

B.10.1 Pipe D/t Ratio and Internal Pressure

The pipe *D*/*t* ratio and internal pressure are the two most recognized influencing parameters to the CSC in the existing CSC models. Sensitivity studies in this project demonstrate a coupled effect between the *D*/*t* ratio and internal pressure, i.e., the increase of the CSC due to increasing pressure is more significant for small *D*/*t* pipes than large *D*/*t* pipes. However, most models do not recognize the coupling between the two parameters and also overestimate the increase of the CSC due to the internal pressure. The CSA models, although recognize the coupling between the internal pressure and pipe *D*/*t* ratio, produce an opposite trend to what is observed in the sensitivity studies. Additional details on this issue can be found in Sections 3.6.1, 4.4.1, 4.4.2, and B.2.

B.10.2 Pipe Properties: Strength, Strain Hardening, Lüder's and Uniform Strains

The pipe yield strength is used to evaluate the pressure effect on the CSC in most existing models, i.e., to calculate the pressure factor - the ratio between the pressure induced hoop stress and yield (or flow) strength. It should be noted that the yield strength for calculating the pressure factor is the hoop property and could be different from the longitudinal strength due to material anisotropy.

In addition to being used for calculating the pressure factor, the yield strength is used in some models to show the dependence of the CSC on pipe properties. In some other models, the strain hardening capacity, such as the pipe Y/T ratio and strain hardening exponent (*n*), is used instead of the yield strength. It should be noted that the pipe yield strength and strain hardening capacity are often related. In general, the pipe with lower yield strength often has higher strain hardening capacity. The sensitivity studies through FEA in the project showed that without the variation of the strain hardening capacity, the change of the yield strength alone has secondary effect on the CSC. On the other hand, the increase of the Y/T ratio can decrease the CSC greatly. The details on the effects of the yield strength and strain hardening capacity on the CSC can be found in Sections 3.6.3 and B.4.

The CSC can be affected by the shape of the linepipe's stress-strain curves. The pipes with discontinuous stress-strain curves containing Lüder's strains (or Lüder's extension) are often believed to have less CSC than the pipes with round and smooth stress-strain curves (assuming other conditions are the same). The sensitivity studies showed that if the CSC of the pipe with the Lüder's strain is higher than the Lüder's strain, the CSC of the pipe with the Lüder's strain is usually higher than the CSC of the pipe with round and smooth stress-strain curves (assuming same yield strength and Y/T ratio) and vise versa. The details on the effect of the Lüder's strain on the CSC can be found in Sections 3.6.5 and B.6.

The pipe uniform strain is not used by the existing CSC models. Small uniform strains are observed in the stress-strain curves of some pipes (especially modern linepipe materials). Similar to the yield strength, the uniform strain and the strain hardening capacity are also often correlated, i.e., the pipes with higher uniform strain often have higher strain hardening capacity. The sensitivity studies in this project showed that the change of the pipe uniform strain alone (i.e., the pipe yield strength and Y/T ratio are kept unchanged) has a secondary effect on the CSC unless the uniform strain becomes extremely low. Methods to taking account of the uniform strain are established and the details can be found in Sections 3.6.4 and B.5.

B.10.3 Pipe Geometry Imperfection

The pipe geometry imperfections can greatly affect the CSC. The imperfections studied in this project are those generated during pipe manufacturing which are typically in the form of an ovality (i.e., out-of-roundness of cross section), eccentricity, and non-uniform diameter or wall thickness. Mechanical damages and corrosion defects are not considered. The outside surface of the pipe is not perfectly round and smooth due to the combination of the imperfections. The variation of the outside surface from the perfect shape can be found in both pipe circumferential and longitudinal directions. The variation in the pipe circumference alone, such as the ovality uniform along the length of the pipe is found to have a limited effect on the CSC. A wave-like surface variation along the length of the pipe (referred to as surface undulation) has been found in UOE pipes and can greatly reduce the pipe CSC. Both the height and the wavelength of the surface undulations are found critical to the CSC. Only the surface undulations with critical wavelengths are found to reduce the CSC greatly and the critical wavelength is the wavelength of the wrinkles formed at the maximum moment.

However, there is very limited data on measured surface undulations. The lack of the data on the surface undulations makes the application of some CSC models which require the geometry imperfection as input difficult. In this project, recommended median, upper, and lower bound surface undulations were developed for the application of those CSC models. It is believed that the surface undulations can be used as the generic representation of the geometry imperfections in different types of pipes due to their large detrimental effect on the CSC compared with other types of geometry imperfections. However, it should be noted that the recommendations are based on limited experimental data for UOE pipes. It is not clear if the other types of pipes, e.g., ERW, spiral, etc., have similar types of surface undulations. Additional details on the pipe geometry imperfections can be found in Sections 3.6.2, 4.4.4, and B.3.

B.10.4 Net-Section Force

Most existing CSC models are targeted for bending-dominant loading conditions and claim to be applicable to combined bending and longitudinal force. Although the longitudinal net-section force is found to affect the CSC, most existing CSC models do not adopt it as an input parameter. In addition, the existing CSC models adopted different loading conditions in their development processes. For example, some models used pure bending without net-section force. Some models allowed the net-section force generated by the pressure on the end plates (i.e., the longitudinal stress is in tension and is half of the hoop stress). Some models used data generated from mixed loading conditions. As a result, the difference in the applied net-section force in the models is partially responsible for the large difference in their computed CSC.

An assessment method for treating the net-section tensile force was developed in this project. Future work is still needed to properly consider the effect of the net-section compressive force on the CSC. Details on the net-section force effects can be found in Sections 3.6.7 and B.9.

B.10.5 Girth Weld

For pipes with girth welds, the CSC can be affected by both the girth welds and the geometry imperfections of the plain pipes. Mixed results have been reported in the published experimental data on the effects of girth welds on CSC. Some test data showed that the girth welds, especially those with high-low misalignment can greatly reduce the CSC. The other tests however, showed that girth welds with or without misalignment do not reduce the CSC.

The work in this project found that within reasonable ranges, the weld profile (e.g., cap size etc), welding residual stress, and strength mismatch have marginal effects on the CSC, compared with the plain pipes with reasonable geometry imperfections, e.g., a surface undulation of 4%t (t is wall thickness).

The high-low misalignment also shows relatively limited effect on the CSC especially under pressurized conditions. For the weld high-low misalignment (h_m) up to 50%t, the effect of the misalignment on the CSC is equivalent to a 4%t and 15%t geometry imperfection in a plain pipe under high and zero pressure conditions, respectively. The 4%t ~ 15%t geometry imperfection is within the range of reasonable geometry imperfections found in plain pipes. The mixed testing results on the effect of the girth welds on the CSC could be explained by the different geometry imperfections in the tested pipes.

It should be noted that excessive high-low misalignment could induce significant stress/strain concentration on the tensile side of the pipe under bending. The maximum bending moment can be reached due to necking on the tensile side. The event corresponds to the tensile limit state and the tensile strain models should be able to capture this limit state. As a result, the compressive strain at the maximum moment should not be used as the critical strain for buckling failure.

On the other hand, the radial shrinkage due to the welding of the girth welds tends to create a geometry imperfection in the form of the surface undulation near the girth weld and reduce the CSC. The geometry imperfection induced by the girth weld shrinkage can be assessed with the surface undulations of plain pipes.

Based on the above observations, the CSC of pipes with girth welds can be assessed with the CSC models for plain pipes using equivalent geometry imperfections. Details on the girth weld studies can be found in Sections 3.6.6 and B.8.

B.11 References of Appendix B

1 Suzuki, N., Kondo, J., Endo, S., Ishikawa, N., Okatsu, M., and Shimamura, J., 2006, "Effects of geometry imperfection on bending capacity of X80 linepipe," *Proceedings of the 6th International Pipeline Conference*, September 25-29, Calgary, Alberta, Canada.

2 Suzuki, N., Kondo, J., Ishikawa, N, Okastu, M., and Shimamura, J., 2007, "Strain capacity of X80 high strain line pipes," *Proceedings of the 26th International Conference on Offshore Mechanics and Arctic Engineering*, San Diego, California, June 10 - 15

3 Suzuki, N. and Igi, S., 2007, "Compressive strain limits of X80 high-strain line pipes", *Proceedings of 17th International Offshore and Polar Engineering Conference*, p3246, Lisbon, Portugal, July 1 - 6

4 Sato T., Mikami, Y., Mochizuki, M., Suzuki, N., and Toyota, M., 2008, "Parametric study on the effect of geometric imperfections on the bending capacity of high strength linepipes", *Proceedings of the 7th International Pipeline Conference*, September 29 - October 3, Calgary, Alberta, Canada.

5 Tsuru, E., Shinohara, Y., and Asahi, H., 2007, "Evaluation of precept of strain capacity of high strength UOE line pipes used in strain-based design applications," *Proceedings of the 17th International Offshore and Polar Engineering Conference*, Lisbon, Portugal, July 1-6

6 Shitamoto, H., 2013, "Welded steel pipe fabrication method and welded steel pipe," World Intellectual Property Organization, Pub. No. WO/2013/031879.

7 Dorey, A.B, Murray, D.W., and Cheng, J.J.R., 2006, "Initial imperfection models for segments of line pipe," *Transactions of the ASME*, v128, p322 -329.

8 Chen, H., Ji, L., Wang, H., Qu, D., Gong, S., Li, H., Huang, C., and Xie, W., 2011, "Test evaluation of high strain line pipe material," *Proceedings of the Twenty-first (2011) International Offshore and Polar Engineering Conference*, Maui, Hawaii, USA, June 19-24.

9 DeGeer, D., Timms, C., Wolodko, J., Yarmuch, M., Preston, R., and MacKinnon, D., 2007, "Local buckling assessments for the Medgaz pipeline", *Proceedings of the 26th International*

Conference on Offshore Mechanics and Arctic Engineering, San Diego, California, June 10 - 15.

10 Timms, C.M.J., DeGeer, D., Chebaro, M.R., and Tsuru, E., 2009, "Compressive strain limits of large diameter X80 UOE linepipe", *Proceedings of the 19th International Offshore and Polar Engineering Conference*, p181, Osaka, Japan, June 21 - 26

11 Carr, M., MacRae, I., and Bruton, D., 2009, "Local buckling of pressurized seamless linepipe: results of the SAFEBUCK JIP", *Proceedings of the Pipeline Technology Conference*, Ostend, Belgium, October 12 - 14

12 Tsuru, E., Shinohara, Y., Asahi, H., and Terada, Y., 2005, "Strain capacity of line pipe with yield point elongation," *Proceedings of the 2005 15th International Offshore and Polar Engineering Conference*, Seoul, Korea, June 19-24.

13 Liu, M., and Wang, Y.Y., 2006, "Modeling of Anisotropy of TMCP and UOE Linepipes," *Proceedings of the 16th (2006) International Offshore and Polar Engineering Conference* San Francisco, California, USA, May 28-June 2.

14 Adeeb, S., Zhou, J., and Horsley, D., 2006, "Investigating the effect of UOE forming process on the buckling of line pipes using finite element modeling," *Proceedings of the 6th International Pipeline Conference*, Calgary, Alberta, Canada, September 25-29.

15 Fathi, A., Cheng, J.J.R., Adeeb, S., and Zhou, J., 2010, "Critical buckling strain in high strength steel pipes using isotropic-kinematic hardening," *Proceedings of the 8th International Pipeline Conference*, Calgary, Alberta, Canada, September 27 - October 1.

16 Hilgert, O., Zimmermann, S., and Kalwa, C., 2012, "Anisotropy - benefits for UOE line pipe," *Proceedings of the 9th International Pipeline Conference*, Calgary, Alberta, Canada, September 24 - 28.

17 Tsuru, E., Agata, J., and Nagata, Y., 2010, "Analytical approach for bucking resistance of UOE linepipe with orthogonal anisotropy under combined loading," *Proceedings of the 8th International Pipeline Conference*, Calgary, Alberta, Canada, September 27 – October 1.

18 Det Norske Veritas, 2010, "Submarine pipeline systems", DNV-OS-F101

19 Yoosef-Ghodsi, N., Kulak, G.L., and Murray, D.W., 1994, "Behavior of girth-welded line pipe", *Structural Engineering Report No. 203*, Department of Civil Engineering, University of Alberta

20 Souza, L.T., and Murray, D.W., 1999, "Analysis for wrinkling behavior of girth-welded line pipe," *Journal of Offshore Mechanics and Arctic Engineering*, v121, p53-61.

21 Souza, L.T. and Murray, D.W., 1994, "Prediction of wrinkle behavior of girth-welded line pipe," *Structural Engineering Report No. 197*, University of Alberta, Department of Civil and Environmental Engineering.

22 Al-Showaiter, A., Taheri, F., and Kenny, S., 2008, "Influencing of pipeline misalignment on the local buckling response," *Proceedings of the 7th International Pipeline Conference*, September 29 – October 3, Calgary, Alberta, Canada.

23 Fatemi, A., Kenny, S., Sen, M., Zhou, J., Taheri, F., and Paulin, M., 2009, "Parameters affecting the buckling and post-buckling behavior of high strength pipelines," *Proceedings of the 28th International Conference on Ocean, Offshore and Arctic Engineering*, Honolulu, Hawaii, USA, May 31 - June 5.

24 Suzuki, N., Zhou, J., and Toyoda, M., 2008, "Compressive strain limits of high-strength linepipes", *Proceedings of 7th International Pipeline Conference*, Calgary, Alberta, Canada, Sep. 29 - Oct. 3.

Appendix C **Experimental Database**

C.1 Experimental Data

An experimental database is compiled using testing data published in public domain and used to evaluate the refined compressive strain models. The database consists of 48 full-scale bending tests and the experimentally measured CSC is provided for 40 out of the 48 tests. The database covers the following range,

- OD (D): 6.6 - 48 (inch)
- WT (t): 0.13 - 0.93 (inch)
- D/t: 22 - 104
- Grade: X52 - X100
- YS (σ_y): 55 - 98 (ksi)
- Y/T: 0.77 - 0.91
- Lüder's strain (ε_e): < 1.6%
- Pressure factor (f_p): 0 - 0.82
- Net-section stress factor (f_n): -0.42 - 0.62
- CSC: 0.23 - 6.2 (%)

The pipe grades covered in the database range from X52 to X100 (as shown in Figure C - 1). The details of the distribution of the testing database are given in Section 4.5.1. The details of each individual test in the database are given in Table C - 1.

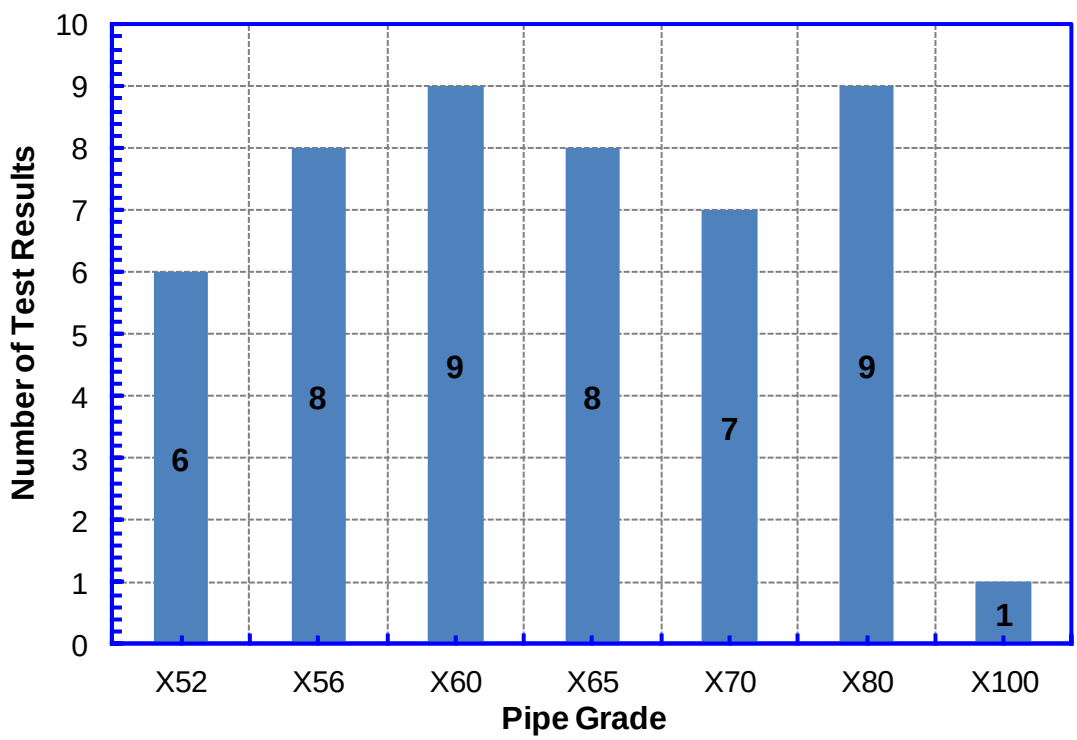

Figure C - 1 Distribution of testing data against pipe grades

Table C - 1 Experimental data

No.	Ref. #	Grade	With girth weld or not	OD (D)	WT (t)	D/t	YS (Y)	UTS (T)	Y/T	Lüder's Strain (ε_e)	p_i	f_p	Net Section Force	f_n	h_g	L_b	h_m	Exp. CSC
				(inch)	(inch)		(ksi)	(ksi)		(%)	(ksi)		(kip)		(mm)	(mm)	(mm)	(%)
1	1	X60	N/A	6.625	0.125	53.0	66	82	0.81	No	1.63	0.65	61	0.35	N/A	N/A	N/A	1.59
2		X60	N/A	6.625	0.125	53.0	64	80	0.80	No	0.00	0.00	0	0.00	N/A	N/A	N/A	0.79
3	2	X60	Yes	48	0.462	103.9	64	82	0.78	No	0.94	0.77	-892	-0.20	N/A	N/A	N/A	0.57
4		X60	Yes	48	0.462	103.9	64	82	0.78	No	0.92	0.75	-937	-0.21	N/A	N/A	N/A	0.47
5		X60	Yes	48	0.462	103.9	64	82	0.78	No	0.03	0.02	-1875	-0.42	N/A	N/A	N/A	0.27
6		X60	Yes	48	0.462	103.9	64	82	0.78	No	0.95	0.78	-217	-0.05	N/A	N/A	N/A	0.82
7		X60	Yes	48	0.462	103.9	64	82	0.78	No	0.15	0.12	-1104	-0.25	N/A	N/A	3.17	0.26
8		X60	Yes	48	0.462	103.9	64	82	0.78	No	0.95	0.78	-217	-0.05	N/A	N/A	3.17	0.41
9		X65	No	48	0.562	85.4	73	87	0.83	No	0.15	0.09	-1362	-0.22	N/A	N/A	No	0.57
10		X60	Yes	48	0.462	103.9	69	82	0.84	1.56	0.15	0.11	-1053	-0.22	N/A	N/A	N/A	0.23
11	3	X70	No	30	0.327	91.7	73	86	0.84	No	0.00	0.00	-465	-0.21	N/A	N/A	No	0.52
12		X70	No	30	0.327	91.7	73	86	0.84	No	0.31	0.20	-330	-0.15	N/A	N/A	No	0.51
13		X70	No	30	0.327	91.7	73	86	0.84	No	0.62	0.39	-195	-0.09	N/A	N/A	No	0.71
14		X70	No	30	0.327	91.7	73	86	0.84	No	1.25	0.78	74	0.03	N/A	N/A	No	1.31
15	4	X70	No	24	0.500	48.0	79	87	0.90	No	2.43	0.74	1854	0.62	N/A	N/A	No	2.80
16		X70	No	24	0.346	69.4	79	90	0.88	N/A	0.83	0.37	371	0.18	N/A	N/A	No	0.70
17		X70	No	24	0.252	95.2	73	82	0.90	N/A	0.00	0.00	-272	-0.19	N/A	N/A	No	0.40
18	5	X65	No	20	0.453	44.2	70	82	0.84	N/A	0.00	0.00	0	0.00	N/A	N/A	No	1.36
19		X65	N/A	20	0.709	28.2	67	77	0.86	N/A	0.00	0.00	0	0.00	N/A	N/A	N/A	1.35
20		X65	No	20	0.748	26.7	69	76	0.90	N/A	0.00	0.00	0	0.00	N/A	N/A	No	1.64
21		X65	No	20	0.929	21.5	65	78	0.84	N/A	0.00	0.00	0	0.00	N/A	N/A	No	2.32
22	6	X80	No	48	0.902	53.2	86	95	0.91	No	0.00	0.00	N/A	0.00	N/A	N/A	No	N/A
23		X80	No	48	0.902	53.2	88	101	0.88	No	1.50	0.45	N/A	0.23	N/A	N/A	No	N/A
24		X80	No	48	0.744	64.5	95	105	0.90	No	1.79	0.61	N/A	0.30	N/A	N/A	No	N/A
25	7	X80	No	30	0.614	48.8	78	101	0.77	N/A	1.81	0.57	1811	0.40	1.00	740	No	2.40
26	8	X80	No	48	0.866	55.4	85	102	0.83	No	1.74	0.57	2459	0.22	0.80	600	No	1.70
27		X80	No	48	0.866	55.4	87	105	0.83	No	1.74	0.55	2416	0.21	0.80	600	No	1.50
28		X80	No	48	0.866	55.4	86	95	0.91	No	1.74	0.56	2479	0.22	1.60	600	No	N/A
29		X80	Yes	48	0.866	55.4	82	103	0.80	No	1.74	0.59	2432	0.23	N/A	N/A	N/A	1.20
30	9	X56	No	20	0.311	64.3	57	63	0.90	No	0.00	0.00	-295	-0.27	N/A	N/A	No	N/A
31		X56	No	20	0.311	64.3	57	63	0.90	No	0.00	0.00	N/A	0.00	N/A	N/A	No	N/A
32		X56	No	20	0.311	64.3	57	63	0.90	No	1.44	0.82	-15	-0.01	N/A	N/A	No	N/A
33		X56	No	20	0.311	64.3	57	63	0.90	No	1.44	0.82	N/A	0.41	N/A	N/A	No	N/A
34		X52	No	12.75	0.250	51.0	55	66	0.83	No	0.00	0.00	-145	-0.26	N/A	N/A	No	1.10
35		X52	No	12.75	0.250	51.0	55	66	0.83	No	0.76	0.36	-84	-0.15	N/A	N/A	No	1.62
36		X52	No	12.75	0.250	51.0	55	66	0.83	No	1.53	0.71	-24	-0.04	N/A	N/A	No	3.29
37	10	X56	Yes	20	0.311	64.3	57	63	0.90	No	0.00	0.00	-295	-0.27	N/A	N/A	N/A	N/A
38		X56	Yes	20	0.311	64.3	57	63	0.90	No	0.00	0.00	-295	-0.27	N/A	N/A	N/A	0.92
39		X56	Yes	20	0.311	64.3	57	63	0.90	No	0.72	0.41	-160	-0.14	N/A	N/A	N/A	1.16
40		X56	Yes	20	0.311	64.3	57	63	0.90	No	1.44	0.82	-25	-0.02	N/A	N/A	N/A	2.13
41		X52	Yes	12.75	0.250	51.0	55	66	0.83	No	0.00	0.00	-145	-0.26	N/A	N/A	N/A	0.68
42		X52	Yes	12.75	0.250	51.0	55	66	0.83	No	0.76	0.36	-84	-0.15	N/A	N/A	N/A	1.26
43		X52	Yes	12.75	0.250	51.0	55	66	0.83	No	1.53	0.71	-28	-0.05	N/A	N/A	N/A	1.93
44	11	X100	N/A	36	0.563	63.9	97	121	0.80	N/A	2.25	0.74	2252	0.37	N/A	N/A	N/A	1.50
45	12	X65	No	20	0.618	32.4	71	80	0.88	N/A	2.70	0.62	632	0.23	0.40	300	No	5.43
46		X65	No	20	0.618	32.4	71	80	0.88	N/A	1.61	0.37	277	0.10	0.40	300	No	4.01
47		X65	No	20	0.618	32.4	71	80	0.88	N/A	2.42	0.55	541	0.20	0.40	300	No	6.16
48	13	X80	N/A	30	0.61	48.9	98	113	0.86	No	1.81	0.45	N/A	0.23	1.00	740	N/A	2.15

As shown in Table C - 1, the complete model input parameters are not available (shown as 'N/A') for every test. The following default values are used for the parameters which are N/A:

- Girth weld: No (i.e., no girth weld, plain pipe);
- Lüder's strain: No (i.e., no Lüder's strain, round house stress-strain curve);

- Net-section force: 0.0 kip
- h_g: see 4.6 for median and lower/upper bound values;
- L_b: critical wavelength;
- h_m: 1/16 in (1.6 mm).

C.2 References of Appendix C

1 Stephens, D. R., Olson, R. J., and Rosenfeld, M. J., 1991, "Pipeline Monitoring - Limit State Criteria," NG-18 Report No. 1888, Battelle, Columbus, Ohio.

2 Bouwkamp, J. and Stephen, R., 1974, " Full Scale Studies on Structural Behaviour of Large Diameter pipes under combined loading," Report No. UC-SESM 74-1, University of California Berkeley.

3 DelCol, P. R., et al., 1998, " Behaviour of Large Diameter Line Pipe Under Combined Loads," Structural Engineering Report 224, University of Alberta.

4 Chen, C. Q., 2008, "Local Buckling and Collapse of Corroded Pipes," PR-244-9827 report, CFER.

5 Foeken, R. J. V. and Gresnigt, A. M, 1998, "Buckling and Collapse of UOE Manufactured Steel Pipes", PR-238-9423, TNO.

6 Fonzo, A. et al., 2011, "Full Scale Investigation on Strain Capacity of High Grade Large Diameter Pipes ", 18th JTM, 16-19 May 2011, San Francisco, CA.

7 Suzuki, N. et al., 2006, "Effects of Geometric Imperfection on Bending Capacity of X80 Line-pipe", Proceedings of the 6th International Pipeline Conference, September 25-29, 2006, Calgary, Alberta, Canada.

8 Tajika, H. et al., 2012, "Compressive and Tensile Strain Capacities of 48" of X80 Line Pipes", Proceedings of the 2012 9th International Pipeline Conference, September 24-28, 2012, Calgary, Alberta, Canada.

8a Suzuki, N. et al., 2010, "Local Buckling Behavior of 48”, X80 High-Strain Line Pipes", Proceedings of the 8th International Pipeline Conference, September 27 - October 1, 2010, Calgary, Alberta, Canada.

8b Tajika, H., et al., 2011, "Full-Scale Bending Test of 48” X80 Linepipes", Proceedings of the Twenty-first (2011) International Offshore and Polar Engineering Conference, June 19-24, 2011, Maui, Hawaii, USA, Vol. 4, pp 653-659.

8c Igi, S., et al., "Strain Capacity of 48" OD X80 Pipeline in Pressurized Full-scale Bending Test", Proceedings of the Twenty-first (2011) International Offshore and Polar Engineering Conference, June 19-24, 2011, Maui, Hawaii, USA, Vol. 4, pp 646-652.

9 Mohareb, M. E., et al., 1994, "Deformational Behaviour of Line-pipe", Structural Engineering Report No. 202, Department of Civil Engineering, University of Alberta, Edmonton, Canada T6G 2G7.

10 Yoosef-Ghodsi, N., Kulak, G. L., and Murray, D.W., 1994, "Behaviour of Girth Welded Line-pipe", Structural Engineering Report No. 203, Department of Civil Engineering, University of Alberta, Edmonton, Canada T6G 2G7.

11 Unpublished communication.

12 Tajika, H., and Suzuki, N., 2009, "Bending Capacity and Seismic Integrity of X65 ERW Line Pipe", Proceedings of the Nineteenth (2009) International Offshore and Polar Engineering Conference, June 21-26, 2009, Osaka, Japan, pp 527-533.

13 Suzuki, N. et al., 2007, "Strain Capacity of X80 High-strain Line Pipes", Proceedings of the 26th International Conference on Offshore Mechanics and Arctic Engineering OMAE2007-29505, June 10-15, 2007, San Diego, California, USA.